DOKUZ EYLÜL UNIVERSITY
GRADUATE SCHOOL OF NATURAL AND APPLIED SCIENCES

DEVELOPMENT OF THERMALLY RESISTANT SOIL MATERIAL WITH PUMICE, PERLITE AND FIBER GLASS ADDITIVES

by
Esra GÜNERİ

December 2022
İZMİR

DEVELOPMENT OF THERMALLY RESISTANT SOIL MATERIAL WITH PUMICE, PERLITE AND FIBER GLASS ADDITIVES

A Thesis Submitted to the
Graduate School of Natural and Applied Sciences of Dokuz Eylul University
In Partial Fulfillment of the Requirements for the Degree of Doctor of Philosophy in Civil Engineering, Geotechnical Program

by
Esra GÜNERİ

December 2022
İZMİR

Ph.D. THESIS EXAMINATION RESULT FORM

We have read the thesis entitled **"DEVELOPMENT OF THERMALLY RESISTANT SOIL MATERIAL WITH PUMICE, PERLITE AND FIBER GLASS ADDITIVES"** completed by **ESRA GÜNERİ** under supervision of **PROF. DR. YELİZ YÜKSELEN AKSOY** and we certify that in our opinion it is fully adequate, in scope and in quality, as a thesis for the degree of Doctor of Philosophy.

Prof. Dr. Yeliz YÜKSELEN AKSOY

Supervisor

Prof. Dr. A. Hakan ÖREN	Assist. Prof. Dr. Ender BAŞARI
Thesis Committee Member	Thesis Committee Member
Assoc. Prof. Dr. Tuğba ESKİŞAR TEFÇİ	Assoc. Prof. Dr. Deniz ÜLGEN
Examining Committee Member	Examining Committee Member

Prof. Dr. Okan FISTIKOĞLU

Director

Graduate School of Natural and Applied Sciences

ACKNOWLEDGMENT

First of all, I would like to thank my honorable advisor, Professor Yeliz YÜKSELEN AKSOY, who always supported me throughout my doctoral study and always shared her knowledge and experiences with me. All her teachings will guide me throughout my life and for that I'm grateful.

I would like to thank my esteemed committee members Professor A. Hakan ÖREN and Assistant Professor Ender BAŞARI for their contributions. For his support in the hydraulic conductivity tests, I would also like to thank Prof. A. Hakan ÖREN very much. I would like to thank Professor Gürkan ÖZDEN and Associate Professor Okan ÖNAL, whose knowledge and experience I benefited from during my doctoral education.

I would like to thank my dear friend Şükran Gizem ALPAYDIN, who devotedly helped me during my experimental studies, and also thanks to my labmates and firends Cihat AŞÇI, Yusuf BATUGE and Emir OKUCU.

Finally, I am grateful to my beloved husband Hüseyin GÜNERİ, who always supported me spiritually during my doctoral thesis, to my dear son Kemal GÜNERİ, who took all my worries and tiredness with his presence, and to my baby, who will be the new member of our family. I am also grateful to my dear mom and dad for supporting me all along my life and making me feel like they were there for me.

I would like to thank scholarship of TÜBİTAK Project 217M553 and YOK 100/2000 Doctoral Scholorship for their financial support and supplying test equipment in order to conduct the study within the scope of the thesis.

Esra GÜNERİ

DEVELOPMENT OF THERMALLY RESISTANT SOIL MATERIAL WITH PUMICE, PERLITE AND FIBER GLASS ADDITIVES

ABSTRACT

There has been a rapid increase in the type and number of energy structures due to the increasing energy requirements in the world in last decades. Due to the high cost of fossil fuels and their damage to the environment, there has been a focus on nuclear resources, geothermal energy, solar energy, etc. in energy generation. On the other hand, these energy structures cause thermal temperature changes in the soil, as they are structures that directly contact the soil. As a result, thermal effects occur in the soils around these structures, such as buried cables, heat piles, solid waste storage facilities, and geothermal facilities. Therefore, there has been an increase in the number of studies on the engineering behavior of soils due to high temperature and thermal cycles in recent years. These studies revealed that thermal cycles (heating-cooling) and high temperatures caused changes in the engineering properties of soils, such as hydraulic conductivity, volumetric change (settlement-swelling), and shear strength.

There is a need for buffer materials which are durable and keeps enginering properties for a long time. For this purpose, it was aimed to develop durable buffer material under high temperature that can preserve its compressibility, hydraulic conductivity and strength properties under high temperatures in the presence perlite, pumice, and fiberglass additives. According to the results, the fiberglass additive is more effective on the thermal conductivity, swelling, shear strength of the sand-bentonite mixtures under high temperature when compared with pumice and perlite.

Keywords: Fiberglass, perlite, pumice, sand-bentonite mixtures, high temperature

POMZA, PERLİT VE CAM ELYAF KATKILI ISIYA DAYANIKLI ZEMİN MALZEMESİ GELİŞTİRİLMESİ

ÖZ

Son on yılda dünyada artan enerji ihtiyacına bağlı olarak enerji yapılarının tür ve sayısında hızlı bir artış olmuştur. Fosil yakıtların maliyetinin yüksek olması ve çevreye verdiği zararlar nedeniyle enerji üretiminde nükleer kaynaklar, jeotermal enerji vb. konulara ağırlık verilmiştir. Bu enerji yapıları ise doğrudan zeminlerle temas eden yapılar oldukları için zeminde sıcaklık değişimlerine neden olurlar. Bunun sonucunda gömülü kablolar, ısı kazıkları, katı atık depolama tesisleri, jeotermal tesisler gibi yapıların etrafındaki zeminlerde termal etkiler meydana gelir. Bu nedenle, son yıllarda yüksek sıcaklık ve termal döngüler nedeniyle zeminlerin mühendislik davranışları üzerine yapılan çalışmaların sayısında artış olmuştur. Bu çalışmalar, termal döngülerin (ısıtma-soğutma) ve yüksek sıcaklığın zeminlerin hidrolik iletkenlik, hacimsel değişim (oturma-şişme), kesme dayanımı gibi mühendislik özelliklerinde değişikliklere neden olduğunu ortaya koymuştur.

Dayanıklı ve mühendislik özelliklerini uzun süre koruyan tampon malzemelerine ihtiyaç vardır. Bu amaçla, perlit, pomza ve fiberglas katkıların varlığında, yüksek sıcaklıklarda sıkıştırılabilirlik, hidrolik iletkenlik ve dayanım özelliklerini koruyabilen, yüksek sıcaklık altında dayanıklı tampon malzeme geliştirilmesi hedeflenmiştir. Elde edilen sonuçlara göre, yüksek sıcaklıkta kum-bentonit karışımlarının termal iletkenliğini, şişmesini, kayma direncini arttırmada cam elyafı katkısı pomza ve perlite göre daha etkilidir.

Anahtar Kelimeler: Cam elyaf, perlit, pomza, kum-bentonit karışımları, yüksek sıcaklık

CONTENTS

PH. D. THESIS EXAMINATION RESULT FORM……..ii

ACKNOWLEDGEMENTS……iii

ABSTRACT……iv

ÖZ……v

LIST OF FIGURES……...xiii

LIST OF TABLES……..…….xxii

LIST OF SYMBOLS……...…xxvi

ABBREVIATIONS……xxvii

CHAPTER 1 - INTRODUCTION 1

1.1 Statement of the Problem 1

1.2 Objective and Scope 2

1.3 Outline of the Thesis 3

CHAPTER 2 - LITERATURE REVIEW 5

2.1 Major Structures Causing Temperature Change in Soils 7

2.1.1 Nuclear Waste Storage Repositories 7

2.1.2 Municipal Solid Waste Landfills 9

2.1.3 Energy Piles 11

2.1.4 Buried Power Cables 13

2.1.5 Geothermal Plants 14

2.2 Temperature Effects on the Engineering Behavior of Soils 14

2.2.1 Temperature Effects on the Volume Deformation Behavior of the Soils 14
2.2.2 Temperature Effects on the Shear Strength Behavior of the Soils 21
2.2.3 Temperature Effects on the Hydraulic Conductivity Behavior of the Soils 23
2.2.4 Thermal Conductivity Behavior of the Soils 28
2.3 Temperature Resistant Materials 29
2.3.1 Pumice 29
2.3.2 Perlite 30
2.3.3 Fiberglass 31

CHAPTER 3 - MATERIAL CHARACTERIZATION and EXPERIMENTAL METHODS 33

3.1 Material Characterization 33
3.1.1 Sand-Bentonite Mixtures 33
3.1.2 Pumice 35
3.1.3 Perlite 36
3.1.4 Fiberglass 38
3.2 Methods 39
3.2.1 Determination of the Engineering Index Properties of the Materials 40
3.2.2 Preparation of the Mixtures 42
3.2.3 Compaction Tests 43
3.2.4 Compressibility Tests 43
3.2.5 Direct Shear Tests 46
3.2.6 Hydraulic Conductivity Tests 48

3.2.9 Finite Element Method (FEM) Analyses of the Sand-Bentonite Mixtures as a Buffer Material 54

CHAPTER 4 - TEMPERATURE EFFECT ON THE VOLUME DEFORMATION, SHEAR STRENGTH, HYDRAULIC CONDUCTIVITY AND THERMAL CONDUCTIVITY BEHAVIOR OF SAND-BENTONITE MIXTURES 55

4.1 Compaction of Sand-Bentonite Mixtures 55

4.2 Volume Deformation Behavior of Sand-Bentonite Mixtures 56

4.2.1 Volume Deformation Behavior of Sand-Bentonite Mixtures Under Room Temperature 56

4.2.2 Volume Deformation Behavior of Sand-Bentonite Mixtures Under High Temperature (80 °C) 57

4.2.3 Volume Deformation Behavior of Sand-Bentonite Mixtures Under Thermal Cycles 59

4.3 Shear Strength Behavior of Sand-Bentonite Mixtures 61

4.3.1 Shear Strength Behavior of Sand-Bentonite Mixtures Under Room Temperature 62

4.3.2 Shear Strength Behavior of Sand-Bentonite Mixtures Under High Temperature 64

4.3.3 Shear Strength Behavior of Sand-Bentonite Mixtures Under Thermal Cycles 66

4.4 Hydraulic Conductivity Behavior of Sand-Bentonite Mixtures Under Room and High Temperatures and Thermal Cycles 67

4.5 Thermal Conductivity of the of Sand-Bentonite Mixtures 70

4.6 SEM Analyses of the Sand-Bentonite Mixtures 71

CHAPTER 5 - PUMICE EFFECT ON THE VOLUME DEFORMATION, SHEAR STRENGTH, HYDRAULIC CONDUCTIVITY AND THERMAL CONDUCTIVITY BEHAVIOR OF SAND-BENTONITE MIXTURES UNDER THERMAL CONDITIONS 72

5.1 Compaction Behavior of Pumice Added Sand-Bentonite Mixtures 72

5.2 Volume Deformation Behavior of Pumice Added Sand-Bentonite Mixtures 75

5.2.1 Volume Deformation Behavior of Pumice Added Sand-Bentonite Mixtures Under Room Temperature 75

5.2.2 Volume Deformation Behavior of Pumice Added Sand-Bentonite Mixtures Under High Temperature 78

5.2.3 Volume Deformation Behavior of Pumice Added Sand-Bentonite Mixtures Under Thermal Cycles 81

5.3 Shear Strength Behavior of Pumice Added Sand-Bentonite Mixtures 86

5.3.1 Shear Strength Behavior of Pumice Added Sand-Bentonite Mixtures Under Room and High Temperatures 86

5.3.2 Shear Strength Behavior of Pumice Added Sand-Bentonite Mixtures Under Thermal Cycles 91

5.4 Hydraulic Conductivity Behavior of Sand-Bentonite Mixtures Under Room-High Temperatures and Thermal Cycles 96

5.5 Thermal Conductivity of the Sand-Bentonite Mixtures in the Presence of Pumice 100

5.6 Scanning Electron Microscope (SEM) Analyses 102

CHAPTER 6 - PERLITE EFFECT ON THE VOLUME DEFORMATION, SHEAR STRENGTH, HYDRAULIC CONDUCTIVITY AND THERMAL CONDUCTIVITY BEHAVIOR OF SAND-BENTONITE MIXTURES 104

6.1 Compaction Behavior of Perlite Added Sand-Bentonite Mixtures 104

6.2 Volume Deformation Behavior of Perlite Added Sand-Bentonite Mixtures 108

6.2.1 Volume Deformation Behavior of Sand-Bentonite Mixtures Under Room Temperature 108

6.2.2 Volume Deformation Behavior of Perlite Added Sand-Bentonite Mixtures Under High Temperature 110

6.2.3 Volume Deformation Behavior of Perlite Added Sand-Bentonite Mixtures Under Thermal Cycles 112

6.3 Shear Strength Behavior of Perlite Added Sand-Bentonite Mixtures 116

6.3.1 Shear Strength Behavior of Perlite Added Sand-Bentonite Mixtures Under Room and High Temperatures 116

6.3.2 Shear Strength Behavior of Perlite Added Sand-Bentonite Mixtures Under Thermal Cycles 122

6.4 Hydraulic Conductivity Behavior of Perlite Added Sand-Bentonite Mixtures Under Room and High Temperatures and Thermal Cycles 124

6.5 Thermal Conductivity of the Perlite Added Sand-Bentonite Mixtures 132

6.6 Scanning Electron Microscope (SEM) Analyses of Perlite Added Sand-Bentonite Mixtures 134

CHAPTER 7 - THE EFFECT OF FIBERGLASS ON THE VOLUME DEFORMATION, SHEAR STRENGTH, HYDRAULIC CONDUCTIVITY AND THERMAL CONDUCTIVITY BEHAVIOR OF SAND-BENTONITE MIXTURES 136

7.1 Compaction Behavior of Fiberglass Added Sand-Bentonite Mixtures 136

7.2 Volume Deformation Behavior of Fiberglass Added Sand-Bentonite Mixtures 137

7.2.1 Volume Deformation Behavior of Fiberglass Added Sand-Bentonite Mixtures Under Room Temperature 138

7.2.2 Volume Deformation Behavior of Fiberglass Added Sand-Bentonite Mixtures Under High Temperature 139

7.3 Shear Strength Behavior of Fiberglass Added Sand-Bentonite Mixtures . 143

7.3.1 Shear Strength Behavior of Fiberglass Added Sand-Bentonite Mixtures Under Room Temperature 143

7.3.2 Shear Strength Behavior of Fiberglass Added Sand-Bentonite Mixtures Under High Temperature 146

7.4 Hydraulic Conductivity Behavior of Fiberglass Added Sand-Bentonite Mixtures Under Room and High Temperatures and Thermal Cycles 150

7.5 Thermal Conductivity of the of Fiberglass Added Sand-Bentonite Mixtures 154

CHAPTER 8 - MODELING THE BUFFER MATERIAL AROUND NUCLEAR WASTE STORAGE AREA 155

8.1 Nuclear Waste Storage Repositories 155

8.2 Modeling with Code Bright Programme 157

8.3 Finite Element Method (FEM) Analysis of Sand-Bentonite Mixtures as a Buffer Material 160

8.3.1 Evaluation of Performance of 10B-90S Mixture with FEM Analysis 160

8.3.2 Evaluation of Performance of 20B-80S Mixture with FEM Analysis 163

8.3.3 Evaluation of Performance of 30B-70S Mixture with FEM Analysis 166

CHAPTER 9 - CONCLUSIONS..... 171

9.1 Compaction Test Results 171

9.2 Oedometer Tests Results 171

9.3 Direct Shear Test Results..... 172

9.4 Hydraulic Conductivity Test Results..... 174

9.5 Thermal Conductivity Test Results 175

9.6 Comparison of the Effects of the Pumice, Perlite and Fiber Glass Additives 175

9.7 Future Studies 177

REFERENCES..... 178

LIST OF FIGURES

Page

Figure 2.1 Influence of overconsolidation ratio on the thermal strain of fine soils (Cekerevac, & Laloui, 2004) 6

Figure 2.2 THM processes involved in the evolution of the barrier during the transient period (Gens et al., 2021) 8

Figure 2.3 Thermal reactions in simulated landfill environment (Tupsakhare et al., 2020) 10

Figure 2.4 Structure diagram of composite energy pile (Xie, & Qin, 2021) 12

Figure 2.5 Geothermal heat exchangers with single and double U-tubes (Özüdoğru, 2015) 13

Figure 2.6 Schematic presentation of volumetric deformation and hydraulic conductivity behavior of soils under thermal effects (adopted from Zang, 1993a) 15

Figure 2.7 Consolidation stress and temperature relationship (Campanella, & Mitchell, 1968; El Tawati, 2010) 18

Figure 2.8 Comparison of the calculated hydraulic conductivity with the measured ones for the FEBEX bentonite at a dry density of 1.38 Mg/m^3 (Villar, & Lloret 2004) 24

Figure 2.9 Hydraulic conductivity vs. temperature for saturated samples compacted to different nominal dry densities (Villar et al., 2010) 27

Figure 2.10 Physical appearance of pumice (Istockphoto , 2010) 30

Figure 2.11 Physical appearance of perlite (Worldperlite, 2013) 31

Figure 2.12 Physical appearance of fiberglass (Lbifiberglass, 2022) 32

Figure 3.1 Sand and bentonite samples 34

Figure 3.2 Grain size distribution curves of sand and bentonite samples 34

Figure 3.3 The X-Ray diffraction analysis (XRD) result of the bentonite 35

Figure 3.4 Pumice sample 35

Figure 3.5 Grain size distribution curve of pumice 36
Figure 3.6 The X-Ray diffraction analysis (XRD) of the pumice sample 36
Figure 3.7 Perlite sample 37
Figure 3.8 Grain size distribution curve of perlite 37
Figure 3.9 The X-Ray diffraction analysis (XRD) of the perlite 38
Figure 3.10 Fiberglass sample 39
Figure 3.12 Devices for pH measurement and XRD analysis a) pHmeter, b) Thermo Scientific ARL X'TRA device 42
Figure 3.13 Mold, jack and automatic compactor 43
Figure 3.14 The oedometer test device 44
Figure 3.15 The heat ring, thermostat and membrane used in oedometer tests under high temperature and temperature cycling 45
Figure 3.16 Path representation of the oedometer experiments under thermal cycles 46
Figure 3.17 Compacted and submerged samples for direct shear tests 46
Figure 3.18 Heat rod and digital thermometer used in the direct shear tests 47
Figure 3.19 Path representation of the direct shear experiments under thermal cycles 48
Figure 3.20 The geotextiles, latex membrane and O-rings used in hydraulic conductivity tests 49
Figure 3.21 The permeameter test set-up a)K-type thermocouple, b) aluminum cell and c) heat rod 49
Figure 3.22 The hydraulic conductivity test equipment under high temperatures 50
Figure 3.23 The equipment of thermal conductivity measurement 51
Figure 3.24 Wooden cells used in thermal conductivity measurements 52
Figure 3.25 Compacted samples before measurement 52

Figure 3.26 TEMPOS Thermal Properties Analyzer instrument and samples 53

Figure 3.27 Freeze-drier device and COXEM EM-30 Scanning electron microscope 54

Figure 4.1 Compaction curves of the sand-bentonite mixtures..... 56

Figure 4.2 Compression and swelling curves of sand-bentonite mixtures under room temperature..... 57

Figure 4.3 Compression and swelling curves of sand-bentonite mixtures under high temperature..... 58

Figure 4.4 The effect of temperature on compression amount under room temperature and 80 °C..... 59

Figure 4.5 Compression and swelling curves of sand-bentonite mixtures under thermal cycles..... 61

Figure 4.6 Shear stress-normal stress relationship of sand-bentonite mixtures at room temperature..... 62

Figure 4.7 τ- ε relationship of sand-bentonite mixtures at room temperature 63

Figure 4.8 τ- ε relationship of sand-bentonite mixtures at room temperature 63

Figure 4.9 Shear stress-normal stress relationship of sand-bentonite mixtures at high temperature based on shear rate (0.5 mm/min)..... 65

Figure 4.10 τ- ε relationship of sand-bentonite mixtures at high temperature based on shear rate (0.5 mm/min) 65

Figure 4.11 Shear stress-normal stress relationship of sand-bentonite mixtures at high temperature based on shear rate (0.003 mm/min)..... 66

Figure 4.12 Shear stress-normal stress relationship of sand-bentonite mixtures under thermal cycle and 196 kPa normal stress..... 67

Figure 4.13 Hydraulic conductivity in terms of pore volume of flow of mixture 10B-90S..... 69

Figure 4.14 Hydraulic conductivity in terms of the pore volume of flow of mixture 20B-80S..... 69

Figure 4.15 Hydraulic conductivity in terms of the pore volume of flow of mixture 30B-70S 69

Figure 4.16 Scanning electron microscope photos of the samples (a) 10B-90S (x1000) at room temperature (RT), (b) 10B-90S (x1000) at 80 ˚C..... 71

Figure 4.17 Scanning electron microscope photos of the samples (a) 20B-80S (x1000) at room temperature (RT), (b) 20B-80S (x1000) at 80˚C 71

Figure 5.1 Compaction curve of pumice additive..... 73

Figure 5.2 Compaction curves of sand-bentonite mixtures with pumice additives a) 10B-90S mixtures, b) 20B-80S mixtures..... 74

Figure 5.3 Effect of pumice additive on maximum dry unit weight for 10B-90S and 20B-80S mixtures..... 74

Figure 5.4 Effect of pumice additive on optimum water content for 10B-90S and 20B-80S mixtures..... 75

Figure 5.5 Compression and swelling curves of pumice 76

Figure 5.6 Compression and swelling curves of sand-bentonite mixtures under room temperature in the presence of pumice a) 10B-90S, b) 20B-80S..... 77

Figure 5.7 Compression and swelling curves of sand-bentonite mixtures under high temperature in the presence of pumice a) 10B-90S, b) 20B-80S..... 79

Figure 5.8 Compression and swelling curves of sand-bentonite mixtures under thermal cycle in the presence of pumice a) 10B-90S, b) 20B-80S 83

Figure 5.9 The effects of thermal cycling on NC clay and 20PU-8B-72S mixtures . 85

Figure 5.10 The effect of sand-bentonite mixtures on compression amount under room temperature and 80°C in the presence of pumice additive..... 86

Figure 5.11 Shear stress-normal stress relationship of sand-bentonite mixtures at room and high temperatures in the presence of 10% and 20% pumice additive a) 10B-90S, b) 20B-80S..... 88

Figure 5.12 τ- ε relationship of sand-bentonite mixtures in the presence of of 10% and 20% pumice..... 90

Figure 5.13 Shear stress-strain relationship of pumice under thermal cycling 91

Figure 5.14 Shear stress-strain relationship of sand-bentonite mixtures under thermal cycling in the presence of pumice a) 10B-90S, b) 20B-80S 93

Figure 5.15 Comparison of maximum shear stresses under room, high temperature and thermal cycles cycling in the presence of pumice a) 10B-90S, b) 20B-80S 95

Figure 5.16 Maximum shear strengths of pumice added sand-bentonite mixtures at room temperature and 80 °C 95

Figure 5.17 Hydraulic conductivity versus pore volume of flow graph of 10B-90S mixture a) 10% pumice b) 20% pumice 97

Figure 5.18 Hydraulic conductivity versus pore volume of flow of 20B-80S mixture a) 10% pumice b) 20% pumice 98

Figure 5.19 Hydraulic conductivity values of sand-bentonite mixtures under different temperatures in the presence of pumice 99

Figure 5.20 Comparison of hydraulic conductivity behavior of pumice added sand-bentonite mixtures under temperature cycling 99

Figure 5.21 Scanning electron microscope photographs of pumice, (a) room temperature (x1000) and (b) 80 ˚C (x1000) 102

Figure 6.1 Compaction curve of perlite 104

Figure 6.2 Compaction curves of sand-bentonite mixtures with perlite a)10B-90S mixtures, b)20B-80S mixtures 106

Figure 6.3 Effect of perlite on the maximum dry unit weight a) 10B-90S mixtures, b) 20B-80S mixtures 107

Figure 6.4 Effect of perlite on the optimum water content a) 10B-90S mixtures, b) 20B-80S mixtures 107

Figure 6.5 The collapse of the perlite sample in the oedometer test 108

Figure 6.6 Compression and swelling curves of sand-bentonite mixtures under room temperature in the presence of perlite a) 10B-90S, b) 20B-80S 109

Figure 6.7 Compression and swelling curves of sand-bentonite mixtures under high temperature in the presence of perlite a) 10B-90S, b) 20B-80S 112

Figure 6.8 Compression and swelling curves of sand-bentonite mixtures under thermal cycle in the presence of pumice a) 10B-90S, b) 20B-80S 114

Figure 6.9 The vertical deformation values of the mixtures under thermal cycle, 80 °C and rrom temperature in the presence of perlite additive..... 116

Figure 6.10 Shear stress-normal stress relationship of sand-bentonite mixtures at room temperature and high temperature (80 °C) in the presence of 10% and 20% perlite additive a) 10B-90S, b) 20B-80S..... 118

Figure 6.11 Shear stress-horizontal displacement relationship of 20B-80S and 16B-64S-20PE mixtures at 80 °C 119

Figure 6.12 τ- ε relationship of sand-bentonite mixtures in the presence of of 10% and 20% perlite 121

Figure 6.13 Shear stress-strain relationship of sand-bentonite mixtures under thermal cycling in the presence of perlite a) 10B-90S, b) 20B-80S..... 123

Figure 6.14 Maximum shear strengths of perlite added sand-bentonite mixtures at room temperature and under 80 °C and thermal cycles……124

Figure 6.15 Hydraulic conductivity of 10B-90S mixture a) 10% perlite b) 20% perlite 126

Figure 6.16 Hydraulic conductivity graphs of 20B-80S mixture a) 10% perlite b) 20% perlite..... 126

Figure 6.17 Change of calculated and measured hydraulic conductivity values as a function of temperature, a) 9B-81S-10PE, b) 16B-64S-20PE..... 129

Figure 6.18 Variation of the hydraulic conductivity during heating-cooling cycles for 9B-81S-10PE mixture 130

Figure 6.19 Hydraulic conductivity values of sand-bentonite mixtures under different temperatures in the presence of perlite..... 131

Figure 6.20 Comparison of hydraulic conductivity behavior of perlite added sand-bentonite mixtures under temperature cycling..... 132

Figure 6.21 Electron microscope photographs of perlite and perlite added sand-bentonite mixtures (a) Perlite (x500) under room temperature, (b) 16B-64S-20PE room temperature (x500), (c) 16B-64S-20PE 80 ˚C (x500)..... 135

Figure 7.1 Compaction curves of 30B-70S and 1FG-30B-70S mixtures 136

Figure 7.2 Effect of perlite on the optimum water content and maximum dry unit weight of 30B-70S mixture..... 137

Figure 7.3 Compression and swelling curves of sand-bentonite mixtures under room temperature in the presence of fiberglass..... 139

Figure 7.4 Compression and swelling curves of sand-bentonite mixtures under high temperature in the presence of fiberglass..... 140

Figure 7.5 Effective stress vs e/e_0 relationships at different temperatures a) 30B-70S, b) 0.5FG-30B-70S..... 141

Figure 7.6 The effect of fiberglass on the compression deformation under room temperature and 80 °C..... 142

Figure 7.7 τ-σ relationship of 30B-70S mixtures in the presence fiberglass at room temperature a) 3 mm fiberglass, b) 6 mm fiberglass..... 144

Figure 7.8 Shear stress-strain relationship of fiberglass added sand-bentonite mixtures at room temperature a) 3 mm fiberglass, b) 6 mm fiberglass 145

Figure 7.9 Cracks in long fibers (Betterman, 1995)..... 146

Figure 7.10 τ-σ relationship of 30B-70S mixtures in the presence fiberglass additive (3 mm) at high temperature..... 147

Figure 7.11 Shear stress-strain relationship of sand-bentonite mixtures under high temperature in the presence of 3 mm fiberglass additives..... 148

Figure 7.12 Shear stress-strain relationship of 1FG-30B-70S mixtures under high temperature in the presence of 3 mm and 6 mm fiberglass additives 149

Figure 7.13 Maximum shear strength values of fiberglass added sand-bentonite mixtures at room temperature and 80 °C..... 150

Figure 7.14 Hydraulic conductivity behavior of 30B-70S mixture under different temperatures 151

Figure 7.15 Hydraulic conductivity behavior of 30B-70S mixture with 0.5% fiberglass at different temperatures 152

Figure 7.16 Hydraulic conductivity behavior of 30B-70S mixture with 1.0% fiberglass at different temperatures 152

Figure 7.17 Change in hydraulic conductivity depending on fiberglass content at different temperatures 153

Figure 7.18 Hydraulic conductivity of sand-bentonite mixtures under different temperatures in the presence of fiberglass additives 154

Figure 8.1 Deep Geological Repository Conceptual Design (Deep Geological Repository Conceptual Design Report, 2016) 156

Figure 8.2 Modeling phases around nuclear waste storages for the 10B-90S mixture 158

Table 8.1 The mechanical and thermal properties needed for modeling (Code Bright Tutorial 2020) 158

Figure 8.3 Interval data window (Code Bright Tutorial 2020) 159

Figure 8.4 Contour fill of temperature representation in the presence of 10B-90S buffer mixture at the end of the time 161

Figure 8.5 Temperature vs. distance relationship 162

Figure 8.6 Point temperature evalution 163

Figure 8.7 Contour fill of temperature representation in the presence of 20B-80S buffer mixture 164

Figure 8.8 Temperature vs. distance relationship 165

Figure 8.9 Point temperature evalution 166

Figure 8.10 Contour fill of temperature representation in the presence of 30B-70S buffer mixture 167

Figure 8.11 Temperature vs. distance relationship 168

Figure 8.12 Point temperature evalution 169

Figure 8.13 Temperature vs. distance of all sand-bentonite mixtures 170

Figure 9.1 Comparison of compression curves of pumice and perlite added 20B-80S mixtures 176

LIST OF TABLES

Page

Table 2.1 General requirements for the buffer material (Kim et al., 2011) 9

Table 2.2 Previous studies on the volumetric deformation behavior of temperature (Jarad, 2016)..... 16

Table 2.3 Previous studies on the shear strength behavior of temperature (adapted from Kuntiwattanakul et al., 1995) 22

Table 2.4 Previous studies on the hydraulic conductivity behavior depending on temperature (Jarad, 2016)..... 25

Table 3.1 The physico-chemical properties of the materials 33

Table 3.2 Technical properties* of fiberglass..... 38

Table 3.3 The Gantt chart of the Ph.D Thesis..... 40

Table 3.4 Abbreviated naming of the mixtures used in the tests 42

Table 4.1 Compaction parameters of sand-bentonite mixtures obtained from Standard Proctor Tests..... 55

Table 4.2 Total compression and swelling deformation values of sand-bentonite mixtures at room temperature 57

Table 4.3 Total compression and swelling deformation values of sand-bentonite mixtures at high temperature (80 °C)..... 58

Tablo 4.4. Compression deformation amounts of the sand-bentonite mixtures under thermal cycles..... 60

Tablo 4.5. Swelling deformation amounts of the sand-bentonite mixtures under thermal cycles..... 60

Table 4.6 Shear rates of sand-bentonite mixtures 62

Table 4.7 Internal friction angle and cohesion values of sand-bentonite mixtures.... 64

Table 4.8 Internal friction angle, cohesion and maximum shear stress values of sand-bentonite mixtures at high temperature..... 64

Table 4.9 Hydraulic conductivity values of the sand-bentonite mixtures depending on the temperature 68

Tablo 4.10 Thermal conductivity values of sand-bentonite mixtures based on the saturation degree and void ratio of the mixtures 70

Table 5.1 Compaction characteristics of sand-bentonite mixtures in the presence of pumice additive 72

Table 5.2 Vertical and swelling deformation values of the pumice added sand-bentonite mixtures under room temperature 76

Table 5.3 Vertical and swelling deformation values of the pumice added sand-bentonite mixtures under high temperature 80

Table 5.4 Compression and swelling deformation values of pumice added 10B-90S and 20B-80S mixtures under a temperature cycle 84

Table 5.5 Internal friction angle and cohesion values of sand-bentonite mixtures in the presence of 10% and 20% pumice additives under room and high temperatures 87

Table 5.6 Maximum shear stress values of sand-bentonite mixtures in the presence of 10% and 20% pumice under room and high temperatures 90

Table 5.7 Maximum shear stress values of sand-bentonite mixtures in the presence of 10% and 20% pumice under room and high temperatures and thermal cycle (under 196 kPa normal stress) 92

Table 5.8 Variation of hydraulic conductivity values of 9B-81S-10PU and 8B-72S-20PU mixtures with temperature cycling 96

Table 5.9 Thermal conductivity values of sand-bentonite mixtures in the presence of 10% and 20% pumice 101

Table 6.1 Compaction characteristics of perlite added sand-bentonite mixtures 105

Table 6.2 The vertical and swelling deformation values of the perlite-added sand-bentonite mixtures under room temperature 110

Table 6.3 Vertical and swelling deformation values of the perlite added sand-bentonite mixtures under high temperature 112

Table 6.4 Compression and swelling deformation values of perlite added 10B-90S and 20B-80S mixtures under temperature cycle 115

Table 6.5. Internal friction angle and cohesion values of sand-bentonite mixtures in the presence of 10% and 20% perlite 117

Table 6.6 Maximum shear stress values of sand-bentonite mixtures in the presence of 10% and 20% perlite under room and high temperatures 117

Table 6.7 Maximum shear stress values of sand-bentonite mixtures in the presence of 10% and 20% perlite under room and high temperatures and thermal cycle (under 196 kPa normal stress) 122

Table 6.8 Variation of hydraulic conductivity values of perlite added sand-bentonite mixtures with temperature cycling 125

Table 6.9 Temperature influence on some properties of water (Lide, 1995) 127

Table 6.10 Thermal conductivity values of sand-bentonite mixtures in the presence of 10% and 20% perlite 133

Table 7.1 Compaction parameters of fiberglass added sand-bentonite mixtures obtained from Standard Proctor Tests 137

Table 7.2 Vertical compression and swelling deformation values of the fiberglass-added sand-bentonite mixtures under room temperature 138

Table 7.3 Compression and swelling deformation values of the fiberglass added sand-bentonite mixtures under high temperature 140

Table 7.4 Shear strength parameters of fiberglass added sand-bentonite mixtures at room temperature 146

Tablo 7.5. Shear strength parameters of fiberglass added-sand bentonite mixtures under room and high temperatures 147

Table 7.6 Maximum shear stress values of sand-bentonite mixtures in the presence of fiberglass additives under high temperature 148

Table 7.7 Hydraulic conductivity values of the mixtures at different temperatures 150

Tablo 7.8 Thermal conductivity values of fiberglass added-sand bentonite mixtures 154

Table 8.2 Parameters used in the modeling obtained from experimental studies of the present study..... 159

LIST OF SYMBOLS

CO_2 : Carbon dioxide

CH_4 : Methane gas

C_c : Compression index

SiO_2 : Silicon dioxide

Al_2O_3 : Aluminum oxide

Fe_2O_3 : Iron oxide

CaO : Calcium oxide

MgO : Magnesium oxide

Na_2O : Sodium oxide

K_2O : Potassium oxide

w_{opt} : Optimum water content

γ_n : Natural unit weight

γ_{dry} : Dry unit weight

ϕ : Internal friction angle

c : Cohesion

τ_{max} : Maximum shear stress

σ_{vc} : Effective stress

ε_v : Vertical strain

k : Coefficient of permeability

λ : The value of thermal conductivity

ABBREVIATIONS

XRD	: X-ray powder diffraction
Swedish KBS-3	: An abbreviation of nuclear fuel safety
HLW	: High level waste
THM	: Thermo-Hydro-Mechanical
GSHP	: The ground-source heat pump
GCHPs	: Ground-coupled heat pumps
SWHPs	: Surface water heat pumps
DDL	: Diffuse double layer
UU	: Unconsolidated-undrained
CU	: Consolidated-undrained
CNL	: Constant normal load
ASTM	: American Society for Testing and Materials
SEM	: Scanning electron microscope
RT	: Room temperature
SBM	: Sand bentonite mixture
100 PE	: is the 100% perlite
100PU	: is the 100% pumice

10B-90S	: is the 10% bentonite and 90% sand
20B-80S	: is the 20% bentonite and 80% sand
30B-70S	: is the 30% bentonite and 70% sand
9B-81S-10PU	: is the 9% bentonite, 81% sand and 10% pumice
8B-72S-20PU	: is the 8% bentonite, 72% sand and 20% pumice
18B-72S-10PU	: is the 18% bentonite, 72% sand and 10% pumice
16B-64S-20PU	: is the 16% bentonite, 64% sand and 20% pumice
0.5FG-30B-70S	: is the 29.85% bentonite, 69.65% sand, 0.5% fiberglass
1FG-30B-70S	: is the 29.7% bentonite, 69.3% sand and 1% fiberglass
ILW	: Intermediate-level waste
LLW	: Low-level waste
OCR	: Over consolidation ratio

CHAPTER 1
INTRODUCTION

1.1 Statement of the Problem

In parallel to the world population growth in recent years, the demand on energy increases day by day. However, considering the cost of fossil fuels and their harmful effects on environment, it is seen that there is a greater need for sustainable energy sources. For this purpose, the number and type of energy geo-structures, such as buried power cables, heat piles, geothermal energy facilities, nuclear waste repositories, increase. These energy geo-structures and facilities increase the interaction of the soils with high temperature by transferring the heat to the surrounding soil.

According to the former studies, the engineering parameters of soils may change in the presence of high temperature and temperature cycles. For example, high temperature caused by radioactive wastes in nuclear waste storage repositories affecting engineering behavior of soils. In addition, it is known that the compressibility parameters, shear strength behavior and hydraulic conductivity of soils change under high temperatures and thermal cycles. However, it should be noted that there is no consensus about the change in engineering parameters of soils under high temperature and thermal cycles. Many studies have shown that change in engineering properties of soils especially under high temperature depends on many factors (Laloui, 2001). There is a need for more research on the engineering behavior of soils under different thermal conditions especially in order to increase the performance of energy geo-structures.

It is essential in terms of geotechnical engineering that soils can preserve and keep their engineering properties at the design stage under high temperature and temperature cycles. In the present study, some additives were added to common buffer material which is sand-bentonite mixture to improve/keep its engineering properties under high temperatures and temperature cycles. For this purpose, the additives which are frequently used in heat insulation in the construction industry were chosen. The effect of pumice, perlite and fiberglass additives on the engineering behavior of a buffer material which is a soil mixture; sand-bentonite was investigated under high temperature and temperature cycles.

1.2 Objective and Scope

The scope of the doctoral thesis is to obtain a new buffer sand-bentonite mixture using pumice, perlite and fiberglass additives in order to keep/improve their engineering properties under high temperatures and thermal changes. In this frame, the aims of this doctoral thesis are listed as follows:

- To determine the compressibility, shear strength, hydraulic conductivity behavior and thermal conductivity values of sand-bentonite mixtures under room temperature, high temperature and temperature cycles.
- To examine the changes in the mentioned above engineering parameters in the presence of pumice, perlite and fiberglass additives.
- As a result of the experiments, to obtain the most effective additive and its optimum ratio which can be used in practice.
- Determine the thermal conductivity of the sand-bentonite mixtures in the presence of additives in order to increase heat conduction especially at nuclear waste repositories and energy piles.
- Modeling the chosen mixture in a chosen energy structure in order to examine the usability of the chosen mixture in the field applications.

Three different sand-bentonite mixtures in different bentonite ratios were used in the experiments. 10%bentonite-90%sand , 20%bentonite-80%sand and 30%bentonite-70%sand were choosen as sand-bentonite mixtures. The pumice and perlite additives were used in 10% and 20% contents, while fiberglass additive was used in 1.0% and 0.5% contents. The compaction tests were conducted on all samples in order to prepare identical samples at same dry unit weight and optimum water content. Then, oedometer, direct shear and hydraulic conductivity tests were performed. The oedometer, shear strength and hydraulic conductivity tests were performed under three conditions: room temperature, high temperature and temperature cycles. The thermal conductivity values of the mixtures were obtained in the presence of additives. Finally, the mixtures were modelled in the nuclear waste repository as a buffer material.

1.3 Outline of the Thesis

Within the scope of the doctoral thesis, nine chapters were created. The content of each chapter in this doctoral thesis as follows:

In Chapter 1, the statement of problem for this doctoral thesis and the aim and scope of the doctoral thesis are given.

Chapter 2 presents an information about the energy geo-structures that cause change in temperature on the surrounding soils. A literature review on the former studies on high temperature effect on soil behavior is given under four sub-headings as volumetric deformation, shear strength, hydraulic conductivity and thermal conductivity. The information about the used additive materials is also given in this chapter.

Chapter 3 presents the material characterization and the methods used in the experiments.

Chapter 4 shows the effect of temperature on the volumetric deformation, shear strength, hydraulic conductivity and thermal conductivity behaviors of additive-free sand-bentonite mixtures. The results under room temperature, high temperature and temperature cycles are presented comparatively.

Chapter 5 presents the effect of pumice additives on the volumetric deformation, shear strength, hydraulic conductivity and thermal conductivity behaviors of sand-bentonite mixtures under room temperature, high temperature and thermal cycles.

Chapter 6 shows the effect of perlite on the volumetric deformation, shear strength and hydraulic conductivity behavior of sand-bentonite mixtures under high temperature and temperature cycles.

Chapter 7 presents the effects of fiberglass additive on the behavior of sand-bentonite mixtures under high temperature and temperature cycles. The thermal conductivity measurement results of sand-bentonite mixtures are also given.

In Chapter 8, modeling results are given by using the data obtained from the experimental studies of this doctoral thesis with the help of the Code Bright Program on the nuclear waste storage repository.

In Chapter 9, conclusions and recommendations for future studies are given.

CHAPTER 2
LITERATURE REVIEW

The number of studies on the thermal behavior of soils increase because of the increase in the number and type of energy geo-structures in last decades. Increase in temperature and thermal cycles occur in the surrounding soils at energy geo-structures such as; gas pipelines, geothermal power plants, buried power cables, energy piles, solid waste and nuclear waste storage areas. The soils around energy geo-structures keep their engineering properties unchanged under high temperature or thermal cycles. Changes in the engineering properties of soils due to high temperatures may cause undesirable situations. The performance of the energy geo-structures depends on the engineering properties of the soils under different thermal conditions.

Previous studies have shown that the engineering properties of soils change under high temperatures. The engineering properties such as; volume deformation, hydraulic conductivity and shear strength are also subject to this change. In the literature, there are many studies reported these changes. Gray (1936), & Paaswell (1967) emphasized that shear strength and sample volume decrease in cohesive soils depending on temperature increase. Lambe (1960) relates decrease in volume due to the double layer compression by the increasing temperature. On the other hand, Campanella and Mitchel (1968), Finn (1951), & Gray (1936) stated that the void ratio decreases depending on the temperature increase. Yossef et al. (1961) revealed that the temperature increase also affects the liquid and plastic limits of the soils and acts as a reducing agent, explain this with a decrease in viscosity when temperature increases. It was determined by many studies that there will be a decrease in volume in heated soils as long as it is allowed and in the absence of drainage excessive pore water pressure will occur (Plum, & Esrig, 1969).

The soils have different phase structures; the intergranular space, solid and liquid parts. It was reported that when soil is heated, all components expand. If this soil is a clay group, this expansion results change in the distance between the clay particles and a decrease in the strength of the adsorbed layers (Fleureau, 1979, & Robinet et al. 1996). These changes, the equilibrium between the Van der Waals attractive forces

and the electrostatic repulsive forces, which results in one of the clays' most characteristic thermal behaviors.

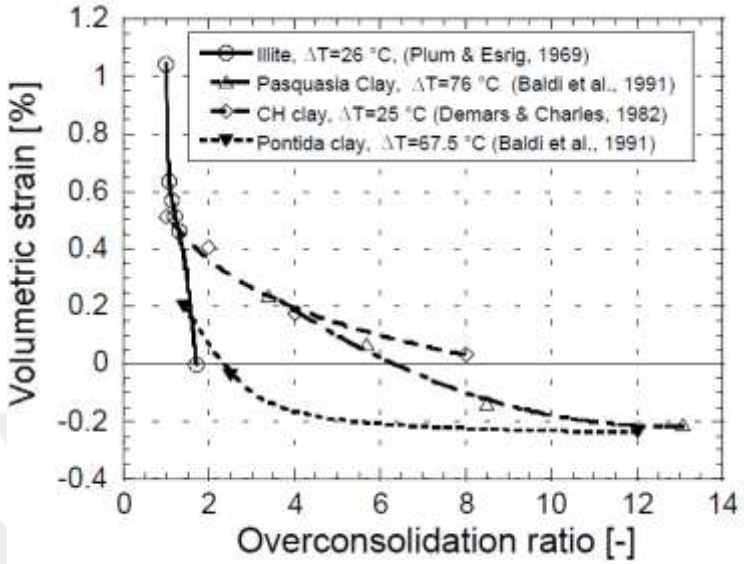


Figure 2.1 Influence of overconsolidation ratio on the thermal strain of fine soils (Cekerevac, & Laloui, 2004)

The intensity of the reversible/irreversible parts of the deformation due to temperature cycling depends upon soil type and plasticity, in addition to stress level measured in terms of the overconsolidation ratio (Laloui, 2001). Figure 2.1 shows that as overconsolidation ratio increases, the expansion behavior increases. In addition, the stress history causes a change in the amount of strain of soil.

It is known that sand-bentonite mixtures, or only bentonite, are used to seal and perform a buffer function in solid waste and nuclear waste storage repositories. The buffer prevents leakage of radioactive wastes from bedrock to groundwater. It should be noted that the materials used as a buffer must have low hydraulic conductivity and high swelling potential. In addition, the capacity to adsorb liquid or water should be high (Yong et al., 1986). To store high-level radioactive wastes (HLW) into bedrock, materials with compressed clay are used as a buffer surrounding HLWs (SKBF/KBS 1983; Simmons, & Baumgartner 1994). Bentonite is preferred as a buffer material due to its low hydraulic conductivity, high absorption capacity, self-sealing properties and durability (Smith et al., 1980; Cho et al., 1999). High gas permeability and low hydraulic conductivity of sand-bentonite mixtures are among the reasons to be

preferred as buffer material. However, bentonite is exposed to high temperatures here and evaporation occurs due to the heat, which causes unexpected deformations (Horseman, & McEwen, 1996). In addition to deformations, chemically illitization of bentonite takes place and a decrease in swelling stress is seen under high temperatures (Zheng et al. 2015).

In the literature it is emphasized that the mechanical properties of sand-bentonite mixtures change depending on the density of the clay, and generally, sand only acts as a filler (Graham et al., 1989; Dixon et al., 1993). The Swedish solid waste disposal practice began in the 1970s, was to bury high-level vitrified waste into containers surrounded by a buffer of 10% bentonite/90% sand at a depth of approximately 500 m in the bedrock. In Canada, sand-bentonite mixtures are widely used as a multi-component buffer (Lingnau et al., 1996). While Dixon et al. (1985) stated that optimum properties would be obtained with equal amounts of sand and bentonite in the use of sand-bentonite for buffering purposes. Akgün et al. (2015) reported that the mixtures formed with 30% bentonite would be more suitable for use. Pakbaz, & Khayat (2004) reported that the strength increased with increasing sand percentage. However, on the contrary, Komine (2004) revealed that bentonite could not fill the voids due to increasing sand amount and decreasing dry density so hydraulic conductivity will increase (Pakbaz, & Khayat, 2004; Komine, 2004). It is seen that many countries have their regulations and preferred buffer materials for nuclear waste repositories.

2.1 Major Structures Causing Temperature Change in Soils

2.1.1 Nuclear Waste Storage Repositories

The disposal of nuclear waste is critical because of any leakage can lead to irreversible catastrophes. Also, the temperature emitted by radioactive wastes occurs around nuclear waste storage areas and is limited by setting a limit value of 100 °C in countries such as Sweden and Finland. Canister elements in which radioactive waste is stored generate heat between 1000 and 2000 Watts during the decay of the waste (Sellin, & Leupin, 2013). Some countries use multiple barrier systems to isolate the waste. Multiple barrier systems are used in most storage systems. Here comes the

bedrock that acts as the primary buffer, followed by the engineered barrier system that surrounds it. While the primary buffer material here is the bedrock itself, the secondarily engineered barrier system is the materials positioned between the canister and the bedrock consisting of only bentonite or sand-bentonite mixture. In cases where bentonite is used as a buffer in structures such as tunnels and deposition holes, the dry density of the buffer material varies between 1450-1650 kg/m^3. In addition, the role of the bedrock as a barrier between the waste and the environment is of great importance (Nuclear Energy Agency, 2007). Figure 2.2 shows the thermo-hydro-mechanical behavior of the bentonite barrier. The heat emitted by radioactive wastes is first transmitted to the bentonite, then to the bedrock and it is observed that the temperature decreases here. The increase in temperature causes the water to evaporate and a process occurs that affects each other from a thermal-hydraulic and mechanical even chemical point of view (Gens et al., 2021).

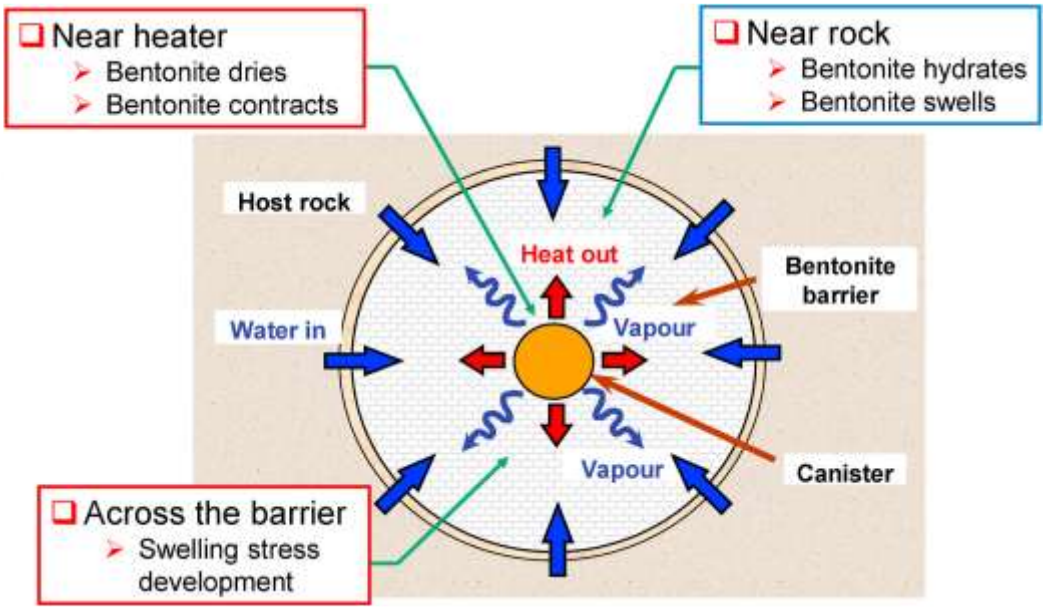


Figure 2.2 THM processes involved in the evolution of the barrier during the transient period (Gens et al., 2021)

Many different countries have different disposal concepts and methods. For example, the Swedish KBS-3 concept includes security scope retardation and containment. While containment emphasizes the complete isolation of radioactive waste, retardation slows the leakage in case of a leak (Sellin, & Leupin, 2013). The burial of radioactive wastes in the bedrock varies according to the country of the

regulations. For example, Switzerland determined this depth between 600-900 m, while Canada determined it as 500-1000 m and Finland about 500 m (Sellin, & Leupin, 2013).

The material to be used as a buffer must have some basic properties. For example, very low hydraulic conductivity and self-sealing ability slow leachate's progress and maintain its service life for a specified period (Sellin, & Leupin, 2013). In addition to these, it should have high durability under high temperatures. The general requirements of the buffer material are shown in Table 2.1.

Table 2.1 General requirements for the buffer material (Kim et al., 2011)

Perormance indicator	**Criterion**	**Background**
Hydraulic conductivity	$k^{buffer} < 10^{-12}$ m/s	Limit mass transport to a diffusion-dominated process
Swelling pressure	$P_{swell} > 1$ MPa	Ensure sealing, self-healing capacity
Maximum temperature	$T^{buffer} < 100$	Ensure that the buffer retains its properties for long periods of time
Minimum temperature	$T^{buffer} > -5°C$	Prevent freezing
Swelling pressure against the canister	$P_{swell} > 0.2$ MPa	Prevent the canister from the sinking
Swelling pressure around the canister	$P_{swell} > 2$ MPa	Prevent microbial activity
Density around the canister	$\rho_{Bulk} > 1{,}650$ kg/m^3	Prevent transport of particles through the buffer
Density around the canister	$\rho_{Bulk} < 2{,}100$ kg/m^3	Limit shear stresses on the canister due to rock movements

2.1.2 Municipal Solid Waste Landfills

Solid waste landfills store many wastes throughout their lifetime. Although the amount of these wastes varies over time, the stacking mainly consists of biomaterials such as food waste, synthetic textiles, wood, paper and plastic. The waste is decomposed and producing 50% CH_4, 50% CO_2 and temperature (Figure 2.3). The

optimum temperature required for decomposing solid wastes by bacteria should be between 35-40 °C and between 50-60 °C depending on the type of bacteria (Tchobanoglous et al., 1993). The general temperature value mentioned for multiple solid waste storage areas is 55 °C and lower (Yeşiller et al., 2005; Hanson et al., 2010; Hanson et al., 2013). In addition, it was determined that the temperature values formed in the areas defined as elevated temperature landfill reached 100 °C (Tupsakhare et al., 2020). Decomposition process occurs aerobic phase, the anaerobic phase, and total decomposition.

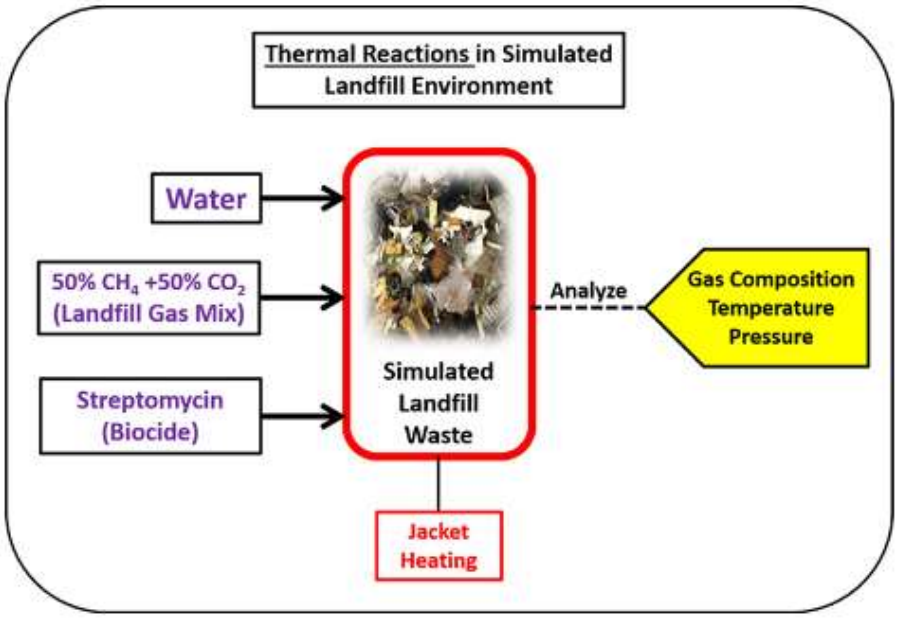


Figure 2.3 Thermal reactions in simulated landfill environment (Tupsakhare et al., 2020)

Farquhar, & Rovers (1973) revealed that waste temperatures are higher in the short term because of decomposition and decrease after about ten years. The height of the waste, the filling rate, and the type of waste are among the factors that directly affect the waste temperature. Previous studies show that the temperature is at the highest level in the middle of the storage areas and is close to the air temperature in the deeper regions (Yeşiller et al., 2005). As it is known, the increase in temperature in solid waste storage areas increases the amount of compression. This situation may decrease the waste's shear strength, even change the waste's slope and cause the stability to deteriorate (Lamothe, & Edgers 1994, Yeşiller et al., 2005). High temperatures are shown to damage gas and leakage infrastructures. At the same time, it has been

determined that the service life of geomembranes used in landfills is adversely affected by high temperatures (Jafari et al., 2014).

2.1.3 Energy Piles

Elements called heat piles or energy piles are used for carrying power and heating and cooling buildings using the ground's natural heat. The first energy pile application was made in 1980 in Austria (Brandl, 2006).

The soil temperature is generally constant throughout a year at underground and the energy piles are designed for this function. For example, in the summer months, a liquid with a higher temperature than the soil temperature is passed inside the piles to cool the water in the pipes and thus to provide cooling by conveying it to the buildings. The opposite of this is applied during the winter months. In other words, the cold liquid is passed through the pipes inside the piles and the soil with a higher temperature heats this liquid (Loveridge, & Powrie, 2012). Energy piles are used in many countries, such as Japan, South Korea and in structures such as bridges and tunnels (Xie, & Qin, 2021). A newly designed energy pile system is shown in Figure 2.4. In this system, both reinforced concrete piles are used. Before these energy piles are placed, cement is injected into the soil and after the energy piles are placed, the cement is covered. In energy piles, heat is used for cooling in summer and heating in winter and is transferred to the ground in summer, while heat is drawn from the ground in winter. When there is a temperature difference between the soil and the outside environment, the energy available on the soil is used to bring the temperature of the building to optimum condition. In summer, the building is cooled with the cooling mode, the heat energy in the building is taken and transferred to the ground. In winter, heat pumps operate to heat the building and transmit the thermal energy available in the soil to the building (Özüdoğru, 2015).

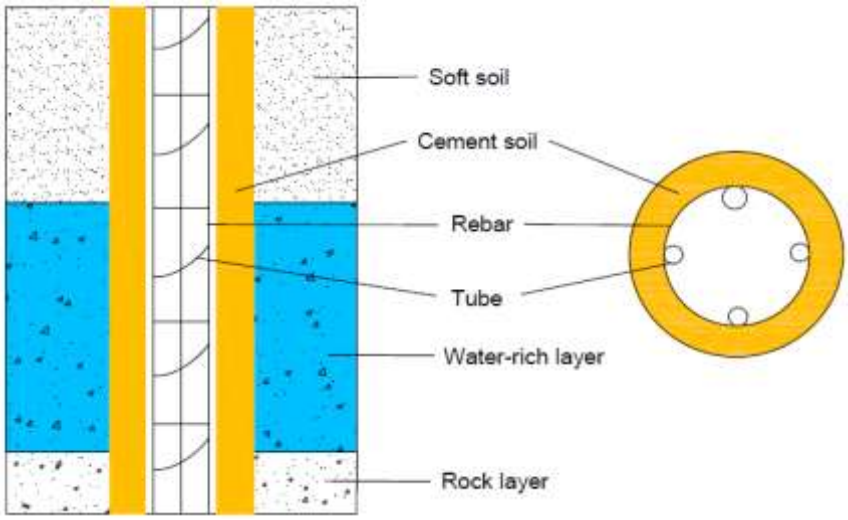


Figure 2.4 Structure diagram of composite energy pile (Xie, & Qin, 2021)

The ground-source heat pump (GSHP) system consists of buried pipes and a pump. The drillings are preferred vertically instead of horizontally because they minimize the effect of temperature changes and reduce the area. Ground-source heat pump systems include groundwater heat pumps (GWHPs), ground-coupled heat pumps (GCHPs) and surface water heat pumps (SWHPs) (Özüdoğru, 2015). Figure 2.5 shows the geothermal heat exchangers with single and double U-tubes.

Pipes used for heating and cooling are placed in the borehole opened at a distance of approximately 50 to 200 meters. The hole inside is closed using materials such as bentonite and sand-bentonite (Özüdoğru, 2015). There are heat pumps in the existing system in the energy piles, and the heat pump helps to heat and cool the fluid inside the pipes faster by using some electrical energy (Loveridge, & Powrie, 2012). However, heat transfer occurs with heat conduction and convection, and temperature stresses arise. As a result, the carrying capacity of the energy piles changes. In addition, many factors affect heat transfer; such as water content, dry density, geometry and mineral structure of materials, the fluid used and tube shape (Figure 2.5). For example, increasing the thermal conductivity from 1.2 W/mK to 2.5 W/mK increases the heat transfer rate to 42% (Xie, & Qin, 2021).

Researches show that temperature change is very effective in energy piles. Because unconsidered changes may cause extra stresses and displacements in the piles

(Abdelaziz, 2013; Knellwolf et al., 2011). Thermal effects are also significant in accurately modeling energy piles' mechanical behavior (Özüdoğru, 2015).

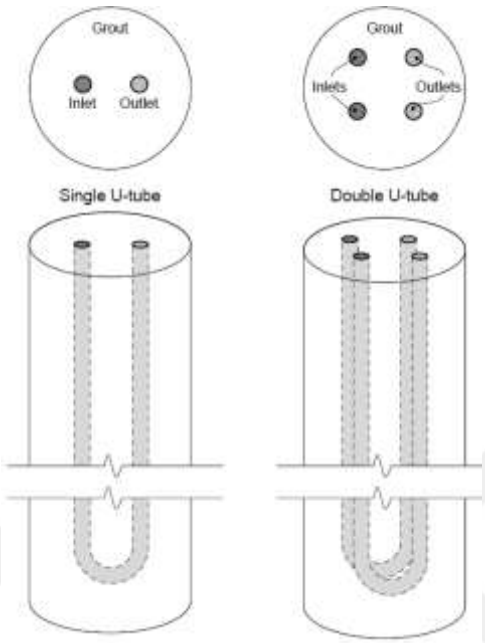


Figure 2.5 Geothermal heat exchangers with single and double U-tubes (Özüdoğru, 2015)

2.1.4 Buried Power Cables

The high temperature caused by buried power cables during their use affects the engineering properties of the soils. Since overheating the cables will cause them to fail to fulfill their duties, the cables must transmit the heat to the surrounding soil. For this reason, the properties of the cable used and the thermal properties of the surrounding material are of great importance (Anders, 1997). In previous studies, the recommended cable temperature was specified as 65 °C and also the limit temperature value was 90 °C (Ocłoń et al., 2015).

It is essential that the material used around the cables is homogeneous, stable and has moisture content. Because if the moisture content of the soil falls under a certain percentage, this causes the soil to dry out and the cables to overheat (Verschaffel-Drefke et al., 2021).

2.1.5 Geothermal Plants

Geothermal energy is the natural heat of the earth. As a result of the excavations, the first humans realized that the temperature increased as they went deeper. Regarding the thermal modeling of the Earth, Lubimova (1968) underlined that heat is released due to the decay of radioactive isotopes of uranium, thorium and potassium and that this is the reason for the continuity of heat (Dickson, & Fanelli, 2003).

The process of converting geothermal energy to electrical energy was made for the first time in 1904 and its development was achieved in the following years. It is said that the gradient in geothermal fields is approximately 2.5-3 °C/100 m. This leads to the determination of the temperature at the desired depths. For example, if the temperature is 15 °C, slightly below ground level, it can be estimated to be 65 °C at 2000 m (Dickson, & Fanelli, 2003).

Geothermal power plants can have two different cycles, steam and binary power cycles. In binary processes, the fluid generally has low enthalpy, and since it is a closed system, it has little or no environmental harm. However, with the developing technology, the temperature of the fluid used in these cycles can reach up to 200 °C. These high temperatures may also affect the surrounding soils on geothermal plants.

2.2 Temperature Effects on the Engineering Behavior of Soils

2.2.1 Temperature Effects on the Volume Deformation Behavior of the Soils

Many researchers investigated the variation of the volumetric deformation behavior of clayey soils with temperature (Table 2.2). There is a general aggrement on that high temperature may have depending on many factors such as; stress history, mineralogy, water content, temperature range, etc. It was observed that under high temperature contraction seen in normally consolidated clays while expansion is seen in overconsolidated clays (Bodas Freitas et al., 2013; Campanella, & Mitchell 1967; Baldi et al. 1988; Cekerevac, & Laloui 2004). It was reported that this effect can be reversed when temperature decreases. However, it is emphasized that this reversibility has a specific temperature range (Bodas Freitas et al., 2013). Researchers relate the contraction behavior with weakening existing bonds, increase in energy of soil grains,

expansion of soil grains, expansion of excess pore water pressure and reducing effective stress. Figure 2.6 is a schematic representation of volume deformation behavior of normally and over-consolidated clays.

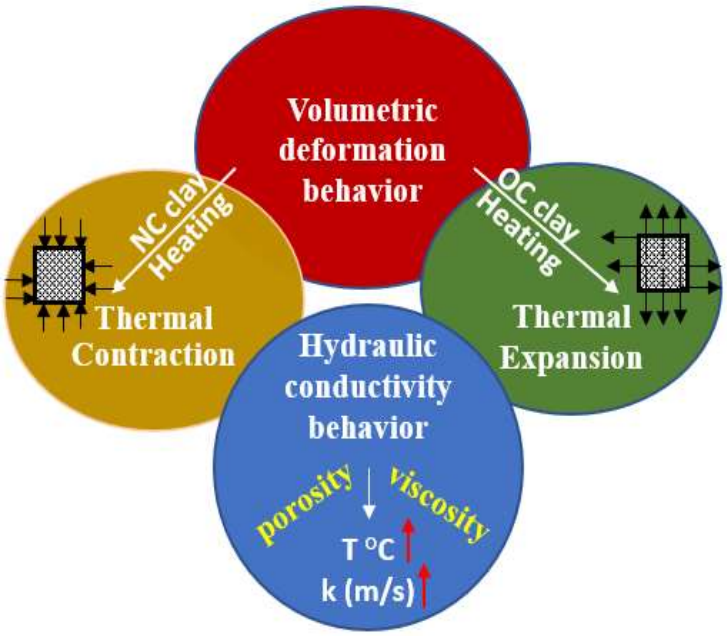


Figure 2.6 Schematic presentation of volumetric deformation and hydraulic conductivity behavior of soils under thermal effects (adopted from Zang, 1993a)

Table 2.2 Previous studies on the volumetric deformation behavior of temperature (Jarad, 2016)

No	Author	Soil	Soil characteristics	Method	Temperature range	Variation with temperature
1	Campanella & Mitchell (1968)	Illite	Remolded Saturated	Drained isotropic cell	24.7, 37.8, 51.4 °C	C_c is independent
2	Lingnau et al.(1996)	1:1 Mixture bentonite-sand	Compacted Saturated LL=230-250%, PI=200%	High pressure and temperature cell/drained	26, 65, and 100 °C	C_s & C_c are independent
3	Tanaka et al. (1997)	Illitic clays	Reconstituted Saturated LL=30%, PI=9%	Drained isotropic cell	28, 65, 100 °C	Non parallel normally consolidated lines
4	Delage et al. (2000, 2004)	Boom clay	PI=50%, Porosity=40%, Stiff clay, saturated	Drained triaxial	Between 20 and 100 °C	C_v & m_v not affected significantly
5	Sultan et al. (2002)	Boom clay	PI=50%, Porosity=40%, Stiff clay, saturated	Drained isotropic cell	23, 40, 70, and 100 °C	Compression curves converged towards the same limit.
6	Cekerevac & Laloui (2004) Laloui & Cekerevac (2003)	Kaolin clay	Remolded Saturated LL=40%, PL=24%	Drained triaxial apparatus	22, 90 °C	C_c is independent
7	Marques et al. (2004)	Sensitive clay from Quebec	Saturated PI= 41 to 49%	Drained oedometer test	between 10 and 50 °C	The slope of the compression curve in the over consolidated domain is not strongly affected
8	Abuel-Naga et al. (2005)	Bangkok clay	Natural, soft, LL=103%, PI=60%, Clay=69%, silt=28%, sand=3%	Drained modified oedometer	25 to 90 °C to 25 °C	C_v increases positively

Table 2.2 Continued

9	François et al. (2007)	Sandy silt	Remoulded Unsaturated Clay fraction = 8% Silty fraction = 72% PI = 8.7%	Isotropic cell	Between 22 to 80 ° C	Compressibility indices are quasiindependent of temperature.
10	Abuel-Naga et al. (2007a)	Bangkok clay	Saturated, natural soft Over-consolidated LL=103%, PI=60%, Clay=69%,silt=28%, sand=3%	Modified oedometer	25 to 90 °C	C_c is independent C_s in the lightly over-consolidated samples is increased positively
11	Tang et al. (2008a)	MX80 bentonite	Compacted, unsaturated LL=520% PL=46%	Triaxial apparatus	25 to 80 °C	The effect on the compressibility parameters was not significant
12	Cui et al. (2009)	Boom clay	Saturated LL = 59-76% PL=22-26% PI = 37-50%	Drained triaxial tests	25 °C - 70-80 °C	Volumetric strain rate coefficient increased with elevated temperature
13	Shariatmadari & Saeidijam (2011,2012)	Bentonite-sand mixture (1:1)	Compacted, saturated LL = 290%, PI = 255%	Drained oedometer	25 to 90 °C	a_v and C_c increased at elevated temperature
14	Tsutsumi & Tanaka (2012)	Kasaoka OsakaMa12 Louiseville	LL=62%, PL=36% LL=109%, PL=43% LL=71%, PL=22% Reconstituted, saturated	Drained CRS tests	10 -50 °C	C_s was independent of temperature C_c at 50 °C was smaller than that at 100 °C.

Towhata et al. (1993) stated that immediately after heating, shrinkage occurred in the soil and volume contraction occurred. It was revealed that the deformation occurs more than the amount of deformation at room temperature with the effect of heating. This situation is caused by the acceleration of the consolidation rate under heating or the deterioration of the hardness of the skeleton of the sample. Cekerevac and Laloui (2004) reported that the elastic limit of soil decreases with increase in temperature and this effect is related with the thermal effects on preconsolidation pressure. It is predicted that the amount of energy that soils have when exposed to high temperatures will increase; accordingly, the energy of soil grains will increase. Molecules with increased energy will become more active, further weakening existing bonds. As a result, the amount of compression in the soil will increase (Gupta et al., 1964; Jarad et al., 2016). Figure 2.7 shows the consolidation stress-void ratio relationship for samples at three different temperatures (first heated and then loaded). It was observed that as the temperature increased, the void ratio decreased and the compression amount increased. The result of these experiments revealed that C_c is independent of temperature (Campanella, & Mitchell, 1968).

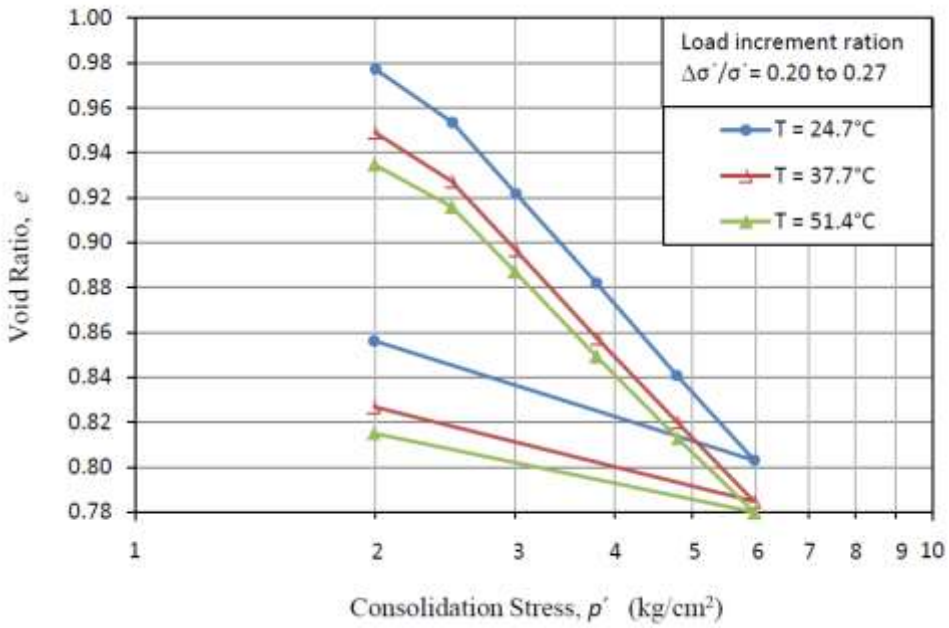


Figure 2.7 Consolidation stress and temperature relationship (Campanella, & Mitchell, 1968; El Tawati, 2010)

In previous studies, it was demonstrated that the heating-cooling cycle affects the volumetric change and behavior of the soil. Still, this effect is dependent on the stress history of the soil but independent of the applied stress level (Abuel-Naga et al., 2005).

Saix et al. (2000) observed contraction behavior in the soil with the effect of temperature in the experiments conducted under three different stresses (Saix et al., 2000; Bag and Rabbani, 2017). Similarly, Towhata et al. (1993) subjected MC clay and bentonite to thermo-mechanical experiments by heating them to 90 °C. According to the results of this study, contraction was seen in normally consolidated clays. Based on this behavior, it is emphasized that the skeletal structure of clay particles may deteriorate with the increase in temperature. The volumetric contraction was determined in the drained experiments carried out by Çekerevac and Laloui (2004) on normally consolidated Kaolin clay with a triaxial test instrument (22°-90 °C) at different temperatures (Çekerevac and Laloui, 2004; Jarad, 2016). Similar to the abovementioned research results, Delage et al. (2004) observed contraction behavior with the effect of temperature in experiments on the Boom clay. It was emphasized that the contraction may be related to the excess water in the soil coming out and being removed from its body, as it usually happens during consolidation (Delage et al., 2004; Jarad, 2016). Also, Abuel-Naga et al. (2005) exposed normally consolidated Bangkok clay to temperature cycling (25-90-25 °C). At the end of the test, it was observed that the normally consolidated clay behaved as if it was overconsolidated, depending on the cycling (Abuel-Naga et al., 2005; Jarad, 2016).

It is known that normally consolidated clays exhibit contraction behavior when left to heating and over-consolidated clays contract more than when heated. In addition, it was determined that over-consolidated clays expand in volume when heated and exhibit reversible behavior (Abuel-Naga et al., 2005). Abuel-Naga et al. (2005) examined the volumetric stress at different temperatures and determined that normally consolidated soils behaved as if they were overconsolidated at a limit temperature value. As a result, the volumetric behavior changed from contraction to expansion (Abuel-Naga et al., 2005). Ghabezloo, & Sulem (2010) emphasized that the pore pressure caused by temperature increases depends on many factors. Factors such as the relationship of compressibility to stress and inelastic volume changes are some of

these factors (Ghabezloo, & Sulem, 2010; Bai and Jiang, 2017). The temperature may have effects on the compressibility parameters as well. Fang and Daniels (2006) revealed that the compression index (C_c) increases with increasing temperature and the volume change amount is related with how much the temperature changes (Fang, & Daniels, 2006; Bag, & Rabbani, 2017).

Expansion behavior is observed in excessively consolidated clays with an increase in temperature. The basis of this behavior is the expansion of excess pore water pressure that occurs with heating. In other words, expansion is the expansion of soil grains (Delage et al., 2000). It is also stated that the expansion behavior increases as the excessive consolidation rate increases. Accordingly, volumetric strain is also affected from the thermal point of view. In addition to these behaviors, the softening in the structure of the clay due to expansion and decrease in the preconsolidation pressure have also been revealed as a result of these studies (Jarad, 2016).

The swelling pressure of bentonite used in nuclear waste landfills is very important parameter in terms of stability of the canister. The swelling pressure must be at a certain level so that the canister, which is the heat source, does not sink into the bentonite used as a buffer, and in order to prevent/close the gaps between the bedrock and the bentonite, a possible leak. In addition, the decrease in swelling pressure causes the shear strength of the soil to decrease. In the case of swelling pressure up to 0.1 MPa, the amount of sinking will be smaller than 2 cm (Sellin, & Leupin, 2013). Former studies revealed that temperature dramatically affects the swelling behavior of bentonite (Xiang et al., 2020). Xiang et al. (2020) reported in their research on GMZ01 bentonite that swelling deformation value increases depending on the initial dry density and decrease with the effect of vertical stress under high temperature. The Gouy-Chapman equation expresses the volume change of bentonites. This model is also called the diffuse double-layer (DDL) model, and it was reported in the previous studies that the thickness of DDLs increases with increasing temperature. Therefore, increasing temperature promote the swelling of clays (Xiang et al., 2020; Ye et al., 2013; Cui et al., 2018). Ye et al. (2013) measured the swelling pressure of bentonite for two different temperature values (20 and 40 °C). Swelling pressure values were determined as 3.02 and 3.41 MPa, respectively. It was revealed that with the increase

in temperature, the swelling pressure increased and reached the peak point. On the other hand, Jarad (2016) revealed that the relationship between swelling index and temperature is not too strong, it affects negligible extents. Campanella and Mitchell (1968) also stated that the swelling index of illitic clays is not dependent on temperature and the rate of influence is minimal.

2.2.2 Temperature Effects on the Shear Strength Behavior of the Soils

The shear strength of the soils may change depending on the temperature. Many researchers have examined the effect of temperature on shear strength, and many results are still controversial. Generally, increase in shear strength is reported as temperature increases. However, some studies were reported decrease in shear strength depending on temperature increase. According to the unconsolidated-undrained (UU) and consolidated-undrained (CU) tests at 20, 50, 80 and 110 °C for a Boom clay, a significant decrease in strength was determined when the temperature increased (De Bruyn and Thimus, 1996). Similarly, Noble and Demirel (1969) reported that since the density and viscosity of the water are affected by temperature, a decrease in the shear strength of clay and silt under 60 °C was investigated.

Moritz (1995) observed that the shear strength decreased as the temperature increased in the study which Swedish clay was used. The reason for this decrease was attributed to the increase in pore water pressure. It was also revealed that the residual stresses involved in shear behavior are not dependent on temperature. On the contrary, Yavari et al. (2016) determined that the shear strength under different temperatures is independent of temperature in line with the results obtained from the direct shear tests. Maghsoodi et al. (2020) reported that both the single and critical shear stresses increased when temperature was increased from 22 to 60 °C as a result of the direct shear experiments performed using kaolin, but the temperature had no effect on the shear strength when the same experiment was performed with sand sample. It has been revealed by some researchers that the internal friction angle, which is one of the parameters of the soil is affected very little by the temperature (Moritz, 1995; Cekerevac, & Laloui, 2004; Maghsoodi et al., 2020). Table 2.3 summarizes some

studies from literature on the shear strength behavior fo soils under different temperatures.

Table 2.3 Previous studies on the shear strength behavior of temperature (adapted from Kuntiwattanakul et al., 1995)

No	Authors	Type of Heating	Type of test	Strength after heating
1	Mitchell (1964)	Drained	Undrained	Decrease
2	Murayama (1969)	Undrained	Undrained	Decrease
3	Sherif and Burrous (1969)	Undrained	Undrained	Decrease
4	Hueckel and Baldi (1990)	Drained	Drained	Decrease
5	Laguros (1969)	Drained	Undrained	Increase
6	Houston et al. (1985)	Drained	Undrained	Increase
7	Nobel and Demirel (1969)	Drained	Undrained	Increase
8	Kuntiwattanakul (1995)	Drained	Undrained	Increase
9	De Beruyn and Thimus (1996)	Undrained and Drained	Undrained and Undrained	Decrease and Decrease
10	Maghsoodi et al. (2020)	Undrained	Undrained	Increase

The triaxial tests on the Pontida silty clay showed that shear strength decreased when the temperature increased from 18 to 115 °C (Hueckel, & Baldi 1990). In the opposite direction, Cekerevac, & Laloui (2004) investigated increase in the shear strength parameters of kaolin clay by increasing the temperature from 22 to 90 °C. It was reported that the increase in shear strength at high temperatures caused by an increase in ductility. Hueckel, & Baldi (1990) attributed the decrease in the shear strength with the decline in the over-consolidation ratio or increase in the void ratio during heating of the over-consolidated soil.

The study on the Fontainebleau sand and kaolin clay, the direct shear test was performed under constant average load (CNL) at temperatures of 5, 22 and 60 °C in a study of Maghsoodi et al. (2019). According to the results of this study, it was observed that the shear strength increased with the increase in temperature for normally consolidated clay. It was emphasized that this increase is about the thermal contraction behavior of normally consolidated clays during heating. In addition, at these temperatures, the internal friction angle increased slightly from 14.4 to 15.3° with the increase in temperature, while the cohesion values showed an increasing trend as 11, 17 and 23 kPa, respectively. It was determined that the cohesion value increased due to the increase in the hardness of the soil with the effect of heating (Maghsoodi et al., 2019).

2.2.3 Temperature Effects on the Hydraulic Conductivity Behavior of the Soils

The high temperature and temperature cycles may affect the hydraulic conductivity behavior of soils. Change in hydraulic conductivity due to high temperature is a very important concern especially for nuclear waste repositories. Many studies have been conducted on the variation of hydraulic conductivity of soils with temperature. In general, the results have been shown that the hydraulic conductivity increases as the temperature increases (Sultan, 1997; Delage et al., 2000; Chen et al.,2014). Increase in hydraulic conductivity is related with changes in the water viscosity mostly (Cho et al. 1999). Table 2.4 summarizes some reaserches on the hydraulic conductivity behavior under different temperatures.

Mingarro et al. (1989) observed that the hydraulic conductivity parameter of the bentonite and granite increased to one degree of magnitude by increasing the temperature from 20 to 100 °C. This increase was associated with an increase in porosity due to the degeneration of water adsorbed in the clay pore wall (Pusch, 1980). Houston, & Lin (1987) investigated that the increase in hydraulic conductivity was smaller than the value expected from the change in the water viscosity due to the temperature increase on the tests using illite. It was also reported that the soil type is essential in the effect of temperature on hydraulic conductivity and that the soil becomes denser due to thermal consolidation. Similarly, Towhata et al. (1993) stated that the hydraulic conductivity increase with the increase in temperature is higher than

that obtained by calculation, and this is due to the effects on the viscosity of the water. Villar, & Lloret (2004) reported similar results in their study using bentonite samples.

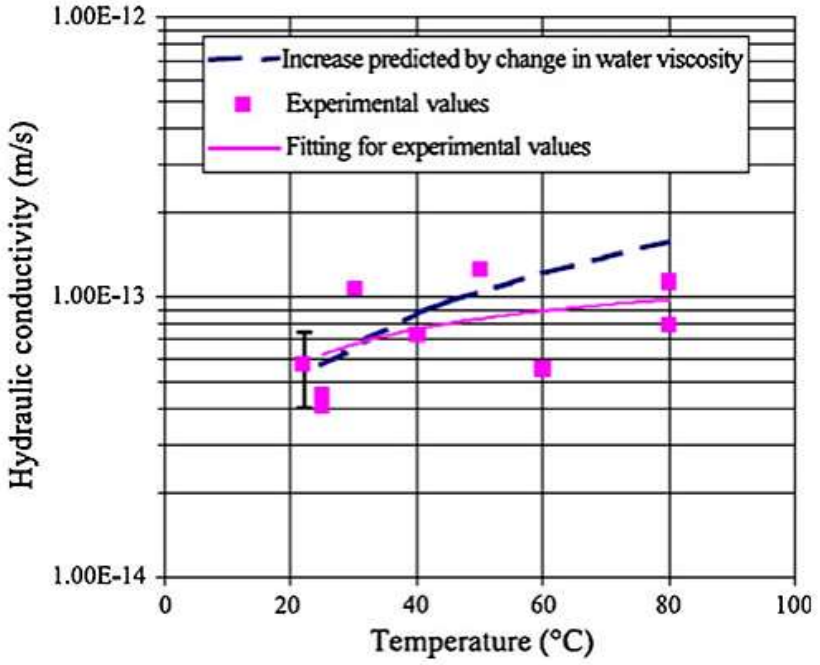


Figure 2.8 Comparison of the calculated hydraulic conductivity with the measured ones for the FEBEX bentonite at a dry density of 1.38 Mg/m^3 (Villar, & Lloret 2004)

As can be seen from Figure 2.8 the estimated hydraulic conductivity value from change in water viscosity depending on temperature was slightly higher than the measured hydraulic conductivity value from the experiment. It was emphasized that the increase in hydraulic condcutivity is not only due to viscosity (Harrington et al., 2014; Villar, & Go´mez-Espina, 2009). The hydraulic conductivity tests with Febex bentonite (1.5 -1.7 m^3/mg) showed that the hydraulic conductivity increased with temperature from the samples prepared at different dry densities (Villar, & Go'mez-Espina, 2009). Previous studies demonstrated that soil-water interaction at the microstructural level is also effective in this behavior (Towhata et al., 1993; Romero et al., 2001; Villar, & Lloret, 2004).

Table 2.4 Previous studies on the hydraulic conductivity behavior depending on temperature (Jarad, 2016)

No	Author	Soil	Soil characteristics	Method	Temperature	k variation with T
1	Subba et al. (1953)	A remoulded alluvial soil	Passing through 1 mm sieve.	Constant head	35 to 1000 °C	35 to 60 °C and above 650 °C: Decrease 60 to 650 ºC: Increase
2	Morin & Silva (1984)	Illite Smectite Siliceous ooze Calcareous ooze	LL: 95%; PL:43% LL: 270%; PL:91% LL: 254%; PL:134% LL: 132%; PL:73%	Rigid ring cell	Between 22 and 220 °C	Increase
3	Cho et al. (1999)	Ca-bentonite	Montmorillonite (70%), feldspar (29%), quartz (1%)	Special apparatus	Between 20 and 80 °C	Increase
4	Delage et al. (2000)	Boom clay	PI=50%, porosity=40%, Stiff clay	Triaxial	Between 20 and 100 °C	Increase
5	Cho et al. (2000)	Ca-bentonite	Montmorillonite (70%), feldspar (29%), quartz (1%)	Special apparatus	Between 20 and 150 °C	Increase
6	Romero et al. (2001)	Unsaturated Boom clay	20%-30% kaolinite, 20%-30% illite and 10%-20% smectite, LL=56%,PL=29%	Oedometer	22, 40, 60, and 80 °C	Increase

Table 2.4 Continued

7	Villar & Lloret (2004)	FEBEX bentonite	LL = 98-106 % Montmorillonite (90%)	Oedometer	Between 20 and 80 °C	Increase
8	Bouazza et al. (2008)	Geosynthetic clay	Sodium/powder bentonite	Modified Rowe cell	Between 20 and 60 °C	Increase
9	Delage et al. (2009)	Boom clay	PI=50%, porosity=40%, stiff clay	Triaxial	Between 20 and 90 °C	Increase
10	Villar & Lloret (2010)	FEBEX bentonite	LL = 98-106 % Montmorillonite (90%)	Oedometer	Between 20 and 90 °C	Increase
11	Cho W. et al (2011)	Kyungju Ca-bentonite	Montmorillonite (70%), feldspar (29%), quartz (1%)	Cylindrical cell	20 to 150 ºC	Increase
12	Tsutsumi & Tanaka (2012)	Kasaoka OsakaMa12 Louiseville	LL=62%, PL=36% LL=109%, PL=43% LL=71%, PL=22%	Modified triaxial	Between 10 and 50 ºC	Increase

Figure 2.9 shows change in the hydraulic conductivity value of bentonite sample with temperature. The results have shown that the k changes depending on both viscosity and density (Lide, 1995; Villar et al., 2010). Park et al. (2021) reported that the hydraulic conductivity increased with temperature and decreased as the density increased. The cooling process was also applied in this study and reported that the microchannels contract due to increase in swelling pressure. As a result of this, a slight decrease in hydraulic conductivity was observed (Park et al., 2021).

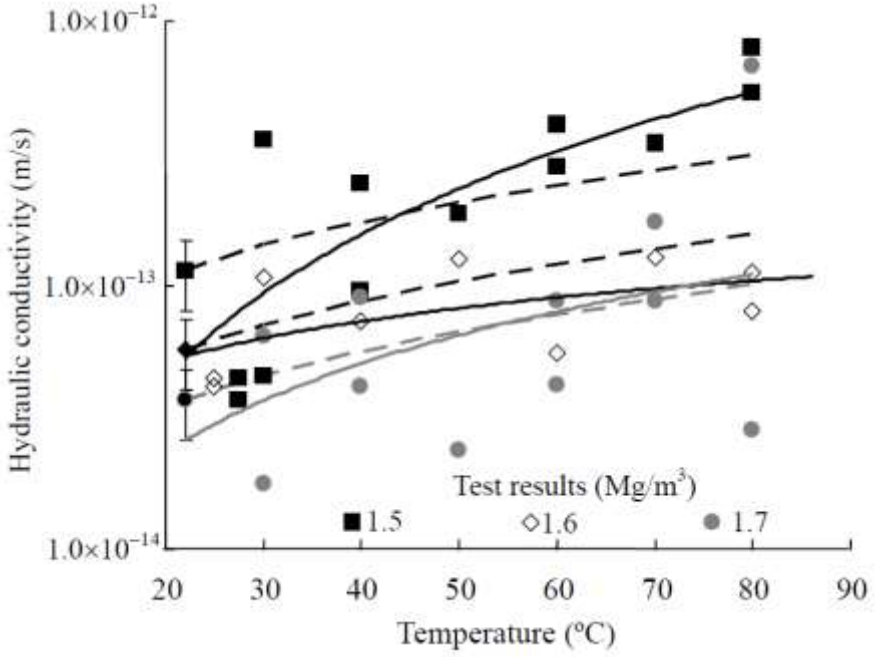


Figure 2.9 Hydraulic conductivity vs. temperature for saturated samples compacted to different nominal dry densities (Villar et al., 2010)

The hydraulic conductivity value can be calculated by help of the emprical equations. For example, an equation showing the relationship between saturated hydraulic conductivity k_s and temperature T were used by Ye et al. (2013). The Equation 2.1 gives the calculated hydraulic conductivity value, while Equation 2.2 shows the temperature dependent viscosity change. In Equation 2.3 k_m is the intrinsic permeability value obtained from the measured hydraulic conductivity values.

$$k_s = k_{in}\rho_w g / \eta(T) \tag{2.1}$$

$$\eta(T) = 0.0002601 + 0.001517\exp[-0.034688x(T - 273)] \tag{2.2}$$

$$k_s = \frac{k_m \, x \, \rho_w g}{0.0002601 + 0.001517 \exp[-0.034688 x (T - 273)]} \quad (2.3)$$

Where $\eta(T)$: is defined as the viscosity of water depending on temperature, k_{in}: intrinsic permeability, g: gravitational acceleration, T: absolute temperature in Kelvin and ρ_w : density of water.

It was also reported that, the predicted saturated hydraulic conductivity value of GMZ01 bentonite was different from the measured one. For that reason, a model which considers both water viscosity and cross area of porous channels was developed for better prediction (Ye et al., 2013). Furthermore, Ye et al. (2013) investigated that heating-cooling cycles have insignificant effect on the saturated hydraulic conductivity.

2.2.4 Thermal Conductivity Behavior of the Soils

Energy geo-structures cause changes in temperatures in the surrounding soils. The thermal conductivity of the soils is one of the most important property for the performance of energy geo-structures. Thermal conductivity represents the heat flow in the soil or any material (Leila, & Nacerddine, 2013). The greater the thermal conductivity value of the soil, the faster conduction of heat. For example, in nuclear waste storage repositories, the temperature values may reach more than 100 °C and the conduction of this temperature by being removed from the canister element, where the nuclear wastes are stored, is directly related to the thermal conductivity of the buffer material (Sellin, & Leupin, 2013). For buried power cables, the dissipation of excess heat on the cables by surrounding soils depends on the thermal conductivity of the soil. In energy piles, the efficiency of the heat energy to be used for heating or cooling the buildings is directly related to the thermal conductivity of the soil surrounding the piles (Wagner, & Clauser, 2005; Özüdoğru, 2015). The correct determination of thermal conductivity is also very important in terms of cost, because this parameter and some additional parameters determine the length of the pipes to be used (Marcotte and Pasquier, 2008; Özüdoğru, 2015).

Thermal conductivity varies depending on many factors, such as porosity, temperature, mineral composition, particle size, dry density, water content and degree of saturation (Nakshabandi, & Kohnke, 1965). The water content is one of the most critical factor in the thermal conductivity of soils (Xu et al., 2020). Since the thermal conductivity of water is higher than that of air, it is expected that soils with high water content will have a high thermal conductivity (Akash et al., 2005). Farouki (1981) determined that the thermal conductivity of free water is about 0.57 $Wm^{-1}K^{-1}$ and the thermal conductivity of ice is about 2.2 $Wm^{-1}K^{-1}$ and explained this situation as follows: If the moisture content is high, more ice is formed at the lower temperature of the sample. The opposite is true at high temperatures. Xu et al. (2020) observed that the thermal conductivity of soils decreases at positive temperatures due to the decrease in the thermal conductivity of water. When it reduces to negative temperatures, the thermal conductivity increases as expected because the volumetric ice amount inside the soil increases.

Porosity is also one of the critical factor affecting thermal conductivity, especially in dry soils. In low porosity soils, the thermal conductivity is measured as high since the particles will contact each other more. In addition, the thermal conductivity is more higher in soils formed by round-shaped grains since the contact surface is more than in angular-shaped grains (Yun, & Santamarina, 2008).

2.3 Temperature Resistant Materials

Within the scope of this doctoral thesis, the additives namely; pumice, perlite and fiberglass were choosen because of their superior properties under high temperatures.

2.3.1 Pumice

Pumice is an amorphous aluminum silicate formed due to volcanic activities. Gas outflow forms pumice's porous structure from sudden cooling during pumice formation (Figure 2.10) (Sarıiz, & Nuhoğlu 1992). The chemical structure of pumice includes SiO_2, Al_2O_3, Fe_2O_3, CaO, MgO, Na_2O and K_2O. Aluminum oxide in the chemical form of pumice is known to provide high heat resistance (Depci et al. 2012).



Figure 2.10 Physical appearance of pumice (Istockphoto , 2010)

Due to its high heat resistance, it can be used to improve the engineering properties of soils under high temperatures. In addition, since the gaps in the pumice's porous structure are independent, it is a material with low hydraulic conductivity (Kılınç Aksay, 2005).

The pumice does not undergo any volume changes below 760 °C and does not enter the chemical reaction with any acid other than hydrofluoric acid. The dissolution rate of pumice in an acid is a maximum of 2.9% (Gündüz et al. 1998; Sezgin, Davraz, & Gündüz 2005). Therefore, the pumice samples have a glassy structure. When they are heated up to 850 °C, no thermal reactions occurred in their form and the pumice does not undergo a structural deterioration (Kılınç Aksay, 2005).

2.3.2 Perlite

Perlite is used in many sectors, such as construction, food, agriculture, medicine, chemistry and metallurgy. Expanded perlite is produced from raw perlite. Its structure is an amorphous aluminosilicate of volcanic origin (Figure 2.11). It has a highly porous structure, low density, low cost and good thermal reliability (Karaman et al. 2011). In the expansion process, raw perlite powder consisting of large particles is heated to about 1150 K (876.9 °C) and the material is softened. With this softening, the water in the structure of the perlite evaporates to form many pores. The pore diameters are generally from 10 μm to about 100 μm. The general porosity of the expanded perlite powder varies between 84% and 98% (Beikircher, & Demharter 2013; Allameh-Haery et al. 2017).



Figure 2.11 Physical appearance of perlite (Worldperlite, 2013)

Thanks to its thermal insulation properties, perlite can be used as an additive material in the buffer materials for energy geostructures. The chemical structure of perlite contains compounds such as SiO_2, Al_2O_3, Fe_2O_3, CaO, Na_2O, K_2O, MgO (Mekaddem et al., 2019). Expanded perlite is widely used in construction as heat and sound insulation material.

2.3.3 Fiberglass

Fiberglass is a material obtained by combining glass fibers. It has two different geometries, as short and long. Fiberglass is frequently used in heat and sound insulation, ship and submarine hulls, automobile engine compartments, ovens, air conditioning units, acoustic wall and ceiling panels and areas to be used for architectural purposes (Figure 2.12). For the formation of fiberglass, some raw materials and chemicals to be added to these raw materials. The main components of fiberglass are silica sand, limestone and soda ash. In addition to these, it also contains calcined alumina (Al_2O_3), borax ($Na_2[B_4O_5(OH)_4]\cdot 8H_2O$), feldspar, nepheline syenite, magnesite ($MgCO_3$) and kaolin clay ($Al_2H_4O_9Si_2$). For the formation of glass, silica sand, soda ash and limestone or waste glass are used (Maher et al., 1994).

Previous studies have shown that reinforcing soils using natural or synthetic fibers increases the strength of soil (Maher et al., 1994). Gray, & Ohashi (1983) reported that fibers increased the peak shear strength of soils under static loads in their study which was about the fiber reinforcement on cohesionless soils. It was also observed that the

fibers positively affect the liquefaction resistance of sands exposed to low and high-amplitude dynamic loads during earthquakes (Maher, & Woods 1990; Noorany, & Uzdavines 1989).



Figure 2.12 Physical appearance of fiberglass (Lbifiberglass, 2022)

CHAPTER 3
MATERIAL CHARACTERIZATION AND EXPERIMENTAL METHODS

3.1 Material Characterization

In the scope of this doctoral thesis, the compaction, consolidation, direct shear, and hydraulic conductivity tests on the pumice, perlite and fiberglass added sand-bentonite mixtures were performed. The pumice and perlite samples were supplied from Pomza Export Company. The fiberglass additive was gathered from Dost Chemistry Company. The bentonite sample was Na-bentonite and gathered from Eczacıbaşı Esan Mining Company. Sand and bentonite samples were dried at 105 °C for 24 hours before being used in the experiments. Pumice, perlite and fiberglass were used without drying. However, the initial water content of the pumice (2-5%) was determined at the beginning of each test and taken into account while making the calculations. Perlite was used without drying and the natural water content content was insignificant (~1-2%). The physico-chemical properties of the materials are given in Table 3.1.

Table 3.1 The physico-chemical properties of the materials

Property	**Sample**				
	Bentonite	**Sand**	**Pumice**	**Perlite**	**Fiberglass**
Specific gravity	2.70	2.63	2.50	1.50	2.60
Liquid limit (%)	476.0	-	37.1	375.0	-
Plastic limit (%)	70.10	-	NP	NP	-
pH	9.50	-	8.86	8.96	-

3.1.1 Sand-Bentonite Mixtures

According to the sieve analysis, 20.7% of the sand is fine material. The sand was sieved through No.6 and used in the mixtures. Figure 3.1 shows the sand and bentonite samples. The bentonite sample was passed through the No.200 sieve. The grain size distributions of bentonite and sand samples are given in Figure 3.2. The clay content of bentonite was 79%.



Figure 3.1 Sand and bentonite samples

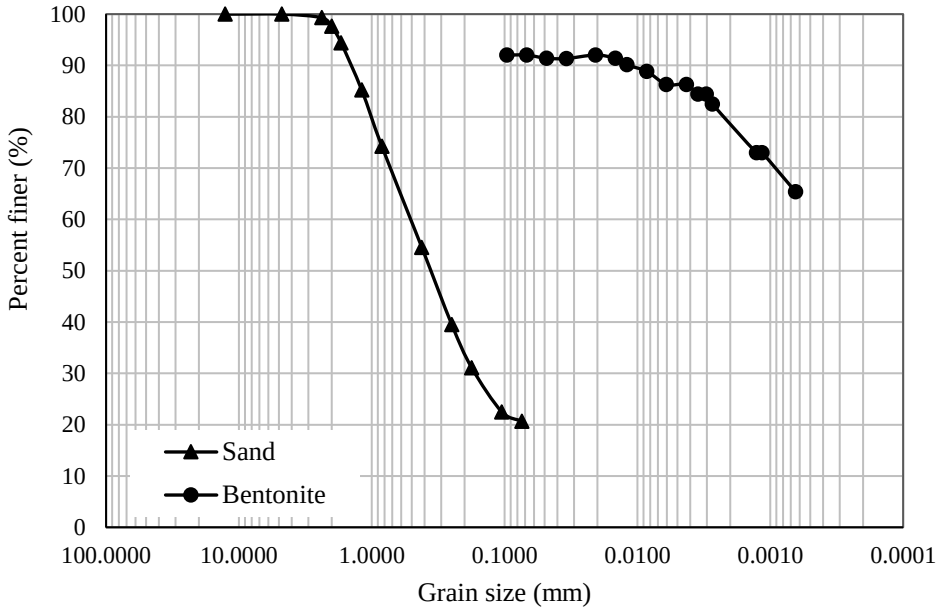


Figure 3.2 Grain size distribution curves of sand and bentonite samples

The X-Ray diffraction (XRD) analyses were performed in the focusing geometry from 0° to 89°, with a scanning speed at 0.1° 2θ/s and radiation at 60 kV, 5-60 mA on Thermo Scientific ARL X'TRA X-Ray diffraction equipment. The XRD analysis showed that the bentonite sample contains montmorillonite, quartz and illite minerals (Figure 3.3).

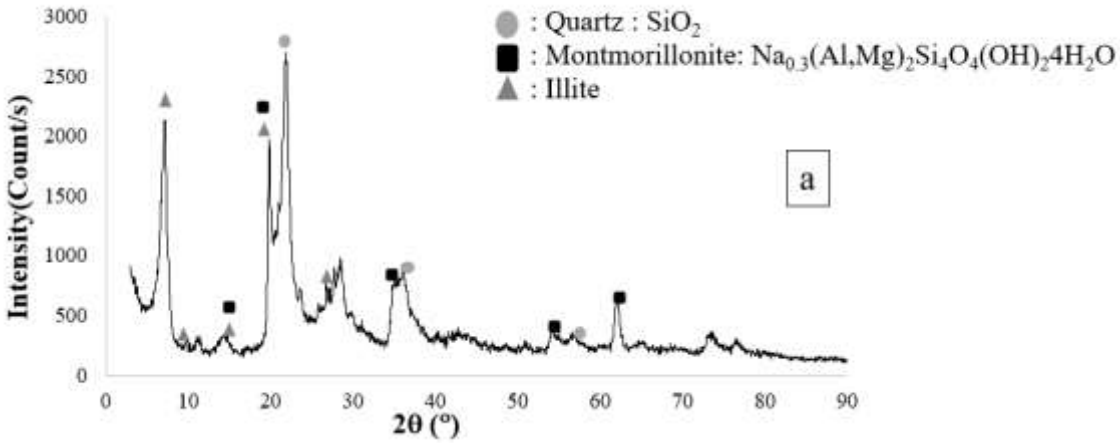


Figure 3.3 The X-Ray diffraction analysis (XRD) result of the bentonite

The sand-bentonite mixtures were prepared in three different bentonite ratios of 10%, 20% and 30%. These mixtures are referred as 10B-90S, 20B-80S, and 30B-70S, respectively.

3.1.2 Pumice

Pumice was used as it is (without drying). However, the initial water content of the pumice (2-5%) was determined at the beginning of each test and taken into account while making the calculations. (Figure 3.4). The grain size distribution of pumice is given in Figure 3.5.



Figure 3.4 Pumice sample

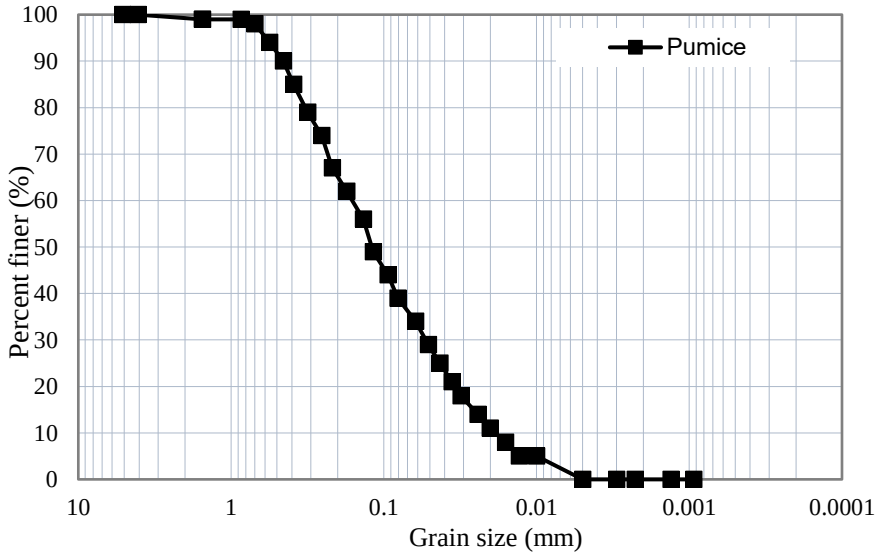


Figure 3.5 Grain size distribution curve of pumice

The XRD analysis result of pumice sample is given in Figure 3.6. According to the XRD results, the calcium silicate and sodium calcium aluminum silicate were observed in the pumice sample.

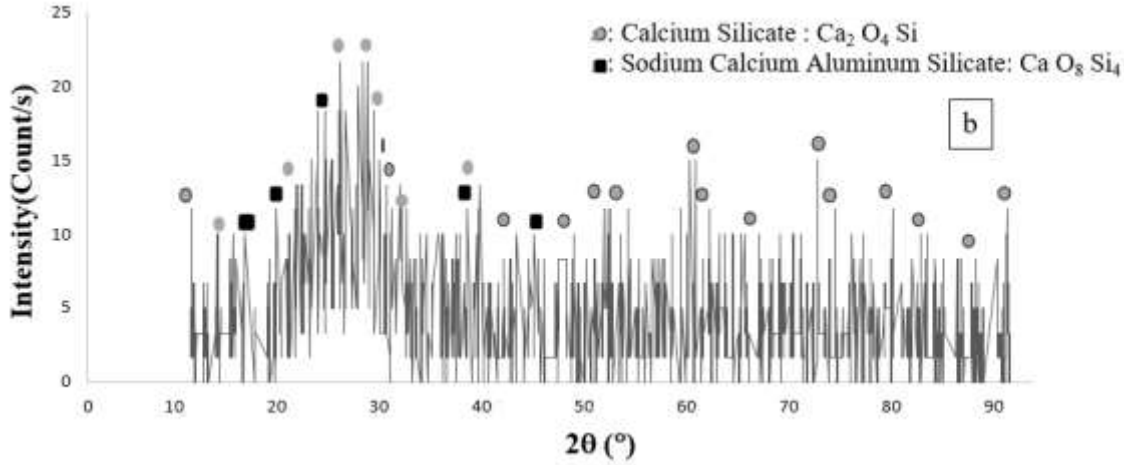


Figure 3.6 The X-Ray diffraction analysis (XRD) of the pumice sample

3.1.3 Perlite

Perlite was used without drying and the natural water content was insignificant (~1-2%). The mixtures were prepared by adding perlite to sand-bentonite mixtures in two different perlite ratios of 10% and 20%. Figure 3.8 shows the grain size distribution curve of perlite.



Figure 3.7 Perlite sample

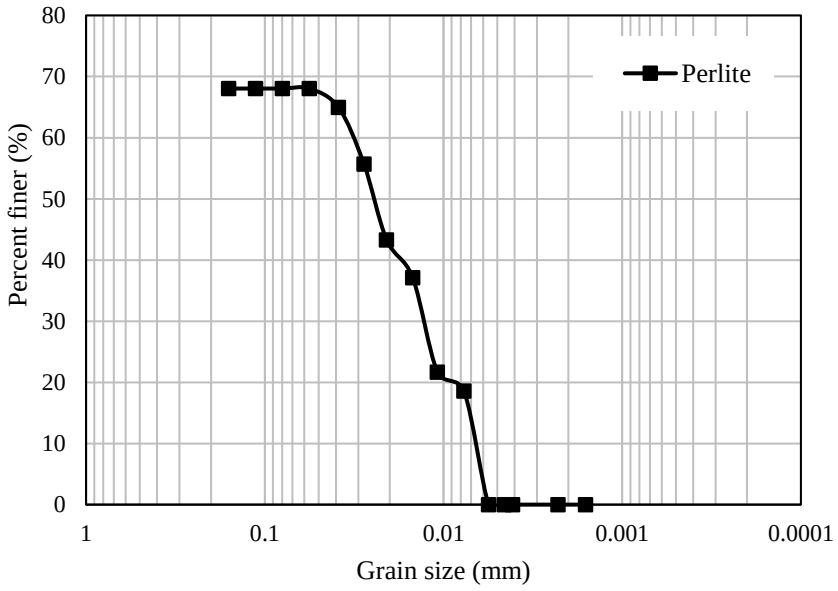


Figure 3.8 Grain size distribution curve of perlite

The XRD analysis result of perlite sample is given in Figure 3.9. The result showed that the perlite sample contains the aluminum oxide, iron oxide, calcium magnesium aluminum oxide, and silicon dioxide.

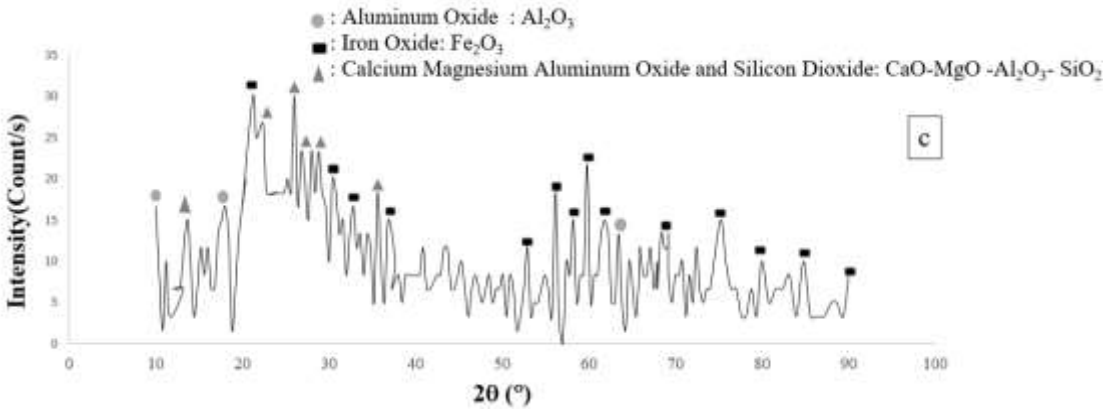


Figure 3.9 The X-Ray diffraction analysis (XRD) of the perlite

3.1.4 Fiberglass

The fiberglass sample was supplied from Dost Kimya Company. Two samples were gathered one of them was 3 mm and the other was 6 mm long. In the tests 3 mm fiberglass was used, however in order to compare the length effect on the shear strength parameters 6 mm fiberglass sample was also used. The technical properties of the fiberglass are given in Table 3.2.

Table 3.2 Technical properties* of fiberglass

Technical Properties	**SI**
Tensile strength	3400 Mpa
Modulus of elasticity	77 Gpa
Temperature limits	-60 °C + 650 °C
Melting temperature	1120 °C
Specific gravity	2.60
Diameter	13 µ
Length	3-6 mm

*Material sheet data

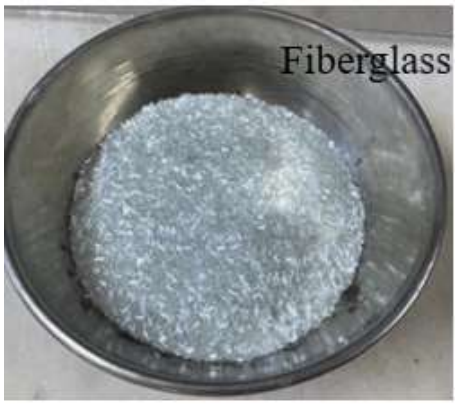
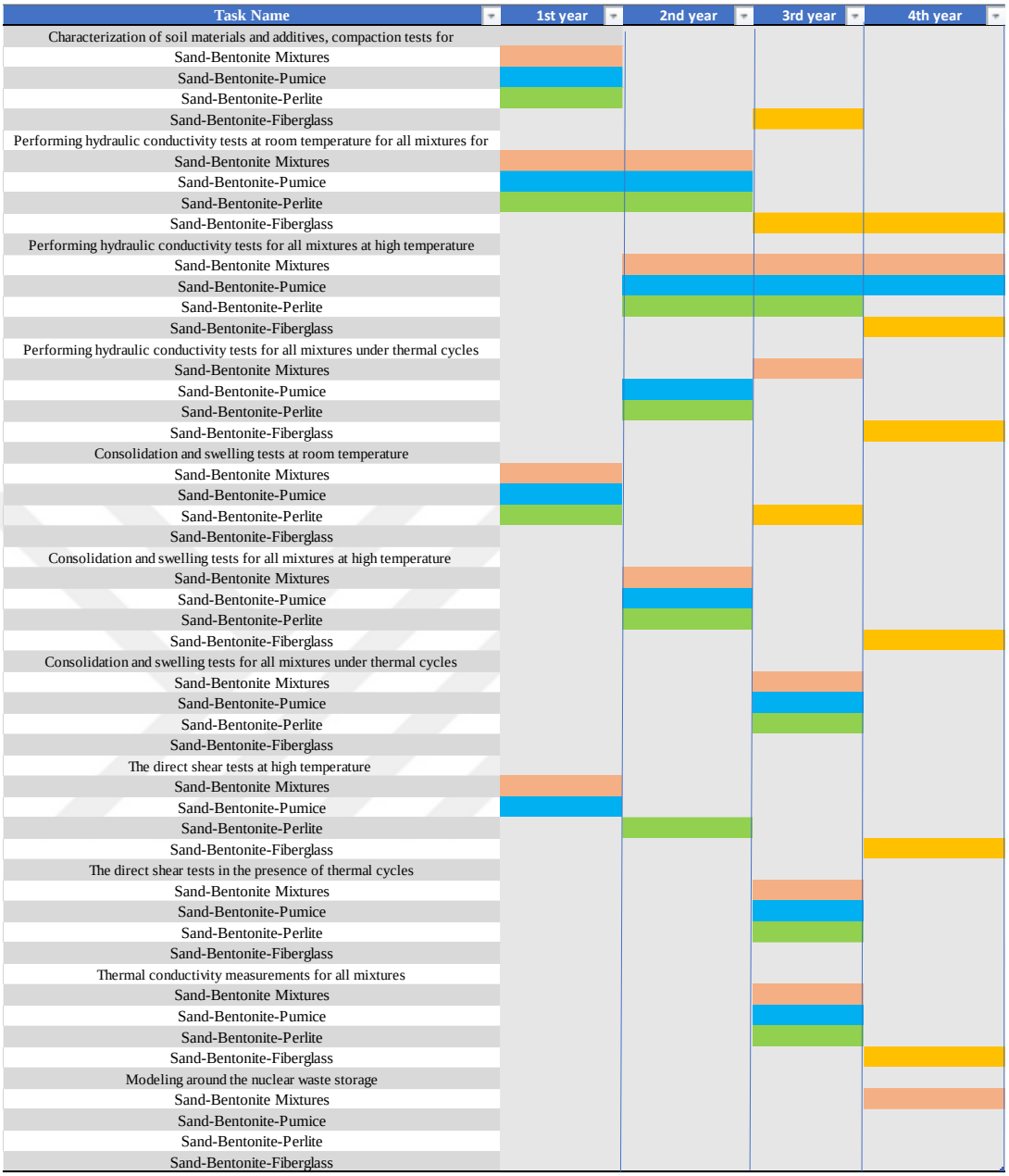


Figure 3.10 Fiberglass sample

3.2 Methods

Within the scope of this study, compaction, oedometer, direct shear, hydraulic conductivity and thermal conductivity tests of pumice, perlite and fiberglass added sand-bentonite mixtures were conducted. Table 3.3 shows the Gantt chart of the Ph.D. thesis. In the first year, the tests to determine the engineering index properties of the materials, compaction tests, consolidation and direct shear tests under room temperature were performed. In the second year, hydraulic conductivity tests of pumice and perlite added sand-bentonite mixtures were started, consolidation and direct shear tests were conducted under high temperature. Experiments were continued under thermal cycles and thermal conductivity measurements were done in the third year. In the fourth year, all tests of fiberglass added sand-bentonite mixtures were started and completed. Modeling analyses were performed in the fourth year.

Table 3.3 The Gantt chart of the Ph.D Thesis



3.2.1 Determination of the Engineering Index Properties of the Materials

Grain size distribution curves of all materials used in the experiments were determined according to ASTM: D422-63 (2007) with the help of wet and dry sieve analyses and hydrometer tests.

The liquid and plastic limit values of the samples were determined according to ASTM: D4318-17e1. While the fall cone test method was used to determine the liquid

limit values of pumice and perlite, the Casagrande test method was performed for bentonite. Specific gravity tests were performed as defined in ASTM: D854-14 (2014). Figure 3.11 shows the photos of the specific gravity and hydrometer tests.

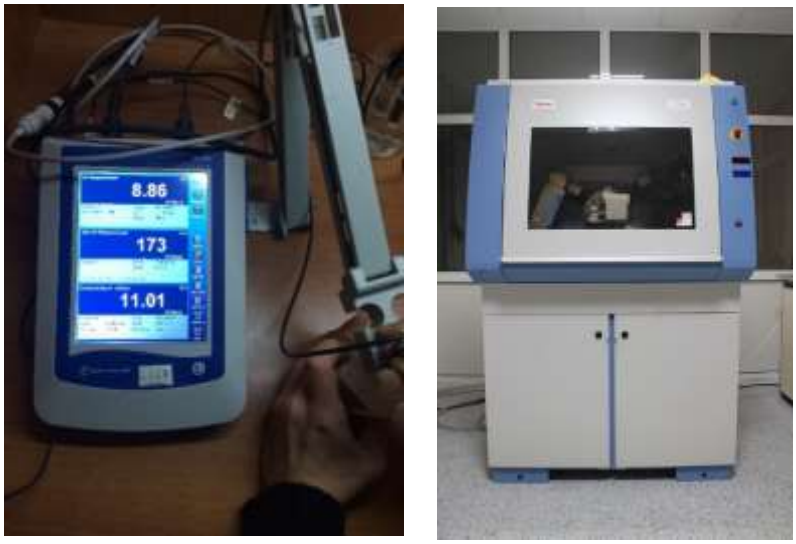


Figure 3.11 Specific gravity and hydrometer tests

The pH values of bentonite, pumice and perlite were measured according to ASTM: D4972-18 (2018). In the tests, bentonite was mixed by adding 50 g of deionized water to 10 g bentonite at a ratio of 1:5. Pumice and perlite were prepared in a ratio of 1:1 (10 g pumice/perlite - 10 g deionized water). After the mixtures were placed in the rotational shaker, they were kept there for about one hour. At the end of this period, after calibration of the pH meter, measurements were done (Figure 3.12a).

The X-ray diffraction (XRD) analyses were performed in the focusing geometry from 0° to 89°, with a scanning speed at 0.1° 2 θ /s and radiation at 60 kV, 5–60 mA on Thermo Scientific ARL X'TRA X-Ray diffraction equipment (Figure 3.12b) for pumice and perlite samples.

Also, Rigaku D/Max-2200/PC X-ray diffractometer device was used for the bentonite sample. The tests were performed on the dry and powdered form of the samples.



(a) (b)

Figure 3.12 Devices for pH measurement and XRD analysis a) pHmeter, b) Thermo Scientific ARL X'TRA device

3.2.2 Preparation of the Mixtures

The samples were prepared by adding 10% and 20% pumice or perlite to 10% bentonite-90% sand (10B-90S) and 20% bentonite-80%sand (20B-80S) mixtures. The 10% and 20% of the total dry weight were weighted as pumice or perlite. The remaining weight was sand-bentonite mixture. The contents were determined based on the dry weight of the samples. For fiberglass experiments 30% bentonite-70% sand (30B-70S) mixtures were used.

Table 3.4 Abbreviated naming of the mixtures used in the tests

	Samples		
	10%Bentonite	**20%Bentonite**	**30%Bentonite**
Pumice	9B-81S-10PU 8B-72S-20PU	18B-72S-10PU 16B-64S-20PU	-
Perlite	9B-81S-10PE 8B-72S-20PE	18B-72S-10PE 16B-64S-20PE	-
Fiberglass	-	-	30B-70S-0.5FG (29.85B-69.65S-0.5FG) 30B-70S-1FG (29.7B-69.3S-1FG)

While preparing the mixtures with fiberglass additives, 1% or 0.5% of the total dry weight of the mixture was weighed as fiberglass. The 30% of the remaining amount was determined as bentonite and the remaining amount was sand. The samples were

abbreviated as; bentonite "B," sand "S," pumice "PU," perlite "PE," and fiberglass "FG." For example, the mixture of 18B-72S-10PE contains 18% bentonite, 72% sand, and 10% perlite. The mixtures with their abbreviations are given in Table 3.4.

3.2.3 Compaction Tests

The maximum dry weight and optimum water content of the samples were determined by compaction tests. For the compaction tests, Standard Proctor Test was performed according to ASTM D698-12 (2012). The prepared samples were compacted by applying two layers in total and 43 drops to each layer. The applied energy was equal to the Standard Proctor energy (Figure 3.13).



Figure 3.13 Mold, jack and automatic compactor

The water was added and the samples were mixed homogenously and kept in a closed container for 24 hours before compaction tests. Figure 3.13 shows the used equipment for the compaction tests.

3.2.4 Compressibility Tests

The compressibility behavior of SBMs were investigated in the presence of pumice and perlite additives at room temperature, high temperature and under temperature

cycling by oedometer tests. Also, compressibility behavior of fiberglass added sand-bentonite mixtures were investigated at room and high temperatures.

The oedometer test samples were compacted on 2% wet side of the optimum water content (w_{opt}). The samples were kept under seating pressure (6.86 kPa) for 24 hours. The oedometer tests were performed according to ASTM D2435 (2011). The load increment ratio (LIR) was unity (24.5, 49, 98, 196, 392 and 784 kPa). After completion of the loading stage, the unloading stage was initiated. At the unloading stage, the load was decreased from 784 kPa to 196 kPa, then to 49 kPa. Figure 3.14 shows one of the used oedometer device.



Figure 3.14 The oedometer test device

The compressibility tests were conducted under high temperatures (80 °C) and temperature cycle in the presence of 10% and 20% pumice and perlite on the 10B-90S and 20B-80S mixtures. In addition, oedometer tests were performed with 30B-70S mixtures in the presence of 1% and 0.5% fiberglass additives at 80 °C. A specially manufactured circular-shaped heat rod (Figure 2) was used in order to maintain high temperature in the oedometer cells. The tests under high temperature were started at 80 °C and continued at this temperature. A thermostat was implemented into the oedometer cell to keep the temperature constant. A thick rubber membrane-structured element was used to prevent the excess evaporation of the water inside the cell (Figure 3.15). In

addition, for the decreasing water level inside the cell because of evaporation, water was supplied from a reservoir with the help of a pipe and pump. The loadings were started from 24.5 kPa and when the deformations reached equilibrium, the next loading was started.



Figure 3.15 The heat ring, thermostat and membrane used in oedometer tests under high temperature and temperature cycling

In addition to high temperature, oedometer tests were performed under temperature cycles. The applied test procedure is shown as paths in Figure 3.16 for better explanation. For temperature cycling, the tests were started at room temperature and when the deformations became insignificant (from 1 to 2) under a stress of 196 kPa the temperature was increased to 80 °C (from 2 to 3). Under this temperature, it was waited until the deformations completed then the samples were cooled to room temperature (from 3 to 4). During the cooling stage, the tests were continued by considering the amount of deformation and at the end of this process, the loading process was started under a stress of 392 kPa (from 4 to 5).

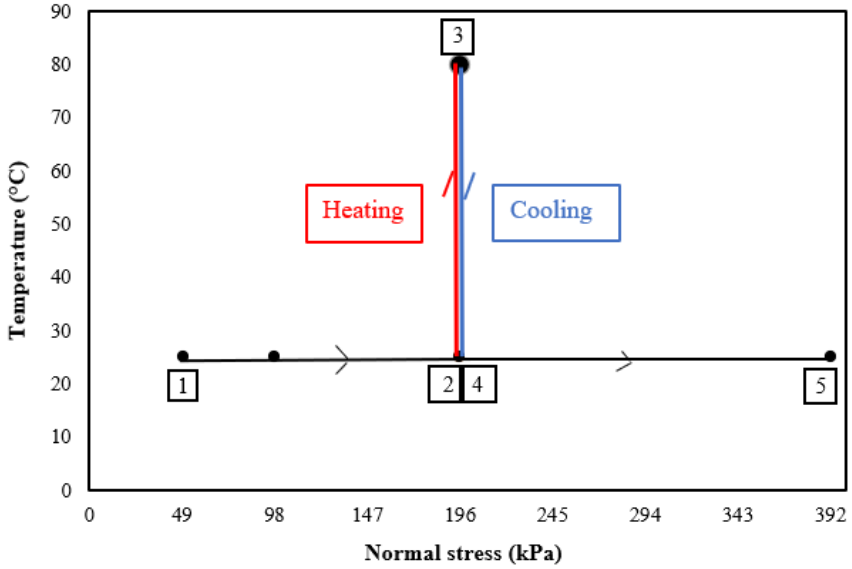


Figure 3.16 Path representation of the oedometer experiments under thermal cycles

3.2.5 Direct Shear Tests

Direct shear tests were performed according to ASTM D3080 (2011). The dry samples were mixed in a vessel until they became homogeneous. The water content was adjusted as 2% wet side of each mixture's optimum water content (w_{opt} + 2%). The samples were compacted in three layers at maximum dry unit weight in the 6x6 cm molds (Figure 3.17).



Figure 3.17 Compacted and submerged samples for direct shear tests

The samples were kept in submerged condition in water for 24 hours and in order to prevent swelling the weight was placed on the samples. After 24 hours, the mold was

placed in the shear box filled with tap water. Under three different normal stress values (49, 98 and 196 kPa), the samples were consolidated and then sheared. The shear rate of the samples was determined as 0.5 mm/min, 0.003 mm/min and 0.004 mm/min under room and high temperature.

The direct shear tests were performed under room temperatures (22~25 °C), high (80 °C) temperature and temperature cycling. To maintain a high temperature, 80 °C, in the shear box specially designed heat rod was used (Figure 3.18). The temperature of the water in the cell was kept constant at 80 °C by using a thermostat. Two K-type thermocouples and a digital thermometer measured and recorded the temperature of the water and soil samples. At the end of the tests, the samples were placed in an oven at 105 °C to determine the final water content.



Figure 3.18 Heat rod and digital thermometer used in the direct shear tests

The direct shear tests of pumice and perlite added SBMs were performed and temperature cycles were also applied. The applied process for temperature cycled direct shear tests is shown in Figure 3.19 as paths. In the temperature cycling tests, the consolidation stage was performed during 8 hours with heating (from 1 to 2) and then cooling stage was applied for 16 hours (from 2 to 3). The temperature was kept constant at 80 °C, and the temperature was reduced to room temperature during cooling (Figure 3.19).

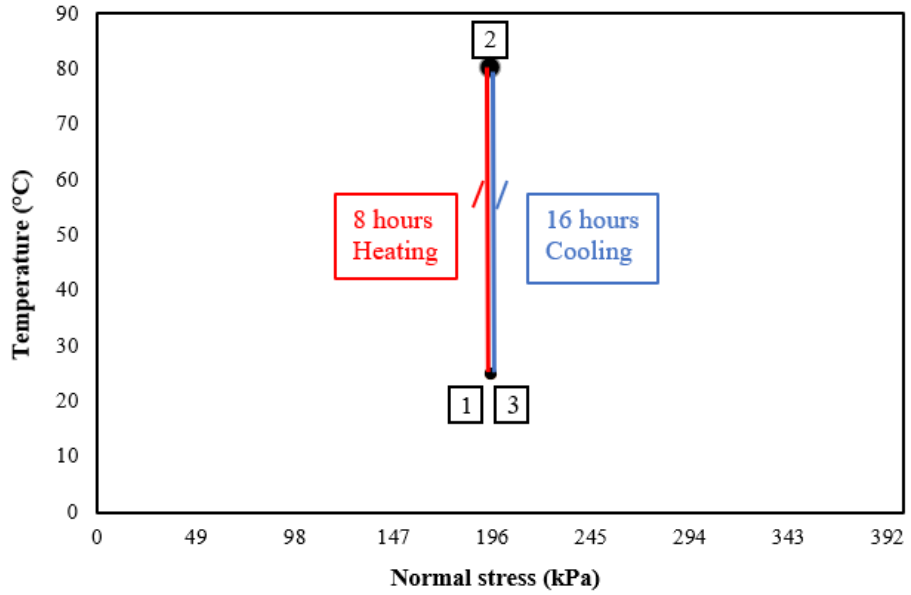


Figure 3.19 Path representation of the direct shear experiments under thermal cycles

3.2.6 Hydraulic Conductivity Tests

Hydraulic conductivity tests were performed of pumice, perlite and fiberglass added sand bentonite mixtures under room and high temperatures and temperature cycles. Hydraulic conductivity tests were performed according to ASTM D5084 (2001) using a flexible wall permeameter. Before the tests, the moist samples were placed in plastic bags in an airtight manner and kept for 24 hours. The samples were compacted at the maximum dry unit weight and w_{opt}+2% water content, then removed from the mold using a hydraulic jack.

Preparing a sample on the wet side of the w_{opt} provides lower hydraulic conductivity. Therefore, all mixtures were prepared at their w_{opt}+2% (wet side). Geotextiles with a diameter of 15 cm on the top and bottom of the sample were placed in the permeameter, latex membrane around it and O-rings on the membrane were used (Figure 3.20).

The hydraulic conductivity tests were conducted in different thermal conditions; room temperature, 80 °C and temperature cycling. The water in the cell, hence the soil, was heated using a specially designed heat rod (Figure 3.21). The applied cell pressure was 50 kPa. Instead of plexiglass, aluminum was preferred as a cell material to prevent adverse temperature effects.



Figure 3.20 The geotextiles, latex membrane and O-rings used in hydraulic conductivity tests

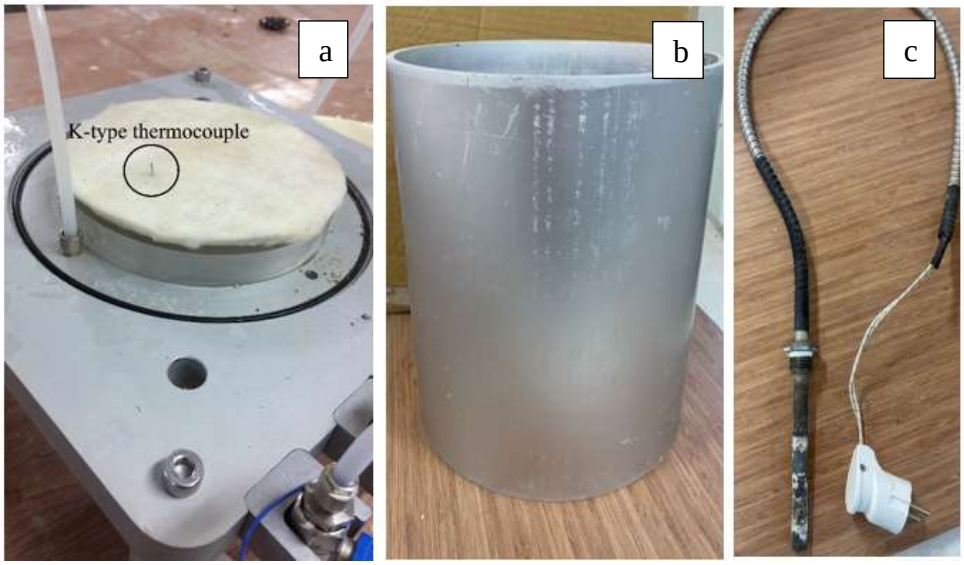


Figure 3.21 The permeameter test set-up a)K-type thermocouple, b) aluminum cell and c) heat rod

In the upper part of the cell, there were three different holes; one for the heat rod and the others for the thermostat and thermocouple, respectively (Figure 3.22). Their surroundings were covered with a heat-resistant liquid gasket in order to prevent any leakage. A gap of approximately a thermocouple diameter was opened on the geotextile and the thermocouple was reeved from this hole by passing through a valve of the permeameter. By this way temperature measurement of the soil was also provided. The water temperature was measured by thermocouple by opening an inlet from the top of the cell.

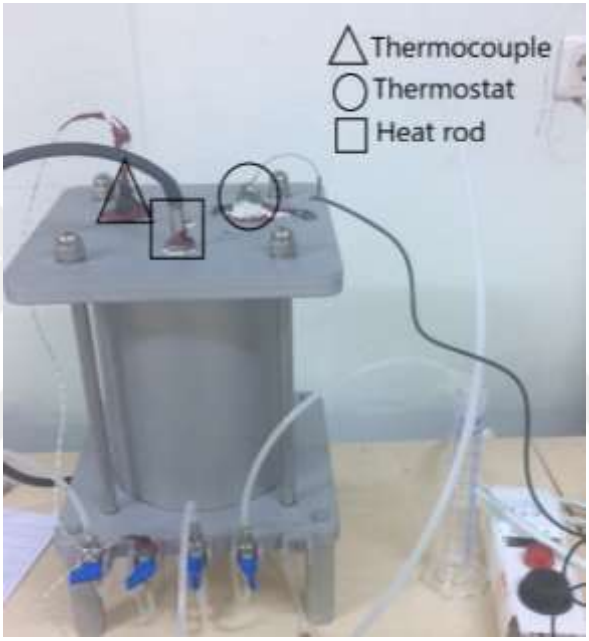


Figure 3.22 The hydraulic conductivity test equipment under high temperatures

The two thermocouples were connected to digital thermometer and temperature values were recorded depending on time. The thermostat system was used to keep the water temperature inside the cell constant at 80 °C. Hydraulic conductivity tests were expressed in terms of pore volume of flow.

Initially, the hydraulic conductivity tests were started at room temperature. Then, when the hydraulic conductivity values reached to steady flow, the temperature was increased to 50 °C. Under this temperature (50 °C), the test was performed until steady flow. Then, the temperature was increased to 80 °C. As a result of this 25-50-80 °C temperature cycle was applied. The tests were run at each temperature increment step until the outflow to inflow ratio became within 0.75~1.25. This limit is essential for

equilibrium before a test is terminated. According to the temperature measurements, it was observed that the soil in the cell reached a lower temperature than the water. Generally, the temperature difference between the water and soil was approximately 10 -15 °C. With the help of a thermocouple placed in the soil, it was determined that the soil temperature was 20, 40 and 60 °C when the water temperature was 25, 60, and 80 °C, respectively.

3.2.7 Thermal Conductivity Tests

The thermal conductivity values of the mixtures were measured with the Shotherm QTM device (Figure 3.23). Measurements were made at an ambient temperature of 20~22 °C. Samples were compacted at the same void ratio and saturation degree and sealed for 24 hours for homogeneity.



Figure 3.23 The equipment of thermal conductivity measurement

For thermal conductivity tests wooden cells were manufactured specially(Figure 3.24). Before the experiments, the samples were mixed with water to ensure homogeneity and the samples were compacted in a mold with a volume of 12x12x4 cm^3 with a total of 3 layers and 104 blows (Figure 3.25). The number of impacts were determined with the help of trial tests. By this way, the samples were compacted at the same energy level. Before measuring the thermal conductivity of the samples, they were covered with a transparent cover (Figure 3.25). Measurements were made from five different locations of the sample to ensure homogeneity. Thermal conductivity values were determined by taking the average of five values.

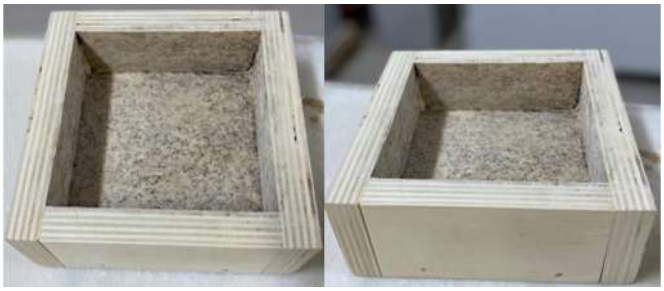


Figure 3.24 Wooden cells used in thermal conductivity measurements

Two different sample preparation methods were used like at same void ratio and at same void ratio and saturation degree values. The saturation degree and void ratio values were determined separately depending on the group of 10B-90S and 20B-80S mixtures. For each mixture an average values of void ratio and sturation degree were determined and the samples were prepared according to these values.



Figure 3.25 Compacted samples before measurement

The thermal conductivity values of fiberglass added SBMs and some other parameters were measured using the TEMPOS Thermal Properties Analyzer instrument (Figure 3.26).

The mixtures were prepared and kept in a sealed container for 24 hours and then compacted at the maximum dry unit weight and optimum water content. Then, using the appropriate probes of the measuring instrument, the thermal conductivity (W/mK) and volumetric heat capacity (MJ/m^3K) of the mixtures were determined.



Figure 3.26 TEMPOS Thermal Properties Analyzer instrument and samples

3.2.8 Scanning Electron Microscope (SEM) Analyses

Scanning Electron Microscope (SEM) analysis is a process that provides an image by scanning the surface of materials utilizing electron beams. The samples were first compacted in a mold with a specific volume at the maximum dry unit weight and optimum water content. These samples, considering the conditions of conducted experiments, were prepared keeping at 80 °C or under room temperature in submerged condition for 24 hours in order to determine the temperature effect on the samples' structure. After this stage, the samples were taken out of the container and wrapped with cling film and placed in the freezer, where they were kept for 24 hours. At the end of this period, the samples were taken in a frozen state and broken with the help of a hammer. The pieces of the samples that were large enough were dried in the freeze-drier device and kept 24 hours (Figure 3.27). Due to the shrinkage process during air-drying or oven-drying, changes occur at microstructure of the sample. It is more convenient to use freeze-dried or critical-point-dried samples for use in the SEM analysis.

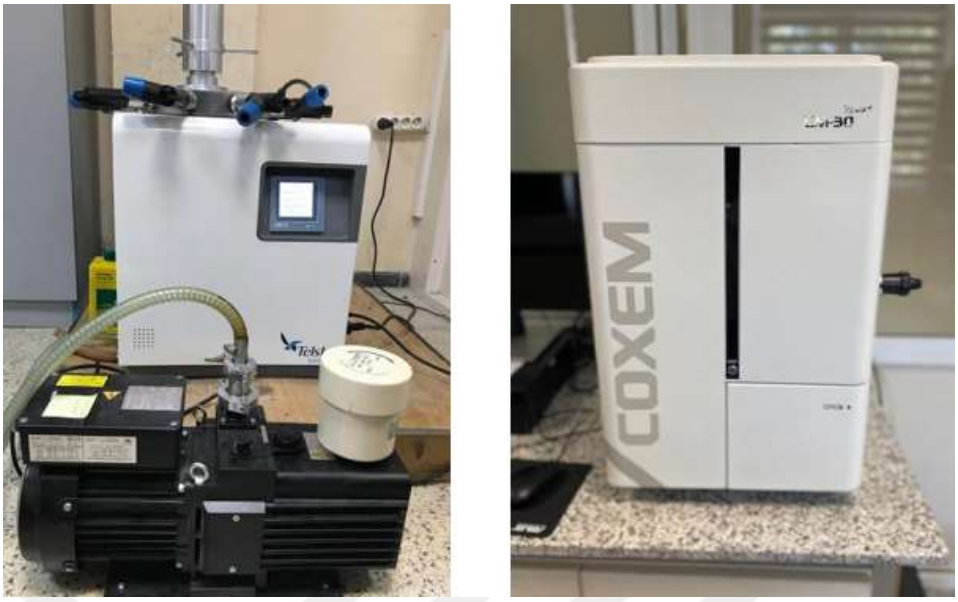


Figure 3.27 Freeze-drier device and COXEM EM-30 Scanning electron microscope

Then the samples were placed in the SEM device in a dry state (without any water) for analysis, images were taken from the desired parts of the material at the selected scales and recorded.

3.2.9 Finite Element Method (FEM) Analyses of the Sand-Bentonite Mixtures as a Buffer Material

Within the scope of this thesis, a modeling study was conducted around the nuclear waste storage repository and as a buffer material sand-bentonite mixtures were selected. For this purpose, Code Bright program was used. The Code Bright is a program that can perform thermo-hydro-mechanical (THM) analysis using the Finite Elements Method (FEM). It was developed by the Department of Civil and Environmental Engineering of the Polytechnic University of Catalonia (UPC) and works in conjunction with an extension called GiD.

The mixture selected as a buffer in the modeling study was simulated using a single layer. The layers that make up the modeling consist of canister (heat source), buffer material (sand-bentonite mixture) and bedrock. While the initial and boundary temperature value of the bedrock was accepted as 25 °C, the initial temperature value of the buffer material was chosen as 20 °C. Analyzes were performed for the final time of 100 years.

CHAPTER 4
TEMPERATURE EFFECT ON THE VOLUME DEFORMATION, SHEAR STRENGTH, HYDRAULIC CONDUCTIVITY AND THERMAL CONDUCTIVITY BEHAVIOR OF SAND-BENTONITE MIXTURES

Former studies show that the engineering behavior of soils changes when it comes to the interaction with temperature. Because with increase in temperature, there is an increase in the volumetric deformation behavior of soils that is an increase in the amount of compression, an increase in the hydraulic conductivity due to the decrease in water viscosity, and an increase in the shear strength according to some researchers and a decline according to some other studies (Towhata et al., 1993; Maghsoodi et al., 2019; Lide, 1995).

Sand-bentonite mixtures are one of the mixtures currently used as a buffer; in some cases, only bentonite is also widely used as a buffer. For that reason, in the scope of this thesis the engineering properties of sand-bentonite mixtures were determined in the presence of different additives under high temperature and temperature cycles.

4.1 Compaction of Sand-Bentonite Mixtures

The Standard Proctor tests of 10B-90S, 20B-80S and 30B-70S mixtures were performed in order to determine the compaction parameters of the samples. The test results showed that as the amount of bentonite increased, the maximum dry unit weight decreased and the optimum water content increased (Figure 4.1). While the dry maximum of the 10B-90S mixture was 16.7 kN/m^3, it decreased to 15.6 kN/m^3 and 14.6 kN/m^3 as the bentonite content was increased to 20% and 30%, respectively.

Table 4.1 Compaction parameters of sand-bentonite mixtures obtained from Standard Proctor Tests

Sample	$\gamma_{d,max}$ (kN/m^3)	w_{opt} (%)
10B-90S	16.70	15.5
20B-80S	15.60	17.5
30B-70S	14.62	22.5

While the optimum water content value was 15.5% of the mixture with 10% bentonite, it increased by 2% and 5%, respectively, with 20% and 30% bentonite contents.

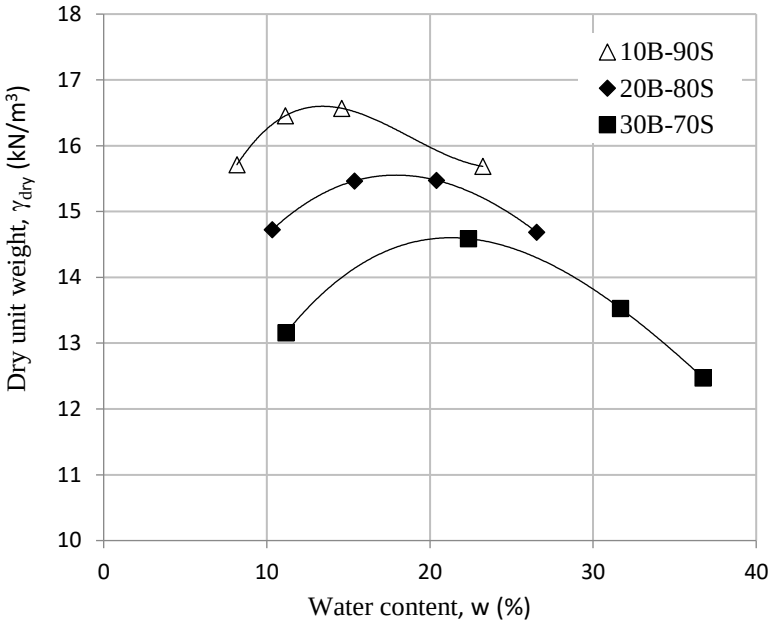


Figure 4.1 Compaction curves of the sand-bentonite mixtures

4.2 Volume Deformation Behavior of Sand-Bentonite Mixtures

The volumetric deformation behavior of SBMs was determined under three different thermal conditions. This section presents the results of the volumetric deformation behavior under room temperature, high temperature and thermal cycles.

4.2.1 Volume Deformation Behavior of Sand-Bentonite Mixtures Under Room Temperature

The volumetric deformation behavior of 10%, 20% and 30% sand-bentonite mixtures were determined with oedometer tests at room temperature and the compression curves are shown in Figure 4.2. From the test results obtained, it was determined that the total vertical deformation values of 10B-90S, 20B-80S and 30B-70S mixtures were 4.56%, 10.07% and 14.07%, respectively. It is known that increase in bentonite content cause increase in the amount of compression and swelling. Table 4.2 shows the compression and swelling deformation amounts of SBMs.

Table 4.2 Total compression and swelling deformation values of sand-bentonite mixtures at room temperature

Sample	Total vertical deformation (%)	Total swelling deformation (%)
10B-90S	4.56	0.34
20B-80S	10.07	0.91
30B-70S	14.07	1.37

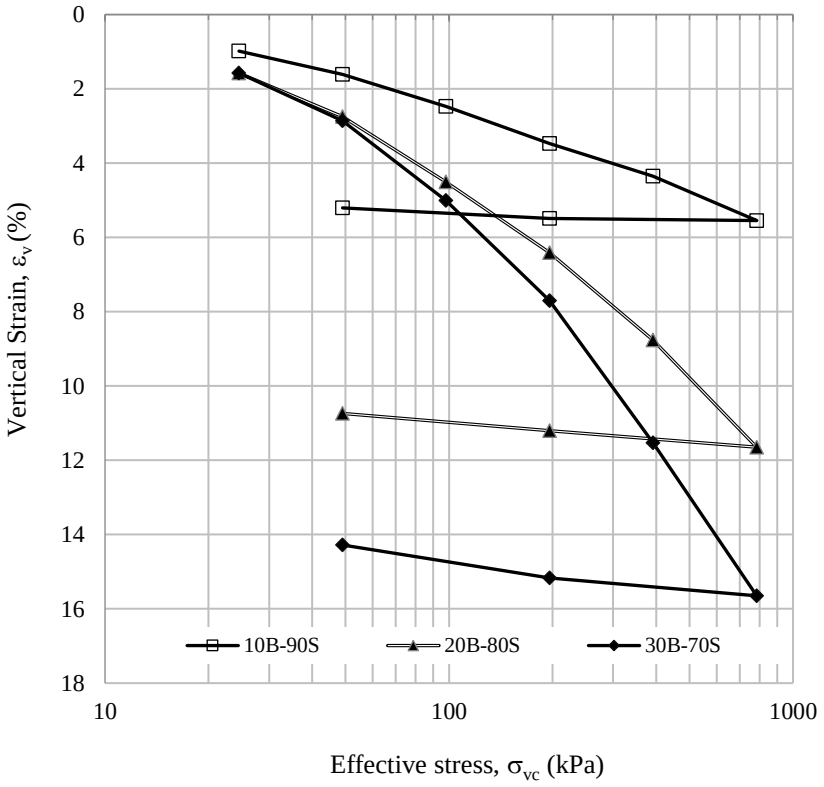


Figure 4.2 Compression and swelling curves of sand-bentonite mixtures under room temperature

4.2.2 Volume Deformation Behavior of Sand-Bentonite Mixtures Under High Temperature (80 °C)

The compression curves of three different sand-bentonite mixtures under high temperature are given in Figure 4.3. As the content of bentonite was increased under high temperature, the compression amount increased (Table 4.3). It was reported in the literature, temperature increase affects the tensile behavior of bentonite or sand-

bentonite mixtures used as buffer material (Lingnau et al., 1996). However, the extent of this effect may vary depending on the material used and level of temperature rise.

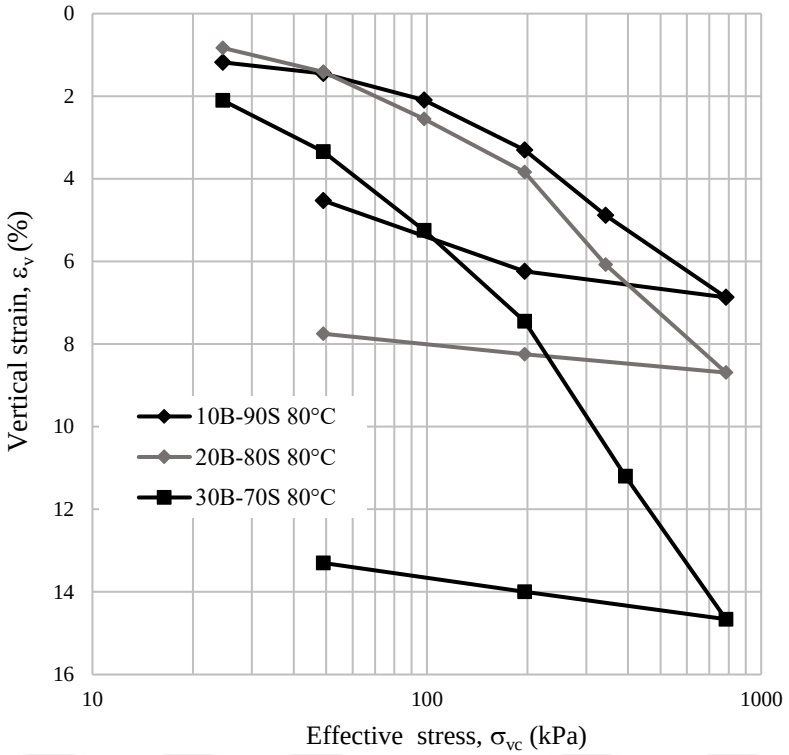


Figure 4.3 Compression and swelling curves of sand-bentonite mixtures under high temperature

Table 4.3 Total compression and swelling deformation values of sand-bentonite mixtures at high temperature (80 °C)

Sample	Total vertical deformation (%)	Total swelling deformation (%)
10B-90S	5.69	2.34
20B-80S	7.86	0.94
30B-70S	12.56	1.36

Eriksson (1989) observed a decrease in the volume of samples during the heating period. Also, Sinha, & Kusakabe (2008) determined that when the temperature was increased to 75 °C, the amount of compression increased of sand-bentonite mixtures. This situation was explained by the shrinkage of the clay grains and decrease in volume due to less space in the diffuse double layer (Yong et al., 1992). It was revealed that the pore water pressure changes with the temperature and the void ratio changes accordingly.

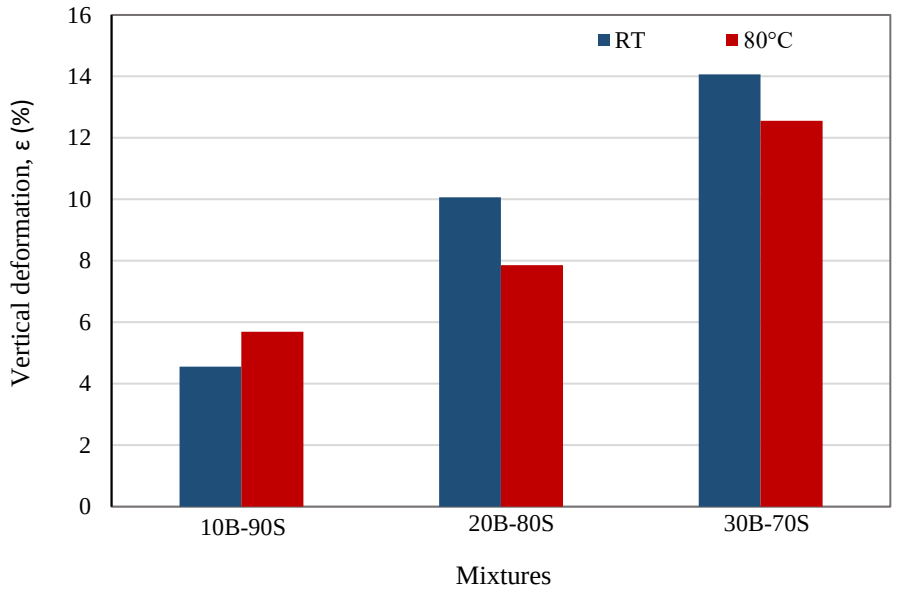


Figure 4.4 The effect of temperature on compression amount under room temperature and 80 °C

Figure 4.4 shows the vertical deformation amounts of additive free sand-bentonite mixtures under room and high temperatures. As the bentonite ratio increased, it was observed that the amount of compression of the mixtures increased both at room and at high temperature.

4.2.3 Volume Deformation Behavior of Sand-Bentonite Mixtures Under Thermal Cycles

The oedometer tests of 10B-90S and 20B-80S mixtures were conducted under temperature cycling. Figure 4.5 shows the compression curves of these sand-bentonite mixtures under the temperature cycle (25-80-25 °C). Table 4.4 and Table 4.5 show the compression and swelling deformation values of the samples, respectively.

Tablo 4.4. Compression deformation amounts of the sand-bentonite mixtures under thermal cycles

Mixture	Loading 24.5-196 kPa compression (RT) (%)	196 kPa compression (80 °C) (%)	196 kPa compression (RT) (%)	392 kPa total compression (%)
10B-90S	1.80	0.16	0.23	4.20 (785kPa)
20B-80S	2.96	0.05	0.26	9.18 (785kPa)

Tablo 4.5. Swelling deformation amounts of the sand-bentonite mixtures under thermal cycles

Mixture	Unloading 392-196 kPa-swell (RT) (%)	196 kPa swell (80 °C) (%)	196 kPa swell (RT) (%)	49 kPa total swell (%)
10B-90S	0.32	0.22	-0.22	0.54
20B-80S	0.43	0.27	-0.25	0.81

The compression stage was started with the test's initiation at room temperature. After it was loaded at a stress level of 196 kPa and completed its compression deformations, the compression behavior of the sample continued with the application of high temperature. It was observed that the samples continued to contraction behavior during the unloading phase. This is because, according to the Kuhn & Mitchell (1993) model, with the increase in temperature, as a result of increase in sliding of particles the rate of creep increases (Kuhn & Mitchell, 1993; Jarad, 2016). Creep behavior occurs during secondary consolidation, where the mechanism is the displacement and rearrangement of grains under effective stress. When this creep behavior is investigated in terms of microstructure, it is seen that pore fluid drainage and change in viscosity of pore fluids cause such a behavior (Das, 2008; Le et al., 2012; Green, 1969). It was noted that the structure weakens and detoriates.

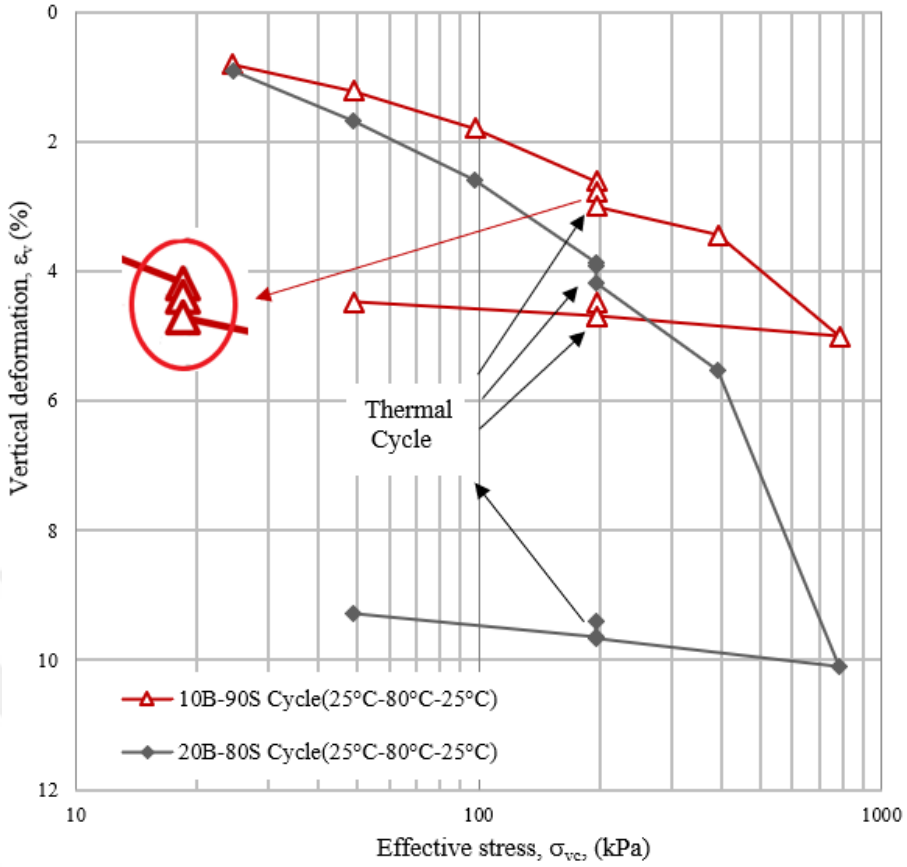


Figure 4.5 Compression and swelling curves of sand-bentonite mixtures under thermal cycles

As can be seen from the zoomed area in Figure 4.5, when the temperature increased to 80 °C even after completion of vertical deformations before temperature increase, by increase in temperature deformations starts again at this stress level. After reaching 80 °C temperature of 10B-90S mixture, an increase in the compression amount of 0.16% was observed. In the 20B-80S mixture, this amount was determined as 0.05% during loading phase. As a result of increase in sliding of particles the rate of creep increases under high temperature.

4.3 Shear Strength Behavior of Sand-Bentonite Mixtures

Within the scope of this doctoral thesis, the direct shear tests were conducted under room temperature, high temperature and thermal cycles to determine the shear strength of additive-free SBMs.

4.3.1 Shear Strength Behavior of Sand-Bentonite Mixtures Under Room Temperature

The direct shear tests on the10B-90S and 20B-80S mixtures were conducted and two different shear rates were applied in order to determine the shear rate effect under high temperature. In addition, 30B-70S sample was subjected to only one shear rate. The applied shear rates are given in Table 4.6.

Table 4.6 Shear rates of sand-bentonite mixtures

Mixture	Shear rate (mm/min)	Shear rate (mm/min)
10B-90S	0.5	0.004
20B-80S	0.5	0.004
30B-70S	-	0.003

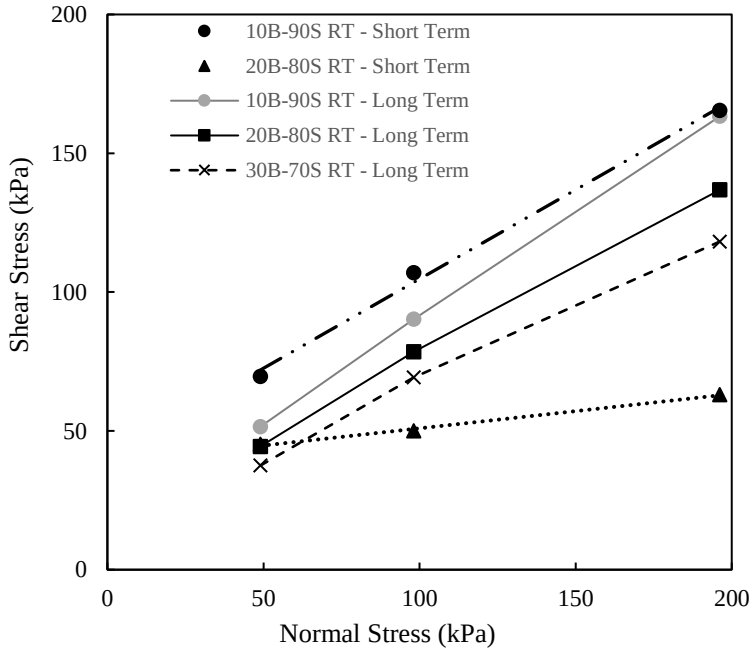


Figure 4.6 Shear stress-normal stress relationship of sand-bentonite mixtures at room temperature

Table 4.7 shows the obtained the internal friction angle and cohesion values of 10B-90S and 20B-80S mixtures. It was observed that the internal friction angle and the maximum shear stress decreased considerably as the bentonite ratio in the mixture increased. However, an insignificant change in cohesion value was observed (Figure 4.6). The maximum shear stress values of 10B-90S and 20B-80S mixtures were 106.9 kPa and 41.7 kPa at room temperature, respectively (Figure 4.7).

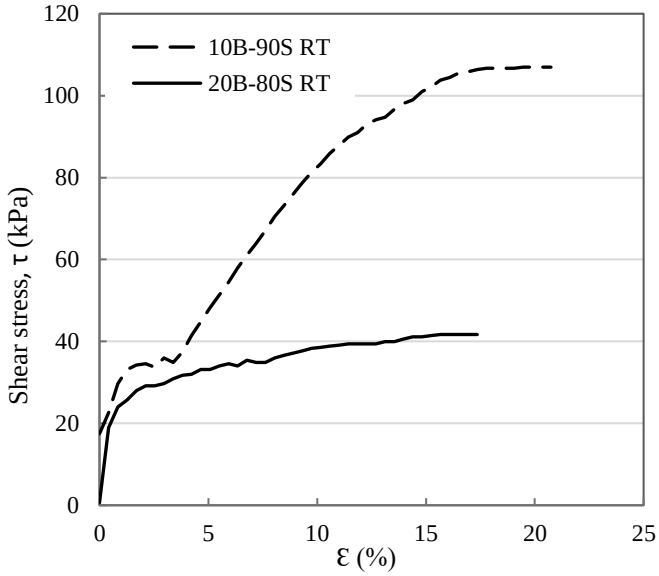


Figure 4.7 τ- ε relationship of sand-bentonite mixtures at room temperature

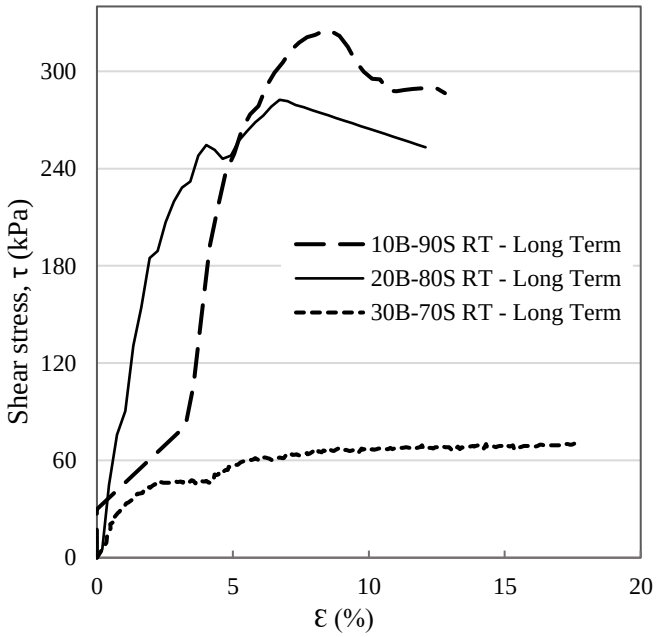


Figure 4.8 τ- ε relationship of sand-bentonite mixtures at room temperature

The direct shear test results of additive-free mixtures under room temperature showed that as the amount of bentonite increased, the internal friction angle decreased and the cohesion value did not change significantly (Table 4.8). As expected, the increase in clay content caused a decrease in strength (Figure 4.7). However, compared

to the direct shear tests performed as short term, the internal friction angle and shear stress values increased.

As shown in Figure 4.8, according to the long-term direct shear test results at room temperature, the maximum shear stress value of the 10B-90S mixture was 324.8 kPa. In comparison, the shear strength value decreased to 282.4 kPa and 70.4 kPa for 20B-80S and 30B-70S mixtures, respectively, as the amount of bentonite increased. The reason of decrease in the maximum shear stress value of the 30B-70S mixture compared to the other additive-free mixtures was that the high amount of bentonite controlled the shear strength behavior.

Table 4.7 Internal friction angle and cohesion values of sand-bentonite mixtures

	Room Temperature (Long Term)		**Room Temperature (Short Term)**	
Mixture	**ϕ (°)**	**c (kPa)**	**ϕ (°)**	**c (kPa)**
10B-90S	37.1	15.0	32.7	40.4
20B-80S	31.9	15.2	7.0	38.5
30B-70S	28.6	12.7	-	-

4.3.2 Shear Strength Behavior of Sand-Bentonite Mixtures Under High Temperature

Within the scope of this thesis, direct shear tests of sand-bentonite mixtures under high temperatures were performed. The 10B-90S and 20B-80S mixtures were sheared at a shear rate (0.5 mm/min), however the 30B-70 mixture was sheared at a shear rate of 0.003 mm/min.

Table 4.8 Internal friction angle, cohesion and maximum shear stress values of sand-bentonite mixtures at high temperature

	High Temperature (80 °C)		
Mixture	**ϕ (°)**	**c (kPa)**	**Maximum shear stress (kPa)**
10B-90S	31.5	31.5	94.4
20B-80S	13.4	20.0	47.4

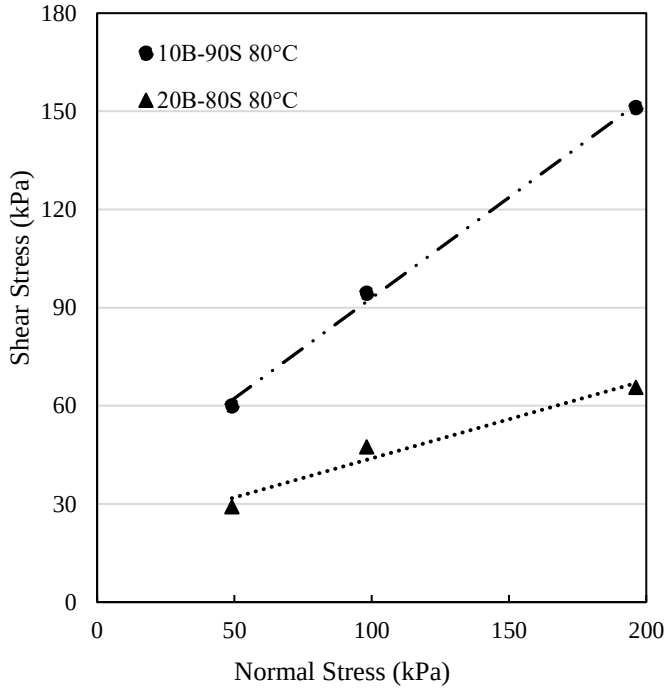


Figure 4.9 Shear stress-normal stress relationship of sand-bentonite mixtures at high temperature based on shear rate (0.5 mm/min)

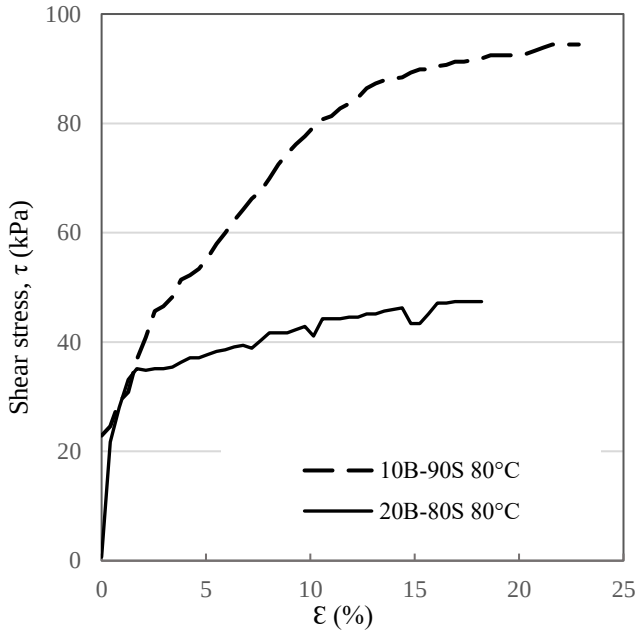


Figure 4.10 τ- ε relationship of sand-bentonite mixtures at high temperature based on shear rate (0.5 mm/min)

The test results showed that the internal friction angle of the 10B-90S mixture at room temperature remained almost same when the temperature was increased to 80 ℃, while the internal friction angle of the 20B-80S mixture increased at high temperature.

Previous studies have shown that the internal friction angle is not affected by temperature (Figure 4.9) and the shear strength of soils reaches higher values when the specimens are heated (Cekerevac and Laloui, 2004) (Figure 4.10). Also, it was observed that the internal friction angle and cohesion value of the 30B-70S mixture increased to 31.1° and 15.0 kPa, respectively with increase in temperature (Figure 4.11).

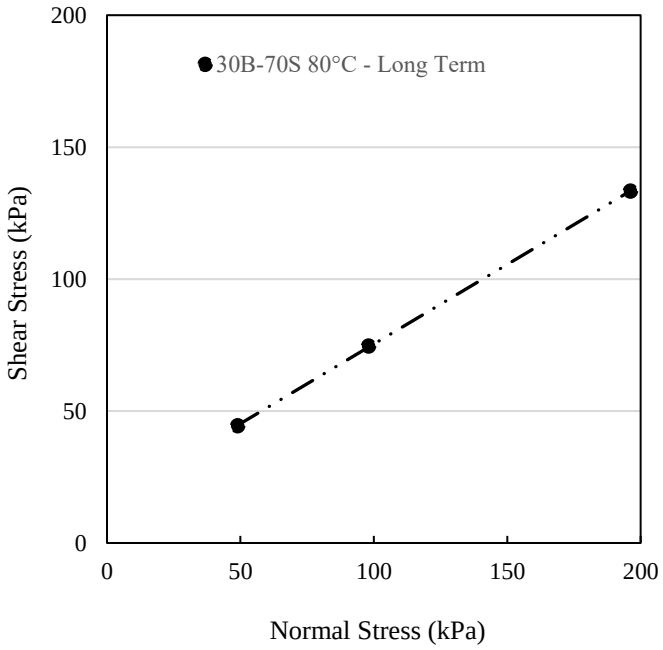


Figure 4.11 Shear stress-normal stress relationship of sand-bentonite mixtures at high temperature based on shear rate (0.003 mm/min)

4.3.3 Shear Strength Behavior of Sand-Bentonite Mixtures Under Thermal Cycles

The shear strength behavior of the 10B-90S and 20B-80S mixtures were investigated under temperature cycling. After subjected to a heating-cooling cycle during the consolidation phase, the samples were sheared at room temperature (22~25 °C). The 10B-90S and 20B-80S mixtures reached to maximum shear stress values of 248.8 and 176.1 kPa, respectively (Figure 4.12). The increase in the bentonite content is the main reasons of this decrease in shear strength.

The main parameters that determine the sliding behavior are; the load to which it has been exposed in the past, the test method is chosen and the method of application, and the mineralogical structure of the soil (Yavari et al., 2016). Previous studies have shown that shear strength affected and increased by temperature increase or the temperature it has been exposed to in the past, regardless of whether the test conditions are drained or undrained.

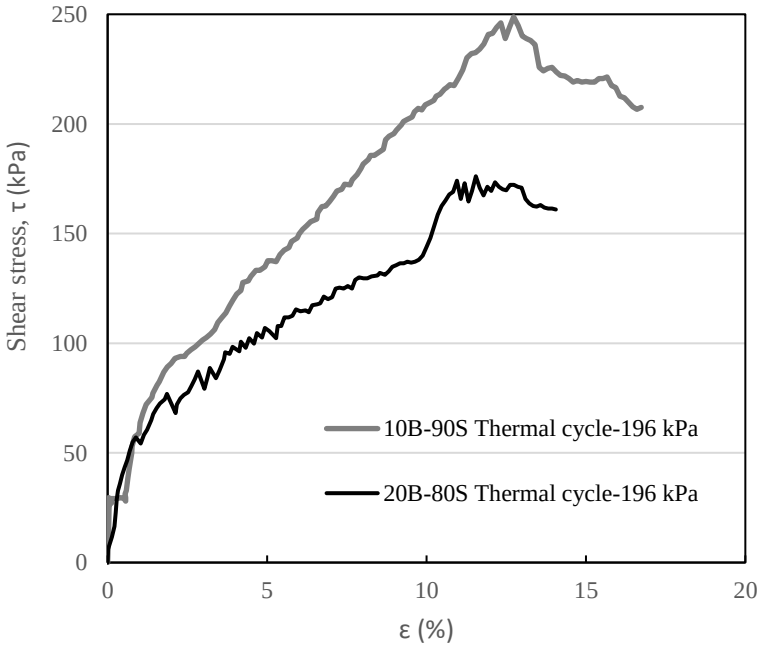


Figure 4.12 Shear stress-normal stress relationship of sand-bentonite mixtures under thermal cycle and 196 kPa normal stress

Changes in the shear strength behavior of soils with temperature may be due to volumetric changes or changes in the texture of the soil (Abuel-Naga et al., 2007). According to Hamidi et al. (2014), with the increase in temperature, the internal friction angle may change or remain constant without being affected by this situation. In addition, Yavari et al. (2016) stated that temperature values between 5 °C and 40 °C affect the shear strength behavior of sand and clay negligibly.

4.4 Hydraulic Conductivity Behavior of Sand-Bentonite Mixtures Under Room and High Temperatures and Thermal Cycles

Within the scope of the doctoral thesis, hydraulic conductivity tests were conducted on the additive-free SBMs. The tests were started under room temperature (25 °C) and

gradually temperature was increased up to 50 °C and then 80 °C and when the stable flow was obtained, it was aimed to apply a thermal cycle by switching to the cooling stage in the cycle and reducing temperature from 80 °C to 50 °C and 25 °C, consecutively. The Table 4.9 shows the measured hydraulic conductivity values depending on the temperature.

Table 4.9 Hydraulic conductivity values of the sand-bentonite mixtures depending on the temperature

Cell Temperature (°C)	**k (m/s)**		
	10B-90S	**20B-80S**	**30B-70S**
25	8.2×10^{-07}	4.5×10^{-11}	4.3×10^{-11}
50	1.1×10^{-06}	5.1×10^{-11}	3.2×10^{-10}
80	1.4×10^{-06}	6.7×10^{-11}	5.0×10^{-10}
50	8.8×10^{-07}	6.3×10^{-11}	-
25	6.3×10^{-07}	3.9×10^{-11}	-
50	6.7×10^{-07}	-	-
80	4.7×10^{-07}	-	-
50	5.7×10^{-07}	-	-
25	4.7×10^{-07}	-	-

As can be seen from Table 4.9, the test results showed that the hydraulic conductivity of all sand-bentonite mixtures increased as the temperature increased. As the temperature increases, the flow rate increases as the viscosity of the fluid decreases (Villar, & Lloret, 2004). Figure 4.13, 4.14 and 4.15 shows the hydraulic conductivity graphs of 10B-90S, 20B-80S and 30B-70S mixtures, repectively.

The hydraulic conductivity values of the 10B-90S, 20B-80S and 30B-70S mixtures were determined as 8.2×10^{-7} m/s, 4.5×10^{-11} m/s and 4.3×10^{-11} m/s, respectively at room temperature. As can be seen from Table 4.9, this value increased by 1.34 times with increase in cell temperature to 50 °C and reached the value of 1.1×10^{-6} m/s for 10B-90S mixture. For 20B-80S and 30B-70S mixtures, it increased by 1.13 and 7.44 times, respectively. The one reason for this situation is decrease in water viscosity of water due to the increasing temperature, hence hydraulic conductivity increases. When the cell temperature was increased to 80 °C, the hydraulic conductivity slightly increased.

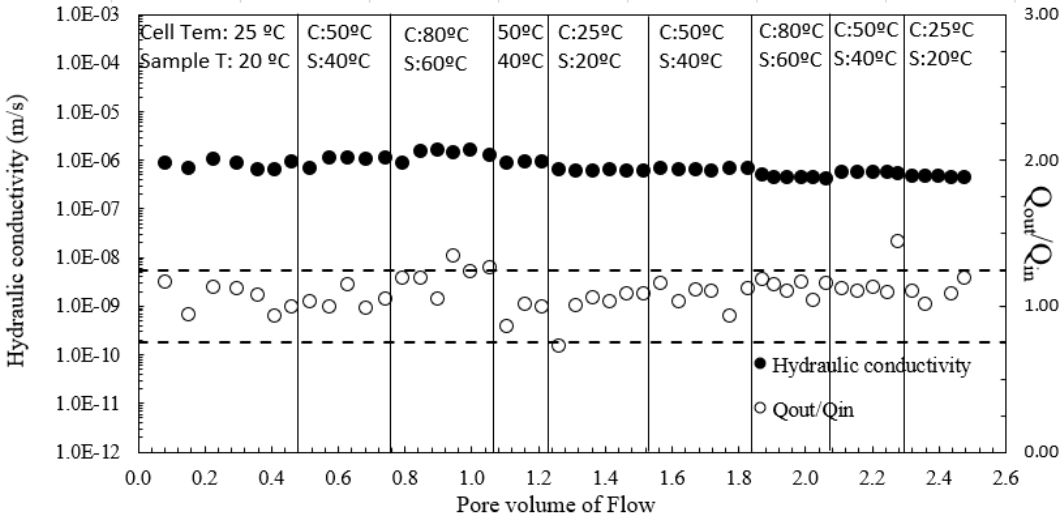


Figure 4.13 Hydraulic conductivity in terms of pore volume of flow of mixture 10B-90S

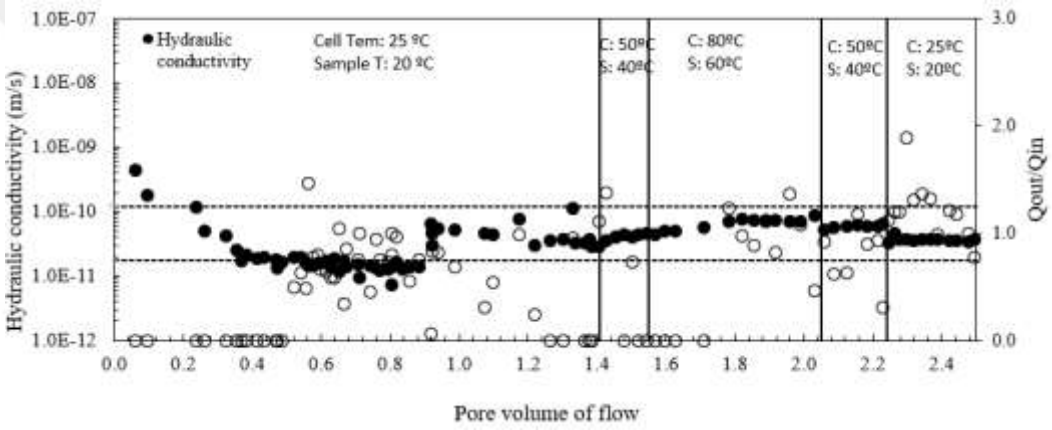


Figure 4.14 Hydraulic conductivity in terms of the pore volume of flow of mixture 20B-80S

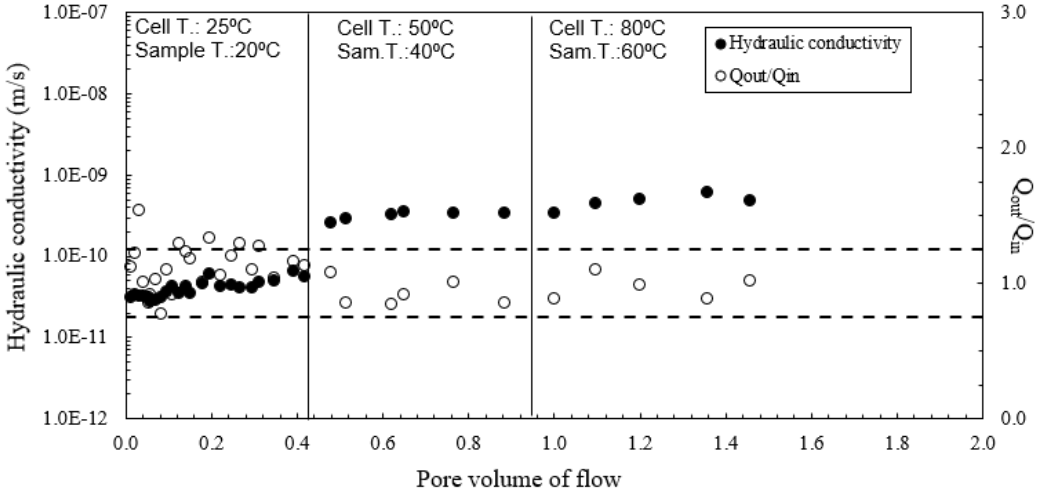


Figure 4.15 Hydraulic conductivity in terms of the pore volume of flow of mixture 30B-70S

After this temperature level, the cooling was applied. It was observed that the hydraulic conductivity of 10B-90S mixture decreased approximately 1.6 and 1.4 times at temperatures from 80 °C to 50 °C and 50 °C to 25 °C, respectively. The same decreasing trend was also available for the 20B-80S mixture. Moreover, the hydraulic conductivity value of the mixture could not return to the point where it started.

Previous studies show that this behavior cannot be explained only by the increase in viscosity of water and that there are changes in the microstructure caused by the soil-water interaction (Chen et al.2017). Hence, the results of the present study showed that not only change in viscosity of water is enough for explaining decreasein hydraulic conductivity. Beside the change in viscosity, detoriation of the pore structure is the another reason for change in hydraulic conductivity.

4.5 Thermal Conductivity of the of Sand-Bentonite Mixtures

The thermal conductivity values of 10B-90S and 20B-80S mixtures were measured. As mentioned in the "Methods" section, the thermal conductivity measurements of the samples were performed on the samples which were prepared according to two different methods.

Tablo 4.10 Thermal conductivity values of sand-bentonite mixtures based on the saturation degree and void ratio of the mixtures

Mixtures	**Thermal Conductivity (λ, W $m^{-1}K^{-1}$)**	
	Based on saturation degree and void ratio	Based on void ratio
10B-90S	1.779	1.153
20B-80S	1.461	1.971

The Table 4.10 shows the test results of the samples prepared based on the saturation degree and void ratio of the mixtures. In addition, the thermal conductivity value of the 30B-70S additive free mixture was also measured and found to be 1.621 W/mK. According to Table 4.10, the thermal conductivity decreased as the amount of bentonite increased. The decrease in the amount of sand in the mixture is one of the main reasons for this because the quartz in the sand is an essential factor in increasing thermal conductivity (Johansen, 1977). On the other hand, when the void ratio keeps constant in

the mixtures reverse behavior was obtained when compared with the constant saturation degree. It can be explained that bentonite can fill the voids sufficiently, the intergranular contact surface will increase and the thermal conductivity will increase (Ahn, & Jung, 2017).

4.6 SEM Analyses of the Sand-Bentonite Mixtures

The SEM photographs of additive-free 10B-90S and 20B-80S mixtures are given in Figure 4.16. Figure 4.16 shows that the 10B-90S mixture did not undergo a significant change when it was cured under room temperature and high temperature. However, the SEM photos of 20B–80S mixtures revealed that as the temperature increased, the voids became smaller and there was a decrease in the pore volume of sample (Figure 4.17).

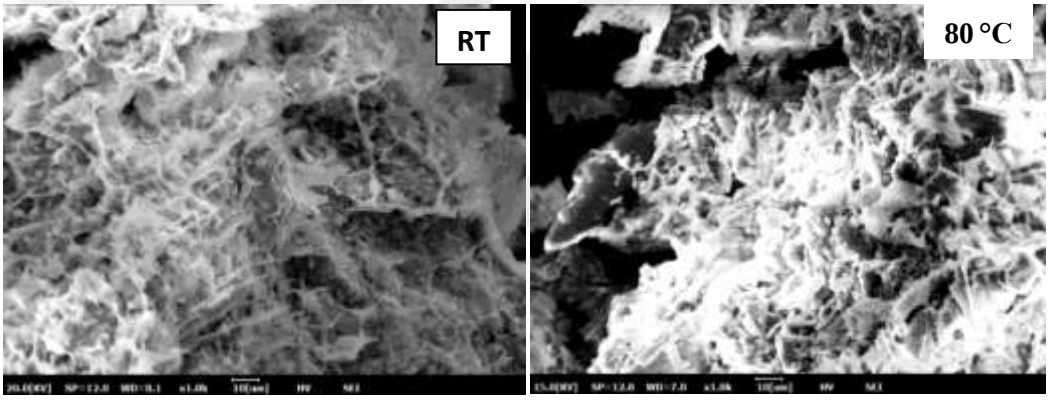


Figure 4.16 Scanning electron microscope photos of the samples (a) 10B-90S (x1000) at room temperature (RT), (b) 10B-90S (x1000) at 80 ˚C

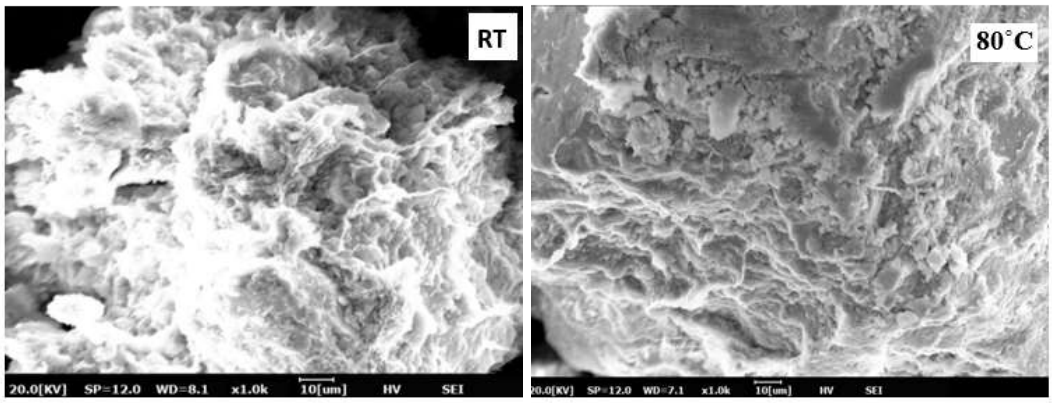


Figure 4.17 Scanning electron microscope photos of the samples (a) 20B-80S (x1000) at room temperature (RT), (b) 20B-80S (x1000) at 80˚C

CHAPTER 5
PUMICE EFFECT ON THE VOLUME DEFORMATION, SHEAR STRENGTH, HYDRAULIC CONDUCTIVITY AND THERMAL CONDUCTIVITY BEHAVIOR OF SAND-BENTONITE MIXTURES UNDER THERMAL CONDITIONS

5.1 Compaction Behavior of Pumice Added Sand-Bentonite Mixtures

The Standard Proctor tests were performed on the 10B-90S and 20B-80S mixtures in the presence of 10 and 20% pumice additives. The dry unit weight and optimum water content values of pumice were determined as 12.98 kN/m^3 and 30%, respectively (Figure 5.1). The compaction test results showed that the γ_{dmax} of the 10% bentonite-sand mixture was 16.7 kN/m^3, then decreased to 16.2 kN/m^3 and 15.6 kN/m^3 in the presence of 10% and 20% pumice, respectively (Table 5.1). The low dry unit weight value of pumice is a reason for such decrease in dry unit weight values of the bentonite-sand mixtures. On the other hand, pumice additive changed the w_{opt} values insignificantly.

Table 5.1 Compaction characteristics of sand-bentonite mixtures in the presence of pumice additive

Group	Sample	$\gamma_{d,max}$ (kN/m^3)	w_{opt} (%)
10% bentonite	Pumice (PU)	12.98	30.0
	10B-90S	16.70	15.5
	9B-81S-10PU	16.20	17.0
	8B-72S-20PU	15.60	16.0
20% bentonite	20B-80S	15.60	17.5
	18B-72S-10PU	15.20	17.0
	16B-64S-20PU	14.70	17.0

When the compaction behavior of 20B-80S mixtures was examined in the presence of 10% and 20% pumice additives in Figure 5.2 b, it was seen that $\gamma_{d,max}$ values are 15.2 kN/m^3 and 14.7 kN/m^3 in the presence of 10 and 20% pumice additive. It was observed that $\gamma_{d,max}$ value decreased from 15.6 kN/m^3 to 15.2 kN/m^3 when the bentonite content was increased from 10% to 20% with 10% pumice additive (Figure 5.2).

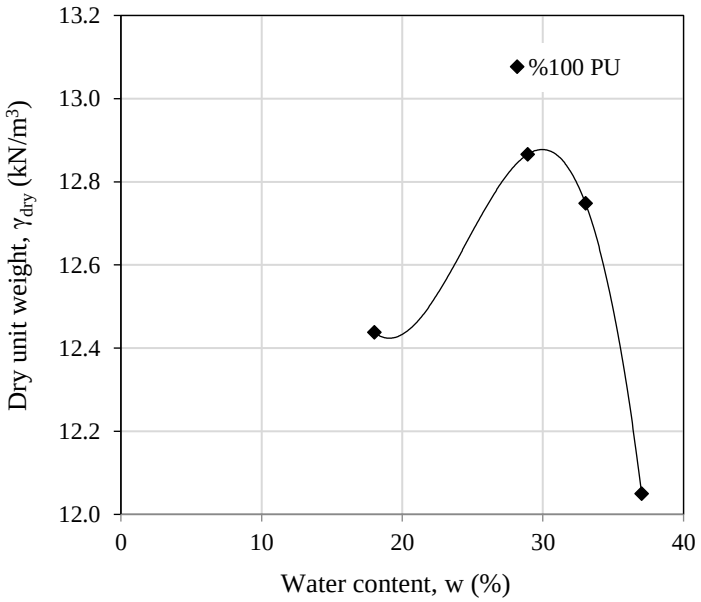
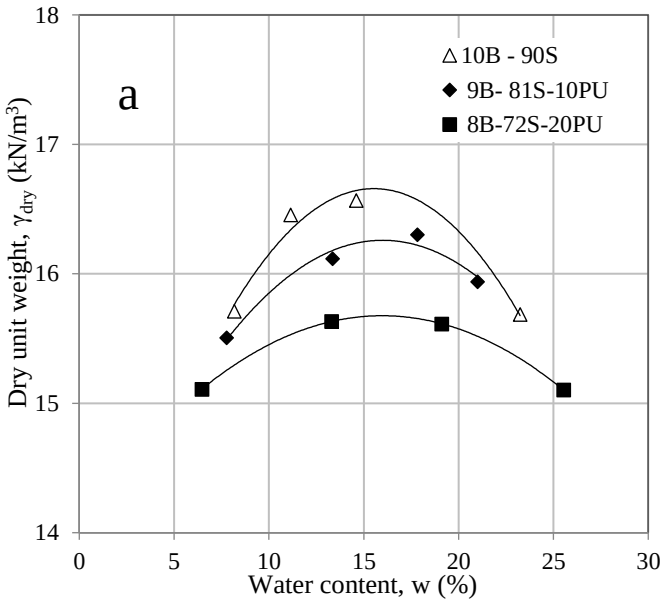


Figure 5.1 Compaction curve of pumice additive



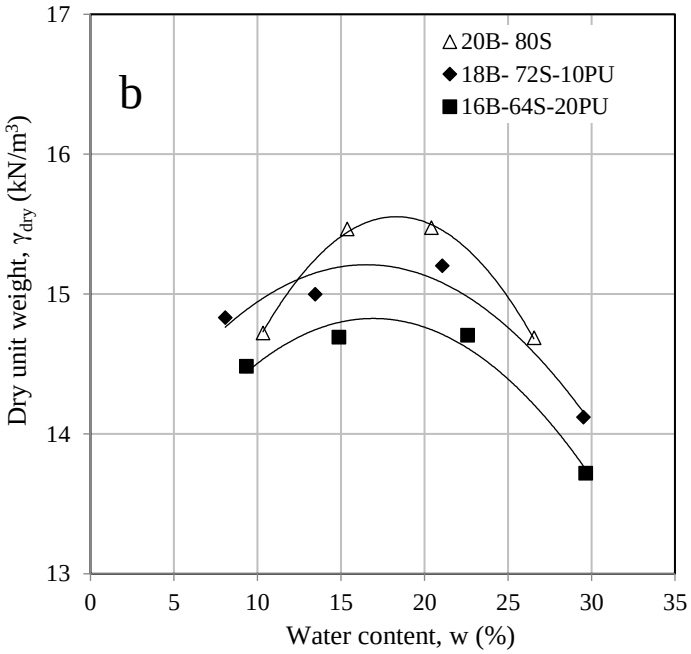


Figure 5.2 Compaction curves of sand-bentonite mixtures with pumice additives a) 10B-90S mixtures, b) 20B-80S mixtures

Figure 5.3 and 5.4 show the effect of pumice additive on the $\gamma_{d,max}$ and w_{opt} values of sand-bentonite mixtures. Both 10% and 20% of pumice contents had a reducing effect on the dry unit weight of 10B-90S and 20B-80S mixtures.

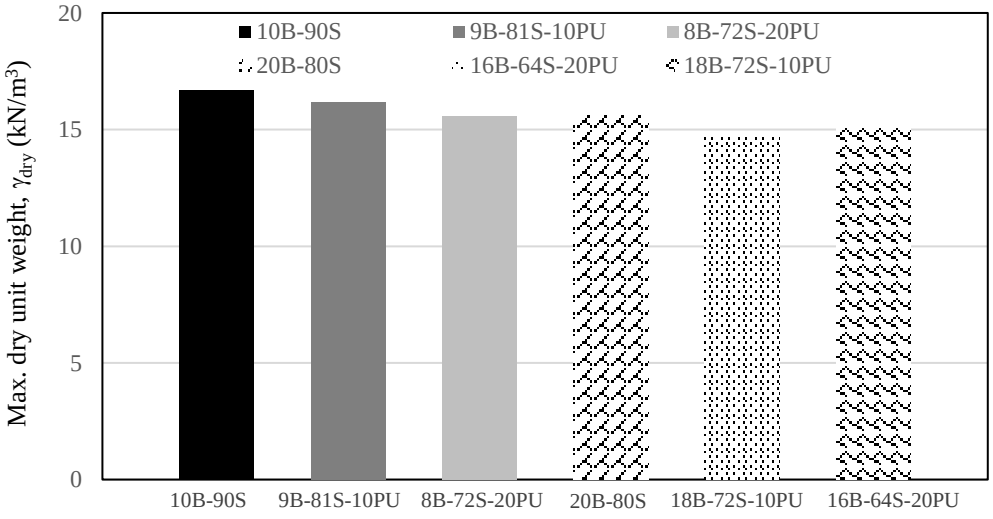


Figure 5.3 Effect of pumice additive on maximum dry unit weight for 10B-90S and 20B-80S mixtures

Pumice additive did not significantly affect the w_{opt} value of the 10B-90S and 20B-80S mixtures. Because when pumice was added to sand-bentonite mixtures, the

mixture's water content did not change significantly. Although the high optimum water content of pumice, low content of pumice could not change the w_{opt} values, significantly.

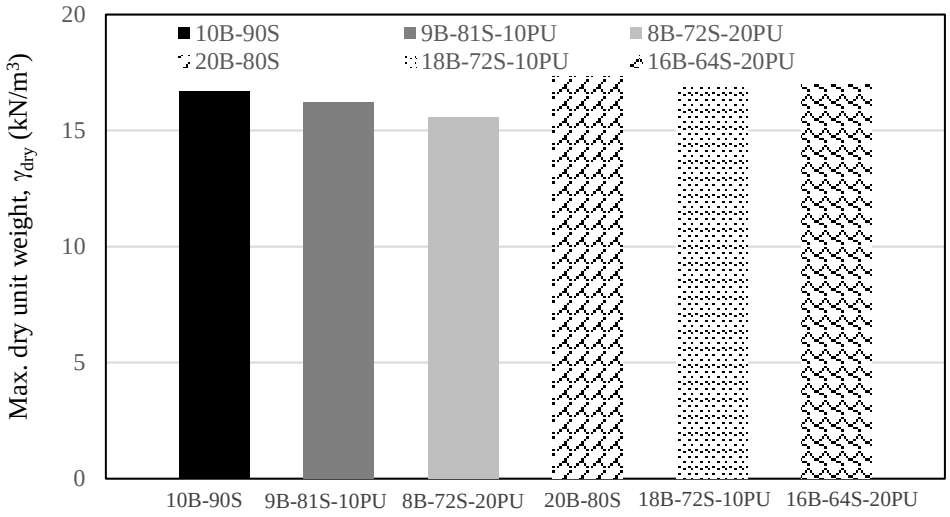


Figure 5.4 Effect of pumice additive on optimum water content for 10B-90S and 20B-80S mixtures

5.2 Volume Deformation Behavior of Pumice Added Sand-Bentonite Mixtures

The volume deformation behavior of pumice added sand-bentonite mixtures was investigated under three different thermal conditions: room temperature, high temperature and thermal cycles.

5.2.1 Volume Deformation Behavior of Pumice Added Sand-Bentonite Mixtures Under Room Temperature

The oedometer test on the pumice sample showed that the total vertical deformation value of pumice under room temperature was determined as 3.98% (Figure 5.5). The swelling deformation value was obtained 0.89%. It was observed that, the pumice has very low swelling potential.

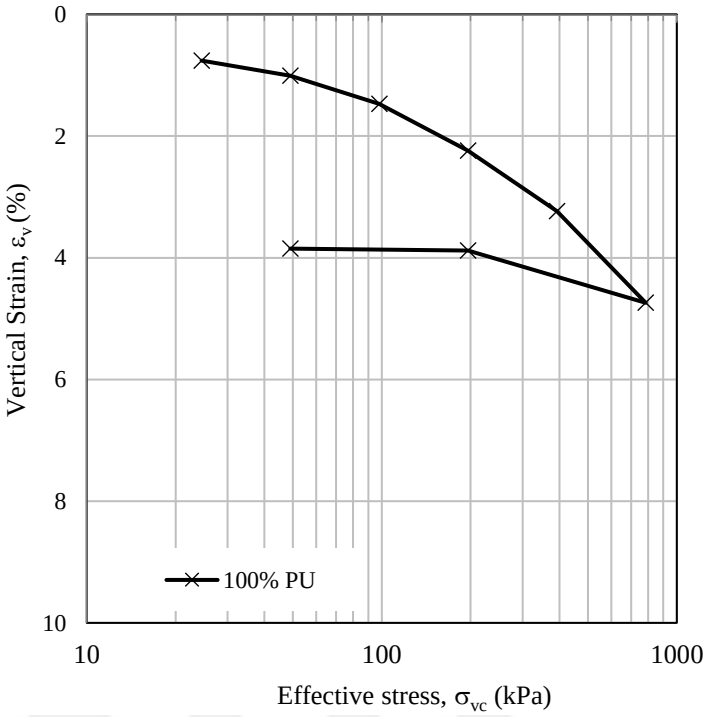


Figure 5.5 Compression and swelling curves of pumice

Table 5.2 Vertical and swelling deformation values of the pumice added sand-bentonite mixtures under room temperature

Mixtures	Vertical Deformation (%)	Swelling Deformation (%)
PU	3.98	0.89
10B-90S	4.56	0.35
10PU-9B-81S	3.71	0.20
20PU-8B-72S	5.92	0.62
20B-80S	10.07	0.91
10PU-18B-72S	17.10	2.62
20PU-16B-64S	16.74	2.60

Compression behavior of 10B-90S and 20B-80S mixtures were determined under room temperature in the presence of 10 and 20% pumice additives (Figure 5.6). The total vertical compression deformation value of the 10B-90S mixture was 4.6%. In the presence of 10% pumice additive of the 10B-90S mixture, the vertical deformation value was determined as 3.7%. It was observed that this value increased to 5.9% with the increase in content of pumice to 20%.

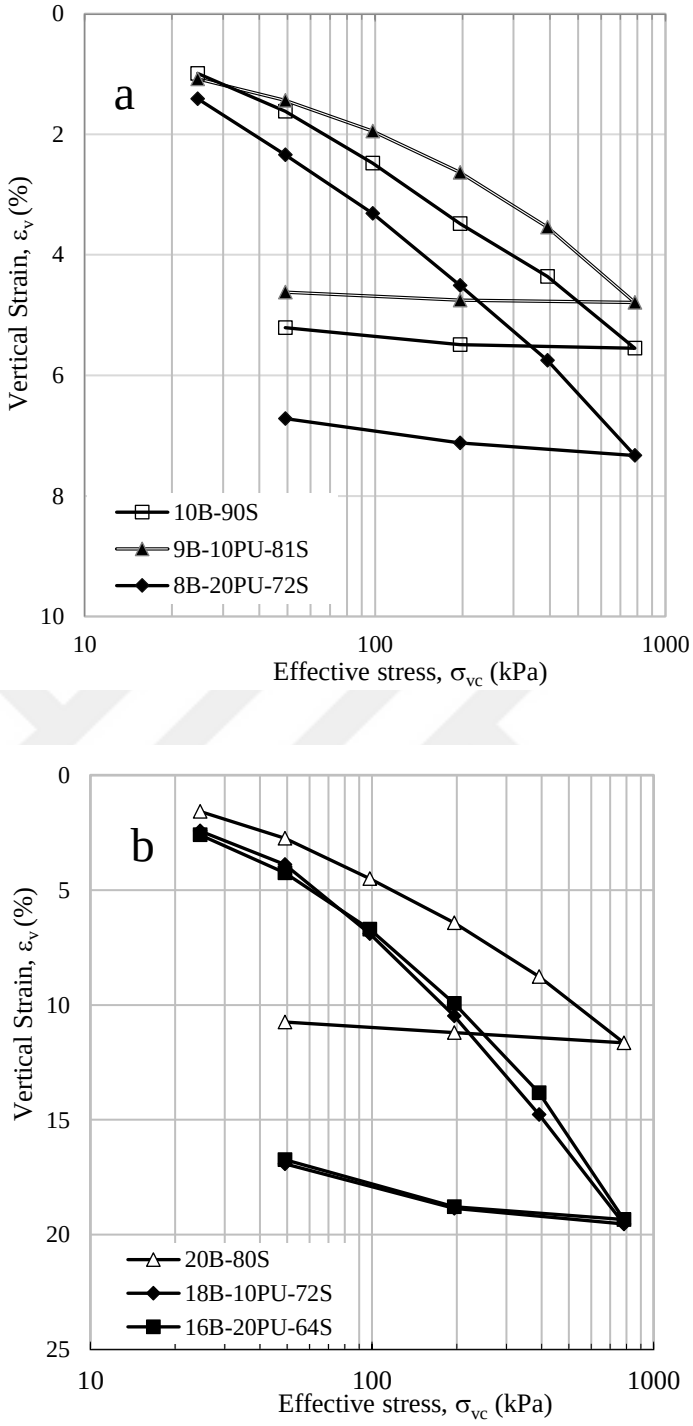


Figure 5.6 Compression and swelling curves of sand-bentonite mixtures under room temperature in the presence of pumice a) 10B-90S, b) 20B-80S

The compression deformation value of the 20B-80S mixture was 10.1%. However, the deformation value increased to 17.1% and 16.7% with 10 and 20% pumice, respectively. Generally, pumice increased the compression deformation values of the 10B-90S and 20B-80S mixtures. When the swelling deformation values were examined,

the pumice increased the swelling deformation amounts in general. The fact that the pumice has a highly porous (spongy) structure and this structure compressed easily when loaded and causes an increase in the amount of compression. When load is unloaded, the pores expand and fill with water with a reversible effect. This behavior causes increase in the amount of swelling.

5.2.2 Volume Deformation Behavior of Pumice Added Sand-Bentonite Mixtures Under High Temperature

The oedometer tests performed under high temperatures in the presence of 10 and 20% pumice on the 10B-90S and 20B-80S mixtures. According to the results, pumice increased the compression deformation of the both mixtures under high temperatures (Table 5.3). The amount of vertical deformation increased 0.4% and 1.3% in the presence of 10% and 20% pumice additives, respectively for 10B-90S mixture. The volumetric deformation behavior of soils in the presence of high temperature investigated by many researchers and it was reported that the amount of vertical deformation (settlement) of soils increases under high temperatures (Cekerevac and Laloui, 2004). However, the amount of deformation depends on the many factors such as the over-consolidation ratio (OCR), temperature range, soil type and soil drainage condition (Jarad, 2016). The reason of this increase in deformation is generally explained with plastic deformation of soils under high temperatures (Delage et al. 2004; Sultan et al. 2002). Although, the samples were compacted and in over-consolidated state, they still continued to contraction under high temperature in this study. This finding is in opposite direction with the some studies in the literature. For example, Cekerevac and Laloui (2004) investigated that samples with a lower OCR value (1.5 and 2) showed contraction behavior at the end of the heating period compared to samples with a higher OCR value (12) as a result of experiments under drained conditions with kaolin. Increase in the OCR value of the soils during heating phase has an increasing effect on the expansion behavior of the soil (Cekerevac, & Laloui, 2004).

There was a negligible decrease in the amount of swelling, due to the decrease in the bentonite ratio in the mixtures. Contrarily, the swelling deformation amounts decreased under high temperature when compared to room temperature. The former studies have

shown that the swelling deformation values were affected negligible under high temperature in general (Jarad, 2016). According to the results, pumice could not reverse this tendency.

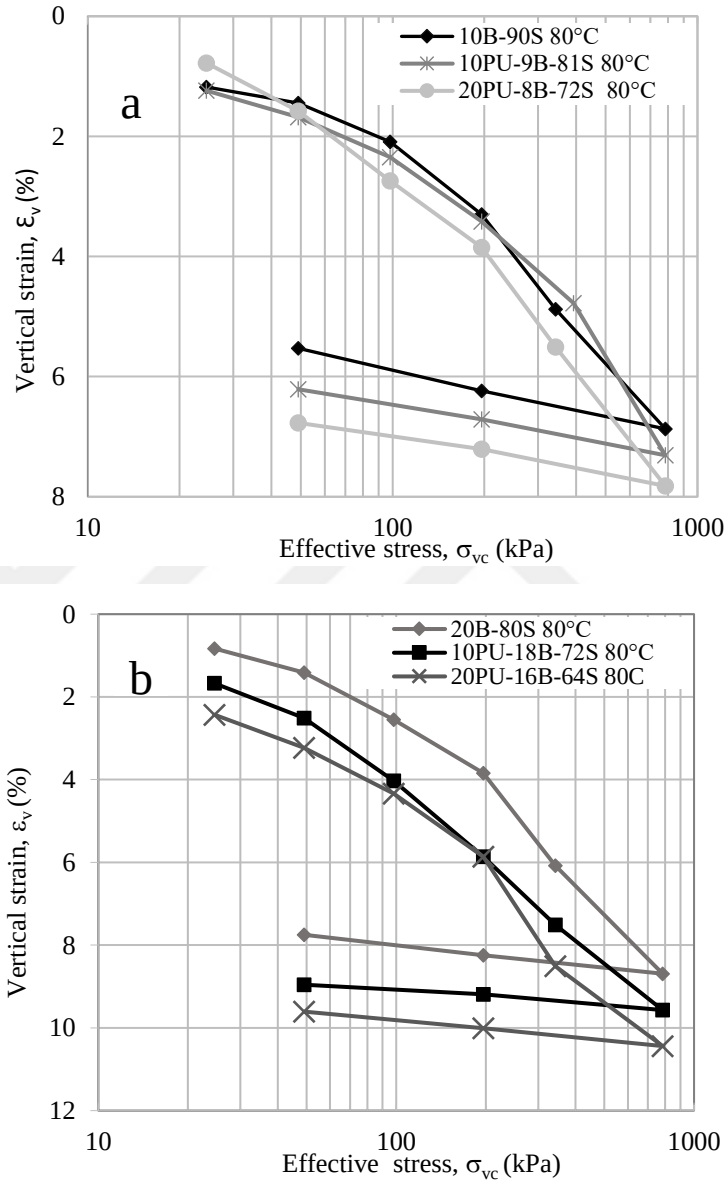


Figure 5.7 Compression and swelling curves of sand-bentonite mixtures under high temperature in the presence of pumice a) 10B-90S, b) 20B-80S

Table 5.3 Vertical and swelling deformation values of the pumice added sand-bentonite mixtures under high temperature

Mixtures	Vertical Deformation (%)	Swelling Deformation (%)
10B-90S	5.69	1.34
10PU-9B-81S	6.07	1.10
20PU-8B-72S	7.04	1.05
20B-80S	7.86	0.94
10PU-18B-72S	7.90	0.61
20PU-16B-64S	8.01	0.83

The compression curves obtained under high temperatures of 20B-80S mixtures in the presence of pumice are given in Figure 5.7. It was observed that the additive-free mixture compression deformation amount decreased from 10.1% to 7.9% with the effect of high temperature. This result is in a good agreement with literature. Under high temperature illitization of bentonite and plastic contraction behavior of soils may cause such decrease in vertical deformation. In additon to these effects Jarad (2016) explained this behavior by the increase in the force between the grains of the clay as a result of heating.

It was determined that pumice additive increased the deformations amounts of the 20B-80S to 7.9% with 10% pumice and to 8.01% with 20% pumice at 80 °C. However, the deformation values attained in both additive contents were negligible. Some researchers performed oedometer tests under high temperature and reported that the compression index did not increase as the temperature was increased, but sometimes it may change negligibly (Finn, 1951; Campanella, & Mitchell, 1968). For example, in this study, while the compression index of 10B-90S mixture was 0.096 under room temperature, it was found to be 0.095 under high temperature, and the compression index of 9B-81S-10PU mixture was determined as 0.043 and 0.066 under room and high temperature, respectively. While the compression index changed negligibly with temperature for 10B-90S of these mixtures, it increased with temperature for the 9B-81S-10PU mixture. It was determined in terms of compression parameters that when pumice is added to the 20B-80S mixture under high temperature, the amount of vertical

deformation did not change significantly and therefore, the mixture can maintain its current state and will not create a situation that restricts its use as a buffer material.

The swelling deformation amount of the 20B-80S mixture at 80 °C was determined as 0.94%. With 10% and 20% pumice additives, the amount of swelling was determined as 0.61% and 0.83%, respectively, and it was observed that the swelling behavior showed a decreasing trend. However, some researchers investigated that the swelling index is independent of temperature (Finn, 1951; Campanella, & Mitchell, 1968). On the contrary, Kale and Ravi (2019) revealed that the swelling pressure of bentonite decreases as the temperature increases. Bag and Rabbani (2017) observed that the swelling pressure increased as the temperature increased. As can be seen from former studies, there is no consensus on the swelling behavior of soils under high temperatures because of several affecting factors. The results of the present study in parallel with the observations of Bag and Rabbani (2017) that swelling potential decreases as temperature increases. Elevated temperature decreases swelling strains in bentonite-sand mixture. It can be attributed to the effect of temperature on double layer state. An increase in temperature causes a decrease in surface potential for a constant surface charge (Mitchell, & Soga, 2005).

5.2.3 Volume Deformation Behavior of Pumice Added Sand-Bentonite Mixtures Under Thermal Cycles

The oedometer tests of 10B-90S and 20B-80S mixtures were performed in the presence of 10% and 20% pumice under temperature cycling. In Figure 5.8a and b, compression curves of 10B-90S and 20B-80S mixtures in the presence of 10% and 20% pumice additives are given under temperature cycling. For temperature cycling, the tests were started at room temperature and when the deformations became insignificant under a stress of 196 kPa, the temperature was increased to 80 °C and deformations were observed. Under this temperature, it was waited until the deformations completed. This stage continued 2 to 5 days depending on the sample. Then the samples were cooled to room temperature. During the cooling stage, the tests were continued (2 to 5 days) by considering the amount of deformation and at the end of this process, the samples were loaded stress level of 392 kPa.

In addition, compression and swelling deformation amounts of 10B-90S mixtures are shown in Table 5.4. According to the test results, for 10B-90S mixture, under normal stress of 196 kPa, although the deformations were completed at room temperature at this stress level, an increase in the compression amount of 0.16% were observed when the temperature was increased to 80 °C. According to the test results, pumice addition to the sand-bentonite mixtures could not prevent increase in vertical deformations during heating phase.

In the unloading stage the additive free samples were unloaded from 784 kPa to 196 kPa, while pumice added samples were unloaded from 392 kPa to 196 kPa. For that reason, the additive free and pumice added samples are not comparable in terms of swelling deformations. As can be seen from Table 5.4 during unloading when the temperature was increased pumice added mixtures start to contraction surprisingly. This behavior was seen for both 10B-90S and 20B-80S samples in the presence of 10% and 20% pumice. It should be noted that this compression behavior under unloading continued during cooling stage, too. It was observed that at the end of heating-cooling cycle generally, swelling and compression deformation amounts neutralized each other.

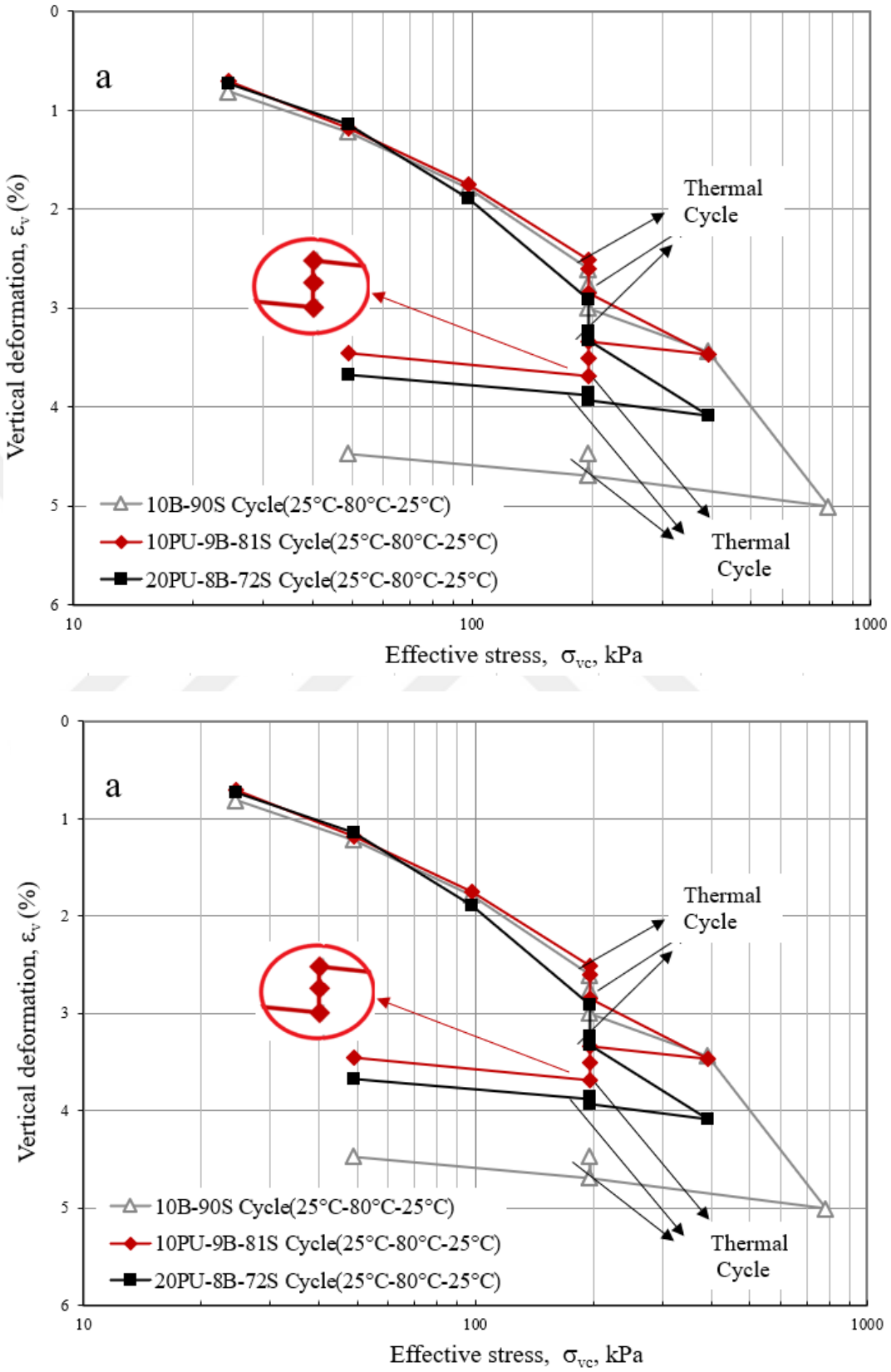


Figure 5.8 Compression and swelling curves of sand-bentonite mixtures under thermal cycle in the presence of pumice a) 10B-90S, b) 20B-80S

Table 5.4 Compression and swelling deformation values of pumice added 10B-90S and 20B-80S mixtures under a temperature cycle

Samples	LOADING				UNLOADING		
	Vertical def. (%) 24.kPa to 196 kPa	Increase in vertical def. (%) after heating 196 kPa	Increase in vertical def. (%) after cooling 196 kPa	Total vertical deformation (%)	Swelling def. unloading 392 kPa to 196 kPa	After heating 196 kPa (%)*	After cooling 196 kPa (%)*
10B-90S	1.8	0.16	0.23	4.2	0.32 (from 784 kPa to 196 kPa)	0.22 ↑	0.22 ↓
10PU-9B-81S	1.8	0.10	0.25	2.8	0.13	0.16 ↓	0.19 ↓
20PU-8B-72S	2.2	0.30	0.10	3.4	0.16	0.13 ↓	0.02 ↓
20B-80S	2.9	0.05	0.26	9.2	0.42 (from 784 kPa to 196 kPa)	0.27 ↑	0.25 ↓
10PU-18B-72S	4.8	0.07	0.22	6.7	0.13	0.18 ↓	0.19 ↓
20PU-16B-64S	4.4	0.58	0.13	6.7	0.13	0.16 ↓	0.30 ↓

↓*: settlement, ↑ swelling

As a result of the heating-cooling cycle applied in the unloading phase, the volume deformation amount of pumice-added mixtures increased in both cases. Towhata et al. (1993) heated MC clay up to 90 °C and observed that volume contraction behavior after heating and noted that the reason of the reason of this is the increase in the consolidation rate or the deterioration of the stiffness of the clay skeleton. Burghignoli et al. (2000) examined the volumetric effects of the thermal cycle in their study on clays under drained conditions and their results were compared with the present study in Figure 5.9, where the void ratio change is shown where a-b: heating phase, b-c: constant temperature, c-d: cooling phase. Similar to Burghignoli et al. (2000) study during (a-b) and immediately after (b-c) heating, the void ratio decreased. However, in the (c-d) part (cooling cycle) the void ratio decreased in the present study. It should be noted that in the present study the samples were over-consolidated. However, Burghignoli et al. (2000) reported that there was no change at the void ratio during cooling. While the void ratio decreases with heating, it does not increase again with cooling, this means that it is not reversible. In support of the former findings mentioned in this study, contraction occurred during heating in both the loading and unloading phases. Expansion behavior

was not observed in the cooling phase and even the contraction behavior continued at negligible level.

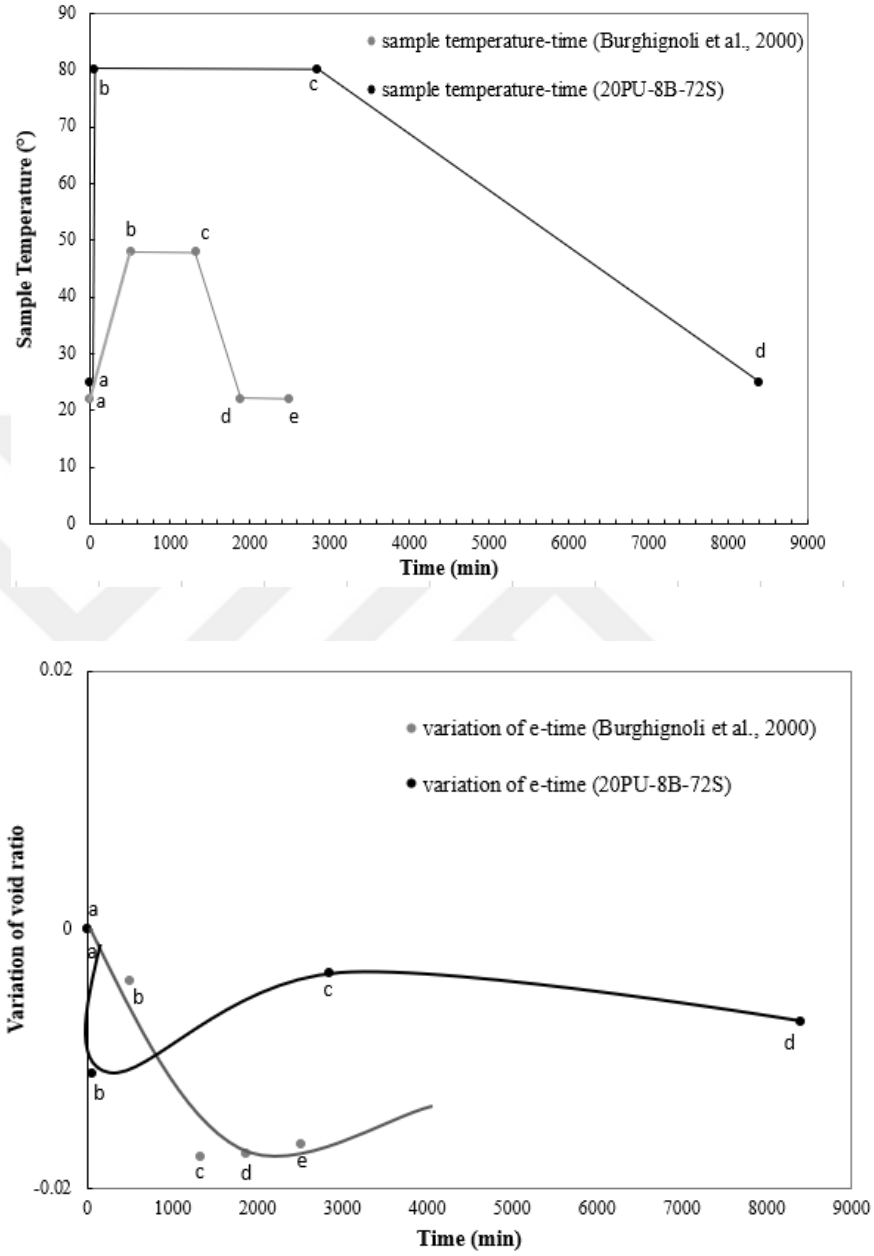


Figure 5.9 The effects of thermal cycling on NC clay and 20PU-8B-72S mixtures

In the literature it is observed that the amount of creep increases as the temperature increases, since the viscosity between particles decreases at high temperatures (Gupta 2013, Schmertmann 2012, Marchall 1960). The results of this study is an agreement with these findings in the literature that as temperature increased creep amount increased as can be seen Figure 5.10.

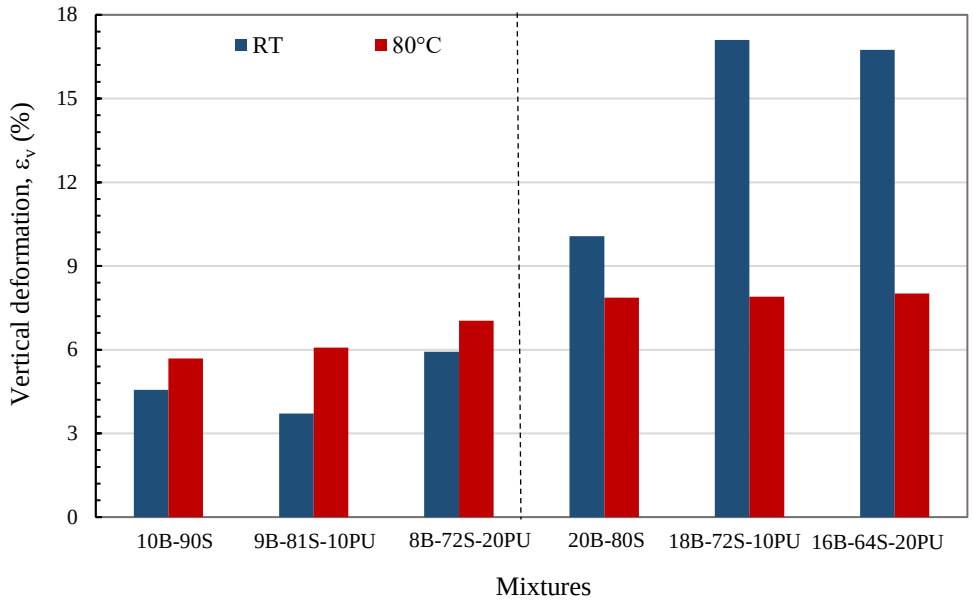


Figure 5.10 The effect of sand-bentonite mixtures on compression amount under room temperature and 80°C in the presence of pumice additive

5.3 Shear Strength Behavior of Pumice Added Sand-Bentonite Mixtures

Direct shear tests of sand-bentonite mixtures were conducted at room temperature and 80 °C in the presence of 10% and 20% pumice additives and the effect of pumice on the shear strength behavior was investigated under high temperature in comparison with room temperature.

5.3.1 Shear Strength Behavior of Pumice Added Sand-Bentonite Mixtures Under Room and High Temperatures

Direct shear tests of sand-bentonite mixtures were performed at room temperature and 80 °C in the presence of 10% and 20% pumice additives. In 10B-90S mixtures, 20% pumice additive increased the internal friction angle both at room and high temperature, while 10% pumice additive caused a slight increase only under high temperature (Figure 5.11). In the variation of their effects between the two additive ratios is negligible, considering the internal friction angle. This effect reflected on the shear strength and affected the maximum shear stress (10% pumice, 102.9 kPa and 20% pumice, 103.8 kPa) values to a negligible extent. Table 5.5 shows the internal friction angle and

cohesion values of 10B-90S and 20B-80S mixtures in the presence of 10% and 20% pumice additives.

Table 5.5 Internal friction angle and cohesion values of sand-bentonite mixtures in the presence of 10% and 20% pumice additives under room and high temperatures

	Room Temperature		**80°C**	
Mixture	**ϕ (°)**	**c (kPa)**	**ϕ (°)**	**c (kPa)**
10B-90S	32.7	40.4	31.5	31.5
9B-81S-10PU	32.7	46.8	34.1	35.4
8B-72S-20PU	36.7	28.7	34.7	29.1
20B-80S	7.0	38.5	13.4	20.0
18B-72S-10PU	11.12	25.4	11.6	29.7
16B-64S-20PU	12.22	32.2	14.5	24.0

In 20B-80S mixtures, both pumice additives increased the internal friction and shear strength under room temperature, while only 10% pumice additive increased the shear stress value under 80 °C. On the other hand, 20% pumice additive increased the internal friction angle insignificantly and almost did not change the shear strength. Therefore, in these tests with 20B-80S mixtures under high temperatures, the pumice additive did not show a significant effect on the shear strength of the mixture.

It was observed that while the drained internal friction angle (ϕ') of the 10B-90S mixture at room temperature was 32.7°, it decreased to 31.5° under high temperature (80°C). The ϕ' values did not change with 10% pumice but increased to 36.7° with 20% pumice content under room temperature. Pumice increased angle of internal friction of the sand-bentonite mixtures even under room temperature. When 10% and 20% pumice were added to 10B-90S mixtures under high temperature, ϕ' values increased to 34.1° and 34.7°, respectively (Table 5.5). It was observed that the ϕ' values increased as pumice was added for the 10B-90S mixture under high temperature.

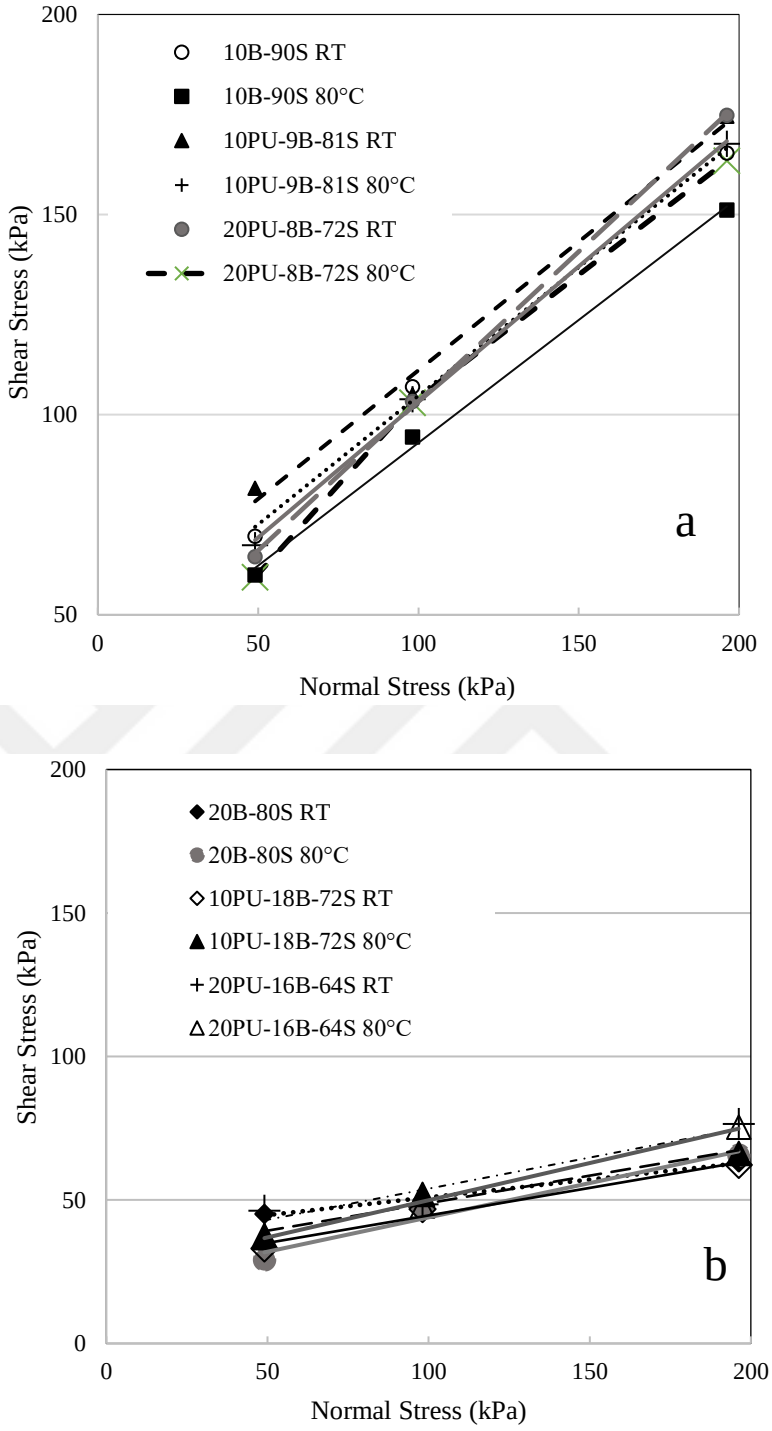
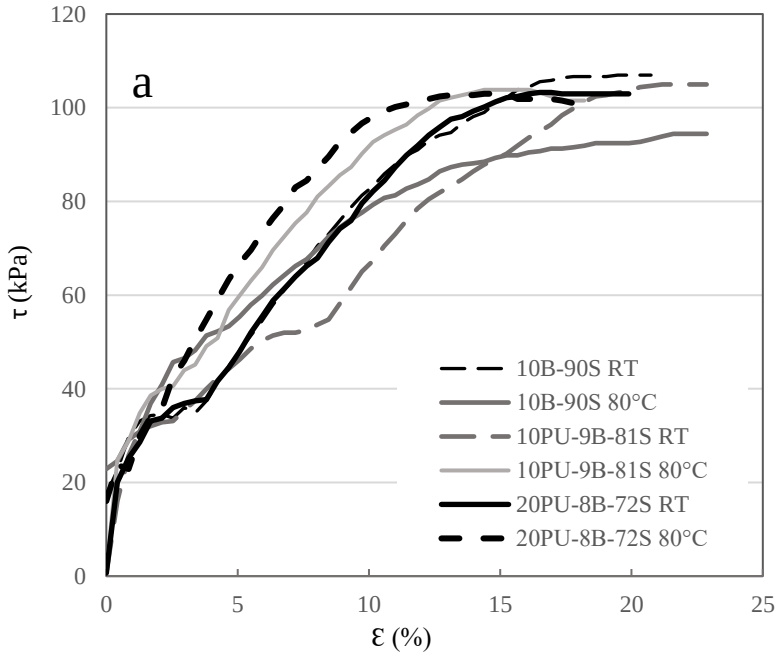


Figure 5.11 Shear stress-normal stress relationship of sand-bentonite mixtures at room and high temperatures in the presence of 10% and 20% pumice additive a) 10B-90S, b) 20B-80S

The maximum shear stress value was 106.9 kPa of the 10B-90S mixture at room temperature (Figure 5.12). Generally, the maximum shear stress values of 10B-90S mixtures decreased slightly when the temperature was increased from room temperature

to 80 °C. In addition, maximum shear stress (τ_{max}) values of the 10B-90S mixture in the presence of 10% and 20% pumice additives increased by approximately 10 kPa under high temperature (Table 5.6).

Direct shear tests results of the 20B-80S mixtures showed that pumice additive increased the internal friction angle values under room temperature similar to 10B-90S mixture. The ϕ' value of the 20B-80S mixture at room temperature was 7.0°, while this value increased to 11.1° and 12.2° with 10% and 20% pumice additives, respectively. However, the cohesion (c') value decreased with 10% and 20% pumice addition under room temperature (Table 5.6). Under high temperatures, adding 10% pumice reduced the internal friction angle from 13.6° to 11.6°. In contrast, the addition of 20% pumice increased the internal friction angle to 14.5°. The maximum shear stress values slightly increased for 20B-80S mixtures when the temperature was increased from room temperature to 80°C. However, it should be noted that the ϕ' values increased especially in the presence of 20% pumice additives under high temperature.



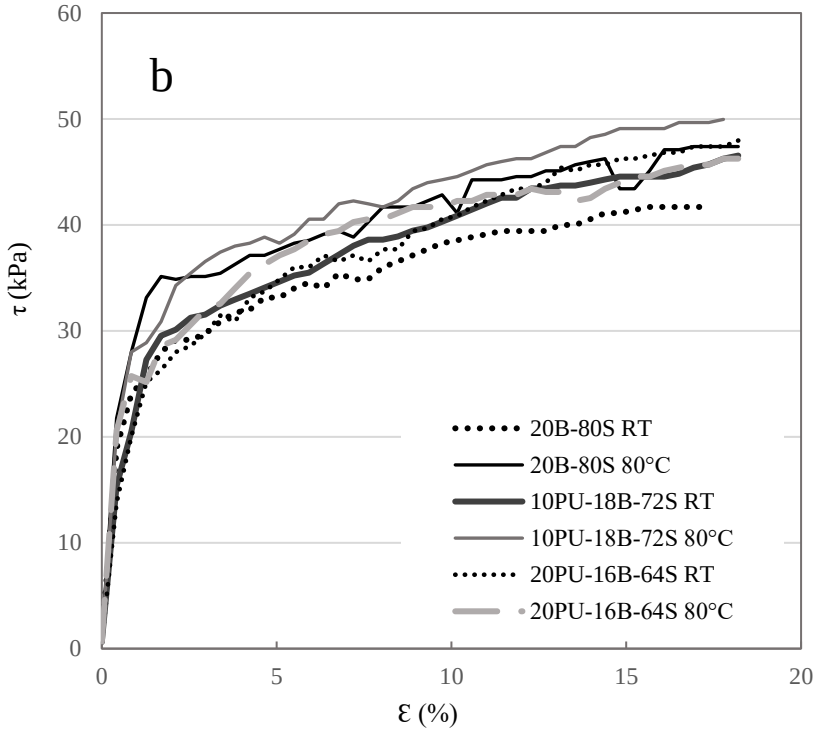


Figure 5.12 τ- ε relationship of sand-bentonite mixtures in the presence of of 10% and 20% pumice a) 10B-90S, b) 20B-80S

Table 5.6 Maximum shear stress values of sand-bentonite mixtures in the presence of 10% and 20% pumice under room and high temperatures

	Room Temperature (under 98 kPa)	**80 °C (under 196 kPa)**
Mixture	**Maximum Shear Stress (kPa)**	
10B-90S	106.97	94.42
9B-81S-10PU	104.97	103.83
8B-72S-20PU	102.98	102.98
20B-80S	41.69	47.39
18B-72S-10PU	46.54	49.96
16B-64S-20PU	47.96	46.25

Former studies have shown that the shear strength increases under high temperature (Cekerevac, & Laloui, 2004). The results of this study showed that pumice contributes to the shear strength of SBMs under high temperature positively. This is because pumice has silanol (Si-OH) groups on its surface and this silanol group binds hydroxyl groups at the edges of the clay platelets (Ogawa et al. 1998). As a result, the pumice is held by the clay surface and positive charge increases on the clay surface. Hence, the shear

strength of bentonite increased even under room temperature. Another reason is when pumice is added to the sample, both the bentonite and sand content of the mixture decreased; with decrease in the amount of bentonite, the shear strength increased.

5.3.2 Shear Strength Behavior of Pumice Added Sand-Bentonite Mixtures Under Thermal Cycles

The direct shear tests of pumice added SBMs were performed under temperature cycle. In the temperature cycling tests, the samples consolidated under normal stress value (196 kPa) and then consolidation stage was continued during 8 hours with heating (80 °C) and then cooling stage was applied for 16 hours. Then, during shearing stage the samples were kept under room temperature.

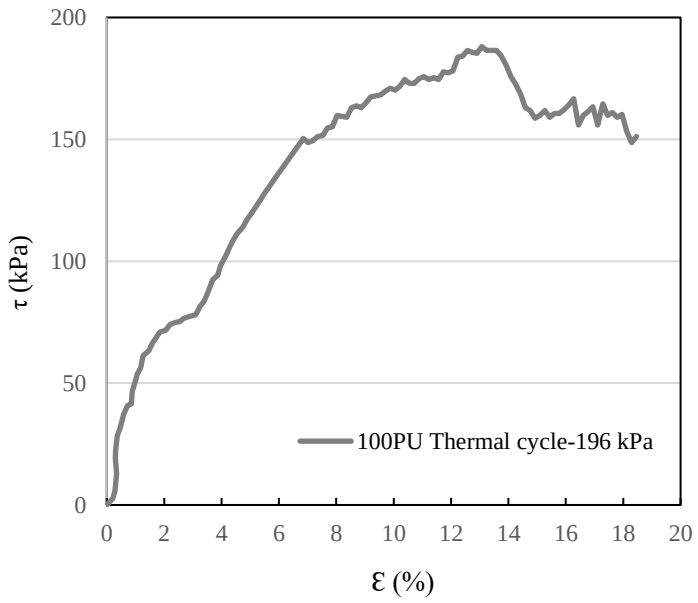


Figure 5.13 Shear stress-strain relationship of pumice under thermal cycling

The maximum shear stress value of the pumice was found to be 188.05 kPa due to the temperature cycle applied under a stress of 196 kPa (Figure 5.13). In the previous tests which were performed under room temperature and 80 °C, it was observed that the maximum shear stress values at were found to be 196.5 kPa and 137 kPa, respectively. It was observed that the shear strength at room temperature decreased under temperature cycling and high temperature when compared with room temperature.

Figure 5.14a shows the shear strength values of 10B-90S mixtures in the presence of pumice and by performing 8 hours heating-16 hours cooling cycle before the specimens were sheared. The maximum shear stress value obtained for the 10B-90S mixture was determined as 248.8 kPa during thermal cycle. It should be noted that, the maximum shear stress value of pumice was determined as 188 kPa. When 10% pumice and 20% pumice were added to this mixture, the maximum shear stress values were obtained as 222.6 kPa and 244.8 kPa, respectively under temperature cycle. The decrease in shear strength of soils with increase in temperature is explained that increase in pore water pressure under temperature reduces strength of the sample and causes it to weaken (Jarad, 2016). Even though the direct shear tests were performed under drained conditions, decrease in shear strength were observed under temperature cycling. However, this decrease was less than those of tests under high temperature. Because of application cooling stages reversed decreasing trend in shear strength.

Table 5.7 Maximum shear stress values of sand-bentonite mixtures in the presence of 10% and 20% pumice under room and high temperatures and thermal cycle (under 196 kPa normal stress)

	Room Temperature	**80 °C**	**Temperature cycling**
Mixture	**Maximum Shear Stress (kPa)**		
PU	112.81	78.48	188.05
10B-90S	165.789	94.42	248.81
9B-81S-10PU	174.618	103.83	222.60
8B-72S-20PU	174.618	102.98	244.84
20B-80S	63.1	47.39	176.13
18B-72S-10PU	61.803	49.96	168.19
16B-64S-20PU	76.518	46.25	166.99

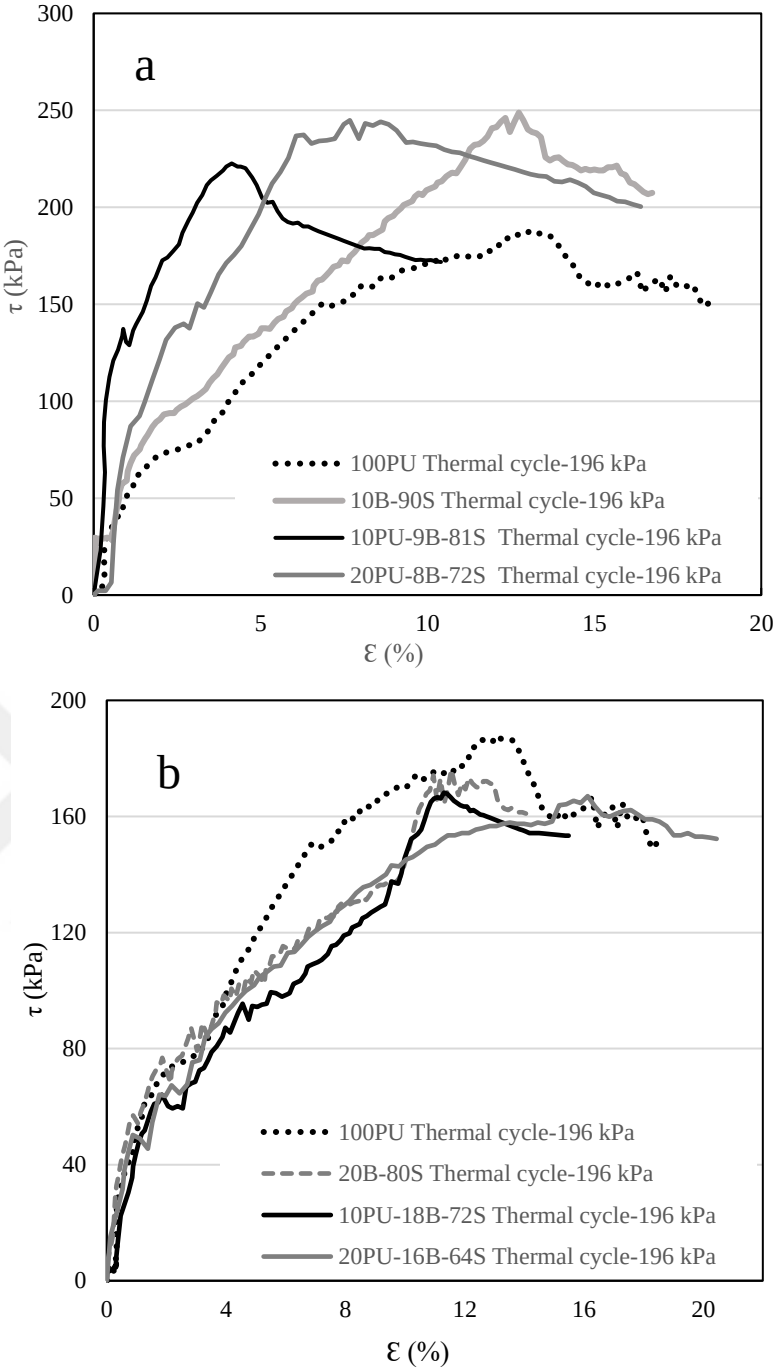
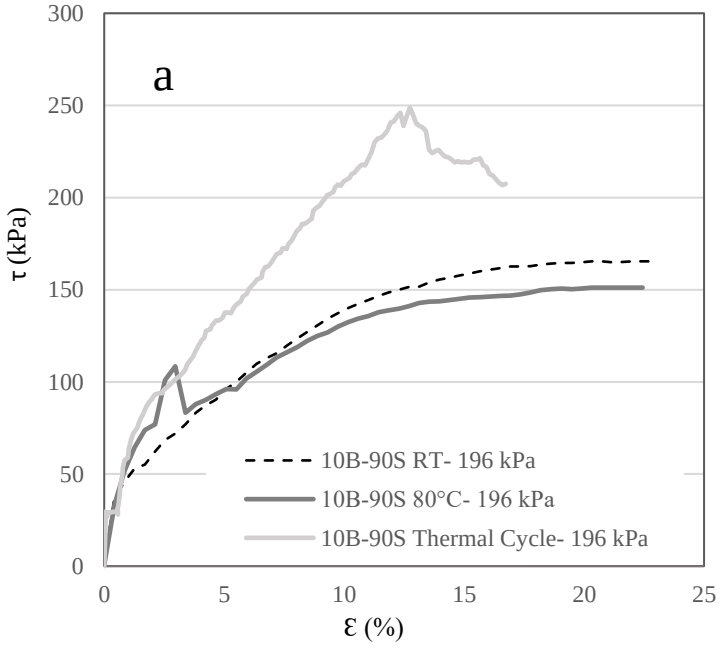


Figure 5.14 Shear stress-strain relationship of sand-bentonite mixtures under thermal cycling in the presence of pumice a) 10B-90S, b) 20B-80S

It was observed that the maximum shear stress values attained highest values under temperature cycling for all mixtures, while the lowest maximum shear stress values were obtained under high temperature conditions.

Figure 5.14b shows the strain-shear stress relationship of 20B-80S mixtures in the presence of pumice additive and temperature cycling. The maximum shear stress value of the 20B-80S mixture was determined as 176.1 kPa. Adding pumice to the mixture decreased the shear strength of the sand-bentonite mixture with thermal cycling. In addition, there were no difference between 10% and 20% pumice contents (168 kPa and 167 kPa, respectively). Table 5.7 shows the maximum shear stress values of sand-bentonite mixtures in the presence of 10% and 20% pumice additives under room and high temperatures and thermal cycle, comparatively. Generally, it was observed that the shear strength increased significantly under thermal cycles.

The τ-ε relationships of 10B-90S and 20B-80S mixtures at 196 kPa normal stress level under room and high temperature and thermal cycle are given in Figure 5.15. It was seen that the maximum shear stress (248.8 kPa) attained during thermal cycle, it was followed by room temperature (165.4 kPa), and the lowest maximum shear stress value (151.1 kPa) was obtained under high temperature for 10B-90S mixtures. On the other hand, the maximum shear stress reached its highest value during the thermal cycle (174.1 kPa), and shear strength values were close to each other at room temperature (63.0 kPa) and high temperature (65.9 kPa) for 20B-80S mixtures.



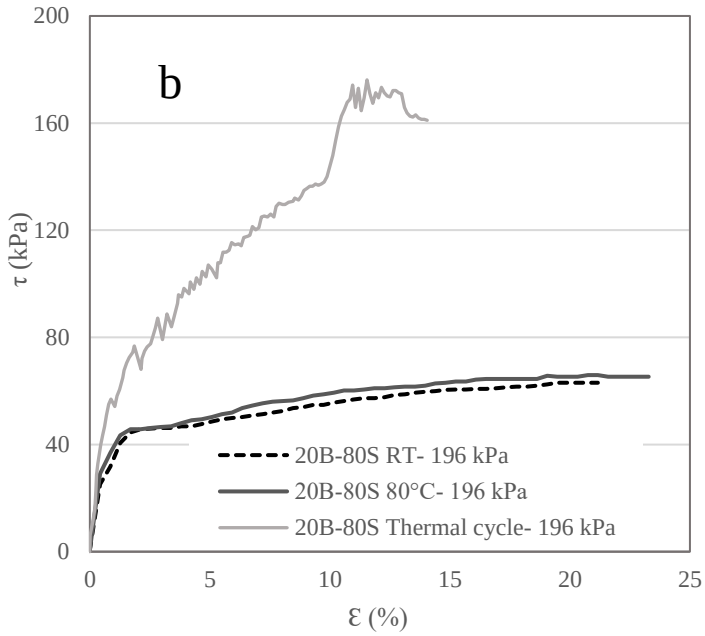


Figure 5.15 Comparison of maximum shear stresses under room, high temperature and thermal cycles cycling in the presence of pumice a) 10B-90S, b) 20B-80S

According to the results of the direct shear test conducted under temperature cycle and at 196 kPa stress level, the shear strength values of the mixtures decreased as the pumice was added to the sand-bentonite mixtures. It was observed that the pumice additive decreased the shear strength of the 10B-90S mixtures, while it had a negligible effect on the 20B-80S mixtures (Figure 5.16).

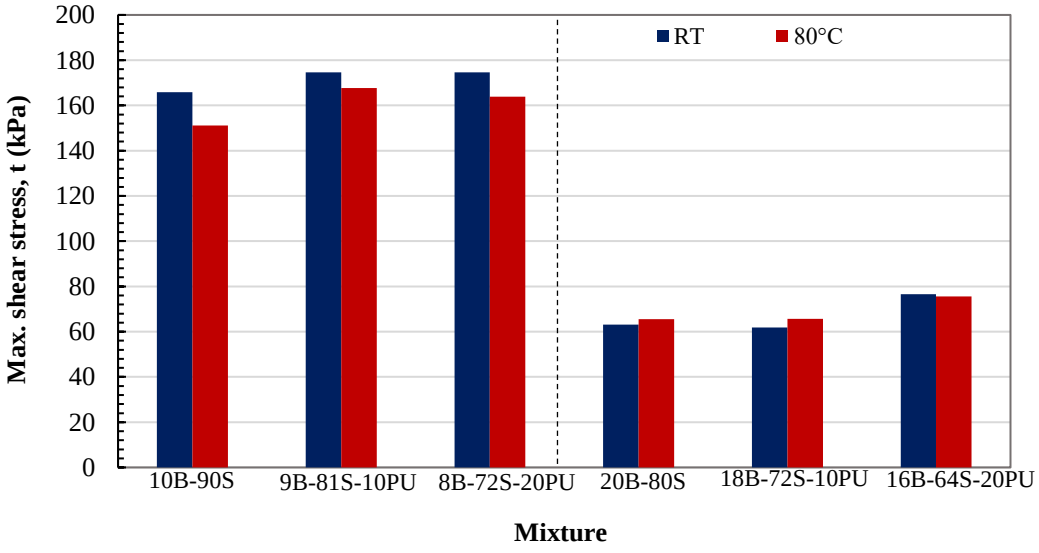


Figure 5.16 Maximum shear strengths of pumice added sand-bentonite mixtures at room temperature and 80 °C

5.4 Hydraulic Conductivity Behavior of Sand-Bentonite Mixtures Under Room-High Temperatures and Thermal Cycles

The hydraulic conductivity values of the 10B-90S and 20B-80S mixtures were determined in the presence of under different temperature values, starting from room temperature and to 80 °C. The water temperature was gradually increased, from 25 to, 50 and 80 °C, respectively and the sample temperature was determined as approximately 20, 40 and 60 °C.

Figures 5.17a and b show the hydraulic conductivity versus pore volume of flow values of the 10B-90S mixtures in the presence of 10% and 20% pumice additives. The temperature dependent k values of the 9B-81S-10PU mixture are given in Table 5.8. It was observed that the hydraulic conductivity of the 9B-81S-10PU mixture increased with increasing temperature. One of the reason of this decrease in water viscosity as the temperature increases. The reduced viscosity allow the water to flow more easily. However, it was reported that structural changes in the soil skeleton may also cause changes in hydraulic conductivity (Villar and Lloret, 2004).

Table 5.8 Variation of hydraulic conductivity values of 9B-81S-10PU and 8B-72S-20PU mixtures with temperature cycling

	Sample			
	9B-81S-10PU	**8B-72S-20PU**	**18B-72S-10PU**	**16B-64S-20PU**
Temperature (°C)	**k (m/s)**			
25	3.1×10^{-11}	1.4×10^{-10}	4.4×10^{-11}	1.5×10^{-10}
50	1.4×10^{-10}	2.0×10^{-10}	4.1×10^{-11}	8.5×10^{-11}
80	2.1×10^{-10}	3.8×10^{-10}	5.9×10^{-10}	9.4×10^{-11}
50	2.1×10^{-10}	2.9×10^{-10}	5.4×10^{-10}	7.6×10^{-11}
25	-	1.6×10^{-10}	-	5.2×10^{-11}

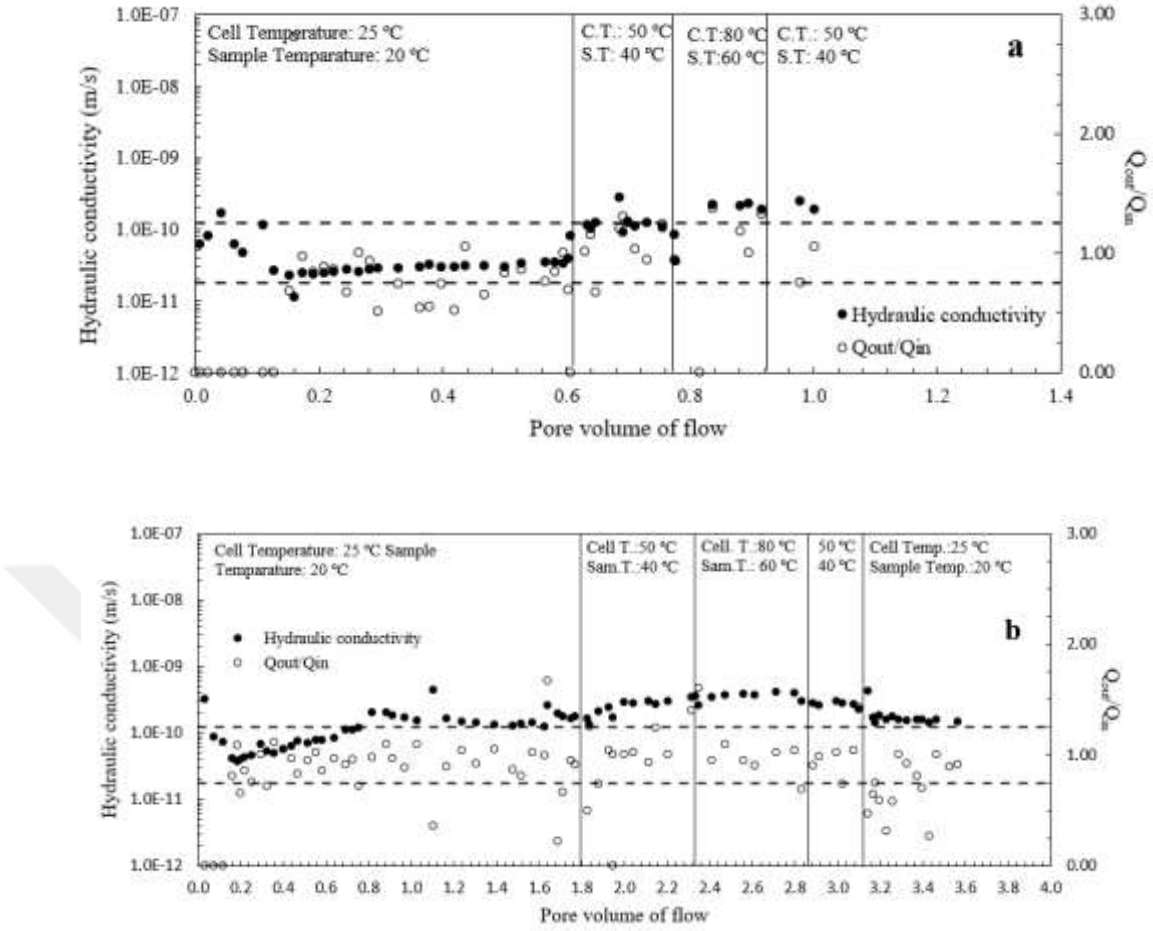


Figure 5.17 Hydraulic conductivity versus pore volume of flow graph of 10B-90S mixture a) 10% pumice b) 20% pumice

It was observed that pumice increased the hydraulic conductivity of 10B-90S mixtures. The hydraulic conductivity tests under the effect of temperature for the 16B-64S-20PU mixture is given in Figure 5.18. The hydraulic conductivity value determined at room temperature as 1.5×10^{-10} m/s, this value decreased to 8.5×10^{-11} m/s with increasing temperature. Although the expected behavior here is an increase in the flow rate, a decrease was observed only in the beginning of the experiment due to pumice existense in the mixture. The results showed that pumice had a positive contribution to the hydraulic conductivity of 20B-80S mixtures. However, in the other heating-cooling phases of the test, the trend turned to opposite direction. As the temperature increased the hydraulic conductivity increased and decreased as the temperature decreased in small amounts, depending on the behavior of the viscosity of the water (Sultan, 1997; Delage et al., 2000; Chen et al.,2014).

Generally, it was observed that the hydraulic conductivity coefficient increased when temperature increased. During cooling stage the hydraulic conductivity started to decrease, however at the end of thermal cycle it was observed that the sample could not return to its initial value. Because as temperature increased, the viscosity of the water decreased and the flow rate increased. However, the results showed that only change in water viscosity cannot explain change in hydraulic conductivity. After thermal cycles samples could not return to initial value, this indicates that structural changes occur in the body of the sample. As the reason for this situation, it can be shown that the temperature changes the pore structure of the grains. Similarly, Romero et al. (2001) reported that hydraulic conductivity is not only affected by changes in viscosity but also thermal changes have effects on soil-water interaction at the microstructural level.

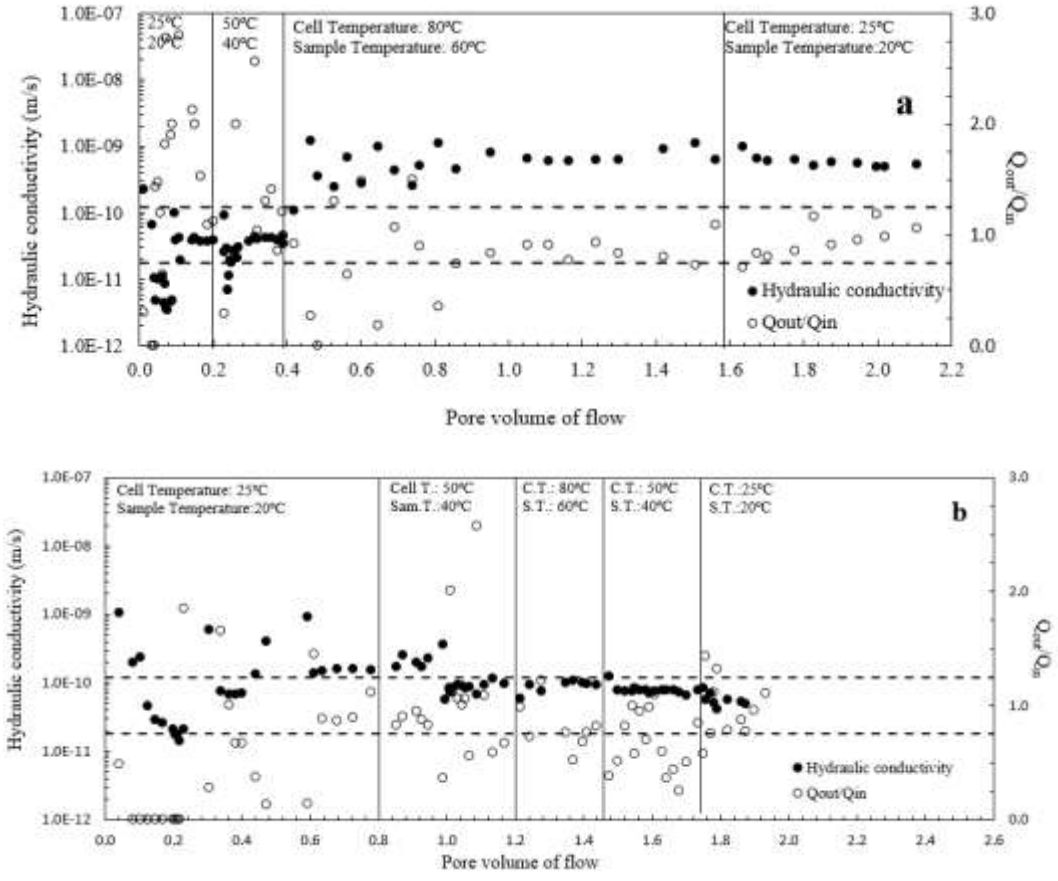


Figure 5.18 Hydraulic conductivity versus pore volume of flow of 20B-80S mixture a) 10% pumice b) 20% pumice

Other studies have shown that as the temperature increases, the texture of the clays changes and larger voids are formed in the soil (Pusch and Güven, 1990; Pons et al.,

1994; Thomas et al., 1994; Romero et al., 2001). It was reported that high temperature causes a weakening of the microstructure as it creates larger voids in the soil (Chen et al., 2017).

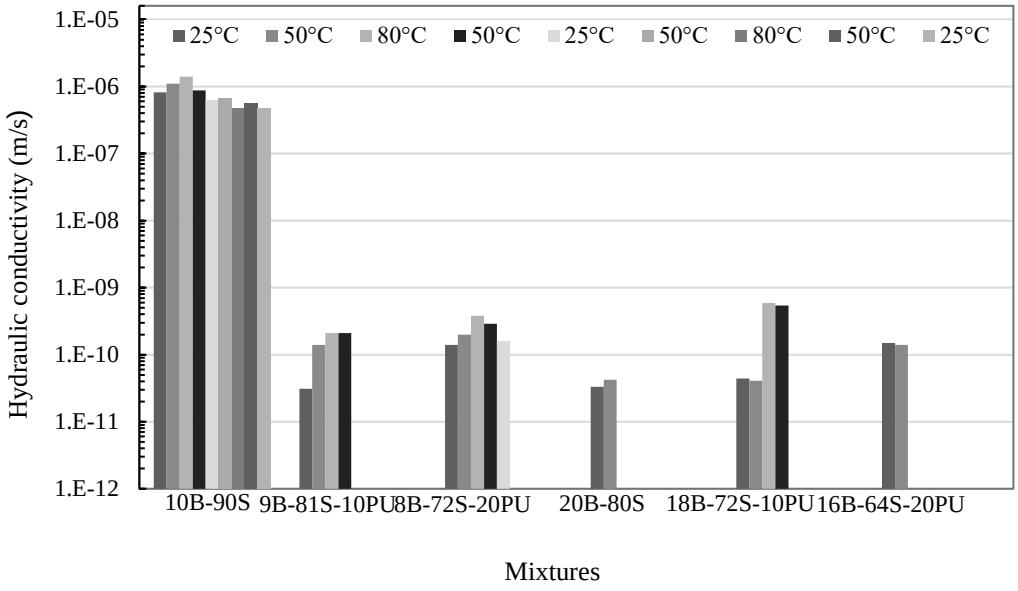


Figure 5.19 Hydraulic conductivity values of sand-bentonite mixtures under different temperatures in the presence of pumice

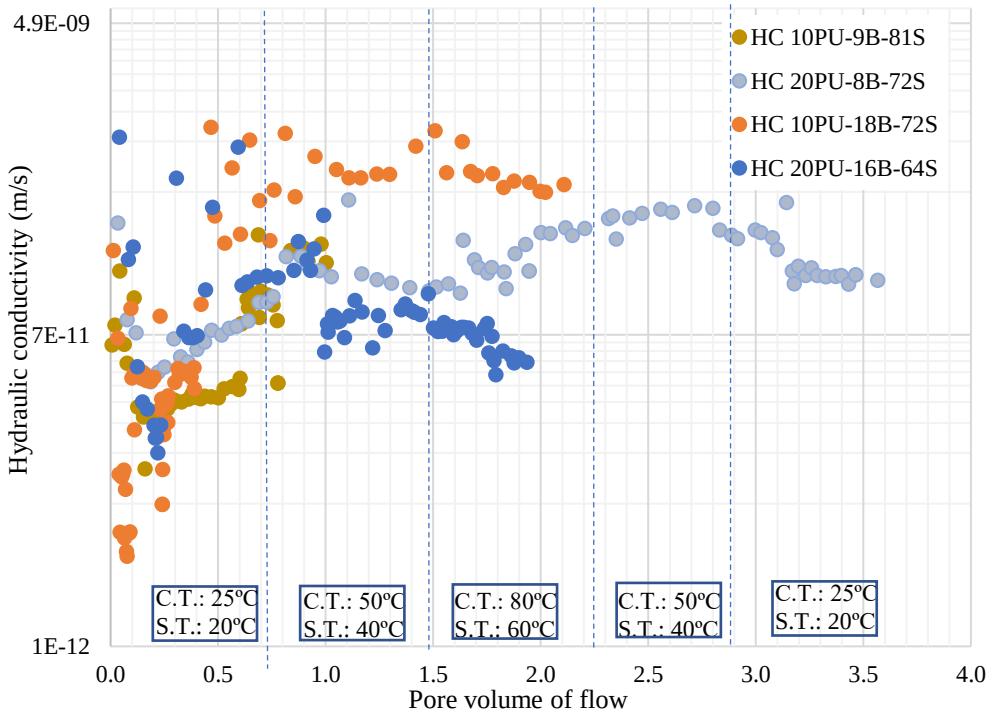


Figure 5.20 Comparison of hydraulic conductivity behavior of pumice added sand-bentonite mixtures under temperature cycling

In general, the hydraulic conductivity test results of sand-bentonite mixtures in the presence of pumice under temperature cycle showed that the hydraulic conductivity increased with the effect of temperature, and decreased during cycle, but did not reach its initial value (Figure 5.19).

In Figure 5.20, hydraulic conductivity values of pumice added sand-bentonite mixtures under the temperature cycle are given, comparatively. It was determined that the 10PU-18B-72S mixture had the lowest hydraulic conductivity under room temperature, but the highest hydraulic conductivity increase was observed in this mixture when room temperature was increased to 50 °C. It was observed that the hydraulic conductivity values of all mixtures increased as the temperature increased and decreased slightly when the temperature decreased depend on the viscosity of water and structural changes (Villar, & Lloret, 2004).

5.5 Thermal Conductivity of the Sand-Bentonite Mixtures in the Presence of Pumice

In this thesis, thermal conductivity values of 10B-90S and 20B-80S mixtures were measured in the presence of 10% and 20% pumice. The thermal conductivity values measured on the samples with constant void ratio and saturation degree are given in Table 5.9. The void ratio and saturation degree values are the most important parameters for that reason these parameters were chosen as parameters, which were constant for all samples, at each sample group as seen in Table 5.9. It should be noted that depending on the mixture the “e” and “S” values were choosen seperately. In the first set of samples, all samples were prepared at same void ratio (e=0.6). In the second set, both saturation degree and void ratio were constant. It should be noted that depending on the mixture, there were too much difference between the “S” and “e” values. For that reason, for each mixture constant values were choosen seperately.

The thermal conductivity value of the pumice was measured as 0.905 W/mK as a result of the tests performed at the void ratio 0.6. When “e” and “S” values were constant for the prepared samples, the termal conductivity value (0.878 W/mK) did not change significantly. The thermal conductivity values of the sand-bentonite mixtures were higher than this value and the thermal conductivity values of the mixtures decreased as

pumice was added to these mixtures. In addition, the test results showed that the thermal conductivity value increased as bentonite content in the mixtures increased. The main reason is that bentonite has a high water-holding capacity, considering that water is a conductive substance.

Table 5.9 Thermal conductivity values of sand-bentonite mixtures in the presence of 10% and 20% pumice

Mixtures	**Thermal Conductivity (W/mK) (e= 0.6 constant)**	**Thermal Conductivity (W/mK) ("S" and "e" constant)**	
100 PU	0.905	0.878	S = 0.82 e = 0.97
10B-90S	1.153	1.779	S = 0.71 e = 0.64
9B-81S-10PU	1.142	1.588	
8B-72S-20PU	1.011	1.426	
20B-80S	1.971	1.461	S = 0.73 e = 0.76
18B-72S-10PU	1.950	1.950	
16B-64S-20PU	1.932	1.776	

The decrease in the thermal conductivity of the mixture as the pumice additive increases shows that pumice, which is used in thermal insulation, can be added to sand-bentonite mixtures and used as an insulation barrier around energy geo-structures and facilities. Previous studies report that the thermal conductivity of the mixture increases as the percentage of sand increases. However, another study shows that, depending on the sample's dry density and water content, the thermal conductivity may remain constant or even decrease with the increase of the sand content (at values above the limit value it will reach) (Xu et al., 2016). In this case, the thermal conductivity value of the 10B-90S mixture is expected to be higher than the 20B-80S mixture. While measurement results based on the constant void ratio and saturation degree support this behavior.

5.6 Scanning Electron Microscope (SEM) Analyses

The 10B-90S and 20B-80S mixtures were analyzed by scanning electron microscope (SEM) at room temperature and 80 °C in the presence of pumice. The mixtures were selected especially where the effects were more significant (especially at high temperatures) and structures of these mixtures at room temperature and 80 °C were investigated by SEM analyses.

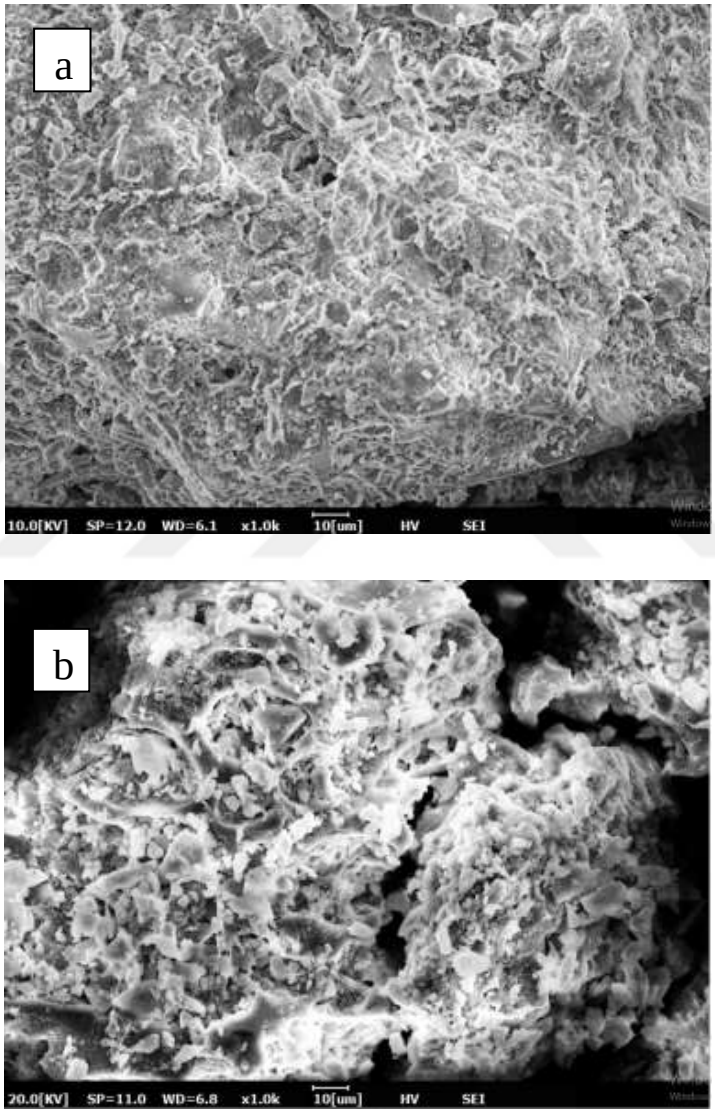


Figure 5.21 Scanning electron microscope photographs of pumice, (a) room temperature (x1000) and (b) 80 ˚C (x1000)

The SEM photographs of pumice sample was taken at room and 80 °C temperatures. The flake-shaped particles of pumice are visible from the SEM photograph in Figure

5.21. The voids in the structure of the pumice increase its water absorption capacity. But at the same time, its porous nature can lead that any fluid passing through. When the SEM photographs under room temparature and 80 °C were compared, decrease in pores and more contracted structure easily can be seen.

CHAPTER 6
PERLITE EFFECT ON THE VOLUME DEFORMATION, SHEAR STRENGTH, HYDRAULIC CONDUCTIVITY AND THERMAL CONDUCTIVITY BEHAVIOR OF SAND-BENTONITE MIXTURES

6.1 Compaction Behavior of Perlite Added Sand-Bentonite Mixtures

The compaction parameters of the perlite added sand-bentonite mixtures were determined by Standard Proctor tests (ASTM D-698, 2012) and the test results were given in Table 6.1. The maximum dry unit weight and optimum water content values of the 10B-90S mixture were determined as 16.6 kN/m^3 and 13%, respectively. The dry unit weight of perlite was 2.9 kN/m^3 and w_{opt} was determined as 240%. It should be noted that perlite have high water holding capacity and low dry density. The maximum dry unit weight of the mixture with 10% perlite decreased to 14.8 kN/m^3 and w_{opt} increased to 20%. When perlite content in the mixture was increased from 10% to 20%, the maximum dry unit weight decreased to 13.1 kN/m^3 and the w_{opt} reached to 30%. The test results showed that the perlite additive decreased the dry unit weight of 10B-90S mixtures and increased the optimum water content.

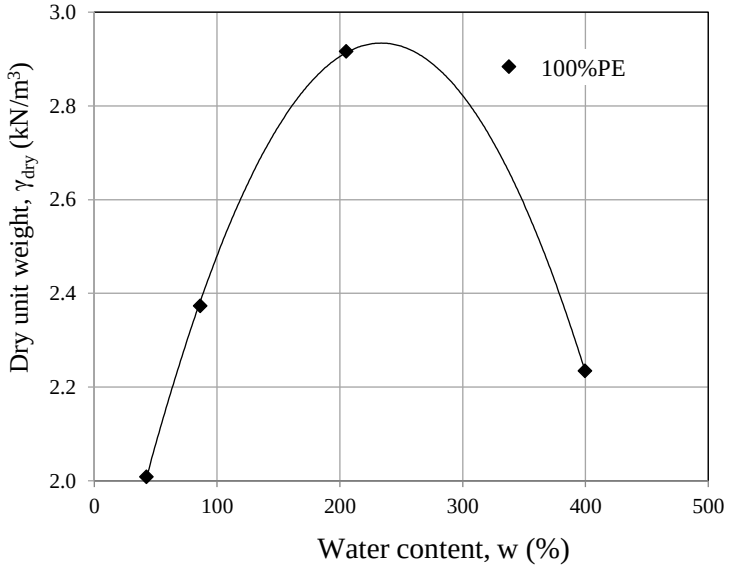
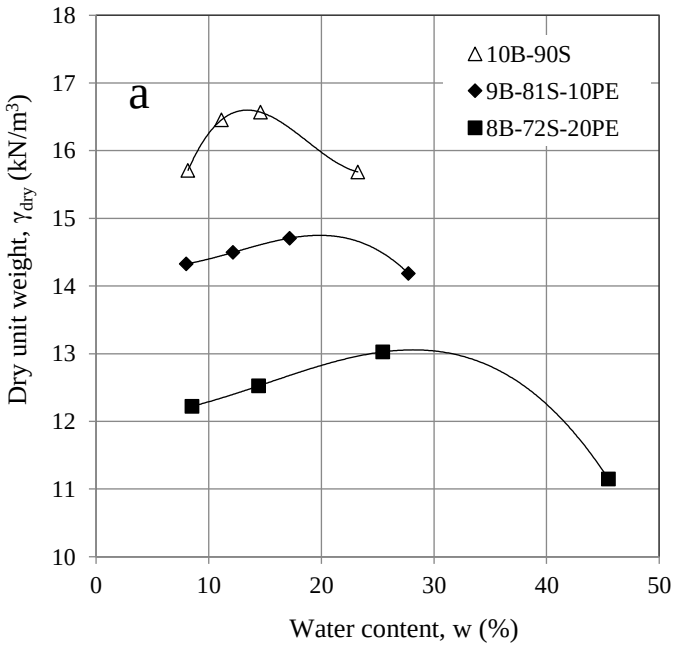


Figure 6.1 Compaction curve of perlite

Table 6.1 Compaction characteristics of perlite added sand-bentonite mixtures

Group	Sample	$\gamma_{d,max}$ (kN/m^3)	w_{opt} (%)
	PE	2.90	240.0
10% bentonite	10B-90S	16.70	15.5
	9B-81S-10PE	14.50	17.5
	8B-72S-20PE	13.10	24.7
20% bentonite	20B-80S	15.60	17.5
	18B-72S-10PE	11.10	30.0
	16B-64S-20PE	8.80	60.0

Addition of perlite to the 20B-80S mixtures showed same trend similar to 10B-90S mixtures. While the dry unit weight of the 20B-80S mixture was 15.6 kN/m^3, this value decreased to 11.1 kN/m^3 and 8.8 kN/m^3, respectively with 10% and 20% perlite contents. On the other hand, the w_{opt} values increased from 17.5% to 25% and 50%, with 10% and 20% perlite additives, respectively.



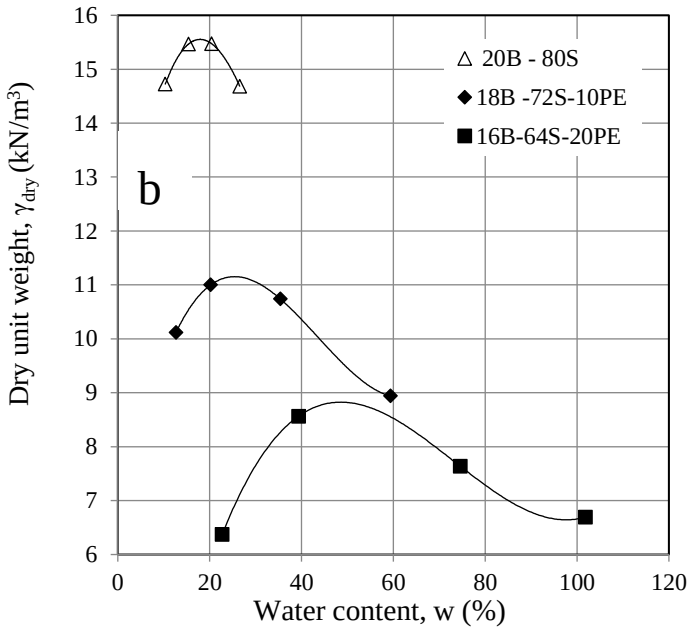
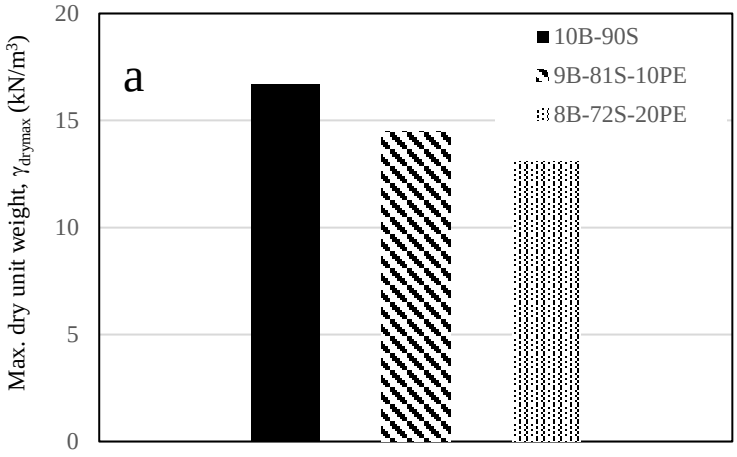


Figure 6.2 Compaction curves of sand-bentonite mixtures with perlite a)10B-90S mixtures, b)20B-80S mixtures

The effect of perlite additive on optimum water content and maximum dry unit weight was investigated. When perlite additive was added to sand-bentonite mixtures, the maximum dry unit weight was reduced due to its low dry unit weight (2.9 kN/m^3) (Figure 6.3).



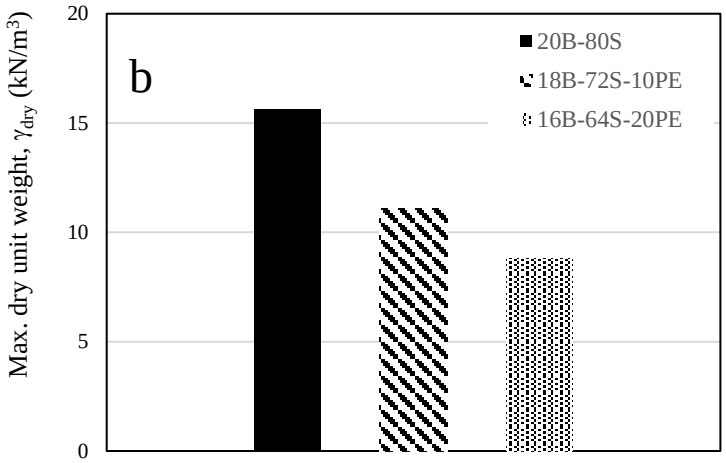


Figure 6.3 Effect of perlite on the maximum dry unit weight a) 10B-90S mixtures, b) 20B-80S mixtures

The perlite additive increased the water content of both mixtures. Because of highly porous material, perlite can adsorb more water and its liquid limit so high (375%) (Figure 6.4).

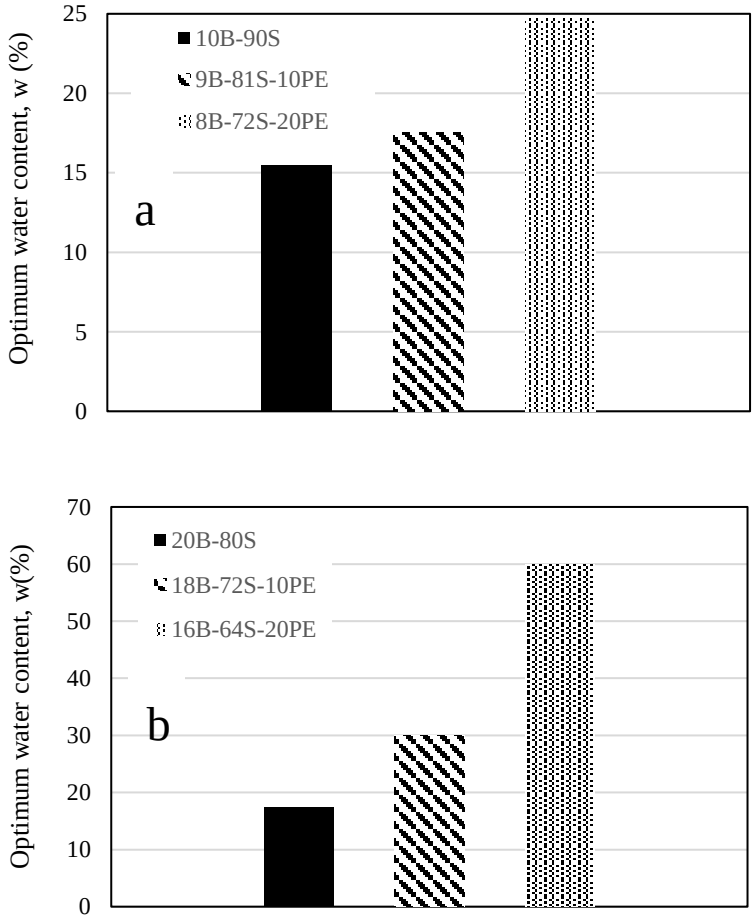


Figure 6.4 Effect of perlite on the optimum water content a) 10B-90S mixtures, b) 20B-80S mixtures

6.2 Volume Deformation Behavior of Perlite Added Sand-Bentonite Mixtures

The volume deformation behavior of perlite and sand-bentonite mixtures was investigated under three conditions: room temperature, high temperature and thermal cycles. The effects of thermal conditions and perlite on the volume deformation behavior of sand-bentonite mixtures were investigated.

6.2.1 Volume Deformation Behavior of Sand-Bentonite Mixtures Under Room Temperature

The oedometer tests of 10% and 20% perlite added sand-bentonite mixtures were performed under room temperature. It was tried to perform oedometer test on the perlite, however it collapsed even under room temperature. Figure 6.5 shows the occurred gap between the loading frame and cap because of collapse of the sample.

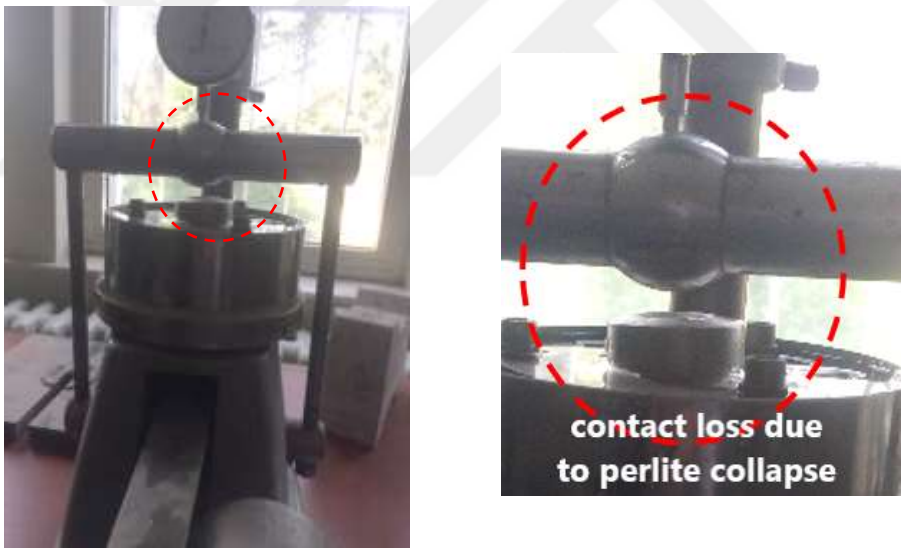


Figure 6.5 The collapse of the perlite sample in the oedometer test

Figure 6.6a and b show the stress-strain relationship of 10B-90S and 20B-80S mixtures in the presence of perlite, respectively. It was observed that the total vertical deformation increased as the perlite content increased in the 10B-90S mixture. The vertical deformation, which was 7.45% with 10% perlite, increased to 11.6% with 20% perlite. As a result of the tests, it was observed that the vertical deformation and swelling deformation values increased as perlite content was increased in the 10B-90S mixture.

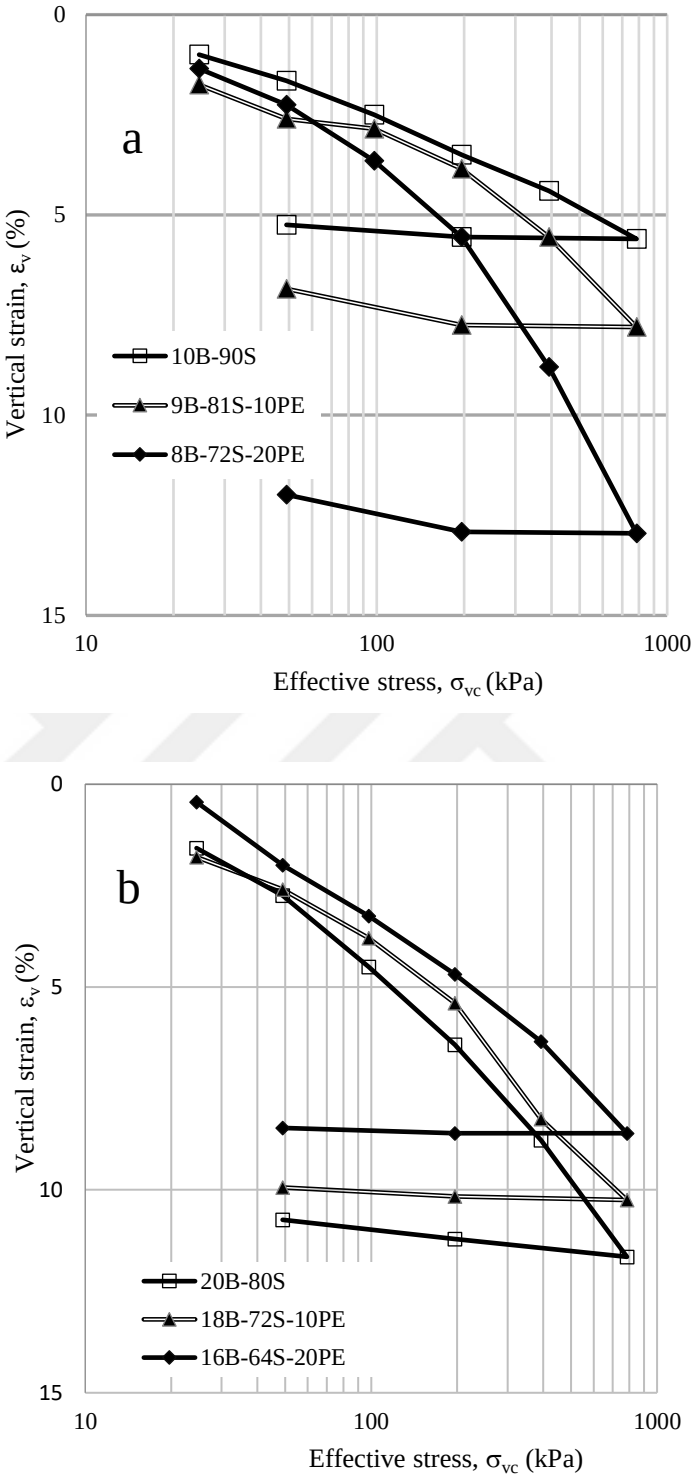


Figure 6.6 Compression and swelling curves of sand-bentonite mixtures under room temperature in the presence of perlite a) 10B-90S, b) 20B-80S

Unlike 10B-90S mixtures, perlite additive shows a deformation reducing effect in the 20B-80S mixtures. While the vertical deformation amount was 10.07% under room

temperature, this value decreased to 8.45% with the addition of 10% perlite and to 8.16% with the addition of 20% perlite. In addition, perlite reduced the swelling deformation of 20B-80B mixtures more than 50%. The results showed that perlite has positive effects (decrease in compression and swelling deformation) on the volume deformation of sand-bentonite mixtures. There are two reasons of this increase; one of them chemical reaction and the other one is the material replacement. Perlite has silanol (Si-OH) groups at the surface and silanol group bounds hydroxyl groups at the edges of the clay platelets (Ogawa et al., 1998). For that reason, perlite is held by the clay surface. Another reason of the increase in shear strength is material replacement. Because when the perlite added to the sample both bentonite and sand contents were decreased. The bentonite material was replaced with perlite mineral which has a very high thermal resistivity and very low thermal expansion.

Table 6.2 The vertical and swelling deformation values of the perlite-added sand-bentonite mixtures under room temperature

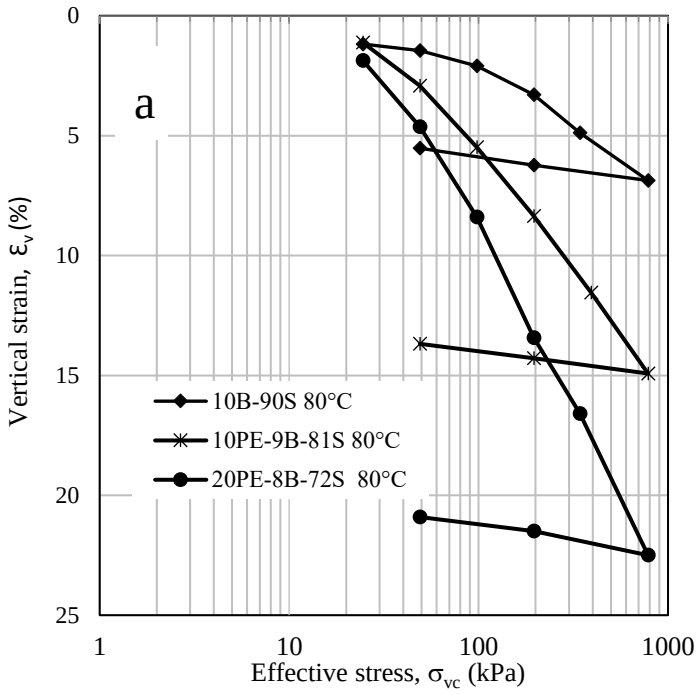
Mixtures	Vertical Deformation (%)	Swelling Deformation (%)
10B-90S	4.56	0.35
10PE-9B-81S	6.05	0.95
20PE-8B-72S	11.60	0.96
20B-80S	10.07	0.91
10PE-18B-72S	8.45	0.31
20PE-16B-64S	8.16	0.37

6.2.2 Volume Deformation Behavior of Perlite Added Sand-Bentonite Mixtures Under High Temperature

The oedometer tests were conducted under high temperatures by adding 10% and 20% perlite to 10B-90S and 20B-80S mixtures. According to the test results, perlite increased the vertical deformation of the 10B-90S mixtures under high temperatures (Table 6.3). Sinha and Kusakabe (2008) obtained from the consolidation experiments conducted under high temperature that the volumetric deformation behavior is affected from the high temperature. In addition, the amount of compression increases with the change of the pore volumes because of change in pore water pressure with temperature.

Similar to this, the vertical deformation amount of 10B-90S sample increased (from 4.56% to 5.69%) by increase in temperature. Perlite additon to this sample increased the vertical deformion almost two fold as can be seen from Table 6.3.

The compression curves of perlite added 20B-80S mixtures obtained under high temperature are given in Figure 6.7. It was observed that the amount of deformation of the 20B-80S mixture decreased from 10.07% to 7.86% with high temperature. It was determined that perlite additives increased the deformation value of the 20B-80S mixture. The vertical deformation value 13.67%, increases to 15.48% with 10% perlite at 80 °C. As can be seen from Table 6.3, similar to vertical deformation, sweelling deformation values increased in the presence of perlite.



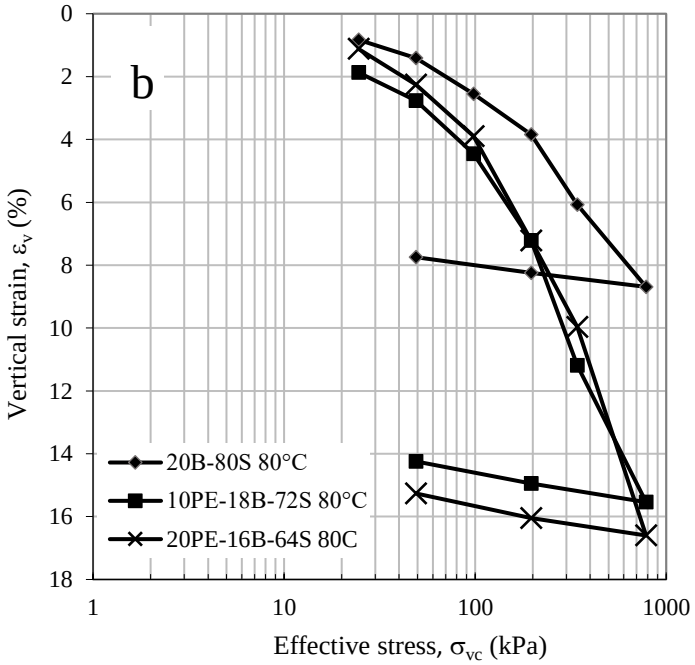


Figure 6.7 Compression and swelling curves of sand-bentonite mixtures under high temperature in the presence of perlite a) 10B-90S, b) 20B-80S

Table 6.3 Vertical and swelling deformation values of the perlite added sand-bentonite mixtures under high temperature

Mixtures	Vertical Deformation (%)	Swelling Deformation (%)
10B-90S	5.69	1.34
10PE-9B-81S	13.80	1.23
20PE-8B-72S	20.63	1.59
20B-80S	7.86	0.94
10PE-18B-72S	13.67	1.3
20PE-16B-64S	15.48	1.34

6.2.3 Volume Deformation Behavior of Perlite Added Sand-Bentonite Mixtures Under Thermal Cycles

In Figure 6.8 a and b, compression and swelling curves of 10B-90S and 20B-80S mixtures in the presence of 10% and 20% perlite additives under temperature cycling are given. For all mixtures, samples continued to compression as a result of the heating-

cooling cycle performed during loading. The highest total vertical deformation value belongs to the 20PE-8B-72S mixture.

According to the test results, in the 10B-90S mixture, under normal stress of 196 kPa at room temperature, although the deformations were completed at this stress level, an increase in the compression amount of 0.16% occurred when the temperature was increased. According to the test results, perlite addition to this mixture generally increased the amount of deformations that occurred during the cycle.

The former studies showed that soils have much more deformation with increase in temperature. Because when soil is exposed to high temperature, the amount of energy increases and accordingly the energy of the soil grains increase. Molecules with increased energy will become more active, leading to further weakening of existing bonds. As a result, there will be an increase in the amount of compression in the soil (Gupta 1964, Jarad 2016). The volumetric deformation occurred after temperature increases under temperature cycling is called as creep deformation (Green, 1969) and expresses volumetric decrease under constant effective stress (Jarad, 2016). Green (1969) reported that the creep behavior is affected by temperature and the effect of this effect increases at low effective stresses. Since the viscosity of the fluid will decrease with high temperature, the contact of the particles with each other decreases and the amount of creep of the soil increases (Gupta, 2013). In the Table 6.4, compression and swelling deformation values obtained under temperature cycle of 10B-90S and 20B-80S mixtures with perlite additive were given. The creep deformation values are given in the second column of the Table 6.4. Even though, the deformations were completed at 196 kPa stress level, with temperature increase deformations occurred under constant stress level.

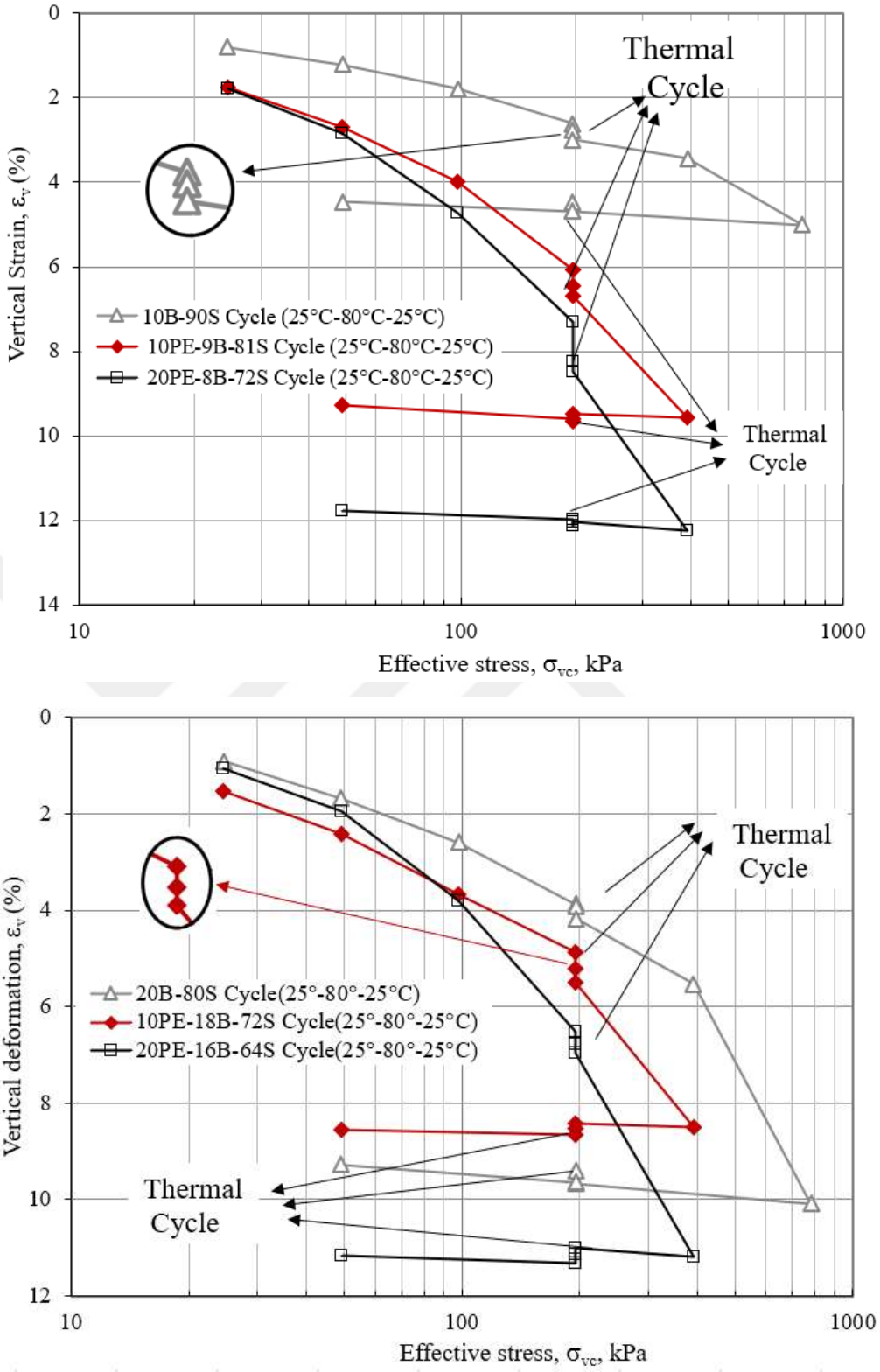


Figure 6.8 Compression and swelling curves of sand-bentonite mixtures under thermal cycle in the presence of pumice a) 10B-90S, b) 20B-80S

Table 6.4 Compression and swelling deformation values of perlite added 10B-90S and 20B-80S mixtures under temperature cycle

Samples	LOADING				UNLOADING		
	Vertical def. (%) 24.kPa to 196 kPa	Increase in vertical def. (%) after heating 196 kPa	Increase in vertical def. (%) after cooling 196 kPa	Total vertical deformation (%)	Swelling def. unloading 392 kPa to 196 kPa	After heating 196 kPa (%)*	After cooling 196 kPa (%)*
10B-90S	1.80	0.16	0.23	4.2	0.32 (from 784 kPa)	0.22 ↑	0.22 ↓
10PE-9B-81S	4.32	0.38	0.21	7.82	0.095	0.17 ↓	0.06 ↓
20PE-8B-72S	5.53	0.95	0.24	10.47	0.21	0.10 ↓	0.14 ↓
20B-80S	2.96	0.045	0.26	9.18	0.42 (from 784 kPa)	0.27 ↑	0.25 ↓
10PE-18B-72S	3.35	0.33	0.29	6.98	0.08	0.10 ↓	0.14 ↓
20PE-16B-64S	5.46	0.27	0.19	10.15	0.20	0.14 ↓	0.19 ↓

↓*: settlement, ↑ swelling

It was observed that the total vertical deformation value of 20B-80S mixture increases with 20% perlite additive. For all three mixtures, it was observed that the compression increased as a result of the heating during loading. It was observed that this compression also occurs in the heating cycle applied during unloading part. Towhata et al. (1993) reported that immediately after heating, shrinkage occurred in the soil and volume contraction occurred. It was revealed that the deformation occurred more than the amount of deformation at room temperature with the effect of heating, and this situation was caused either by the acceleration of the consolidation rate or the deterioration of the skeleton of the sample under heating.

Figure 6.9 shows the effect of perlite additive on vertical deformation under room and high temperatures and thermal cycles, comparatively. It was determined that the compression amount of all mixtures increased in the presence of perlite under high temperature. It was observed that the amount of compression generally increased under thermal cycles. It is known that when the soil particles are heated, they become more active, and as a result, the bonds weaken and the amount of compression increases. (Gupta 1964, Jarad 2016). In general perlite additive increased the amount of vertical

deformation of 10B-90S mixtures under room temperature. However, perlite additive created a deformation reducing effect on 20B-80S mixtures under room temperature. It was observed that perlite additive had a deformation increasing effect under high temperature for all mixtures. According to the results, it can be concluded that under high temperature perlite had no positive (decreasing effect on deformation) effect on the sand-bentonite mixtures.

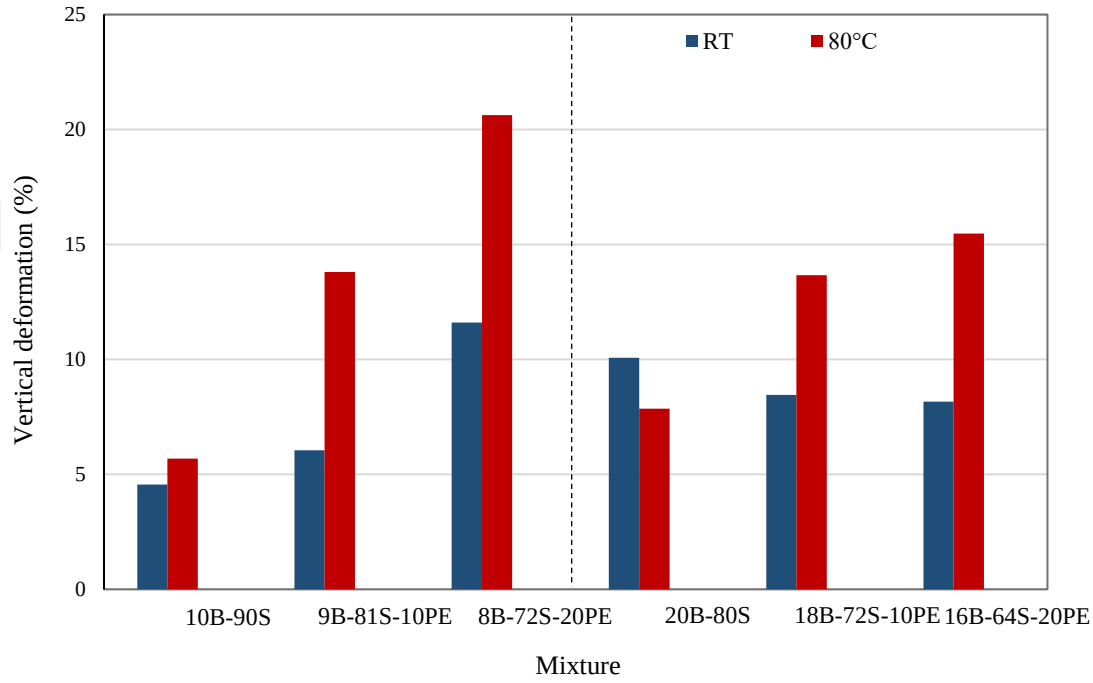


Figure 6.9 The vertical deformation values of the mixtures under thermal cycle, 80 °C and rrom temperature in the presence of perlite additive

6.3 Shear Strength Behavior of Perlite Added Sand-Bentonite Mixtures

The direct shear tests of sand-bentonite mixtures were performed at room temperature and 80 °C in the presence of 10% and 20% perlite additives. The effects of high temperature and perlite were investigated under different thermal conditions.

6.3.1 Shear Strength Behavior of Perlite Added Sand-Bentonite Mixtures Under Room and High Temperatures

The direct shear tests of sand-bentonite mixtures were performed in the presence of 10% and 20% perlite additives under room temperature and 80 °C. It was observed that

the shear strength of 10B-90S mixture decreased when the temperature was increased from room temperature to 80 °C (Figure 6.10). The angle of internal friction values did not change significantly, however the cohesion value decreased from 40.4 to 31.5 kPa. Unlike 10B-90S mixtures, the perlite addition increased the angle of internal friction of sand-bentonite mixtures under room and high temperature for 20B-80S mixtures (Table 6.5). However, it was observed that this increase was more pronounced in the presence of 20% perlite additive so that the angle of internal friction value increased from 7.0 to 23.3° under room temperature. This effect is also valid under 80 °C, the angle of internal friction increased from 13.4 to 27.9°.

Table 6.5. Internal friction angle and cohesion values of sand-bentonite mixtures in the presence of 10% and 20% perlite

	Room Temperature		**80 °C**	
Mixture	**ϕ (°)**	**c (kPa)**	**ϕ (°)**	**c (kPa)**
10B-90S	32.7	40.4	31.5	31.5
9B-81S-10PE	28.9	34.4	28.6	26.3
8B-72S-20PE	25.1	26.0	31.5	6.4
20B-80S	7.0	38.5	13.4	20.0
18B-72S-10PE	20.0	17.6	12.1	38.3
16B-64S-20PE	23.3	31.1	27.9	24.5

Table 6.6 Maximum shear stress values of sand-bentonite mixtures in the presence of 10% and 20% perlite under room and high temperatures

Mixture	**Maximum Shear Stress (kPa)**	
	Room Temperature	**80 °C**
10B-90S	106.97	94.42
9B-81S-10PE	104.97	103.26
8B-72S-20PE	75.00	62.79
20B-80S	41.69	47.39
18B-72S-10PE	62.22	69.63
16B-64S-20PE	77.04	73.33

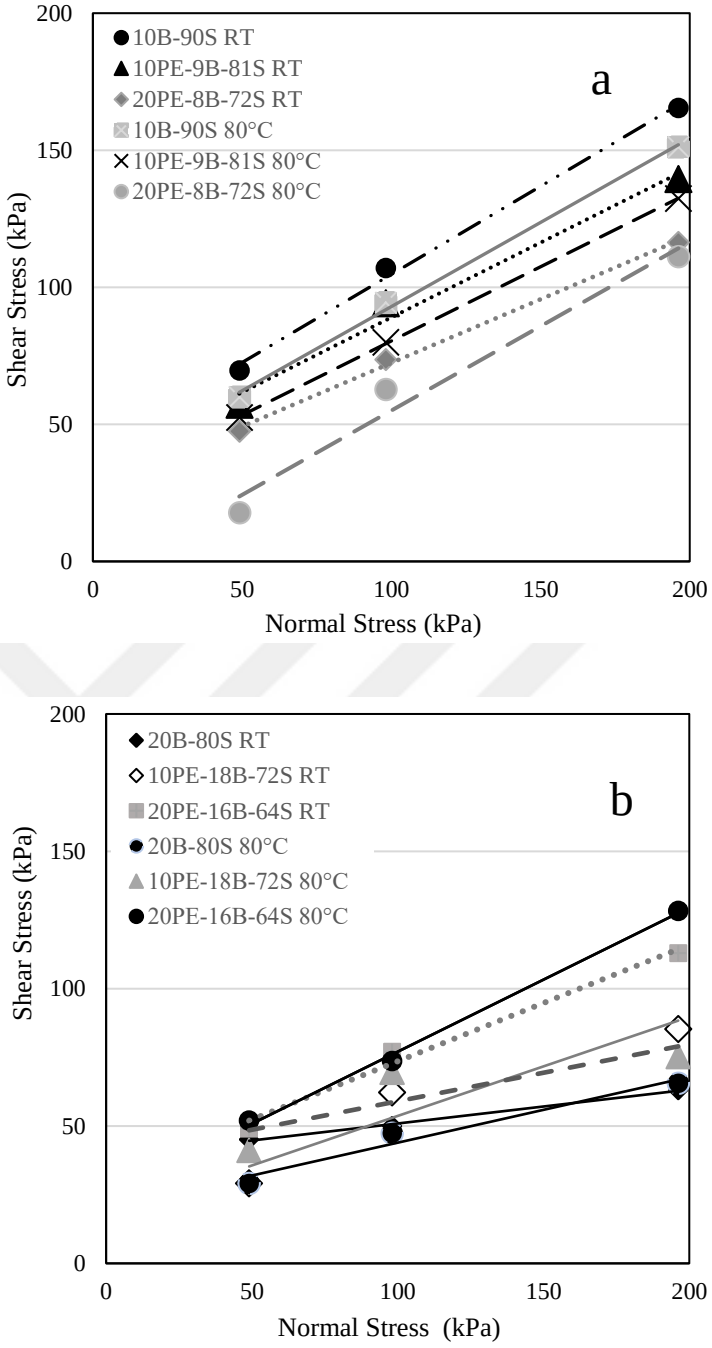


Figure 6.10 Shear stress-normal stress relationship of sand-bentonite mixtures at room temperature and high temperature (80 °C) in the presence of 10% and 20% perlite additive a) 10B-90S, b) 20B-80S

In Figure 6.10b, direct shear test results of 20B-80S mixtures in the presence of 10% and 20% perlite under room and high temperatures are given. The internal friction angle of the 20B-80S mixture was 7.0° and the cohesion value was 38.5 kPa at room temperature. Under room temperature, angle of internal friction value increased to 20.0°

and 23.3° with 10% and 20% perlite, respectively. In general cohesion values decreased compared to the additive-free mixture.

Figure 6.11 shows the shear stress-horizontal displacement relationship of the 20B–80S and 16B–64S–20PE mixtures at 80 °C. It was observed that compared to the additive-free sand–bentonite mixture in the presence of 20% perlite attained higher shear stress values at the same deformation value. For example, in the tests performed under 50 kPa normal stress, the shear stress value of the 20B–80S mixture was found to be 24.8 kPa at 9.7% horizontal displacement, while the shear stress value of the 20% perlite added mixture was found to be 41.7 kPa. When the applied normal stress was increased to 200 kPa, the behavior did not change and the shear stress value for the 20B–80S mixture was 58.8 kPa for 9.7% horizontal displacement, while the shear stress value for the 16B–64S–20PE mixture was 112.9 kPa. It was observed that the 20% perlite additive increased the shear stress values of the 20B–80S mixture under three different normal stresses at high temperature (80 °C).

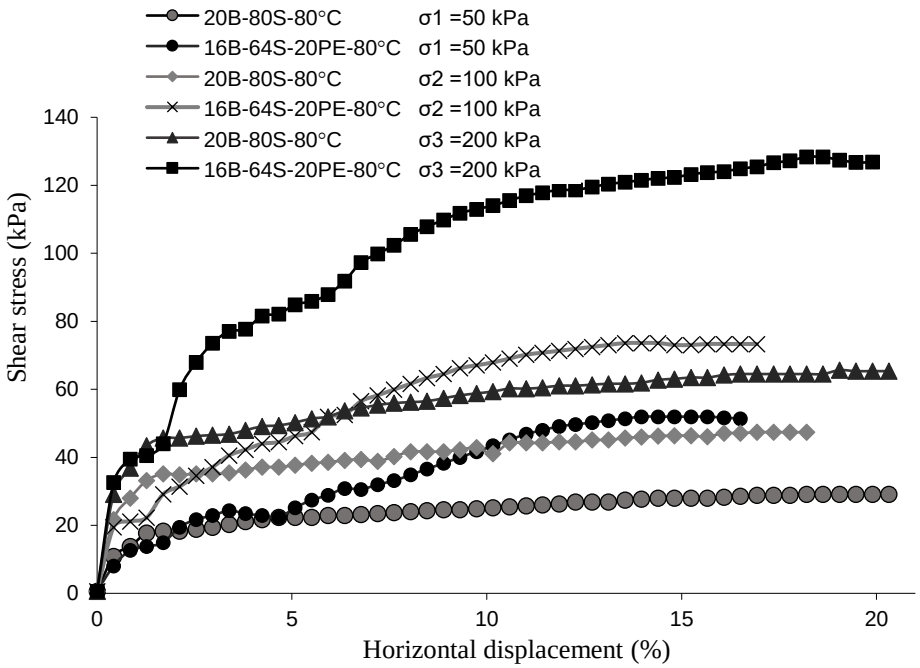


Figure 6.11 Shear stress-horizontal displacement relationship of 20B-80S and 16B-64S-20PE mixtures at 80 °C

In 10B-90S mixtures, it was observed that the perlite additive increased the maximum shear stress value of the mixtures at high temperature with only 10% perlite additive, while in 20B-80S mixtures, perlite additive increased the maximum shear stress value of the mixtures with all perlite contents under room and high temperatures (Table 6.6). When the results were examined on the basis of mixture, it was observed that the maximum shear stresses generally decrease or change in negligible extents when the temperature increased from room temperature to 80 °C.

The effect of temperature on the mechanical properties of soil depends on its overconsolidation ratio, plasticity, expansibility and compaction water content (Baldi et al. 1988; Romero et al. 2001). Delage et al. (2000) investigated the plastic contraction behavior of normally consolidated Boom clay at high temperatures. According to the results, the water expulsion caused thermal contraction. In addition, the plastic volumetric strains caused by contraction had a hardening impact on the soil. De Bruyn and Thimus (1996) and Kuntiwattanakul et al. (1995) reported that the soil strength decreases under undrained condition immediately after heating. Reversely, Laguros (1969) observed that the shear strength increases with the temperature as a result of uniaxial compression tests. These opposite findings show that the mineralogy, overconsolidation ratio, water content, test condition (drained-undrained) are the most important factors affecting on the shear strength behavior. In the present study, the samples were compacted at their maximum dry unit weight. It was observed that during shear according to the vertical deformations samples contracted.

The increase in temperature caused increase in shear strength especially for additive-free 20B-80S mixture. The reason of this behavior may be hardening behavior of sample as a result of plastic contraction. Another reason may be increase in temperature transforms the smectite mineral into more constant silicate phases (Wersin et al. 2006). As a result of this phenomenon, the water adsorption capacity of clay reduces so the strength of clayey soil increases. The results showed that perlite has positive effects on the shear strength of sand-bentonite mixtures. There are two reasons of this increase; one of them chemical reaction and the other one is the material replacement. Perlite has silanol (Si-OH) groups at the surface and silanol group bounds hydroxyl groups at the edges of the clay platelets (Ogawa et al. 1998). For that reason, perlite is held by the

clay surface. Eventually the shear strength of the sand-bentonite mixture increases. Another reason of the increase in shear strength is the material replacement. Because when the perlite added to the sample both bentonite and sand contents were decreased. The bentonite material was replaced with perlite mineral which has a very high thermal resistivity and very low thermal expansion. For that reason, the material replacement may be another reason of the increase in shear strength of sand-bentonite mixtures under high temperature.

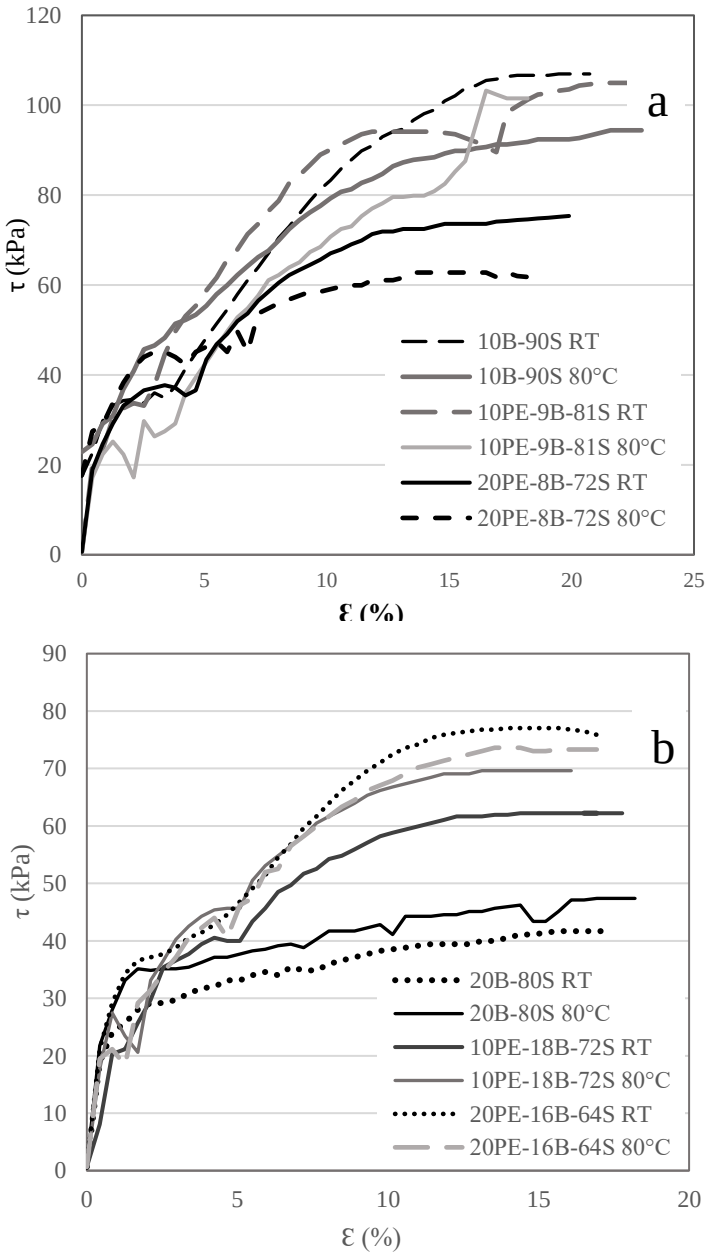


Figure 6.12 τ- ε relationship of sand-bentonite mixtures in the presence of of 10% and 20% perlite a) 10B-90S, b) 20B-80S

6.3.2 Shear Strength Behavior of Perlite Added Sand-Bentonite Mixtures Under Thermal Cycles

The shear strength values of 10B-90S and 20B-80S mixtures in the presence of perlite additive obtained after 8 hours of heating-16 hours of cooling cycles. The results are shown in Figure 6.13 and Table 6.7. The maximum shear stress value obtained for the 10B-90S mixture was determined as 248.8 kPa. This value decreased to 141.1 kPa and 184 kPa, in the presence of 10% and 20% perlite additives, respectively. It is shown that when perlite is added to the mixture, both bentonite and sand content were reduced and bentonite was replaced with perlite mineral, which has a very high thermal durability and low thermal expansion property.

Table 6.7 Maximum shear stress values of sand-bentonite mixtures in the presence of 10% and 20% perlite under room and high temperatures and thermal cycle (under 196 kPa normal stress)

	Room Temperature	**80 °C**	**Temperature cycling**
Mixture	**Maximum Shear Stress (kPa)**		
10B-90S	165.789	94.42	248.81
9B-81S-10PE	139.302	103.26	141.18
8B-72S-20PE	116.739	62.79	184.07
20B-80S	63.1	47.39	176.13
18B-72S-10PE	85.347	69.63	110.99
16B-64S-20PE	112.815	73.33	130.06

Figure 6.13b shows the shear strength values obtained by consolidating 20B-80S mixtures in the presence of perlite, with 8 hours of heating-16 hours of cooling cycle, and then performing the shearing stage at the end of this period. The maximum shear stress value of the 20B-80S mixture decreased to 176.1 kPa due to the increase in the bentonite ratio compared to the 10B-90S mixture. In addition, perlite additives decreased the shear strength of the 20B-80S mixture, which is similar to the trend in 10B-90S mixture, but 20% perlite additive reached higher strength than 10% perlite

additive. Since the consolidation test could not be performed due to collapse of the perlite sample, it could not to be subjected to the direct shear tests.

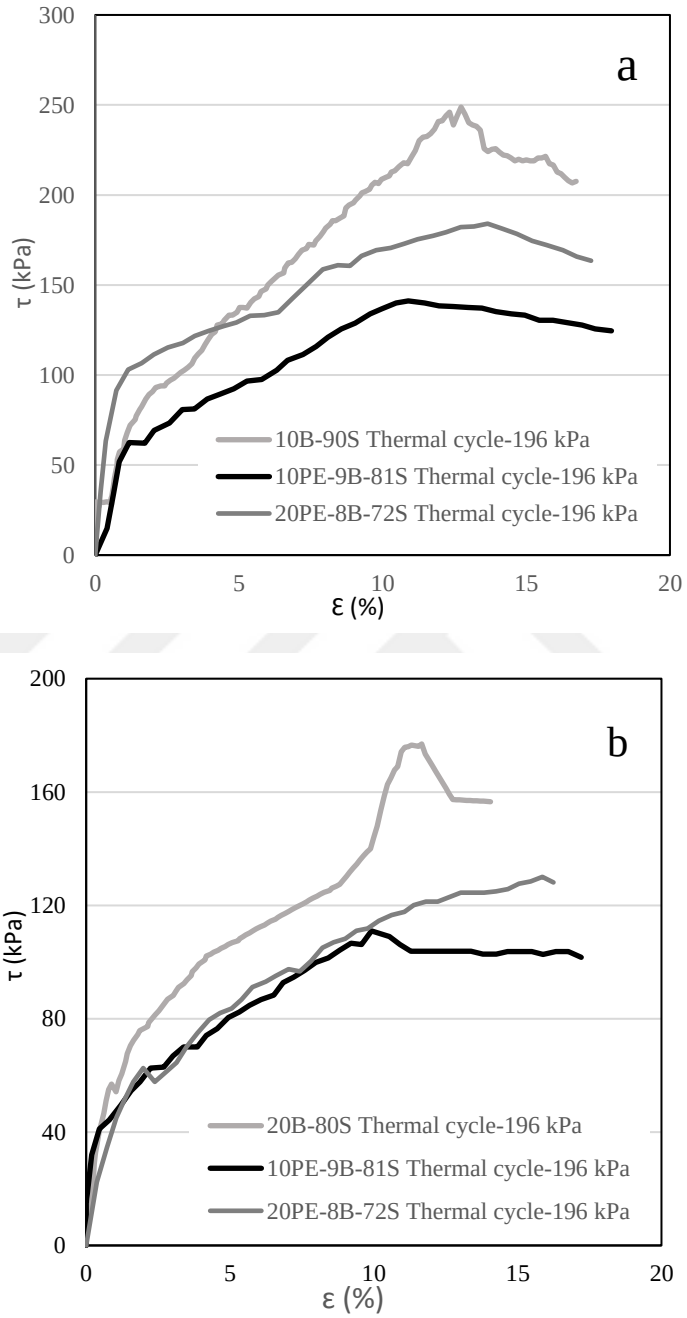


Figure 6.13 Shear stress-strain relationship of sand-bentonite mixtures under thermal cycling in the presence of perlite a) 10B-90S, b) 20B-80S

Perlite additive reduced the shear strength for 10B-90S mixtures at both room and high temperatures. However, the addition of perlite to the 20B-80S mixtures increased the shear strength both at room and high temperatures (Figure 6.15). When the perlite

added to the sample both bentonite and sand content was decreased. The bentonite material was replaced with perlite mineral which has a very high thermal resistivity and very low thermal expansion. Also, perlite has silanol (Si-OH) groups at the surface and silanol group bounds hydroxyl groups at the edges of the clay platelets (Ogawa et al. 1998). For that reason, perlite is held by the clay surface. Eventually the shear strength of the sand-bentonite mixture which have higher bentonite content increased.

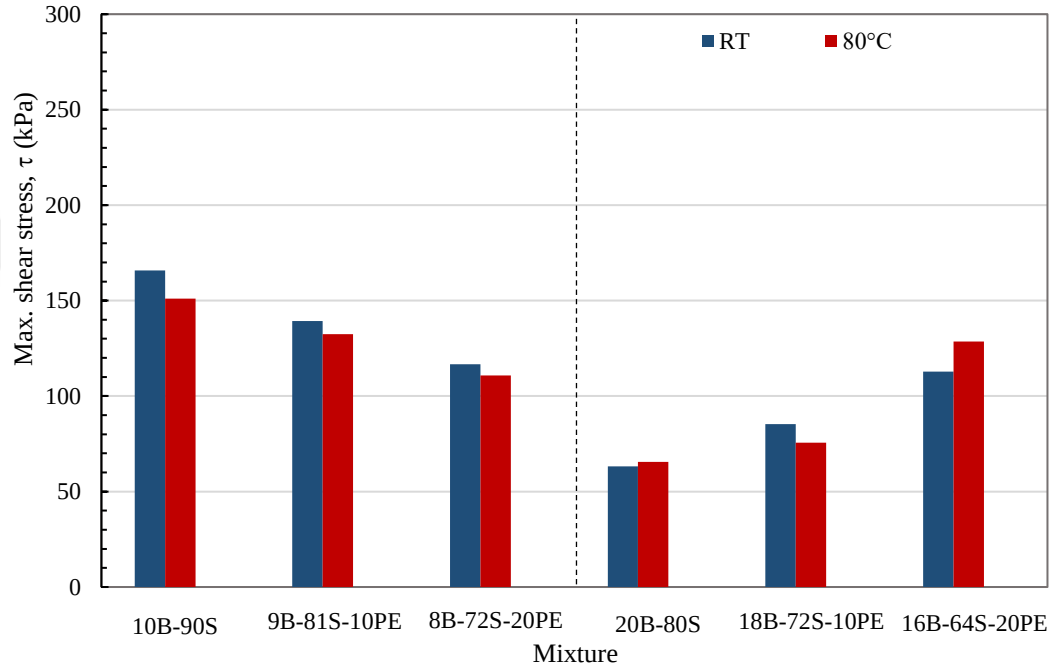


Figure 6.14 Maximum shear strengths of perlite added sand-bentonite mixtures at room temperature and under 80 °C and thermal cycles

6.4 Hydraulic Conductivity Behavior of Perlite Added Sand-Bentonite Mixtures Under Room and High Temperatures and Thermal Cycles

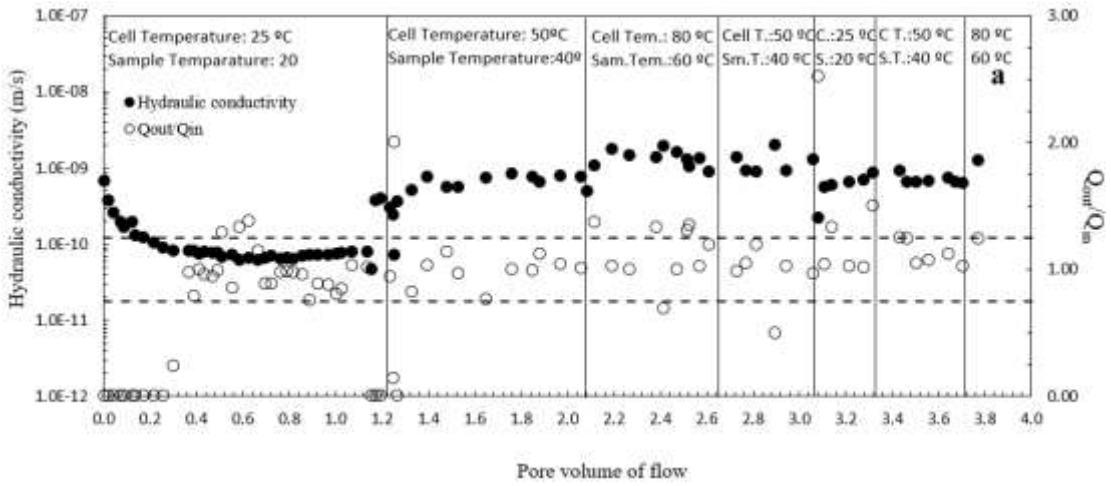
Within the scope of this doctoral thesis, the hydraulic conductivity tests of 10% and 20% perlite added sand-bentonite mixtures were conducted under different temperatures that was gradually increased up to 80 °C, starting from room temperature. The hydraulic conductivity values are given in Table 6.8 depending on the temperatures.

Since the hydraulic conductivity of the 8B-72S-20PE mixture had a very high value ($1.2x10^{-9}$ m/s) under room temperature the tests were not performed under high temperatures. Because, the obtained hydraulic conductivity values were too high and

exceeds the barrier limit (Figure 6.15). The barrier limit is determined as $k \leq 1 \times 10^{-9}$ m/s in landfills in the USA, UK and European countries (Rashid et al., 2017). The hydraulic conductivity coefficient of the soil liners has been determined to be less than 10^{-9} m/s (Daniel 1997; Van Impe 1998; Rowe et al. 2004; Rowe 2005) in order to prevent chemical hazards caused by buffer material, leachate and leakage. However, for nuclear waste repositories the limit k value is 1×10^{-11} m/s (Westsik et al., 1982).

Table 6.8 Variation of hydraulic conductivity values of perlite added sand-bentonite mixtures with temperature cycling

Temperature (°C)	**k (m/s)**		
	9B-81S-10PE	**18B-72S-10PE**	**16B-64S-20PE**
25	7.0×10^{-11}	1.0×10^{-10}	2.2×10^{-10}
50	7.5×10^{-10}	1.5×10^{-10}	7.1×10^{-10}
80	1.4×10^{-09}	2.9×10^{-09}	2.9×10^{-10}
50	1.2×10^{-09}	-	9.7×10^{-10}
25	5.4×10^{-10}	-	8.7×10^{-10}
50	6.7×10^{-10}	-	7.5×10^{-09}
80	1.3×10^{-10}	-	-



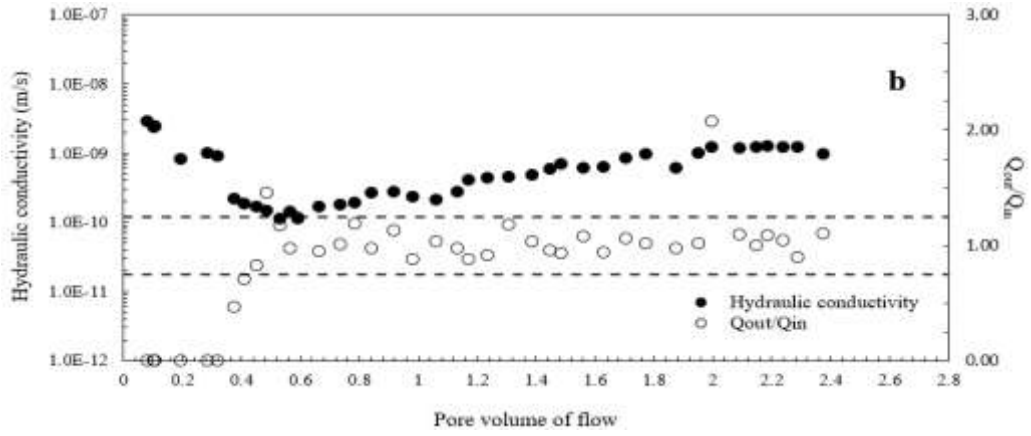


Figure 6.15 Hydraulic conductivity of 10B-90S mixture a) 10% perlite b) 20% perlite

It was observed that the hydraulic conductivity value of the 9B-81S-10PE mixture at room temperature at the beginning of the test increased 10.7 times to 7.5×10^{-10} m/s when the temperature increased to 50 °C. It was investigated that this increase continued as the temperature increased, but when the cooling cycle was started, the hydraulic conductivity values decreased.

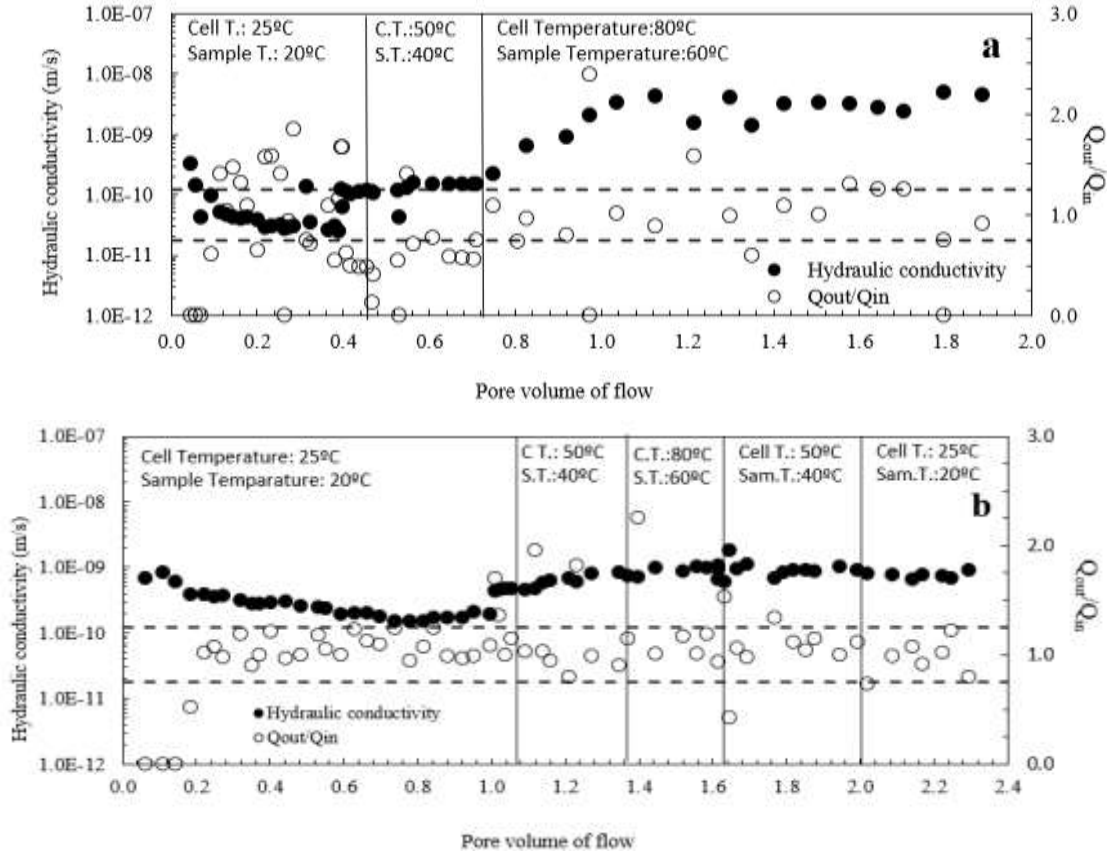


Figure 6.16 Hydraulic conductivity graphs of 20B-80S mixture a) 10% perlite b) 20% perlite

Similarly, it was determined that the hydraulic conductivity coefficients of 20B-80S mixtures increased with increase in temperature in the presence of perlite (Figure 6.16). When the temperature increases, the thickness of the adsorbed water layer decreases, resulting in larger flow channels so higher hydraulic conductivity (Habibagahi, 1977). In addition, the decrease in the viscosity of the water is among the main reasons for the increase in hydraulic conductivity as the temperature increases (Cho et al., 1999; Pusch, 2001).

Table 6.9 Temperature influence on some properties of water (Lide, 1995)

Temperature (°C)	**Water density (g/cm^3)**	**Water viscosity (10^{-6} Pa s)**
10	0.9997	1307
20	0.99821	1002
30	0.99565	797.7
50	0.98803	547
80	0.97182	354.4

The change in water viscosity is accepted as a main reason for increase in hydraulic condcutivity. Table 6.9 shows the change in water density and viscosity at different temperatures. As temperature increases, the viscosity of water decreases. The hydraulic conductivity value can be calculated by help of the emprical equations. For example, an equation showing the relationship between saturated hydraulic conductivity k_s and temperature T were used by Ye et al. (2013). The Equation 6.1 gives the calculated hydraulic conductivity value, while Equation 6.2 shows the temperature dependent viscosity change. In Equation 6.3 k_m is the intrinsic permeability value obtained from the measured hydraulic conductivity values.

Equation 6.3 is defined as a relation that only takes into account the effect of temperature on water viscosity. The hydraulic conductivity values of 9B-81S-10PE and 16B-64S-20PE mixtures at 25, 50 and 80 °C were calculated by using Equation 6.3. Figure 6.17 compares calculated and measured hydraulic conductivity values of 9B-81S-10PE and 16B-64S-20PE mixtures. It can be seen that the measured hydraulic conductivity values were lower than predicted values.

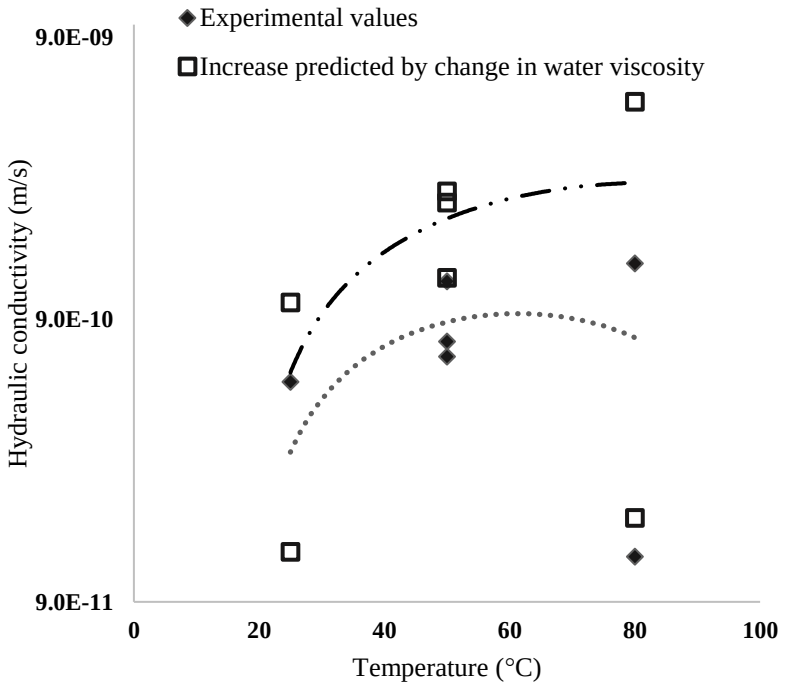
$$k_s = k_{in}\rho_w g / \eta(T) \quad (6.1)$$

$$\eta(T) = 0.0002601 + 0.001517\exp[-0.034688x(T - 273)] \quad (6.2)$$

$$k_s = \frac{k_m \, x \, \rho_w g}{0.0002601 + 0.001517\exp[-0.034688x(T-273)]} \quad (6.3)$$

Where $\eta(T)$: is defined as the viscosity of water depending on temperature, k_{in}: intrinsic permeability, g: gravitational acceleration, T: absolute temperature in Kelvin and ρ_w : density of water.

The difference between the measured and predicted hydraulic conductivity values means that beside the water viscosity there are some other reasons which affect hydraulic conductivity under high temperatures. Similar differences between calculated and measured values were reported by Ye et al. (2013) and Rivas et al. (1991). It means that only change in water viscosity is not enough to fully explain the change in hydraulic conductivity values. The former studies have shown that, as temperature increases fabric structure changes in clays and larger gaps form in the soil (Pusch and Güven, 1990; ; Pons et al., 1994; Thomas et al., 1994; Romero et al. 2001). The hydraulic conductivity values of 9B-81S-10PE mixture increased more than 16B-64S-20PE mixture.



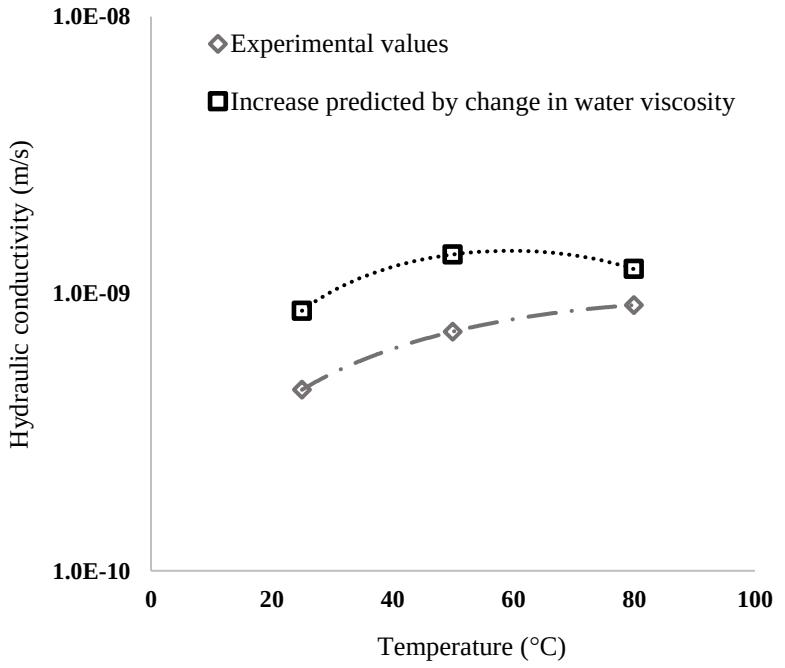


Figure 6.17 Change of calculated and measured hydraulic conductivity values as a function of temperature, a) 9B-81S-10PE, b) 16B-64S-20PE

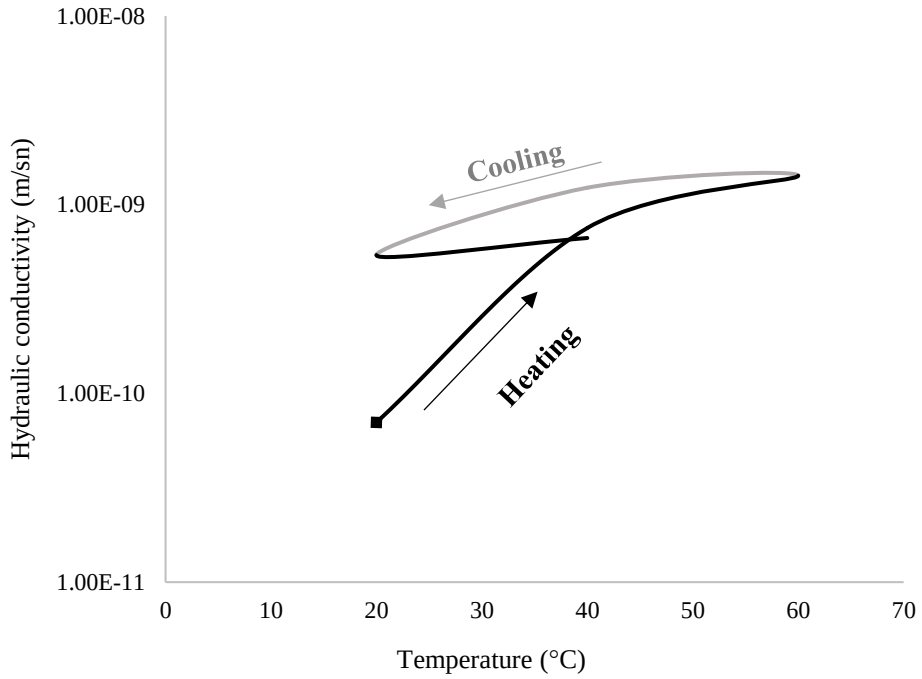


Figure 6.18 Variation of the hydraulic conductivity during heating-cooling cycles for 9B-81S-10PE mixture

Figure 6.18 shows the heating-cooling cycle effect on the hydraulic conductivity of the 9B-81S-10PE mixture. According to the results, with increasing temperature hydraulic conductivity increased whereas it decreased with decreasing temperature (cooling). As a result of thermal cycles, it was seen that the samples could not turn back to their initial k values. It means that, high temperature also changes the pore structure of the samples. Similarly, Romero et al. (2001) reported that hydraulic conductivity affected not only by changes in viscosity, but also thermal changes have effects on soil-water interaction at the microstructural level. It was reported that heating leads to weakening of microstructure, because larger voids are formed by heating (Chen et al. 2017).

The contribution of perlite to the hydraulic conductivity of sand-bentonite mixtures were determined under different temperature conditions; room and high temperatures and temperature cycles. It was observed that perlite additive had an increasing effect on the hydraulic conductivity in10B-90S and 20B-80S mixtures under high temperatures. The highly porous structure of perlite allowed water to find its flow path (Gül, 2016). Figure 6.19 shows the change in hydraulic conductivity values under different

temperatures of sand-bentonite mixtures with and without additives. The experimental results showed that the hydraulic conductivity value of each mixture increased as the temperature increased and the flow rate slowed down with the decrease in temperature. Although perlite did slown down the flow rate in 10B-90S mixtures, perlite additive had an increasing effect on flow rate in 20B-80S mixtures. When the temperature was lowered, the mixtures experienced a slight decrease in their hydraulic conductivity values, but they could not return to their initial values.

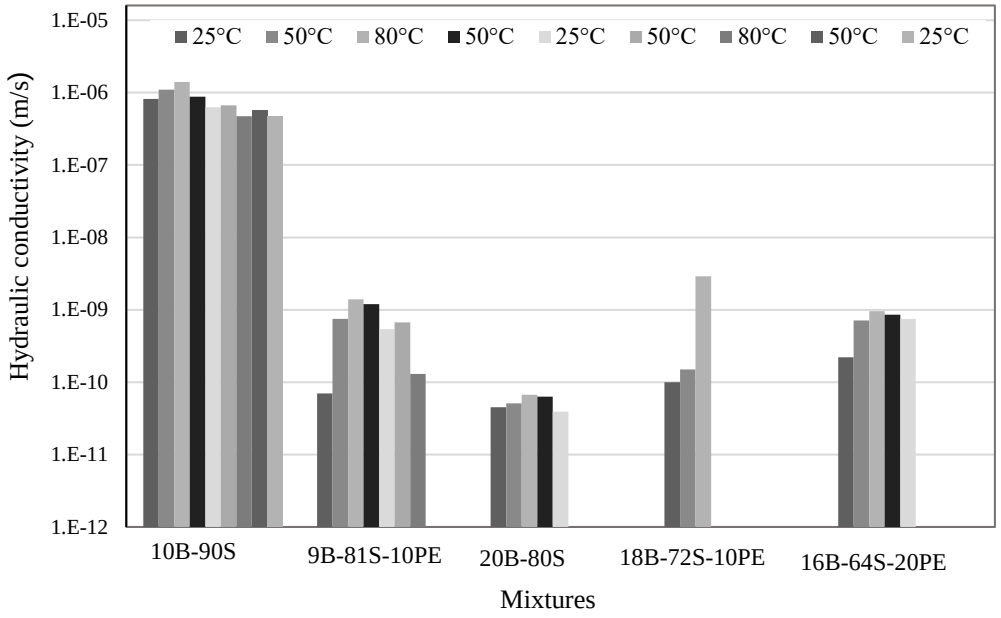


Figure 6.19 Hydraulic conductivity values of sand-bentonite mixtures under different temperatures in the presence of perlite

In Figure 6.20, hydraulic conductivity versus pore volume of flow graphs of perlite added sand-bentonite mixtures under different temperatures are given together. It was determined that the 10PE-18B-72S mixture had the lowest hydraulic conductivity under room temperature, but the highest hydraulic conductivity was observed with 10PE-18B-72S mixture when the temperature was increased 25 to 50 °C. It was observed that the hydraulic conductivity values of all mixtures increased as the temperature increased and decreased slightly when temperature was decreased.

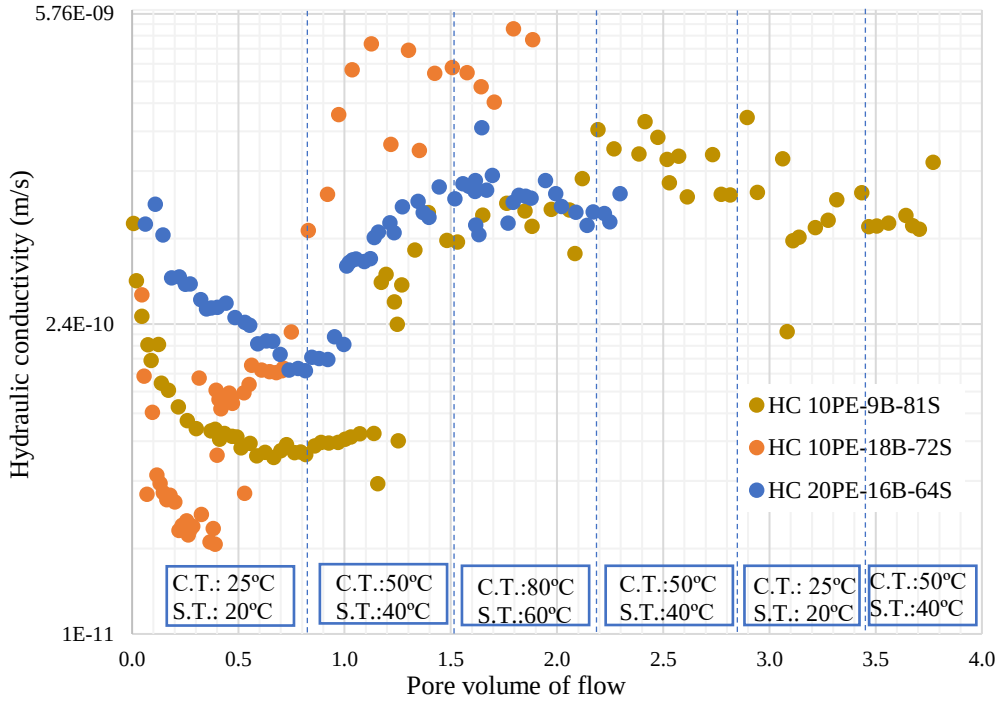


Figure 6.20 Comparison of hydraulic conductivity behavior of perlite added sand-bentonite mixtures under temperature cycling

6.5 Thermal Conductivity of the Perlite Added Sand-Bentonite Mixtures

Thermal conductivity values of 10B-90S and 20B-80S mixtures were measured in the presence of perlite. The results showed that the thermal conductivity values decreased when perlite was added to the sand-bentonite mixtures (Table 6.10).

Thermal conductivity values of perlite added sand-bentonite mixtures were measured according to void ratio and saturation degree values. Under two different conditions the thermal conductivity values were measured. In the first method, only void ratio kept constant while in the second method both void ratio and saturation degree kept constant. The results were similar to pumice added sand-bentonite mixtures. Because of light weight character of perlite, perlite takes up a lot of space by volume. The 80% saturation degree was taken as a constant value according the saturation degree of the mixtures and the void ratio was calculated to be quite high. The result showed that the thermal conductivity value of perlite as 0.477 W/mK.

Table 6.10 Thermal conductivity values of sand-bentonite mixtures in the presence of 10% and 20% perlite

Mixtures	Thermal Conductivity (W/mK) (e= 0.6 constant)	Thermal Conductivity (W/mK) ("S" and "e" constant)	
10B-90S	1.153	1.779	
9B-81S-10PE	0.868	0.611	S = 0.53 e = 1.13
8B-72S-20PE	0.299	0.465	
20B-80S	1.971	1.461	
18B-72S-10PE	0.992	0.873	S = 0.63 e = 1.33
16B-64S-20PE	0.715	0.877	

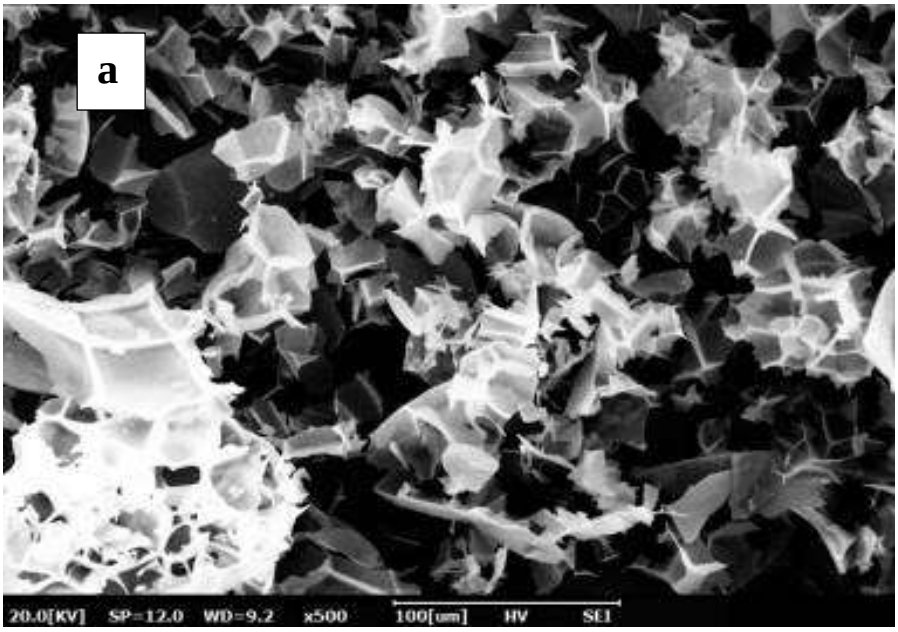
As a result of the thermal conductivity tests in which the void ratio and saturation degree constant, it was determined that the perlite additive made the sand-bentonite mixtures more thermally resistant (insulator). For example, with the addition of 10% perlite to the 10B-90S mixture, the thermal conductivity value decreased from 1.153 W/mK to 0.868 W/mK in the method where the void ratio was kept constant, while it decreased from 1.789 W/mK to 0.611 W/mK when the void ratio and saturation degree was kept constant. When 20% perlite was added, these values decreased to 0.299 W/mK and 0.465 W/mK, respectively.

Previous studies report that the thermal conductivity of the mixture increases as the percentage of sand increases. In this case, the thermal conductivity value of the 10B-90S mixture is expected to be higher than the 20B-80S mixture. The thermal conductivity decreased as the perlite content in the mixture increased. Perlite is a insulating material for that reason it decreases the thermal conductivity of the sand-bentonite mixtures. For that reason, perlite added mixtures can be used as insulation material around energy geo-structures, thus preventing the dissipation of heat in these structures.

6.6 Scanning Electron Microscope (SEM) Analyses of Perlite Added Sand-Bentonite Mixtures

Within the scope of this doctoral thesis, SEM images of the perlite and perlite added sand-bentonite mixtures were analyzed. SEM photographs of the expanded perlite sample at room temperature, 16B-64S-20PE mixture at room temperature and 80 ˚C are given in Figure 6.21. Perlite in the mixtures occupied a large volume due to its light weight. The flake shape of perlite clearly can be seen in Figure 6.21a. It was reported that flake-shaped perlite particles clog the pores and can form an impermeable filter layer (Bageri et al., 2020). However, according to the results of this study, the mentioned clogging effect was not observed in the hydraulic conductivity tests. In terms of hydraulic conductivity, the highly porous structure of expanded perlite facilitated the acceleration of the flow by helping to water to find a flow path throughout the perlite body.

In Figure 6.21b, if it is assumed that perlite has a leafy appearance under room temperature, it was seen that the leaves of this leafy appearance became lighter and the material weakened structurally when the temperature was increased to 80 °C.



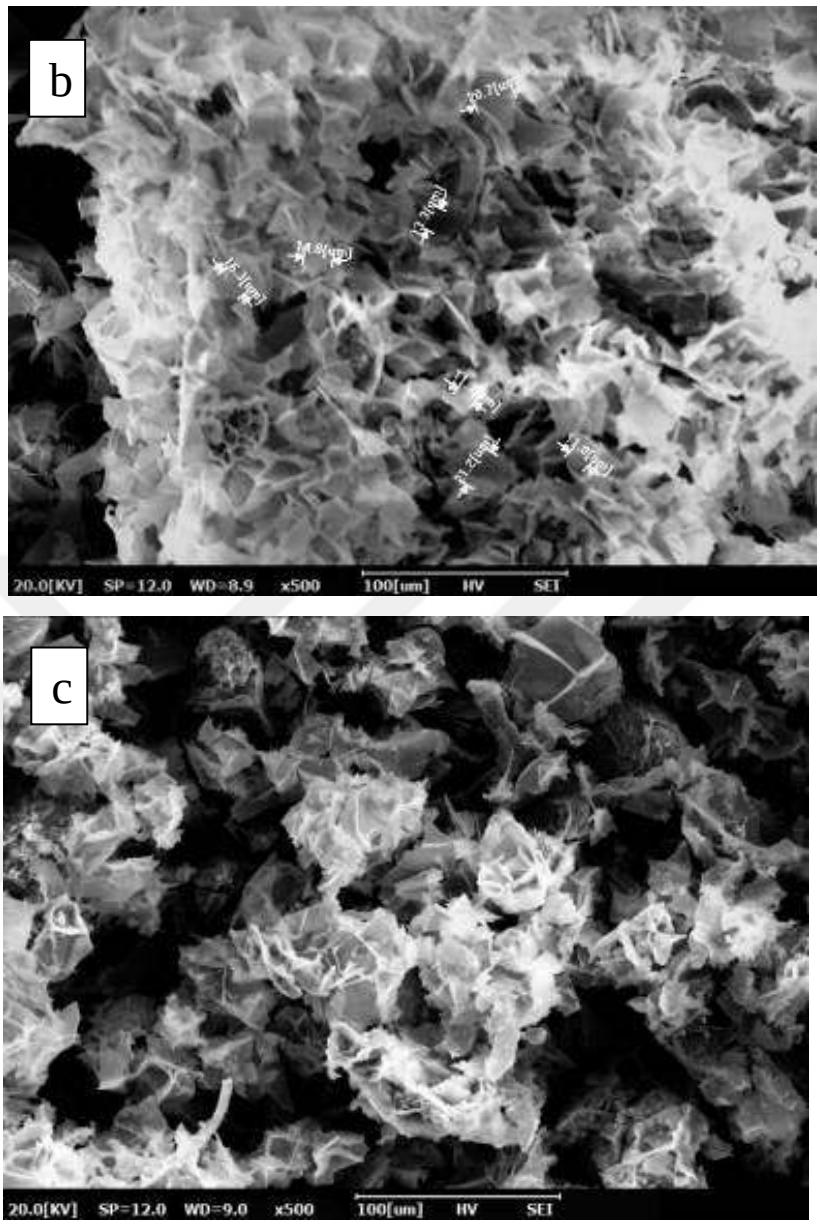


Figure 6.21 Electron microscope photographs of perlite and perlite added sand-bentonite mixtures (a) Perlite (x500) under room temperature, (b) 16B-64S-20PE room temperature (x500), (c) 16B-64S-20PE 80 ˚C (x500)

CHAPTER 7
THE EFFECT OF FIBERGLASS ON THE VOLUME DEFORMATION, SHEAR STRENGTH, HYDRAULIC CONDUCTIVITY AND THERMAL CONDUCTIVITY BEHAVIOR OF SAND-BENTONITE MIXTURES

7.1 Compaction Behavior of Fiberglass Added Sand-Bentonite Mixtures

Fiberglass is one of the additives which was chosen in scope of this study because of its superior thermal characteristics. Fiberglass was added to 30% bentonite-70% sand mixtures in two different ratios; 1% and 0.5%. Because of fiber structure compaction tests could not be performed on the fiberglass sample. Figure 7.1 shows the compaction curve of the 30B-70S mixture, and the line with diamond dots shows the compaction curve in the presence of 1.0% fiberglass. The results have shown that, the effect of fiberglass on the optimum water content and maximum dry unit weight at a negligible level.

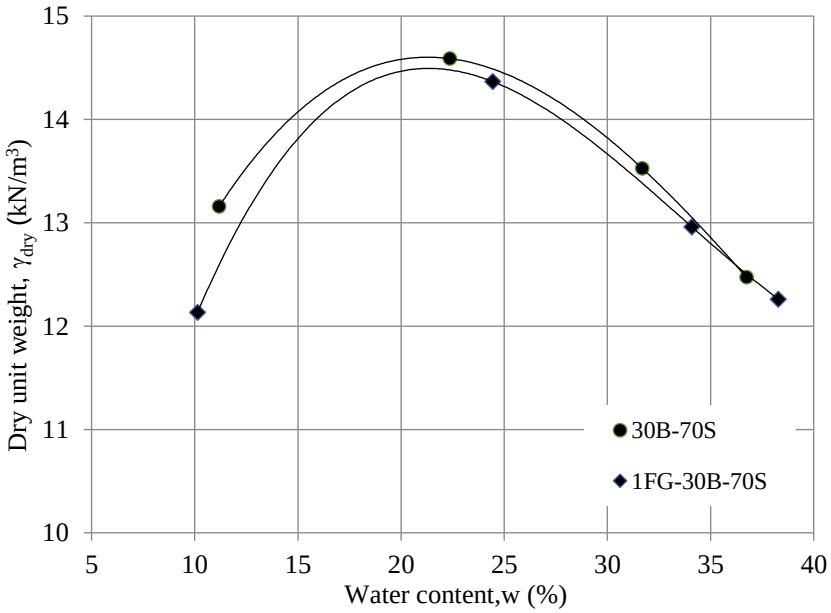


Figure 7.1 Compaction curves of 30B-70S and 1FG-30B-70S mixtures

Table 7.1 Compaction parameters of fiberglass added sand-bentonite mixtures obtained from Standard Proctor Tests

Group	Sample	$\gamma_{d,max}$ (kN/m^3)	w_{opt} (%)
30% bentonite	30B-70S	14.61	22.5
	1FG-30B-70S	14.50	21.5

According to the Standard Proctor test results, it was determined that fiberglass additive has a negligible effect on reducing the optimum water content and maximum dry unit weight of the sand-bentonite mixture (Figure 7.2).

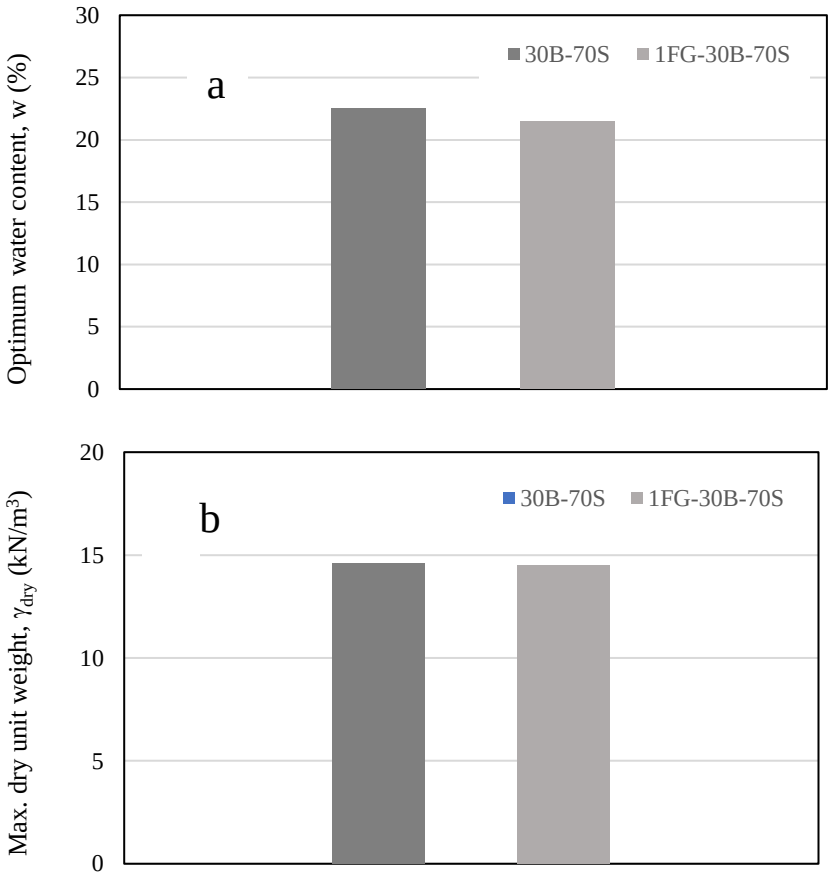


Figure 7.2 Effect of perlite on the optimum water content and maximum dry unit weight of 30B-70S mixture

7.2 Volume Deformation Behavior of Fiberglass Added Sand-Bentonite Mixtures

The volumetric deformation behavior of fiberglass added sand-bentonite mixtures was investigated under two thermal conditions: room temperature and high temperature.

7.2.1 Volume Deformation Behavior of Fiberglass Added Sand-Bentonite Mixtures Under Room Temperature

Within the scope of thesis, oedometer experiments of 0.5% and 1.0% fiberglass added sand-bentonite mixtures were conducted under room temperature. The compressibility parameters of 100% fiberglass could not be determined at room temperature due to fiber structure of the sample. The test results showed that the fiberglass additive increased the vertical deformation amount of the 30B-70S mixture insignificantly in the presence of 0.5 and 1.0% fiberglass (Table 7.2).

Table 7.2 Vertical compression and swelling deformation values of the fiberglass-added sand-bentonite mixtures under room temperature

Mixtures	**Compression Deformation (%)**	**Swelling Deformation (%)**
30B-70S	14.07	1.37
0.5FG-30B-70S	14.01	1.30
1FG-30B-70S	15.00	1.79

The compression and swelling deformation amounts of the 30B-70S mixture was 14.07% and 1.37% under room temperature, respectively. When 0.5% fiberglass additive was added to the 30B-70S mixture the compression deformation did not change and determined as 14.01%. However, when the fiberglass content was increased to 1%, the compression deformation amount increased to 15%. While the swelling deformation amount remained constant with 0.5% fiberglass, it increased to 1.79% with 1% fiberglass additive. According to the results, the 0.5% and 1.0% fiber glass additives, did not have a significant effect on compression deformations under room temperature. However, the swelling deformation increased in the presence of 1% fiberglass (Figure 7.13).

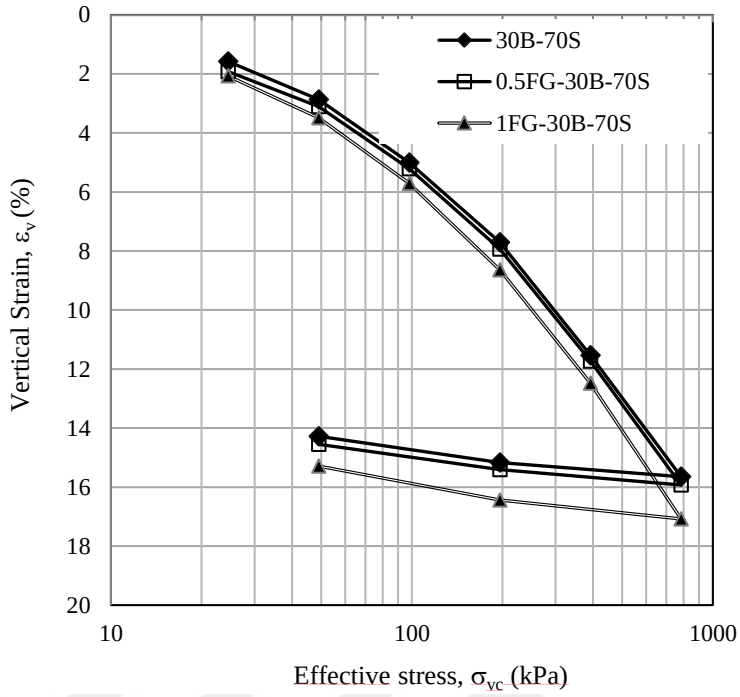


Figure 7.3 Compression and swelling curves of sand-bentonite mixtures under room temperature in the presence of fiberglass

7.2.2 Volume Deformation Behavior of Fiberglass Added Sand-Bentonite Mixtures Under High Temperature

The compressibility and swelling behavior of the fiberglass added mixtures was determined with oedometer tests under high temperatures. In Figure 7.4, the compressibility curves of 0.5% and 1% fiberglass added sand-bentonite mixtures at 80 °C were given. Table 7.3 shows the obtained compression and swelling deformation values.

The results of the oedometer tests performed under high temperature (80 °C) showed that the compressibility deformation amounts from 14.4% increased to 16.2% and 19.8%, with 0.5% and 1% with fiberglass additives, respectively. The compression deformation of the mixtures increased in the presence of high temperature when compared room temperature. The amount of swelling deformation amount was found to be 1.73% for the 30B-70S mixture without additives, while it was 1.49% with 0.5% fiber glass (Figure 7.4).

Table 7.3 Compression and swelling deformation values of the fiberglass added sand-bentonite mixtures under high temperature

Mixtures	Compression Deformation (%)	Swelling Deformation (%)
30B-70S	14.4	1.73
0.5FG-30B-70S	16.2	1.49
1FG-30B-70S	19.8	1.49

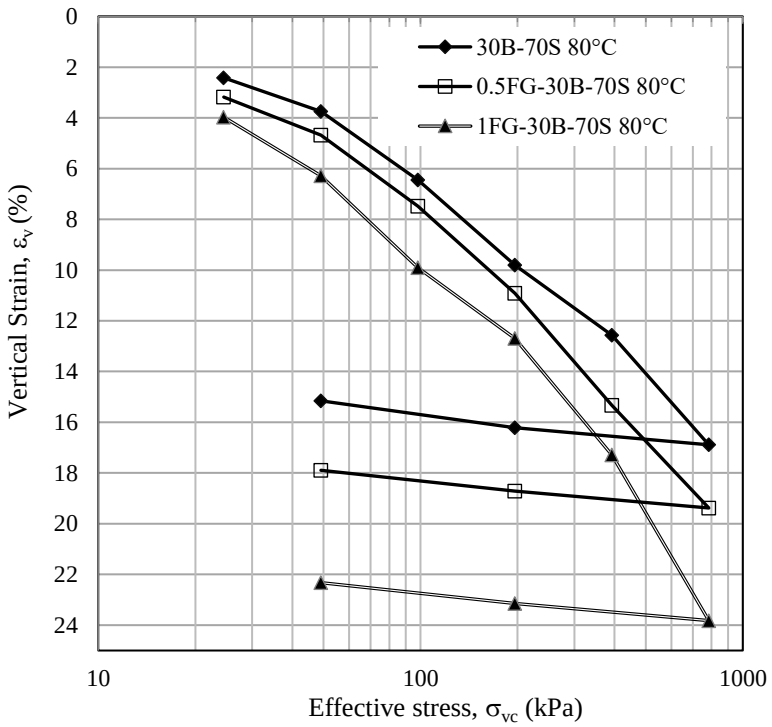


Figure 7.4 Compression and swelling curves of sand-bentonite mixtures under high temperature in the presence of fiberglass

Shariatmadari, & Saeidijam (2011) examined the compressibility parameters of sand-bentonite mixtures under high temperature and reported an increase in the slope of the compressibility curves. The reason for this phenomenon is explained as the temperature increases, void ratio decreases and accordingly the amount of compression increases (Jarad, 2016). Delage et al. (2000) observed contraction behavior in the normally consolidated clay soil as a result of their tests in the presence of high temperature. The plastic volumetric deformations occur in the soil after contraction. In Figure 7.5, the compression curves are shown under different temperatures. The change

in slope of the compression curves by high temperature clearly can be seen in Figure 7.5. It was seen that the slope of the compression curves of the sand-bentonite mixture increased under high temperature and the amount of compression increased by decrease in void ratio. It can be said that 0.5% fiberglass slightly increased the compression deformation amount, since the slope of the compression curve increased more under high temperature compared to the sand-bentonite mixture. The reason for this is that as the temperature increases, the gaps between the grains decrease and the amount of compression increases (Jarad, 2016).

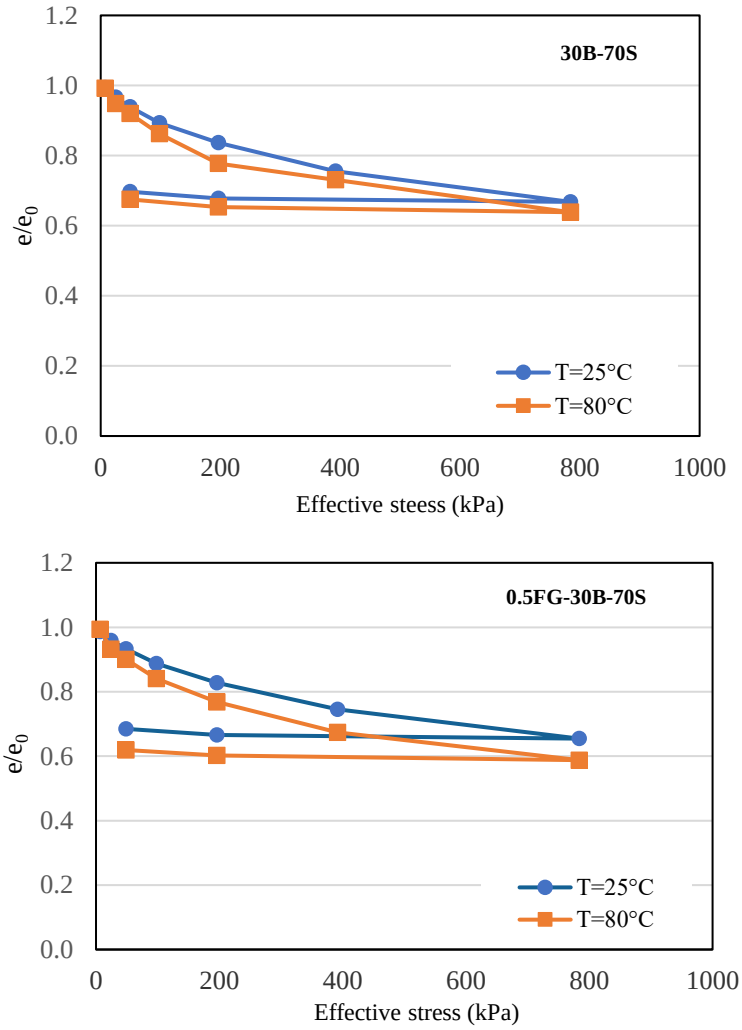


Figure 7.5 Effective stress vs e/e_0 relationships at different temperatures a) 30B-70S, b) 0.5FG-30B-70S

Ye et al. (2013) measured the swelling pressure at two different temperature values (20 and 40 °C) using bentonite. The swelling pressure values were determined as 3.02

and 3.41 MPa, respectively. It was revealed that with the increase in temperature, the swelling pressure increased and reached the peak point. It was also emphasized that the swelling pressure decreased before bentonite reached full saturation. On the other hand, as a result of experiments conducted at different temperatures, Jarad (2016) revealed that the relationship between swelling index and temperature is not strong, it affects negligible extents. Campanella and Mitchell (1968) also stated that the swelling index of illitic clays is not dependent on temperature and the rate of influence is minimal. The test results of the present study show that the swelling deformation amount of the mixtures decrased in the presence of fiberglass. It can be concluded that fiberglass has negligible effect on the volume deformation of sand-bentonite mixtures under high temperature.

The effect of fiberglass additive on the volumetric deformation behavior of sand-bentonite mixtures is given in Figure 7.6 under room and high temperatures, comparatively. The test results showed that the fiberglass additive changed the amount of compression under room temperature insignificantly, while it was observed that the amount of compression increased under high temperature. According to the results of the present study, the vertical compression deformation of mixtures increased under high temperature even in the presence of fiberglass. It can be concluded that fiberglass has no positive contribution to the volume deformation of sand-bentonite mixtures under high temperature.

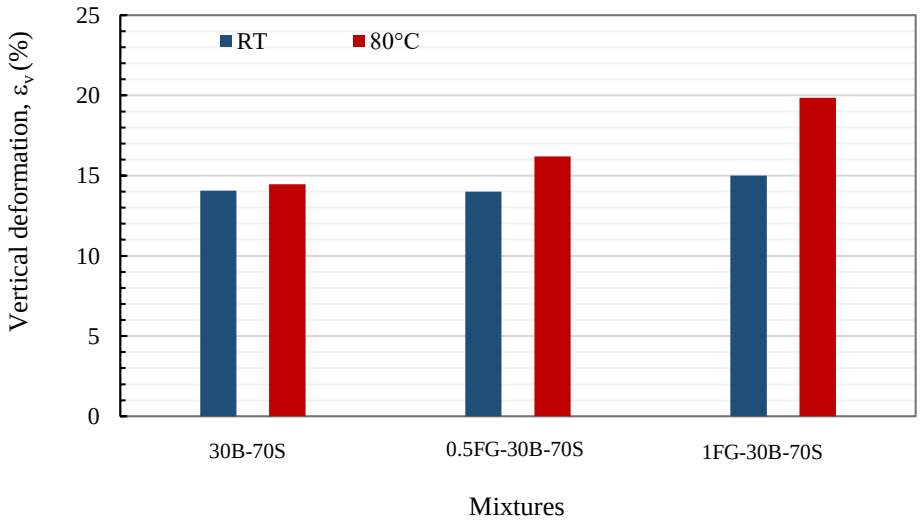


Figure 7.6 The effect of fiberglass on the compression deformation under room temperature and 80 °C

Contraction is interpreted as the deterioration of the skeleton of the soil due to heating, while expansion is interpreted as the enlargement of the spaces in the soil skeleton due to temperature (Towhata et al., 1993). It means that, the soil skeleton detoriates under high temperature and caused much more compression under high temperatures. The results of this study confirm this statement.

7.3 Shear Strength Behavior of Fiberglass Added Sand-Bentonite Mixtures

In this study, the fiberglass effect on the shear strength parameters of sand-bentonite mixtures at room temperature and high temperature was determined.

7.3.1 Shear Strength Behavior of Fiberglass Added Sand-Bentonite Mixtures Under Room Temperature

The direct shear tests were performed on the fiberglass added sand-bentonite mixtures under room temperature. The length of the used fiberglass samples were 3 mm and 6 mm in the tests. Table 7.4 shows the internal friction angle, cohesion and the maximum shear stress values obtained from the tests. It was obtained that fiberglass additives increased the maximum shear stress at 196 kPa stress level of the 30B-70S mixture, but there is no significant difference between 0.5% and 1% fiberglass additives.

In the experiments conducted with 6 mm fiberglass, it was observed that 0.5% fiberglass additive changed the internal friction angle and cohesion insignificantly, but 1.0% fiberglass additive increased the internal friction angle of the mixture from 28.6° to 32.3° (Figure 7.8). In the conducted tests, the positive effect of the length effect on the shear strength was not found to a high extent.

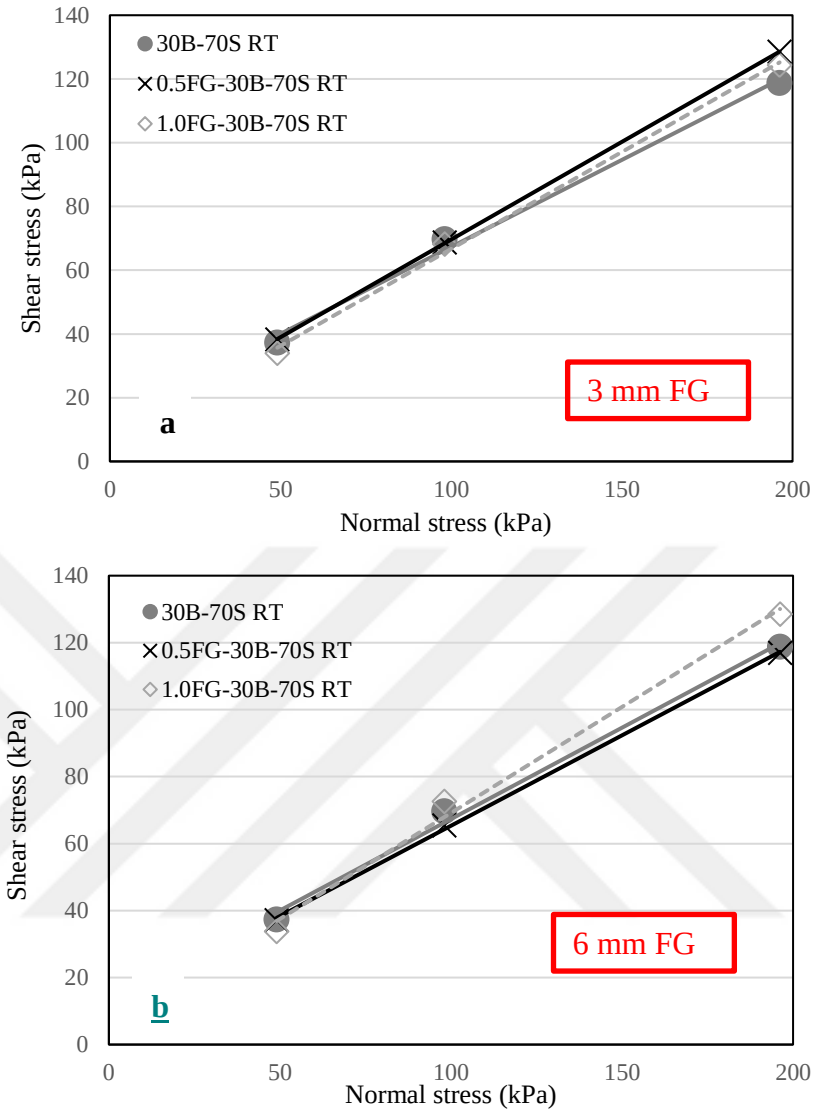


Figure 7.7 τ-σ relationship of 30B-70S mixtures in the presence fiberglass at room temperature a) 3 mm fiberglass, b) 6 mm fiberglass

The test results show that the increase in fiberglass length did not have a significant effect on the shear strength. Increasing the fiber length is preferred for reasons such as increasing the strength and optimizing the bending performance. However, the disadvantage of increase length of fiberglass is that as the length increases, the fibers become agglomerated and the homogeneity of the distribution of the fibers in the material deteriorates, forming a weak dispersion matrix (Lankard, 1972; Li, 2012). Özel, & Öz (2016) examined the fiber length, determined that the 28 days compressive strength of the material decreased by 1.5% as a result of increasing the fiber length from 16 mm to 30 mm. Similarly, Yoo et al. (2014) increased the fiber length from 16.3 mm

to 30 mm, resulting in a 1.2% reduction in strength. The reason for this is that as the length increases, the fragility increases and it becomes more difficult to repair the cracks formed in the fiber by moving away from each other (Figure 7.9) (Özel, & Öz, 2016). Similarly, the results of this study show that that as the fiberglass length increased from 3 mm to 6 mm, the maximum shear strength under normal stress of 196 kPa for 1.0FG-30B-70S mixture decreased by about 3.2%.

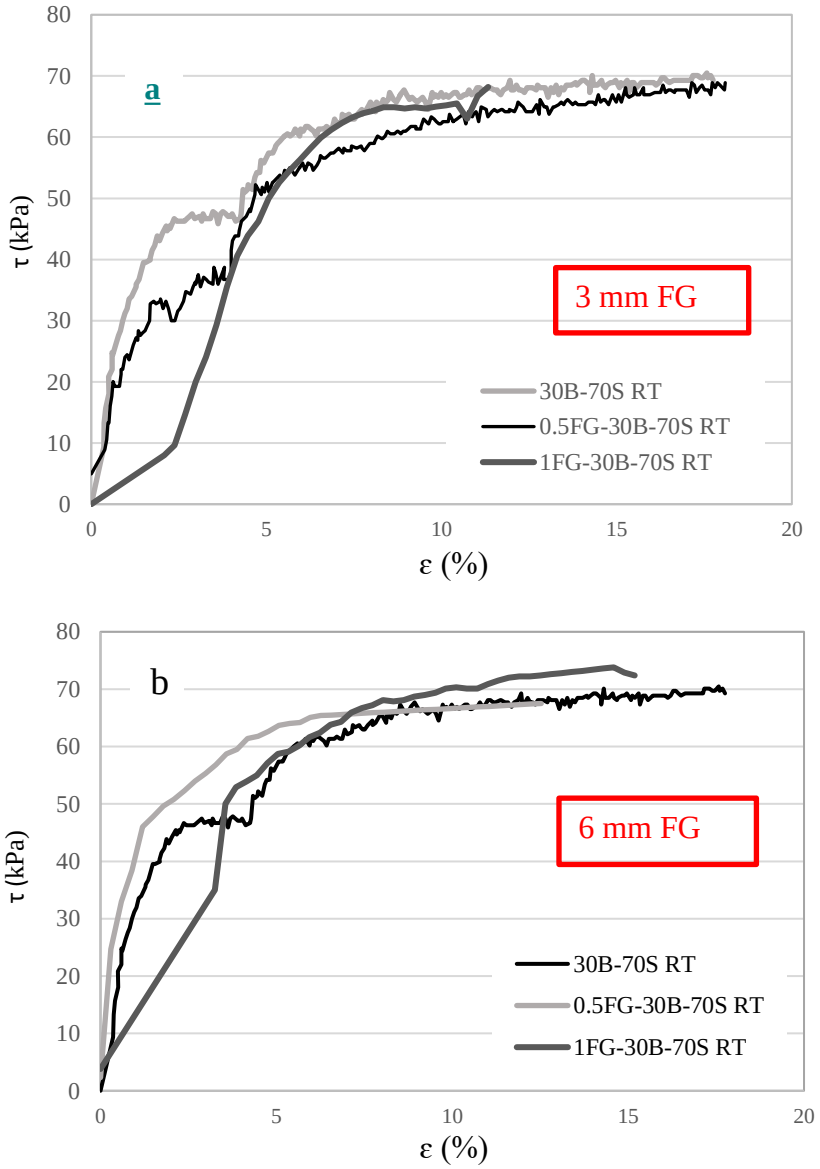


Figure 7.8 Shear stress-strain relationship of fiberglass added sand-bentonite mixtures at room temperature a) 3 mm fiberglass, b) 6 mm fiberglass

Table 7.4 Shear strength parameters of fiberglass added sand-bentonite mixtures at room temperature

		3 mm Fiberglass			6 mm Fiberglass		
Mixture	Normal stress (kPa)	Max. Shear stress (kPa)	Ø (°)	c (kPa)	Max. Shear stress (kPa)	Ø (°)	c (kPa)
30B-70S	49	37.5	28.6	12.7	37.5	28.6	12.7
	98	69.3			69.3		
	196	118.2			118.2		
0.5FG-30B-70S	49	38.3	31.6	8.3	37.1	28.4	11.4
	98	68.8			65.4		
	196	128.8			116.9		
1.0FG-30B-70S	49	33.9	31.3	5.9	33.8	32.3	5.9
	98	68.2			72.6		
	196	124.3			128.5		

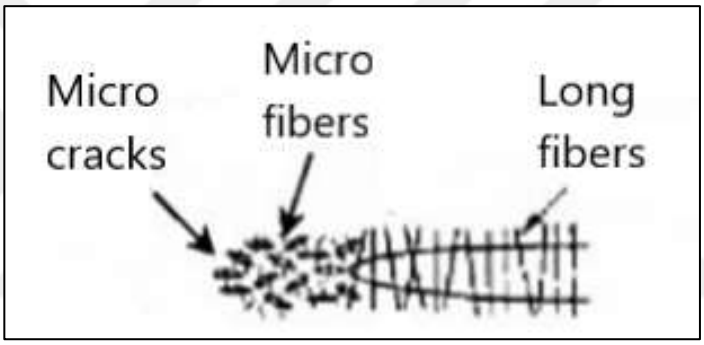


Figure 7.9 Cracks in long fibers (Betterman, 1995)

7.3.2 Shear Strength Behavior of Fiberglass Added Sand-Bentonite Mixtures Under High Temperature

The direct shear tests of fiberglass added sand-bentonite mixtures were performed under room and high temperature in order to determine the contribution of fiberglass to the mixtures' shear strength especially under high temperature (Figure 7.10). The experimental results showed an improvement at the shear strength parameters was obtained under high temperature of 30B-70S sample without any additive (Table 7.5). The effect of fiber glass was more significant under high temperature. The crystalline and amorphous region forming the structure of the fibers greatly affects the behavior of the material. The low melting point of the amorphous region and its lower heat resistance than the crystalline region affect the fiber matrix (hammaddekurutma.com).

For this reason, the expected strength increase with temperature was not observed more than expected.

Tablo 7.5. Shear strength parameters of fiberglass added-sand bentonite mixtures under room and high temperatures

Mixtures	Room Temperature		80 °C	
	ϕ' (°)	c' (kPa)	ϕ' (°)	c' (kPa)
30B-70S	28.6	12.7	31.1	15.0
0.5FG-30B-70S (3 mm)	28.0	8.3	30.3	14.2
1FG-30B-70S (3 mm)	31.3	5.9	31.8	12.5

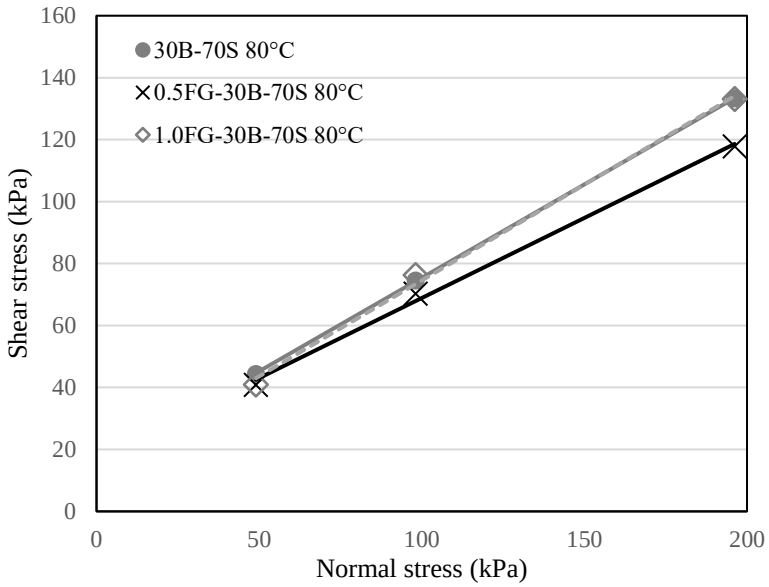


Figure 7.10 τ-σ relationship of 30B-70S mixtures in the presence fiberglass additive (3 mm) at high temperature

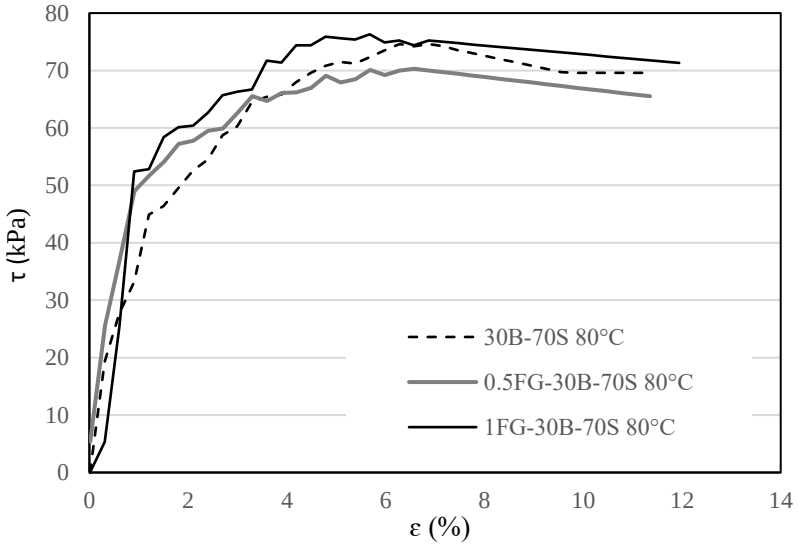


Figure 7.11 Shear stress-strain relationship of sand-bentonite mixtures under high temperature in the presence of 3 mm fiberglass additives

Figure 7.11 shows the effect of fiberglass additives on the maximum shear stress value of sand-bentonite mixtures under high temperature. While 0.5% fiberglass additive was not enough to increase the maximum shear stress value, a slight increase in the maximum shear stress value was observed with 1% fiberglass additive, however, this increase was negligible.

Table 7.6 Maximum shear stress values of sand-bentonite mixtures in the presence of fiberglass additives under high temperature

Mixture	**Maximum Shear Stress (kPa)**
30B-70S	74.6
0.5FG-30B-70S	70.3
1.0FG-30B-70S	76.3

Within the scope of this thesis, the change in shear strength with different fiberglass lengths was investigated and it was seen that the increase in fiberglass length did not increase the shear strength, contrary to expectation. The shear stress and strain values of 3 and 6 mm fiberglass lengths are given in Figure 7.12 and the maximum shear stress values were determined as 72.6 kPa and 76.3 kPa, respectively. The results showed that

the increase in fiberglass length did not increase the shear strength. Similar to Yoo et al. (2014) findings, it was observed that when the fiber length was increased from 16.3 mm to 30 mm, approximately 1.2% strength loss was observed.

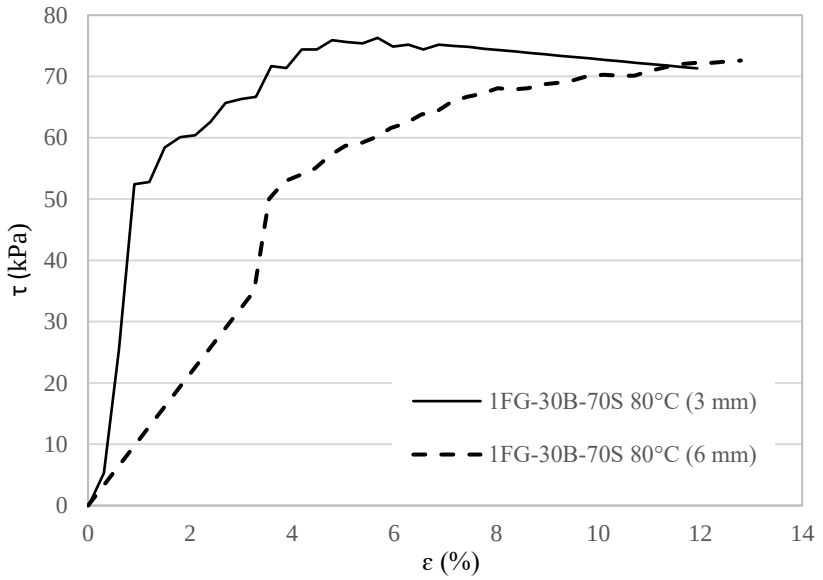


Figure 7.12 Shear stress-strain relationship of 1FG-30B-70S mixtures under high temperature in the presence of 3 mm and 6 mm fiberglass additives

The results of the experiments showed that the fiberglass additive had a reducing effect on the maximum shear stress value under room temperature (Figure 7.13). It was observed that only 1% fiberglass additive had a strength-enhancing effect under high temperature. However, it should be noted that this increase appeared to a negligible extent. Harmancıoğlu (1981) revealed that the strength of the fiberglass will change after 250 °C and over time. In this study, the test temperature was not so high as 250 °C. For that reason, the loss of strength in the fiberglass additive can be explained by the fact that the amorphous region in the structure of the fiber is affected by the temperature and the crystal also affects the region. The reason why this loss does not occur in 1% fiberglass contribution may be due to the different ratio of amorphous and crystalline regions in each fiber structure (Harmancıoğlu ,1981).

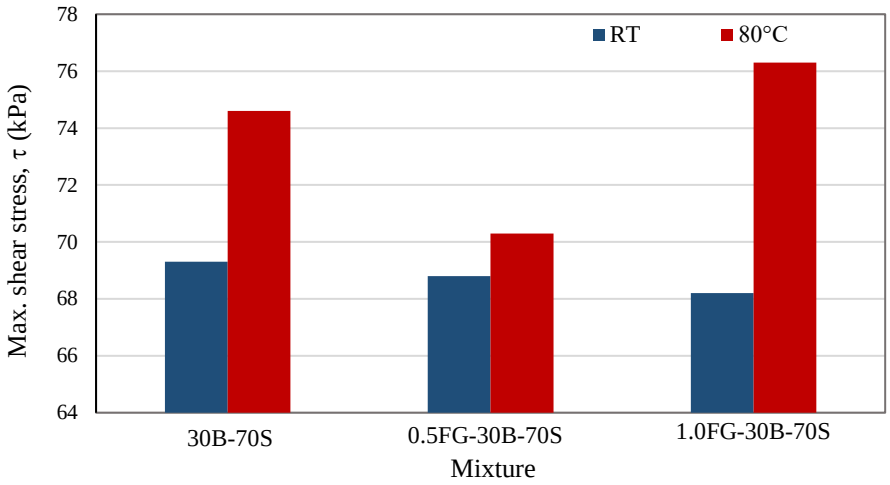


Figure 7.13 Maximum shear strength values of fiberglass added sand-bentonite mixtures at room temperature and 80 °C

7.4 Hydraulic Conductivity Behavior of Fiberglass Added Sand-Bentonite Mixtures Under Room and High Temperatures and Thermal Cycles

The hydraulic conductivity tests of 30B-70S, 0.5FG-30B-70S and 1FG-30B-70S mixtures were conducted in the flexible wall permeameters. The temperature of the tests was started from room temperature (~25 °C) and increased to 50 and 80 °C, respectively. While the cell water temperature was 25, 50, 80 °C, the sample temperature was measured as 20, 40, 60 °C. The obtained hydraulic conductivity coefficients (k) under different temperatures are given in Table 7.7.

Table 7.7 Hydraulic conductivity values of the mixtures at different temperatures

Cell Temperature (°C)	**k (m/s)**		
	30B-70S	**0.5FG-30B-70S**	**1.0FG-30B-70S**
25	4.3E-11	2.5E-10	3.3E-10
50	3.2E-10	3.8E-10	4.1E-10
80	5.0E-10	5.4E-10	5.6E-10
50	*	3.2E-10	3.7E-10
25	-	3.1E-10	3.4E-10

*The test is continuing.

The results have shown that the hydraulic conductivity values increased with increase in temperature. This increase is mainly due to the decrease in the viscosity of water as

the temperature increases, as emphasized in the former studies in the literature. At the same time, the interaction of the soil with water also has an effect on this situation (Romero et al., 2001; Pusch & Güven, 1990; Pons et al, 1994). On the other hand, it was observed that as the fiberglass additive content was increased, the hydraulic conductivity of the mixtures increased and the fiber acted as a path for flow of water.

According to the results, it should be noted that the fiberglass does not contribute to the hydraulic conductivity, increased the hydraulic conductivity of the sand-bentonite mixture under high temperature. Djeghader and Redjel (2017) revealed that in contact of fiberglass with water, water can enter between the fiber and whatever other material forming the mixture, due to capillarity, and this may weaken the structure of the fiberglass and lead to crack formation (Imielińska, & Guillaumat, 2004; Zhang, & Zhan, 2004; Kootsooks, & Mouritz, 2004).

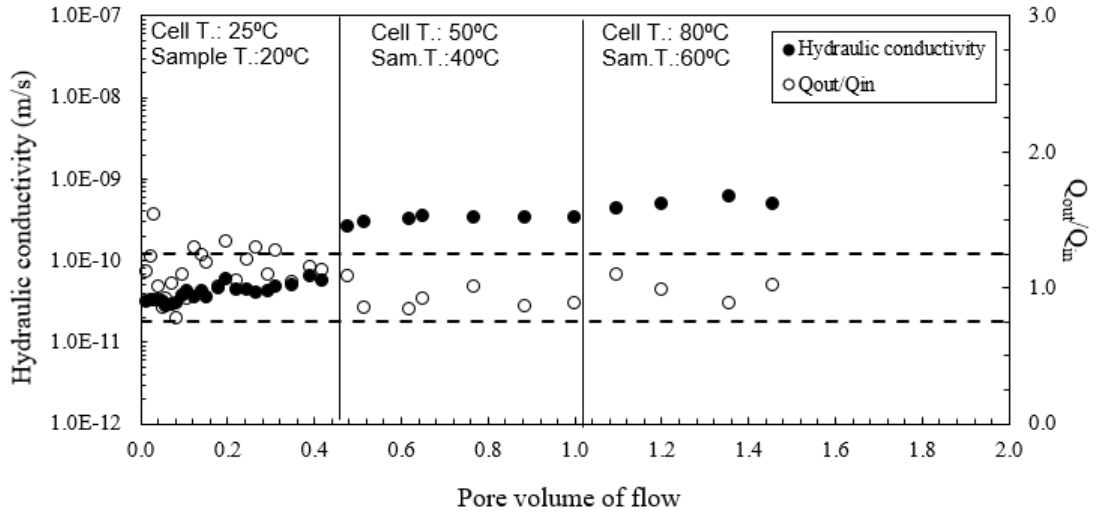


Figure 7.14 Hydraulic conductivity behavior of 30B-70S mixture under different temperatures

Figure 7.14, 7.15 and 7.16 shows the hydraulic conductivity values of the 30B-70S mixture and the fiberglass added mixtures in terms of pore volume of flow under different temperatures. It was observed that the hydraulic conductivity increased as the temperature increased due to the decrease in viscosity, as observed in former studies (Abuel-Naga, 2005; Ye et al., 2013). According to this, the fluctuations in the hydraulic conductivity values depending on the temperature clearly can be seen from Figures 7.14, 7.15 and 7.16.

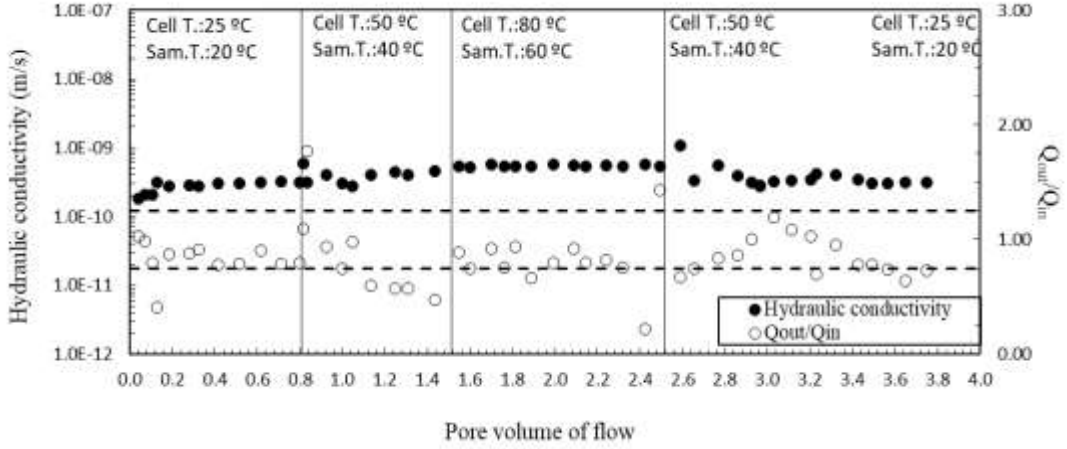


Figure 7.15 Hydraulic conductivity behavior of 30B-70S mixture with 0.5% fiberglass at different temperatures

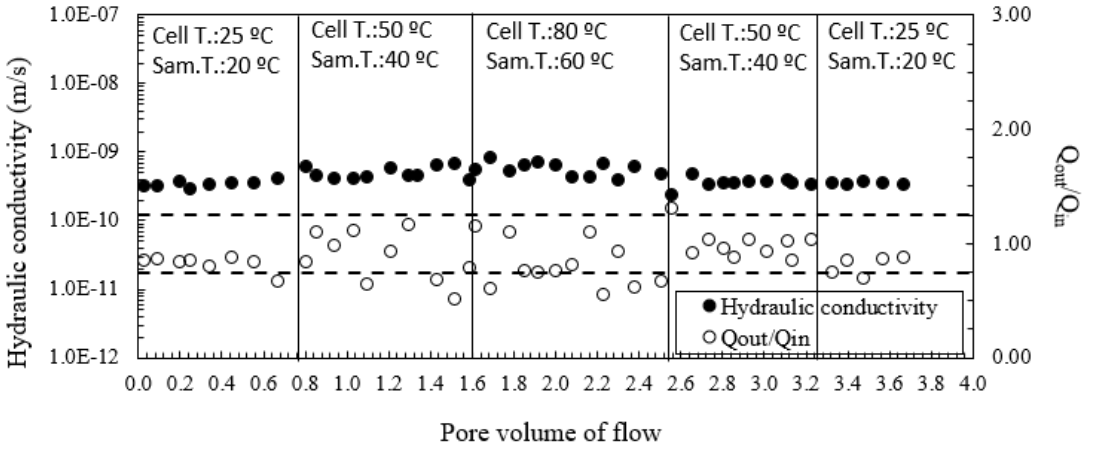


Figure 7.16 Hydraulic conductivity behavior of 30B-70S mixture with 1.0% fiberglass at different temperatures

Figure 7.17 shows the hydraulic conductivity values under different temperatures when 0.5% and 1% fiberglass additives were added to the 30B-70S mixtures. It was observed that the hydraulic conductivity increased as the fiberglass content increased at all temperatures, but the most significant increase occurred under room temperature. As can be seen from Figure 7.17, the increase in the ratio of fiberglass additive in the mixture caused the increase in hydraulic conductivity the most under room temperature. While each mixture experienced an increase in hydraulic conductivity with the increase in temperature observed. Furthermore, the differences between different additive contents for the same temperature were in small. It was determined that the role of the

fiberglass additive in affecting the hydraulic conductivity was quite low as the amount of additive increases under high temperature.

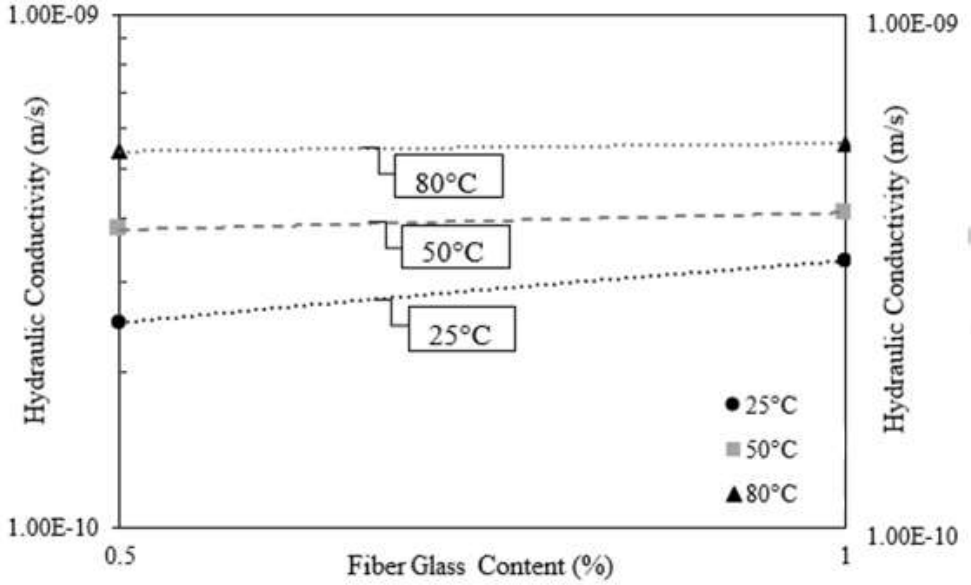


Figure 7.17 Change in hydraulic conductivity depending on fiberglass content at different temperatures

The Figure 7.18 shows the hydraulic conductivity values under different temperatures when 0.5% and 1% fiberglass additives were added to the 30B-70S mixtures. It was observed that the hydraulic conductivity increased as the fiberglass content increased at all temperatures. As can be seen from Figure 7.18, increase in the fiberglass additive in the mixture caused increase in hydraulic conductivity the most under room temperature.

It should be notedt that that the differences between 0.5% and 1.0% additives were too small. It was determined that the role of the fiberglass additive in affecting the hydraulic conductivity is quite low as the amount of additive increases under high temperature.

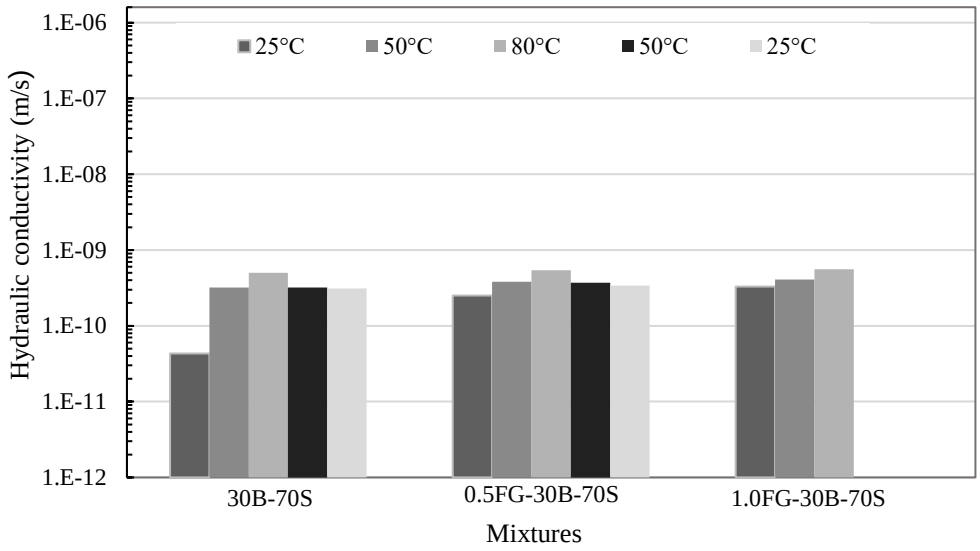


Figure 7.18 Hydraulic conductivity of sand-bentonite mixtures under different temperatures in the presence of fiberglass additives

7.5 Thermal Conductivity of the of Fiberglass Added Sand-Bentonite Mixtures

By virtue of fiberglass high thermal conductivity, it can rapidly conduct heat. For that reason, the thermal conductivity values of 30B-70S samples were measured in the presence of 0.5% and 1.0% fiberglass additives and the results are given in Table 7.8. It was observed that both fiberglass contents have increasing effect on the thermal conductivity of the 30B-70S mixture. The use of fiberglass additives in areas such as buried power cables or nuclear waste landfills may have a positive effect on the heat transfer.

Tablo 7.8 Thermal conductivity values of fiberglass added-sand bentonite mixtures

Samples	**Thermal Conductivity (λ, W $m^{-1}K^{-1}$)**
30B-70S	1.621
0.5FG-30B-70S	1.697
1.0FG-30B-70S	1.698

CHAPTER 8
MODELING THE BUFFER MATERIAL AROUND NUCLEAR WASTE STORAGE AREA

8.1 Nuclear Waste Storage Repositories

Disposal of nuclear waste is of great importance in terms of human and environmental health. Nuclear wastes are formed as a result of the irradiation of uranium fuels in their reactors. The main components of nuclear waste can be listed as unburned uranium, plutonium, curium, americium, neptunium (Crowley, 1997). Nuclear waste is categorized into three different groups as high-level waste (HLW), intermediate-level waste (ILW), and low-level waste (LLW). Briefly, in LLW the effluents contain traces of long-lived nuclides and are compressed prior to storage (Kurniawan et al., 2022; Omoto, 2005). The sludge formed chemical wastes, fuel wastes and dirty materials from reactors are stored. Even after 1000 years, radioactivity will continue (Kurniawan et al., 2022; Conca et al., 1998). HLW contains both long- and short-lived radionuclide-containing wastes and represents highly concentrated wastes that require very high protection (Kurniawan et al., 2022).

In the storage of nuclear wastes (radionuclides), the wastes are regularly placed in a sealed, gas and water-free copper container called a canister. In order to prevent the canister from being damaged by a movement in the bedrock or by dangerous substances that may be present in the groundwater, it is covered with a buffer material. This material is usually clay-containing, due to its low permeability. Buffer materials should be in harmony with the canister and the bedrock. The mechanical support of the bedrock and the closure of the transport paths that may occur are directly related to the buffer material. Another important issue is the burial depth of the wastes into the bedrock. The depth for such wastes is generally foreseen as 400-500 m below the ground (Figure 8.1). Because at such depths, human error or intervention is close to impossible and there is slow movement of groundwater at the same time (Raiko et al., 2012).

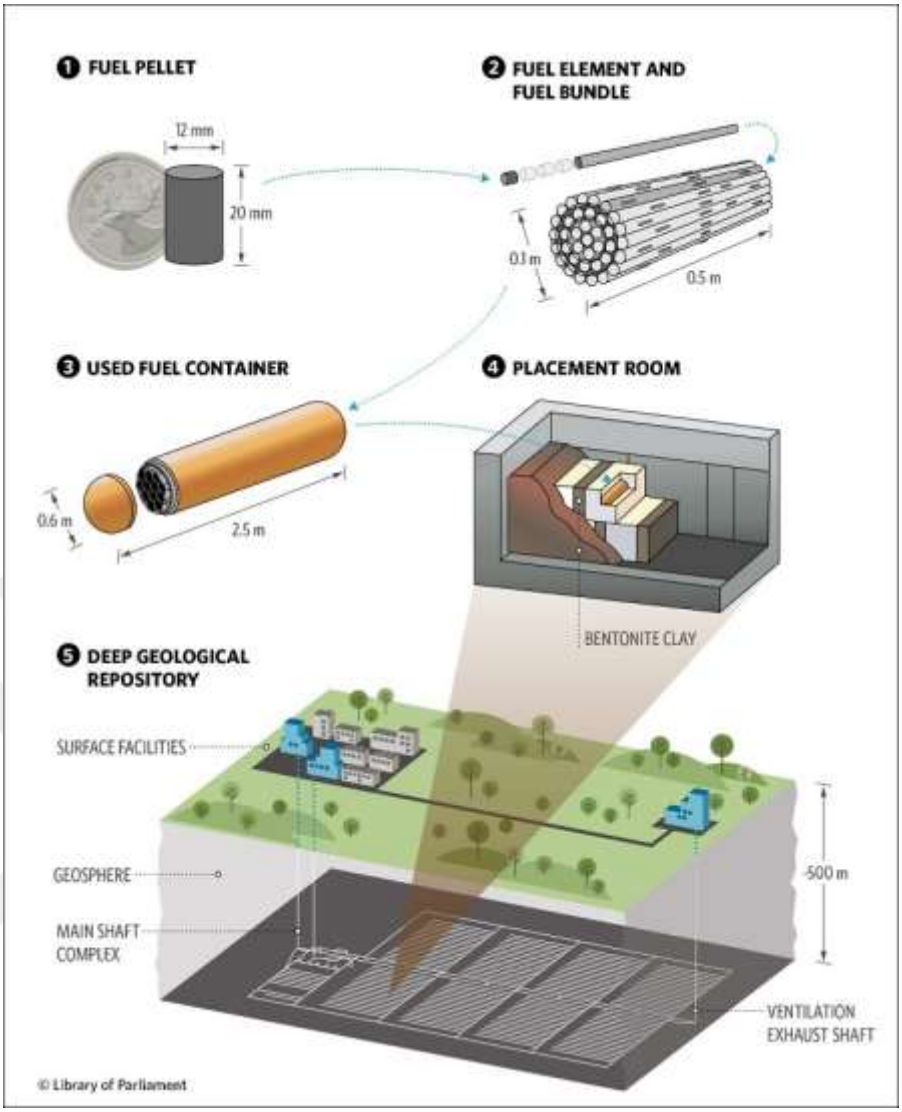


Figure 8.1 Deep Geological Repository Conceptual Design (Deep Geological Repository Conceptual Design Report, 2016)

The safe and rapid disposal of radioactives is an issue of great importance. The possibility, speed and importance of leakage of radioactive wastes should be examined from many chemical, mathematical and scientific aspects (Kurniawan et al., 2022). For example, although granite is found in rock formations in the Lake District in the United Kingdom, it is not preferred because fractures in the rocks cause effluent leakage (Stewart, 2002, Veliscek-Carolan, 2016).The burial of radioactive wastes in the bedrock varies according to the country regulations. For example, Switzerland determined this depth between 600-900 m, while Canada determined it as 500-1000 m and Finland about 500 m (Sellin and Leupin, 2013). Finland uses a warehouse, copper drums and bedrock to store nuclear waste at a depth of about 420 m in Olkiluoto (Raiko et al., 2012).

Sweden and Russia prefer to use a crystalline rock for the disposal of nuclear waste. The depth of bedrock in Sweden is about 600-800 m and there are about 6.000 canisters (Muller et al., 2019). These copper elements were coated with a clay buffer (bentonite) in order to prevent them from corrosion due to groundwater. The material to be used as a buffer must have some basic properties. For example, very low hydraulic conductivity and self-sealing ability slow leachate's progress and maintain its service life for a specified period (Sellin and Leupin, 2013). In addition to these, it should have high thermal resistance material against high temperatures. Radioactive wastes are stored deep in the ground in canisters for years (Kurniawan et al., 2022).

Within the scope of this doctoral study, the modeling of additive free sand-bentonite mixtures as a buffer material around the nuclear waste landfill was performed using the Code Bright program.

8.2 Modeling with Code Bright Programme

It was aimed to use the sand-bentonite mixtures as a buffer around the nuclear waste storage areas with the Code Bright Program and to compare the analysis results by modeling. The Code Bright is a program that can perform thermo-hydro-mechanical (THM) analysis using the Finite Elements Method (FEM). It was developed by the Department of Civil and Environmental Engineering of the Polytechnic University of Catalonia (UPC) and works in conjunction with an extension called GiD.

In this context, host rock size was chosen as 60x60 m, buffer diameter and canister diameter of 6 m and 1 m, respectively. All required data for modeling for the 10B-90S, 20B-80S and 30B-70S mixtures (buffer) were obtained from the experiments of this study (Table 8.2). In Figure 8.2, the geometry of the storage area, the plan view of one of the sand-bentonite mixture to be used as a buffer and the bedrock are given. In addition, the generated meshes are shown as representative.

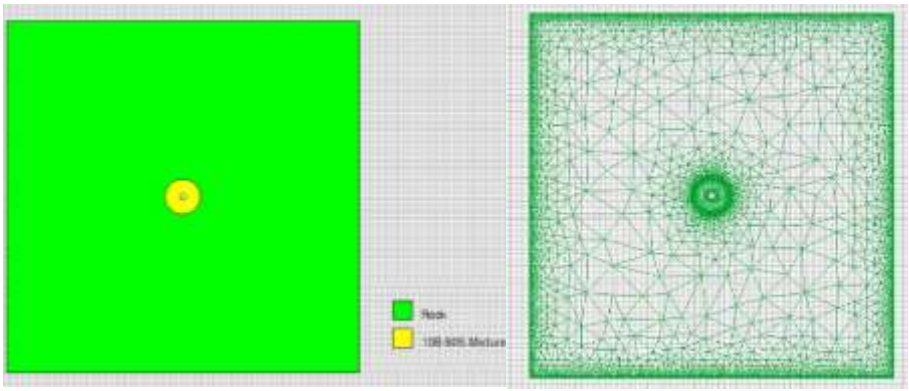


Figure 8.2 Modeling phases around nuclear waste storages for the 10B-90S mixture

Table 8.1 The mechanical and thermal properties needed for modeling (Code Bright Tutorial 2020)

Problem	**Problem**	**Parameter**
Mechanical	Rock	Density (ρ_{nat})
	Buffer zone	Density (ρ_{nat})
Thermal	Rock	Thermal conductivity (λ_{dry} & λ_{sat})
		Spesific heat (C_s)
	Buffer zone	Thermal conductivity (λ_{dry} & λ_{sat})
		Spesific heat (C_s)
	Canister	Heat flow (induced by nuclear waste)

In order to model; density, thermal conductivity, specific heat and heat flow data of the bedrock and mixture selected as the buffer and the canister are needed (Table 8.1). The data required for bedrock and canister are taken from Code Bright Tutorial. The data of the sand-bentonite mixtures (10B-90S, 20B-80S and 30B-70S) to be used as a buffer were obtained as a result of the experiments conducted within the scope of this doctoral thesis. The time factor is important for the formation of boundary conditions and the interval value must be determined. In the modeling study, the final time was chosen as 100 years (Figure 8.3).

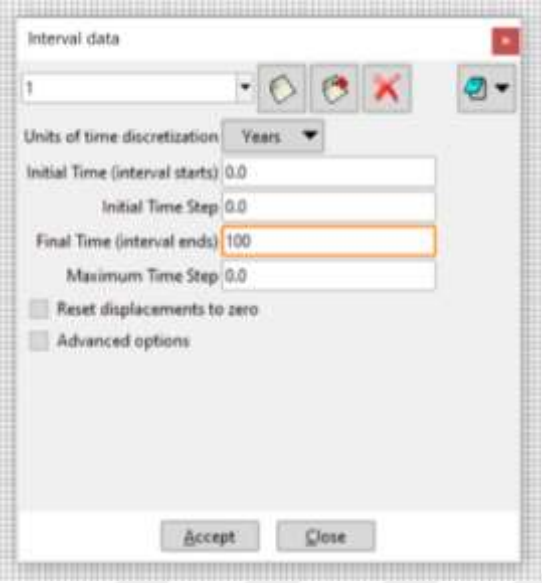


Figure 8.3 Interval data window (Code Bright Tutorial 2020)

Table 8.2 Parameters used in the modeling obtained from experimental studies of the present study

Mixtures	Thermal Conductivity (w/mK)	Vol. Heat capacity (MJ/m^3K)	Heat Capacity (J/m^3K)	γ_n (kg/m^3)	Specific heat (J/kgK)	Hydraulic conductivity (m/s)
10B-90S	1.877	2.260	2260000	1875	1205	8.2×10^{-7} m/s
20B-80S	1.874	2.619	2619000	1833	1429	3.3×10^{-10} m/s
30B-70S	1.621	2.611	2611000	1825	1431	4.3×10^{-11} m/s
Rock*	3.000	-	-	2500	800	-

*Code Bright manual data for host rock

Thermal conductivity, volumetric heat capacity, heat capacity, natural unit weight, specific heat and hydraulic conductivity values of sand-bentonite mixtures are given in Table 8.2. Hard crystalline rocks, clayey rocks and salty rocks are generally chosen for the bedrock in which nuclear waste is buried. For example, France uses mudstone for this concept (Gens, & Olivella, 2001). The main rock considered in the design phase of this study is andesite. Thermal conductivity values were determined for all mixtures by measuring with Tempos instrument. With the same instrument but with a different probe, the volumetric heat capacity was determined and converted to its heat capacity

with unit conversion. The specific heat value is obtained as the ratio of the heat capacity value to the unit weight. The natural unit weight values were obtained from maximum dry unit weight values which were obtained with Standard Proctor tests. The hydraulic conductivity values were determined under room temperature with flexible wall permeameters within the present study.

8.3 Finite Element Method (FEM) Analysis of Sand-Bentonite Mixtures as a Buffer Material

Within the scope of this doctoral thesis, a modeling study was performed to simulate and analyse the use of 10B-90S, 20B-80S and 30B-70S mixtures as a buffer material in nuclear energy storage areas. Two conditions were used for this analysis: a) Initial unknown surface temperature condition b) Flux B.C. Boundary flow rate conditions. Boundary flow rate for rock mass limits and initial temperature for bentonite/rock interface surfaces conditions were determined. The temperature along the bedrock boundary was determined as 25 °C. The initial unknown value of bentonite surfaces was chosen as 20 °C. The boundary flow rate for the canister is the heat flow 200 J/s.

In this modeling study, the dimensions of the bedrock were selected as 60x60 m, the diameter of the buffer element was 6 m and the length was 6 m in the horizontal (horizontal storage) direction. Drilling depth was taken as 30 m. A canister element with a diameter of 1 m was placed in this hole. The radial thickness of the buffer zone was 2.5 m.

8.3.1 Evaluation of Performance of 10B-90S Mixture with FEM Analysis

The time for half of the amount of a radioactive element decay is called as half-life, and this time varies depending on the structure of the nucleus. In this analysis, the half-life was taken as 100 years.

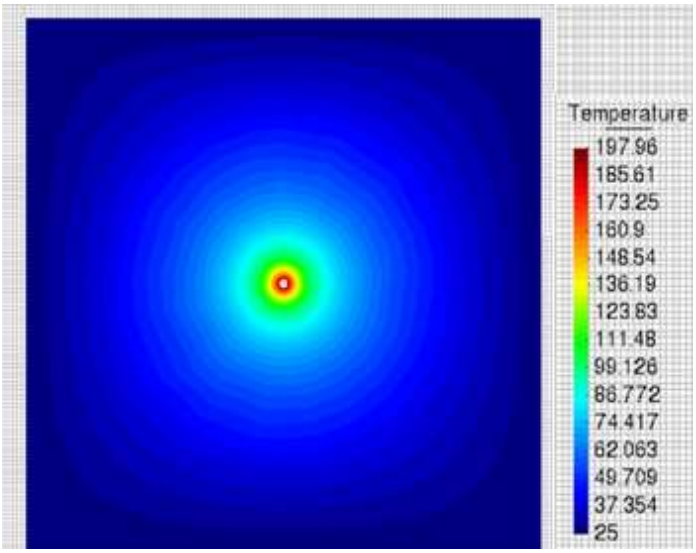
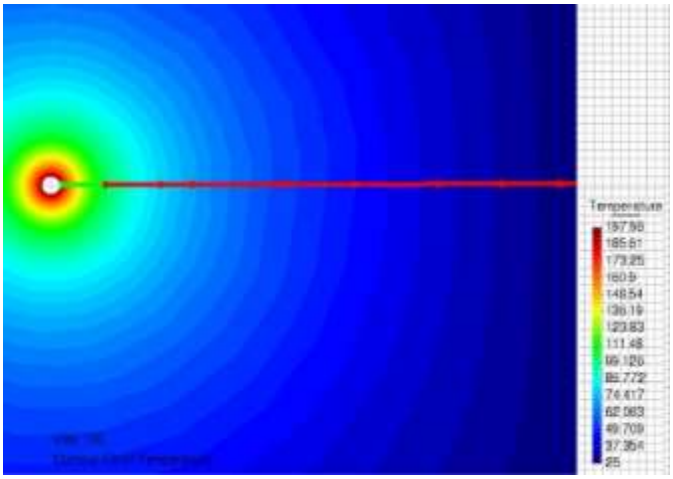


Figure 8.4 Contour fill of temperature representation in the presence of 10B-90S buffer mixture at the end of the time

The temperature change from canister to host rock at the end of this period is shown in Figure 8.4. At the end of the 100-year final interval value, it was determined that the temperature in the canister reached 197.96 °C, and 111.48 °C in a part of the green colored zone where the 10B-90S mixture was used as a buffer. The decreased conduction of the temperature from the canister to the bedrock was supplied with the help of the primary buffer bedrock and the secondary buffer sand-bentonite mixture. Figure 8.5 shows the variation of temperature with respect to distance from the axis of the canister. It shows the decrease in temperature of the canister based on the distance of 30 m from the center of the canister to the bedrock.



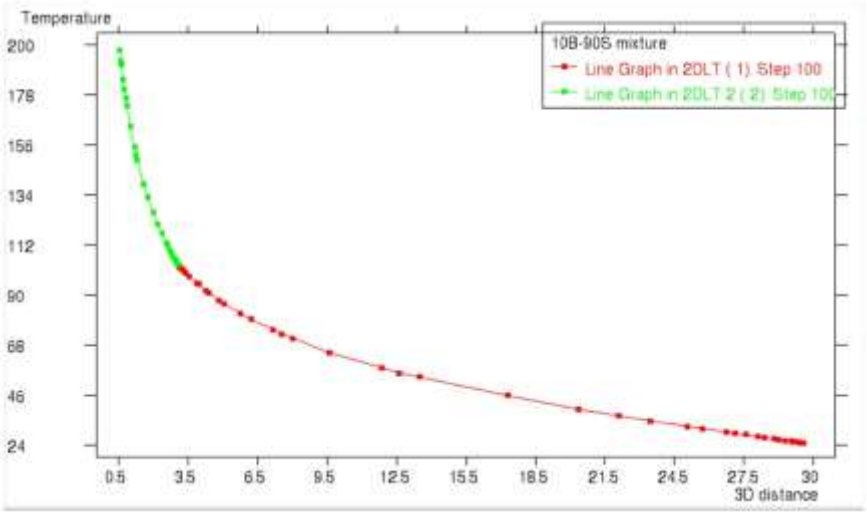
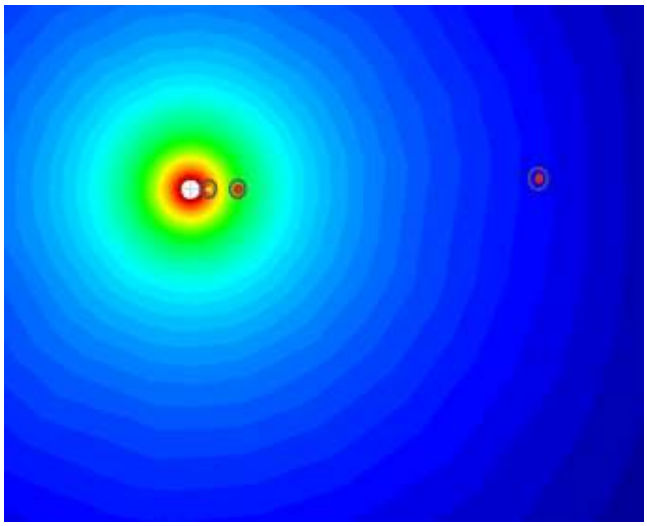


Figure 8.5 Temperature vs. distance relationship

Figure 8.6 indicates that the heat conducted from the canister can be distributed from the 10% bentonite-90% sand mixture, which means that this mixture can act as a buffer. For a selected point (10 isochrone), the temperature of the canister (red zone-line) was determined to be approximately 160 °C, in the buffer zone (green zone-line) 100 °C, and close to the boundary zone of the bedrock (blue zone-dark green line) approximately 40 °C.



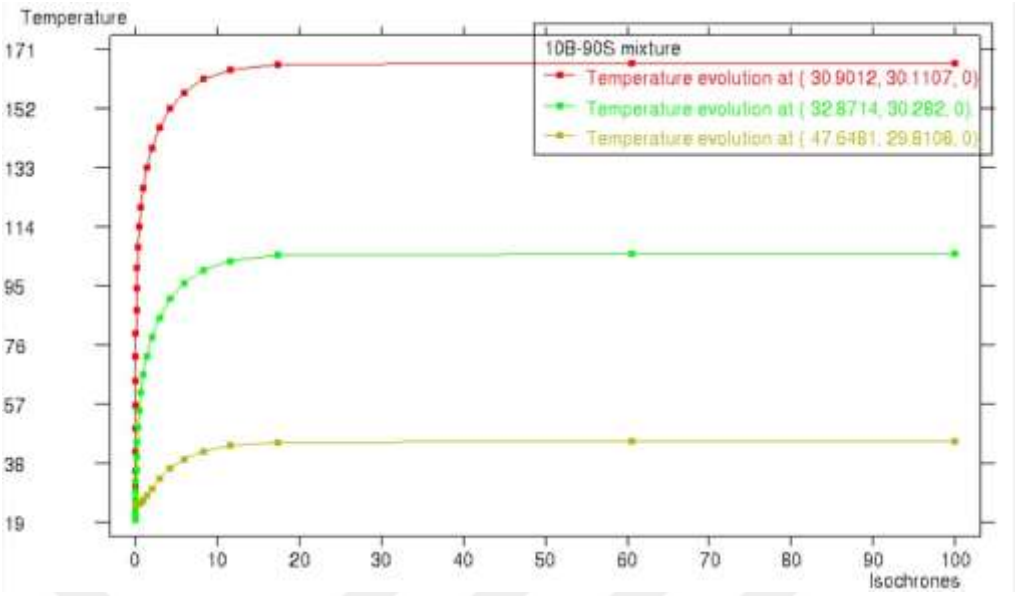


Figure 8.6 Point temperature evalution

8.3.2 Evaluation of Performance of 20B-80S Mixture with FEM Analysis

In this study, 20B-80S sand-bentonite mixture was used as a buffer material to conduct the heat from spreading the canister. According to the results, the temperature values reached at the end of the 100-years are given in Figure 8.7. The temperature values reached with the 20B-80S mixture were quite close to the values when the 10B-90S mixture is used as a buffer. The reason for this is that the thermal conductivity values of these two sand-bentonite mixture materials used as buffers were very close to each other. Where the rapid transfer of heat from the heat source (canister) depends on the higher thermal conductivity. It should be noted that, other engineering properties like swelling potential, volume deformation are also important parameters for buffer material.

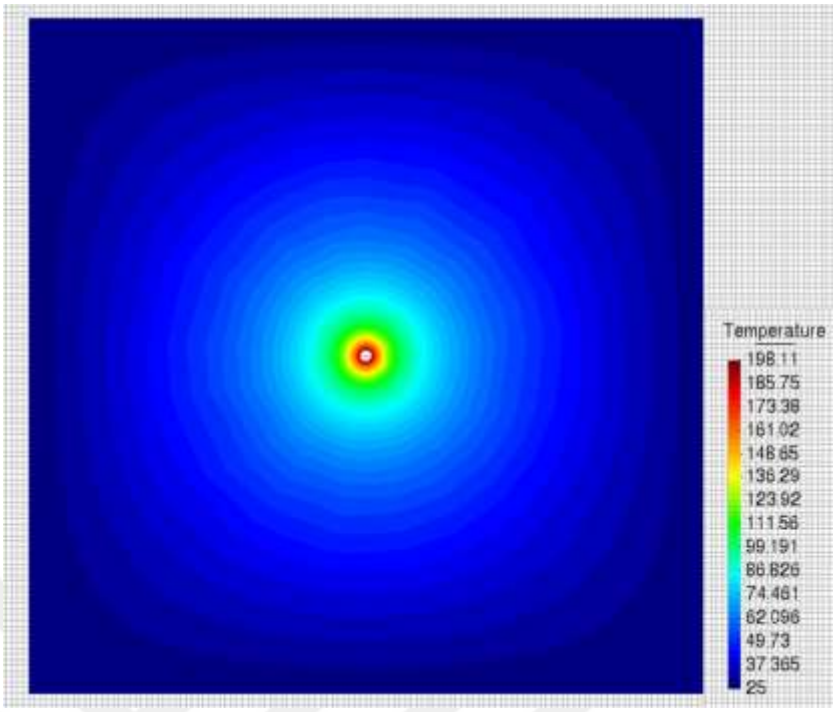
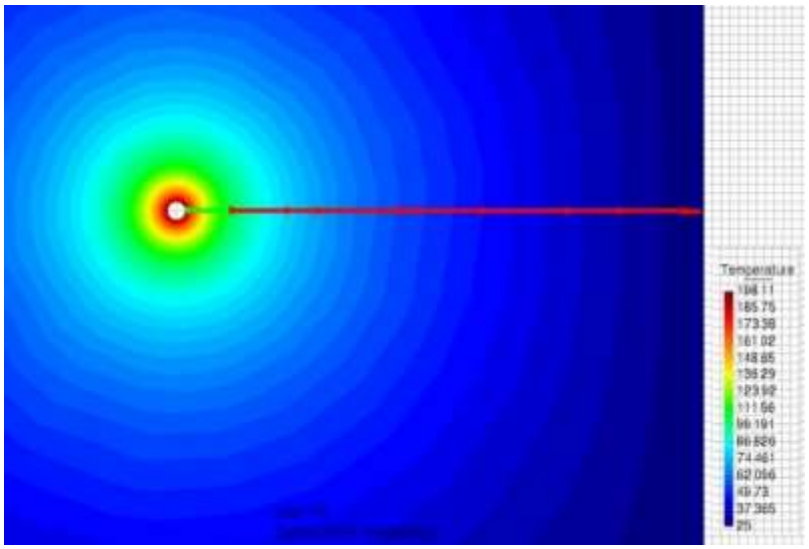


Figure 8.7 Contour fill of temperature representation in the presence of 20B-80S buffer mixture

Figure 8.8 shows the temperature change on a virtual line determined from the canister to the bedrock. It is seen that the temperature decreased with distance from the canister.



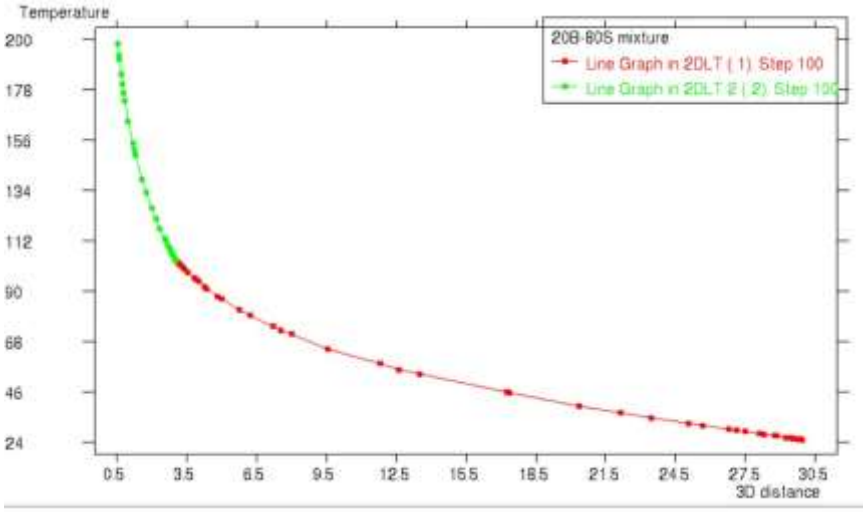
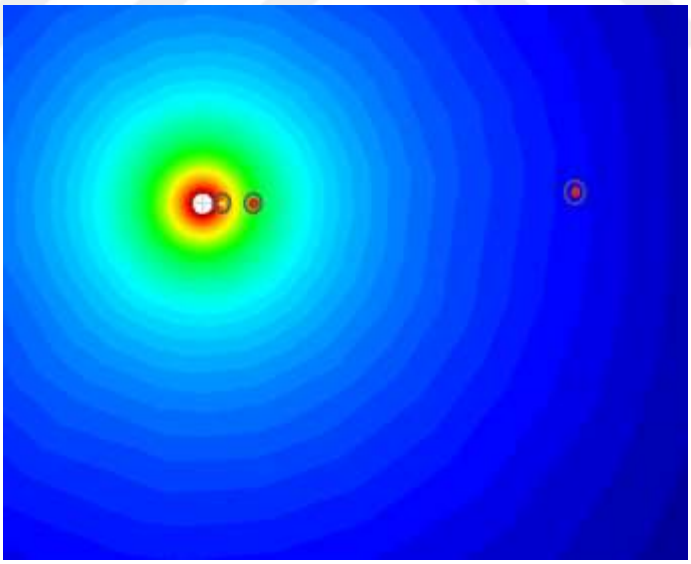


Figure 8.8 Temperature vs. distance relationship

Figure 8.9 shows the temperature values of point-based canister (red zone), buffer zone (green zone) and bedrock (blue zone). For instance, based on 100 isochrons (total bedrock size of 60 meters), temperature values for 50 isochronous distances were analyzed as approximately 160, 105 and 40 °C for the red, green and blue zones, respectively.



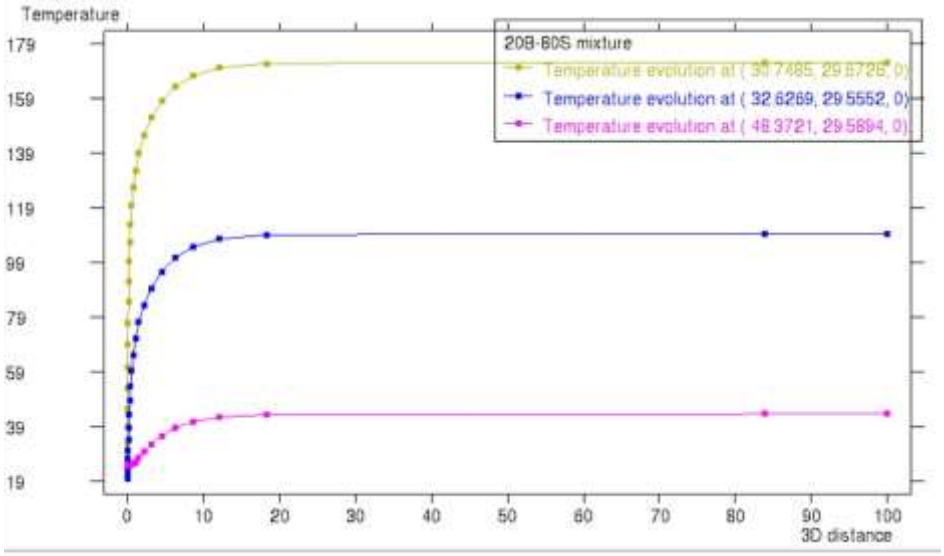


Figure 8.9 Point temperature evalution

8.3.3 Evaluation of Performance of 30B-70S Mixture with FEM Analysis

In this section, modeling results of the use of 30B-70S sand bentonite mixture as a buffer material around the canister element where radioactive wastes were stored are given.

Figure 8.10 shows the temperature change on a virtual line determined from the canister to the bedrock. The test results revealed that the final temperature values reached as a result of using the 30B-70S mixture as a buffer were higher than the 10B-90S and 20B-80S mixtures. The main reason for this is that the thermal conductivity of the 30B-70S mixture is lower than the other two mixtures, such as 1.621 W/mK, and accordingly, the lower heat conduction potential in transferring the heat generated in the canister caused the temperature to be higher for all three zones (canister surface, buffer, host rock).

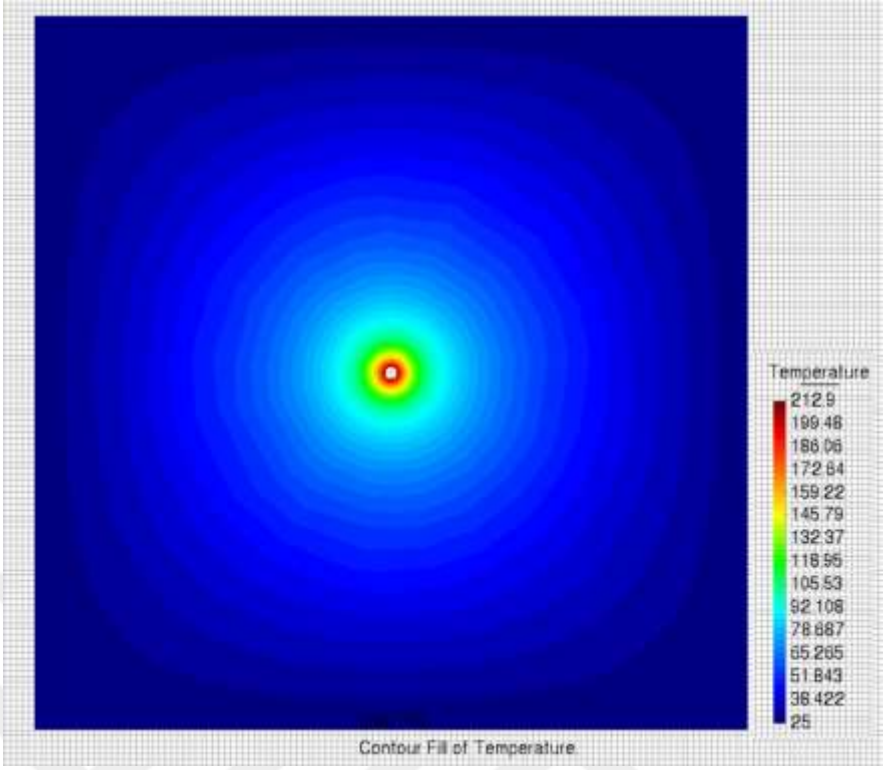


Figure 8.10 Contour fill of temperature representation in the presence of 30B-70S buffer mixture

The low hydraulic conductivity value of the 30B-70S mixture compared to the other two sand-bentonite mixtures indicates that the impermeability will be lower. However, this feature is also a positive factor in slowing down the rate of progress of the leachate and is not important in terms of removing the heat emitted from the heat source (canister). Because the main idea is the ability of the buffer material to transmit heat, that is, its thermal conductivity.

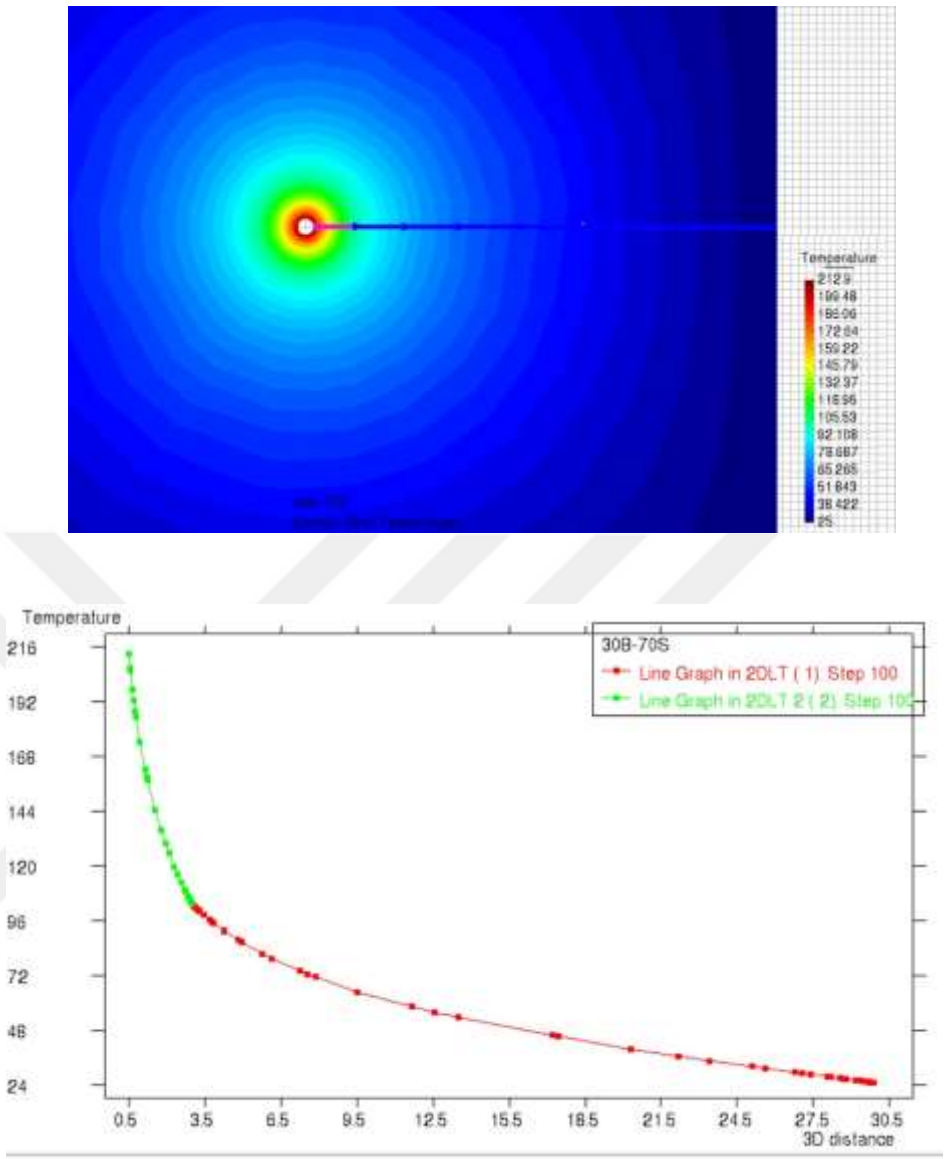


Figure 8.11 Temperature vs. distance relationship

Figure 8.11 shows the decreasing temperature from the canister surface temperature to the bedrock. Figure 8.12 represents point-based temperature values. Canister, buffer and bedrock temperatures are approximately 177, 110, 45 °C for 50 isochron values, respectively.

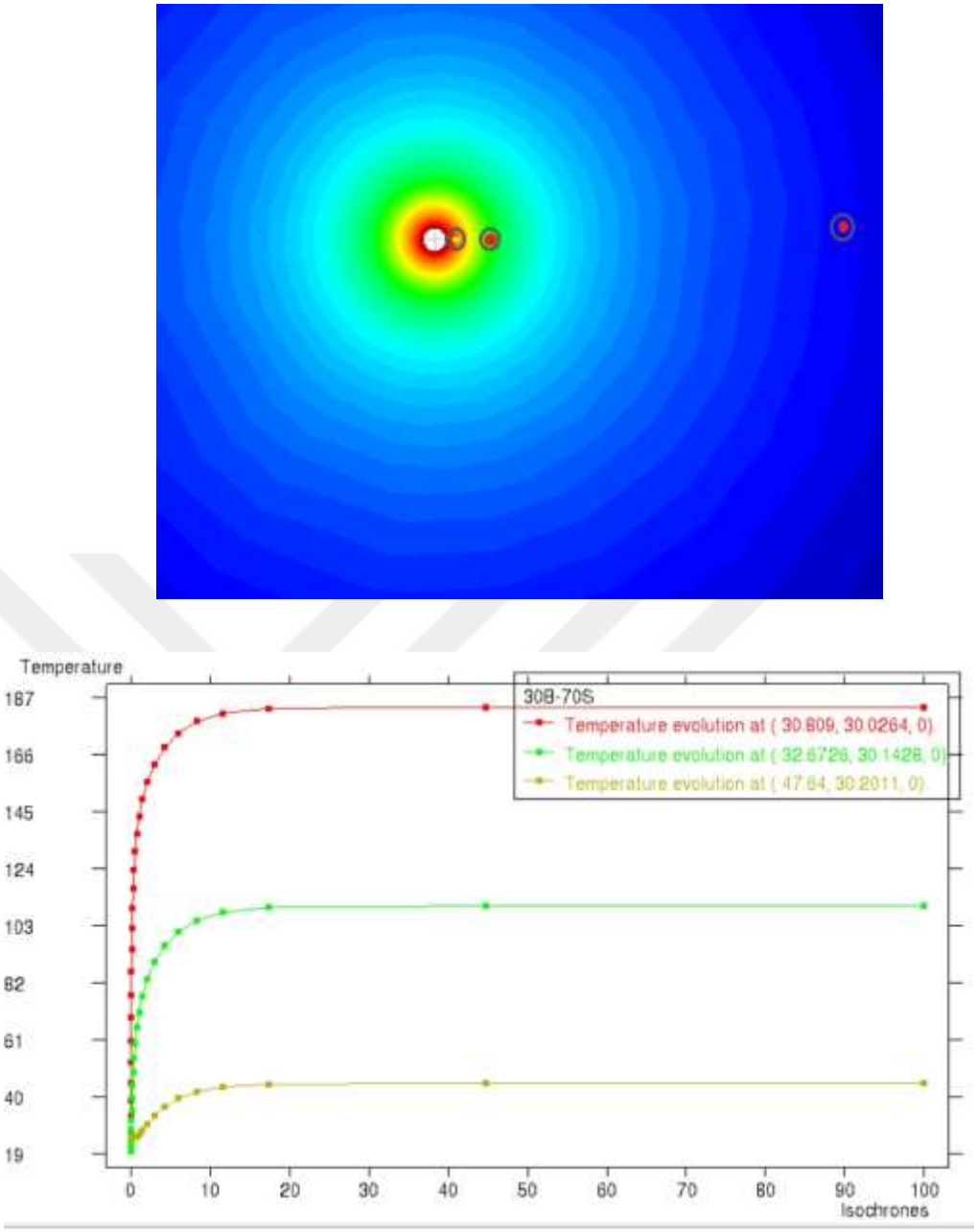


Figure 8.12 Point temperature evalution

As a result of the analyzes performed with the Code Bright Program, the results obtained with three different buffer materials showed that 10B-90S and 20B-80S mixtures reached similar final temperature values due to their close thermal conductivity values. The 30B-70S buffer, on the other hand, reached higher final temperatures due to its lower thermal conductivity.

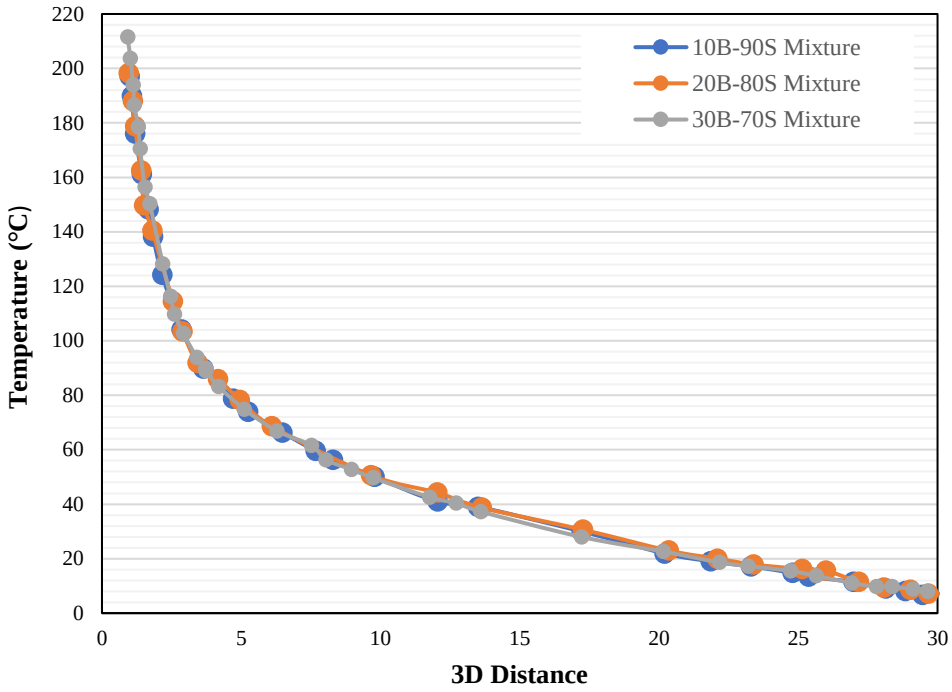


Figure 8.13 Temperature vs. distance of all sand-bentonite mixtures

In Figure 8.13, the cahnge in temperature obtained from 10B-90S, 20B-80S and 30B-70S sand-bentonite mixtures from canister to bedrock is given. Since the mixture with the lowest thermal conductivity will conduct the heat from the heat source slowly, that mixture will reach the highest temperature in its layers. In this modeling study, the highest temperature values were attained since the 30B-70S mixture had the lowest thermal conductivity. The other sand-bentonite mixtures reached very close temperature values, due to the close thermal conductivity values. For this reason, the mixtures were recommended to be used as buffer material. However, it should be noted that only thermal conductivity is not enough for the performance of nuclear waste repositories. The hydraulic conductivity, swelling potential and short- and long-term durability are the other engineering properties should be considered.

CHAPTER 9
CONCLUSIONS

Within the scope of this doctoral thesis, pumice, perlite and fiberglass were added as additives to sand-bentonite mixtures used as buffer material, and the engineering properties of these mixtures were investigated under room, high temperature (80 °C) and thermal cycles (25-80-25 °C). The effect of these thermally resistant materials on the engineering properties of sand-bentonite mixtures were investigated under different thermal conditions. In this context, compaction, oedometer, direct shear, hydraulic conductivity tests and thermal conductivity measurements were carried out performed on the mixtures. The findings of the study are summarized below:

9.1 Compaction Test Results

- As the amount of bentonite was increased from 10% to 20% , the $\gamma_{d,max}$ value decreased slightly, while there was a slight increase in the w_{opt} value.
- Pumice additive decreased the $\gamma_{d,max}$ value of sand-bentonite mixtures, w_{opt} changed negligibly.
- Perlite additive decreased the $\gamma_{d,max}$ value of sand-bentonite mixtures while it increased the w_{opt} value.
- Fiberglass additive changed the $\gamma_{d,max}$ and w_{opt} values of sand-bentonite mixtures negligibly.

9.2 Oedometer Tests Results

Oedometer and swelling experiments were performed under room temperature, high temperature (80 °C) and thermal cycles (25-80-25 °C). According to the test results obtained, the following conclusions can be drawn:

- A decrease in the amount of compression was determined under 80 °C for the sand-bentonite mixtures.
- The total compression amount of sand-bentonite mixtures under thermal cycles decreased compared to room temperature and 80 °C.

- While only 10% pumice additive had a reducing effect on vertical deformation of 10B-90S mixtures, it was observed that the amount of deformation increased as the amount of pumice increased in 20B-80S mixtures under room temperature.
- It was observed that compression and swelling deformation values increased as perlite content was increased in 10B-90S and decreased in 20B-80S mixtures under room temperature.
- It was determined that pumice additives increased the deformation value of the 10B-90S and 20B-80S mixtures at 80 °C. However, the obtained deformation values for both additive contents were negligible.
- It was observed that swelling deformation amounts decreased with addition of pumice to the 10B-90S and 20B-80S mixtures at 80 °C.
- It was determined that perlite additives increased the compression deformation value of 10B-90S and 20B-80S mixtures with 10% and 20% perlite under high temperature (80 °C).
- The pumice and perlite addition to the sand-bentonite mixtures as a result of both heating and cooling cycles increased the compression deformation amounts. It should be noted that the obtained deformation amounts were at negligible levels (0.07% ~ 0.95%).
- According to the results, the 0.5% and 1.0% fiber glass additives, did not have a significant effect on compression deformations under room temperature. However, the swelling deformation increased in the presence of 1% fiberglass.
- The fiberglass additive changed the amount of compression negligibly under room temperature, while it was observed that the amount of compression increased under high temperature.

9.3 Direct Shear Test Results

The shear strength parameters were obtained by performing the direct shear tests at room temperature and high temperature (80 °C). In addition, shear stresses of the mixtures under 196 kPa vertical stress were determined under thermal cycles (25-80-25

°C). Based on the test results, the effects of additives and temperature changes on the shear strength behavior sand-bentonite mixtures can be summarized as follows:

- When the temperature increased to 80 °C, the internal friction angle of the 10B-90S mixture decreased slightly, while that of 20B-80S mixture increased approximately twofold. On the other hand, cohesion valuesof all mixtures decreased.
- When the temperature increased to 80 °C, the maximum shear stress values decreased slightly for 10B-90S, but increased slightly for 20B-80S mixture.
- In 10B-90S mixtures, 20% pumice additive increased the internal friction angle both at room and high temperatures, while 10% pumice additive showed a slight increase only under high temperature.
- In 20B-80S mixtures, both pumice contents (10% and 20%) increased the internal friction angle and maximum shear strength values under room temperature, while only 10% pumice additive increased the shear stress value under 80 °C. On the other hand, 20% pumice additive increased the internal friction angle at a very low rate and almost did not change the maximum shear stress significantly.
- The addition of perlite to 10B-90S mixtures had a reducing effect on shear strength both at room and high temperatures. When perlite was added to the 20B-80S mixtures, it was observed that the maximum shear stress increased both at room and high temperature. However, it was observed that this increase was more pronounced in the presence of 20% perlite additive.
- Pumice and perlite additives reduced the shear stress value under the temperature cycle.
- According to the results both fiberglass contents increased the maximum shear stress values of 30B-70S mixtures. It was observed that the internal friction angle did not change significantly (increased only 3°) with 3 mm fiberglass aditives under room temperature.
- In the experiments conducted with 6 mm fiberglass, it was observed that 0.5% fiberglass additive changed the internal friction angle and cohesion values

insignificantly, but 1.0% fiberglass additive increased the internal friction angle of the mixture much more.

- The experimental results revealed that the fiber glass addition contributes to the internal friction angle and cohesion values positivitely under high temperatures.

9.4 Hydraulic Conductivity Test Results

Hydraulic conductivity experiments were performed at room temperature and high temperature (50-80 °C). One thermal cycle for hydraulic conductivity experiments was conducted by applying the temperature as 25-50-80-50-25 °C, consecutively. In the light of the results obtained, the following conclusions can be drawn:

- The hydraulic conductivity value of the 20B-80S mixture at room temperature was lower than by the order of 10^4 than 10B-90S mixture.
- When a thermal cycle was applied for the 10B-90S mixture, an increase in hydraulic conductivity in the heating phase, and a decrease in the cooling phase was observed. As the number of cycles increased, the amount of increase in hydraulic conductivity decreased.
- It was observed that the hydraulic conductivity value of the pumice added sand-bentonite mixtures increased as the temperature increased. It was determined that even if the hydraulic conductivity decreased in the cooling cycle, it could not return to the initial value.
- According to the hydraulic conductivity test results of perlite and fiberglass added sand-bentonite mixtures under temperature cycling, the hydraulic conductivity of the mixtures increased depending on the viscosity of the water, water-soil interaction and detoriation of pore structure.
- It was observed that the hydraulic conductivity increased as the fiberglass content increased at all temperatures, but the most significant increase occurred under room temperature than high temperature.

9.5 Thermal Conductivity Test Results

The thermal conductivity values of sand-bentonite mixtures with pumice, perlite and fiberglass additives were measured. The measurements were conducted with two different methods based on the degree of saturation and void ratio. According to the measurement results;

- The thermal conductivity value of the mixture decreased as pumice was added to the sand-bentonite mixtures, so that the mixture becomes more insulative.
- Perlite additive also showed similar behavior to pumice additive, it decreased the thermal conductivity value of the mixtures.
- Both fiberglass contents increased the thermal conductivity, it should also be noted that there was no significant change between the 0.5% and 1.0% contents.

9.6 Comparison of the Effects of the Pumice, Perlite and Fiber Glass Additives

According to the oedometer test on the sand-bentonite mixtures in the presence of pumice and perlite additives, the vertical deformation amounts increased under both heating and cooling cycles in the oedometer experiments. Odeometer experiments were not carried out under thermal cycling of fiberglass added sand-bentonite mixtures. Considering this compression increasing effect, it is recommended not to be used in cases where volumetric deformation behavior is important.

When the effect of pumice and perlite additives on 20B-80S mixtures under high temperature was examined and when the additives were compared with each other, it was seen that the perlite added sand-bentonite mixture reached approximately two times more compression than the pumice added sand-bentonite mixture (Figure 9.1). The fact that perlite causes a much more porous structure than pumice is one of the reasons why the amount of compression appears higher under high temperature. Fiberglass additive could not be compared with these two additives due to the difference in bentonite and additive contents.

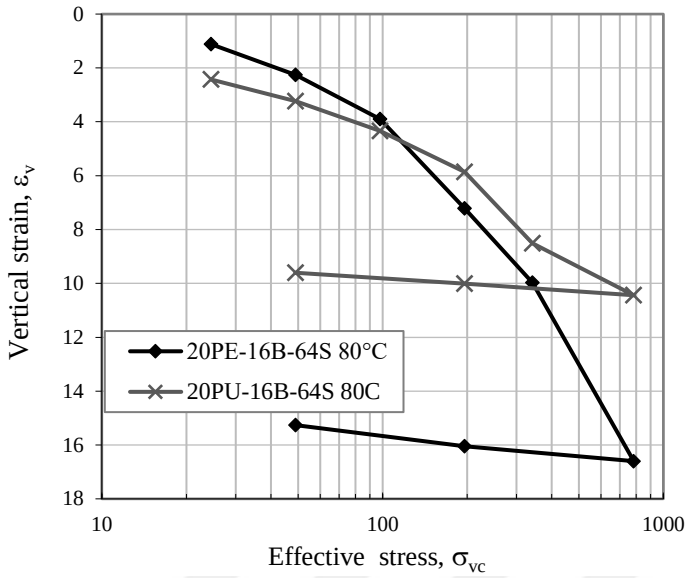


Figure 9.1 Comparison of compression curves of pumice and perlite added 20B-80S mixtures

When the pumice and perlite effects were analyzed, the positive effects on the shear strength of 20B-80S mixture were observed especially under high temperature. The pumice and perlite additives decreased the shear stress values of the sand bentonite mixtures under temperature cycle. The results revealed that the temperature negligibly affects the internal friction angle and cohesion values of fibergglass added sand-bentonite mixtures under room and high temperatures.

According to the hydraulic conductivity test results, the hydraulic conductivity of sand-bentonite mixtures with pumice, perlite and fiberglass increased with the increase in temperature. For this reason, it is not recommended to use these mixtures as buffer materials. However, the initial hydraulic conductivity values of 20B-80S and 30B-70S mixtures under room temperature are 4.5 x 10^{-11} m/s and 4.3 x 10^{-11} m/s, respectively and because of these values remain below the barrier limit (10^{-9} m/s) in municipal solid waste landfills these mixtures are suitable for use. In addition, the hydraulic conductivity value of 20PU-16B-64S mixture determined under 25 °C at the end of the first cycle is 5.2 x 10^{-11} m/s, which can be recommended for use as a barrier in landfills. It should be noted, none of the mixtures supply the hydraulic conductivity limit value (10^{-12} m/s) for nuclear waste repositories.

According to the results of thermal conductivity measurements, pumice and perlite additives decreased the thermal conductivity of sand-bentonite mixtures, in other words they increased the insulating property of the mixtures. These mixtures could be used as insulating materials in areas where heat conduction should be prevented in energy geo-structures. Both fiberglass contents have increasing effect on the thermal conductivity of the sand-bentonite mixtures. These mixtures can be used where heat condcution is needed, for example around the canister in nuclear waste repositories.

The fact that fiberglass additive has an increasing effect on thermal conductivity compared to pumice and perlite additives is important in terms of conducting the heat generated around energy structures faster. For this reason, it can be used with sand-bentonite mixtures to remove the excess heat from the high power cables. At the same time, compared to the other two additives, the amount of compression of fiberglass under room and high temperatures is less, which supports its use around energy geo-structures such as energy piles.

9.7 Future Studies

The buffer materials should have some properties in order to supply continuity of performance of energy geo-structures. For that reason, there is a need to improve engineering properties of buffer materials. The long-term behavior of sand-bentonite mixtures under different thermal conditions should be investigated. Differences in the behavior of normally consolidated and overconsolidated soils require further investigation. The effect of the overconsolidation ratio (OCR) on thermal behavior needs to be investigated extensively. The effect of different additives with higher thermal conductivity such as graphite, copper slag, etc. on the engineering properties of soils should be investigated. The suitability of different soil mixtures for buffer materials such as zeolite-bentonite and zeolite-sand-bentonite mixtures should be investigated for better performance of energy geo-structures.

REFERENCES

Abdelaziz, S. L. (2013). Deep energy foundations: geotechnical challenges and design considerations. PhD Thesis, Department of Civil and Environmental Engineering, Virginia Polytechnic Institute and State University, Blacksburg, VA, USA, 347p.

Abuel-Naga, H.M., Bergado, D., Soralump, S., & Rujivipat, P. (2005). Thermal consolidation of soft Bangkok clay. *Lowland Technol. Int*. J. 7 (1), 13–22. ISSN 1344-9656.

Abuel-Naga, H. M., Bergado, D. T., & Bouazza, A. (2007). Thermally induced volume change and excess pore water pressure of soft Bangkok clay. Engineering Geology, 89: 144–154.

Ahn, J., & Jung, J. (2017). Effects of fine particles on thermal conductivity of mixed silica sands. *Applied Sciences*. 7(7):650. https://doi.org/10.3390/app7070650

Akash, B., Nijmeh, S., & Odeh, S. (2005). Measurement of effective thermal conductivity of soils at various moisture contents. Proceedings of the International Conference on Recent Advances in Mechanical & Materials Engineering 30-31 May, Kuala Lumpur, Malaysia, Paper No. 45.

Akgün, H., Ada, M., & Koçkar, M.K. (2015). Performance assessment of a bentonite–sand mixture for nuclear waste isolation at the potential akkuyu nuclear waste disposal site, southern Turkey, Environ. Earth Sci. 73(10) 6101-6116.

Allameh-Haery, H., Kisi, E., Pineda, J., et al. (2017) Elastic properties of green expanded perlite particle compacts. Powder Technol. https://doi.org/10.1016/j.powtec.2017.01.045

Anders, G. J. (1997). Rating of Electric Power Cables: Ampacity Computations for Transmission, Distribution, and Industrial Applications, 1st ed.; McGraw-Hill Professional: New York, NY, USA; 428p.

ASTM:D3080/D3080M-11. (2011). Standard test method for direct shear test of soils under consolidated drained conditions. *ASTM International, West Conshohocken, PA, USA*, 1–9.

ASTM:D2487-17. (2017). Standard practice for classification of soils for engineering purposes (Unified soil classification system), *ASTM International, West Conshohocken, PA, USA*, 1–10.

ASTM:D5084-00. (2000). Standard test methods for measurement of hydraulic conductivity of saturated porous materials using a flexible wall permeameter. *ASTM International, West Conshohocken, PA, USA*, 1–24.

ASTM:D698-12. (2012). Standard test methods for laboratory compaction characteristics of soil using standard effort (12 400 ft-lbf/ft3 (600 kN-m/m3)). *ASTM International, West Conshohocken, PA, USA*, 1–13.

ASTM:D422-63. (2007). Standard test method for particle-size analysis of soils (Withdrawn 2016), *ASTM International, West Conshohocken, PA, USA*, 1-8.

ASTM:D854-14. (2014). Standard test methods for specific gravity of soil solids by water pycnometer. *ASTM International, West Conshohocken, PA, USA*, 1-8.

ASTM:D4318-17e1. (2017). Standard test methods for liquid limit, plastic limit, and plasticity index of soils. *ASTM International, West Conshohocken, PA, USA*, 1-20.

ASTM:D4972-18. (2018). Standard test methods for ph of soils. ASTM International, West Conshohocken, PA, USA, 1-6.

Bag, R., & Rabbani, A. (2017). Effect of temperature on swelling pressure and compressibility characteristics of soil. *Applied Clay Science*. Volume 136, Pages 1-7, ISSN 0169-1317, https://doi.org/10.1016/j.clay.2016.10.043.

Bageri, B.S., Adebayo, A.R., Al Jaberi, J., & Patil, S. (2020). Effect of perlite particles on the filtration properties of high-density barite weighted water-based drilling fluid. Powder Technol., 360pp. 1157-1166.

Bai, B., & Jiang, S. (2017). Thermally induced pore pressure and consolidation volumetric strain for saturated soils. *Bulgarian Chemical Communications.* Special Edition H. (pp. 19 – 24).

Baldi, G., Hueckel, T., & Pellegrini, R. (1988). Thermal volume changes of the mineral-water system in low-porosity clay soils. *Can Geotech J*. https://doi.org/10.1139/t88-089.

Beikircher, T., & Demharter, M. (2013). Heat transport in evacuated perlite powders for super-insulated long-term storages up to 300 °c. *J Heat Transfer*. https://doi.org/10.1115/1.4023351.

Bodas Freitas T.M., Cruz Silva F., & Bourne-Webb P.J. (2013). The response of energy foundations under thermo-mechanical loading. Proceedings of the 18th International Conference on Soil Mechanics and Geotechnical Engineering, Paris.

Brandl, H. (2006). Energy Foundations and Other Thermo-Active Ground Structures. Géotechnique, 56, 81–122. doi:10.1680/geot.2006.56.2.81.

Burghignoli, A.; Desideri, A., & Miliziano, S. (2000). A laboratory study on the thermomechanical behaviour of clayey soils. Can. Geotech. J. 37: 764-780.

Campanella, R., & Mitchell, J. (1968). Influence of Temperature Variations on Soil Behavior. *Journal of the Soil Mechanics and Foundations Division*.

Cekerevac, C., & Laloui, L. (2004). Experimental study of thermal effects on the mechanical behaviour of a clay. *Int J Numer Anal Methods Geomech*. https://doi.org/10.1002/nag.332

Chen, G.J., Maes, T., Vandervoort, F., Sillen, X., Van Marcke, P., Honty, M., & Vanderniepen, P. (2014). Thermal impact on damaged Boom Clay and Opalinus Clay: permeameter and isostatic tests with μCT scanning. Rock Mech. Rock. Eng. 47 (1), 87–99.

Chen, W.Z., Ma, Y.S., Yu, H.D., Li, F.F., Li, X.L., & Sillen X. (2017). Effects of temperature and thermally-induced microstructure change on hydraulic conductivity of Boom Clay, Journal of Rock Mechanics and Geotechnical Engineering, Volume 9, Issue 3, Pages 383-395,

Cho, W. J., Lee, J. O., & Kang, C. H. (1999). Influence of salinity on the hydraulic conductivity of compacted bentonite. *MRS Proceedings*, *713*.

C O D E _ B R I G H T. Tutorial Manual (2020). Retrieved April 21, 2020, from https://deca.upc.edu/en/projects/code_bright/downloads/tutorials.pdf

Conca, J.L., Apted, M.J., Zhou, W., Arthur, R.C., & Kessler, J.H. (1998). Flow barrier system for the long-term high-level-waste isolation - Experimental results. Nucl. Tech., 1124, 88-100.

Crowley, K. D. (1977). Nuclear Waste Disposal: The Technical Challenges. American Institute of Physics, S-0031-9228-9706-030-4. June 1997 .

Cui, Y., Le, T. T., Tang, A. M., Delage, P., & Li, X. L. (2009). Investigating the time dependent behaviour of Boom clay under thermo mechanical loading, *Géotechnique,* 59, 319-329.

Cui, S.L., Du, Y.F., Wang, X.P., Huang, S., & Xie, W.L. (2018). Influence of temperature on swelling deformation characteristic of compacted GMZ bentonite-sand mixtures. J. Cent. South Univ. 25, 2819–2830.

Danieli D. E. (1997). Clay liners. In: Daniel DE (ed) Geotechnical practice for waste disposal. Chapman & Hall, London, pp 137–163.

Das, B. M. (2008). Advanced Soil Mechanics. Washington, New York, London.

De Bruyn, D., & Thimus, J.F. (1996). The influence of temperature on mechanical characteristics of Boom clay: the results of an initial laboratory programme. Engineering Geology. 41, Nos. 1 – 4, 117 – 126.

Delage, P., Sultan, N., & Cui, Y.J. (2000). On the Thermal Consolidation of Boom Clay. Canadian Geotechnical Journal.

Delage, P., Cui, Y. J., & Sultan, N. (2004). On the thermal behavior of Boom clay. Proceeding Eurosafe 2004 Conference. Berlin, Germany.

Depci, T., Efe, T., Tapan, M., Özvan, A., Açlan, M., & Uner, T. (2012). Chemical characterization of Patnos Scoria (Ağrı, Turkey) and its usability for production of blended cement. Physicochemical Problems of Mineral Processing, Volume 48, Issue 1, Pages 303 – 315.

DeWalle, F. B., Chian, E. S. K., & Hammerberg, E. (1978). Gas production from solid waste in landfills. J. Environ. Eng. Div. (Am. Soc. Civ. Eng.), 104, (EE3), 415–432.

Dickson M. H. & Fanelli, M. (2003). Geothermal energy: utilization and technology. Paris: UNESCO.

Dixon, D.A., Gray, M.N., & Thomas, A.W. (1985). A study of the compaction properties of potential clay–sand mixtures for use in nuclear fuel waste. Engineering Geology, 21: 247–255.

Dixon, D.A., Gray, M.N., Lingnau, B.E., Graham, J., & Campbell, S.L. (1993). Thermal expansion testing to determine the influence of pore water structure on water flow through dense clays. 46th Canadian Geotechnical Conf., Saskatoon, Sask., Sept. 1993, pp. 177-184.

Djeghader, D., & Redjel, B. (2017). Fatigue of glass-polyester composite immerged in water. Journal of Engineering Science and Technology. 12. 1204-1215.

El Tawati, A. (2010). Impact of the rate of heating on the thermal consolidation of compacted silt. Master of Science Thesis. B.S., University of Garyounis.

Eriksson, L. G. (1989). Temperature effects on consolidation properties of sulphide clays. In Proceedings of the 12th International Conference on Soil Mechanics and Foundation Engineering, Rio de Janeiro, 3: 2087–2090.

Fang, H.Y., & Daniels, J.L. (2006). Engineering and environmental perspective. Taylor and Francis New York 10016.

Farouki, O.T. (1981). The thermal properties of soil in cold regions. *Cold Reg. Sci. Technol*. 5, 67–75.

Farquhar, G. J., & Rovers, F. A. (1973). Gas production during refuse decomposition. Water, Air, Soil Pollut., 2(4), 483–495.

Finn, F. N. (1951). The effects of temperature on the consolidation characteristics of remolded clay. Symposium on Consolidation Testing of Soils, ASTM, Special Technical Publication, No. 126: 65–72.

Fleureau, J. M. (1979). Influence d'un champ thermique ou électrique sur les phénomènes d'interaction solide-liquide dans les milieux poreux, Doctoral thesis. Ecole Centrale de Paris.

Gens, A., Alcoverro, J., Blaheta, R., Hasal, M., Michalec, Z., Takayama, Y., Lee, C., Lee, J., Kim, G., Kuo, C., Kuo, W., & Lin, C. (2021). HM and THM interactions in bentonite engineered barriers for nuclear waste disposal. International Journal of Rock Mechanics and Mining Sciences. 137. 104572. 10.1016/j.ijrmms.2020.104572.

Ghabezloo, S. & Sulem, J., (2010). Temperature induced pore fluid pressurization in geomateirals. Italian Geotechnical Journal. 1, 29., Master thesis. The Missouri University of Science and Technology, Rolla, Missouri, USA.

Graham, J., Saadat, F., Gray, M.N., Dixon, D.A., & Zhang, Q.-Y. (1989). Strength and volume change behaviour of a sand-bentonite mixture. Can. Geotech. J., 26: 274-281.

Gray, H. (1936). Progress Report on Research on the Consolidation of Fine-Grained Soils. Proc. Internat. Conf. On Soil Mech. and Found. Eng., Harvard University, Vol. 2, p. 138-141.

Gray, D. H., & Ohashi, H. (1983). Mechanics of fiber reinforcement in sand. *J. Geotech. Engrg., ASCE,* 109(3), 335-353.

Green, W. J. (1969). The influence of several factors on the rate of secondary compression of soil. Master thesis, The Missouri University of Science and Technology, Rolla, Missouri, USA.

Gupta, B. (1964). Creep of saturated soil at different temperatures. Master Thesis, The University of British Columbia, Canada.

Gupta, V. K. (2013). An Experimental Study on Secondary Consolidation of Organic Clay. Master Thesis, Jadavpur University, Kolkata, India.

Gündüz, L., Sarıışık, A., Tozaçan, B., Davraz, M., Uğur İ. & Çankıran, O. 1998. Pomza Teknolojisi (Pomza Karakterizasyonu). Isparta.

Habibagahi, K. (1977). Temperature effect and the concept of effective void ratio Indian Geotechnical Journal, 7 (1) , pp. 14-34.

Hamidi, A., Tourchi, S., Khazaei, C. (2014). Thermomechanical constitutive model for saturated clays based on critical state theory International Journal of Geomechanics 15 1 04014038 https://doi.org/10.1061/(ASCE)GM.1943-5622.0000402

Hanson, J.L., Yeşiller, N., & Oettle, N.K. (2010). Spatial and temporal temperature distributions in municipal solid waste landfills. Journal of Environmental Engineering, 136(8), pp.804-814.

Hanson, J.L., Yeşiller, N., Onnen, M.T., Liu, W.L., Oettle, N.K., & Marinos, J.A. (2013). Development of numerical model for predicting heat generation and temperatures in MSW landfills. Waste management, 33(10), pp.1993-2000.

Harmancioğlu, M. (1981). Tekstil maddeleri 2, Rejenere ve sentetik lifler. s. 338-347.

Harrington, J., Volckaert, G. & Noy, D. (2014). Long-term impact of temperature on the hydraulic permeability of bentonite. Geological Society London Special Publications. 400. 10.1144/SP400.31.

Hartz, K. E., Klink, R. E., & Ham, R. K. (1982). Temperature effects: methane generation from landfill samples. J. Environ. Eng. Div. (Am. Soc. Civ. Eng.), 108(4), 629–638.

Horseman, S.T., & McEwen, T.J. (1996). Thermal constrains on disposal of heat-emitting waste in argillaceous rocks Eng. Geol., 41, pp. 5-16.

Houston, S. L. & Lin, H. D. (1987). A thermal consolidation model for pelagic clays. Marine Geotechnology. 7: 79-98.

Hueckel, T., & Baldi, G. 1990. Thermoplasticity of saturated clays: Experimental constitutive study. J Geotech Eng. https://doi.org/10.1061/(ASCE)0733-9410(1990)116:12(1778)

Imielińska, K., & Guillaumat, L. (2004). The effect of water immersion ageing on low-velocity impact behaviour of woven aramid-glass fibre/epoxy composites. Composites Science and Technology,64(13-14), 2271-2278.

İstockphoto. (25 May, 2010). Pumice Stone Detail Isolated on White. https://www.istockphoto.com/tr/foto%C4%9Fraf/pumice-stone-detail-isolated-on-white-gm119398150-14327072

Jafari, N. H., Stark, T. D., & Rowe, R. K. (2014) Service life of HDPE geomembranes subjected to elevated temperatures. J. Hazard. Toxic Radioactive Waste 18(1), 16–26.

Jarad, N. (2016). Temperature impact on the consolidation and creep behaviour of compacted clayey soils. *Mechanics of materials [physics.class-ph]*. Université de Lorraine. English. NNT :2016LORR0251. tel-01532182

Johansen, O. (1977). Thermal Conductivity of Soils. 322.

Kale, R. C., & Ravi, K. (2019). Influence of thermal history on swell pressures of compacted bentonite. Process Saf Environ 123:199–205. https://doi.org/10.1016/j.psep.2019.01.004

Karaman, S, Karaipekli, A., Sari, A., & Biçer, A. (2011). Polyethylene Glycol (PEG)/Diatomite Composite as A Novel Form-Stable Phase Change Material for Thermal Energy Storage. Solar Energy Materials and Solar Cells. 95. 1647-1653. 10.1016/j.solmat.2011.01.022.

Kılınç Aksay, E. (2005). İzmir-Menderes Yöresi Pomza Cevherinin Kullanımına Yönelik Teknolojik 435 Özelliklerinin Araştırılması. Dokuz Eylül Üniversitesi.

Kim, J. S., Kwon, S. K., Sanchez, M., & Cho, G. C. (2011). Geological storage of high level nuclear waste. KSCE Journal of Civil Engineering, 15(4), 721‑737.

Knellwolf, C., Peron, H., & Laloui, L. (2011) Geotechnical analysis of heat exchanger piles, J. Geotech. Geoenviron. Eng., 137, 890–902. doi:10.1061/(ASCE)GT.1943 5606.0000513.

Komine, H., & Ogata, N. (2004). Predicting swelling characteristics of bentonites. Journal of Geotechnical & Geoenvironmental Engineering, 130, 818_830.

Kootsooks, A., & Mouritz, A.P .(2004). Seawater durability of glass and carbonpolymer composites. Compos Sci Technol;64:1503–11.

Kuhn, M. R., & Mitchell, J. K. (1993). New perspectives on soil creep. Journal of Geotechnical Engineering, 119, 507–524, doi: 10.1061/(ASCE)0733-9410, 119:3(507).

Kuntiwattanakul, P., Towhata, I., Ohishi, K., & Seko, I. (1995). Temperature e_ects on undrained shear characteristics of clay, Soils and Foundations 35(1): 147-162.

Kurniawan, T.A., Othman, M.H., & Singh, D. et al. (2022). Technological solutions for long term storage of partially used nuclear waste: A critical review Ann. Nucl. Energy, 166 , Article 108736.

Laguros, J.G. (1969). Effect of temperature on some engineering properties of clay soils Highway Res. Board Spec. Rep., 103 pp.186-193.

Laloui, L. (2001). Thermo-mechanical behavior of soils. Revue Française de Genie Civil.,5(6), 809-843.

Lambe, J. C. (1960). Influence Of Temperature, Moisture And Method Of Application On The Fungitoxicity Of Mylone And Vapam. A Thesis. Submitted to Oregon State College In Partid Fulfillment Of The Requlrementd For The Degree Of Doctor Of Philosophy June 1960.

Lamothe, D., & Edgers, L. (1994). The effects of environmental parameters on the laboratory compression of refuse. Proc., 17th Int. Madison Waste Conf., Dept. of Engineering Professional Development, Univ. of Wisconsin, Madison, Wisc., 592–604.

Lankard, D.R. (1972). Prediction of the flexural strength properties of steel fibrous concrete. In: Proceedings CERL conference on fibrous concrete. Construction Engineering Research Laboratory, Champaign; p. 101‑23.

LBI FIBERGLASS. (10 May, 2022). Chopped Fiberglass Strand. https://www.lbifiberglass.com/product/chopped-fiberglass-strand/

Le, T. M., Fatahi, B., & Khabbaz, H. (2012). Viscous behaviour of soft clay and inducing factors. Geotechnical and Geological Engineering 30, 1069-1083.

Leila, R., & Nacerddine, D. 2013. Influence Of Thermal Conductivity On Energy Consumption Of Building. International Journal of Engineering Research & Technology (IJERT) ISSN: 2278-0181 www.ijert.org Vol. 2 Issue 6, June.

Li, V. C. (2012). Tailoring ECC for special attributes: A review. Int J Concr Struct M,6(3), 135–144.

Lide, D. (1995). Handbook of chemistry and physics, 75th edn. CRC Press, New York.

Lingnau, B.E., Graham, J., Yarechewski, D., et al. (1996). Effects of temperature on strength and compressibility of sand-bentonite buffer. *Eng Geol*. https://doi.org/10.1016/0013-7952(95)00028-3.

Loveridge, F., & Powrie, W. (2012). Pile heat exchangers: thermal behaviour and interactions. Proceedings of the Institution of Civil Engineers - Geotechnical Engineering 2013 166:2, 178-196.

Lubimova, E. A. (1968). Thermal history of the Earth. In: The Earth's Crust and Upper Mantle, pp. 63–77, American Geophysics Un., Geophysics Monographs, Series 13.

Maghsoodi, S., Cuisinier, O., & Masrouri, F. (2019). Thermo-mechanical behaviour of clay-structure interface. E3S Web of Conferences. 92. 10002. 10.1051/e3sconf/20199210002.

Maghsoodi, S., Cuisinier, O., & Masrouri, F. (2020). Thermal effects on mechanical behaviour of soil–structure interface. Can. Geotech. J. 57 (1), 32–47.

Maher, M. H., & Woods, R. D. (1990). Dynamic response of sands reinforced with randomly distributed fibers. *J. Geotech. Engrg*., ASCE, 116(7).

Maher, M. H., & Ho, Y. C. (1994). Mechanical properties of kaolinite/fibre soil composite. Journal of Geotechnical Engineering. Vol.120 (8), pp.1381-1393.

Marcotte, D., & Pasquier, P. (2008). On the estimation of thermal resistance in borehole thermal conductivity test. Renew. Energy, 33, 2407–2415. doi:10.1016/j.renene.2008.01.021.

Marshall, P. W. (1960). Permeability Studies on Selected Saturated Clays. A High Honors Project under a Fellowship from the National Science Foundation, University of Florida.

Mekaddem ,N., Ali S., Ben., Fois, M., & Hannachi, A. (2019). Paraffin/expanded perlite/plaster as thermal energy storage composite. *In: Energy Procedia*.

Mingarro, E., Rivas, P., del Villar, L.P., de la Cruz, B., Gómez, P., Hernández, A., Turrero, M.J., Villar, M.V., Campos, R., & Cozar, J. (1989). Characterization of clay (bentonite)/crushed granite mixtures to build barriers against the migration of radionuclides: diffusion studied and physical properties. Commission of the European Communities Report EUR 13666.

Mitchell, J.K., & Soga, K. (2005). Fundamentals of Soil Behavior, J. Wiley & Sons, Hoboken, New Jersey, 558 p.

Moritz, L. (1995). Geotechnical properties of clay at elevated temperatures, Int. Sym. Compression and Consolidation of Clayey Soils, IS-Hiroshima, Japan, 267–272.

Nakshabandi, G., & Kohnke, H.. (1965). Thermal conductivity and diffusivity of soils as related to moisture tension and other physical properties. Agricultural Meteorology 2:271-279.

Nuclear Energy Agency, (2007). Nuclear Energy Agency Organisation for Economic Co-operation and Development.

Noble, C. A., & Demirel, T. (1969). Effect Of Temperature On Strength Behavior Of Cohesive Soil. Proceedings of an International Conference Held at Washington, D.C., January 16 1969 With the Support of the National Science Foundation.

Noorany, 1., & Uzdavines, M. (1989). Dynamic behavior of saturated sand reinforced with geosynthetic fabrics. Proc., Geosynthetics '89 Conf., Vol. II, San Diego, Calif., 385-396.

Ocłoń P, Cisek P, Pilarczyk M, et al. (2015). Numerical simulation of heat dissipation processes in underground power cable system situated in thermal backfill and buried in amultilayered soil [J]. Energy Conversion & management, 95:352-370.

Ogawa, M., Okutomo, S., & Kuroda, K. (1998). Control of interlayer microstructures of a layered silicate by surface modification with organochlorosilanes J. Am. Chem. Soc., 120 (1998), pp. 7361-7362.

Omoto, A. (2005). Nuclear power for sustainable development and relevant IAEA activities for the future. Progress in Nuclear Energy. 47. 16-26. 10.1016/j.pnucene.2005.05.056.

Özel, C., & ÖZ, B. (2016). Lif Boyu ve Su/Çimento Oranının Ultra Yüksek Dayanımlı Fiber Katkılı Betonların Basınç Dayanımlarına Etkileri. Cumhuriyet Science Journal. 37. 412. 10.17776/csj.24569.

Özüdoğru, T. Y. (2015). The Use Of Geothermal Heat Exchanger Piles For Sustainable Design. Ph.D. Thesis. Istanbul Technical University, Graduate School Of Science Engineering And Technology. September 2015.

Paaswell, R. (1967). Temperature Effects on Clay Soil Consolidation. Journal of the Soil Mechanics and Foundations Division, 93, 9-22.

Pakbaz, M.C., & Khayat, N. (2004). The effect of sand on strength of mixtures of bentonitesand. Engineering Geological Methods. Modeling of Soil and Rock Behaviour. Engineering Geology for Infrastructure Planning in Europe. 104, 316–320.

Park, S., Yoon, S., Kwon, S., Lee, M.S. & Kim, G.Y. (2021). Temperature effect on the thermal and hydraulic conductivity of Korean bentonite buffer material. *Progress in Nuclear Energy.* Volume 137, 103759. https://doi.org/10.1016/j.pnucene.2021.103759.

Plum L., & Esrig M.I. (1969). Some temperature effects on soil compressibility and pore water pressure. Special report, Report 103, Highway Research Board, Washington.

Pons, C.H,. Franzetti, N., & Tchoubar, D. (1994). Analyse de la structure multiéchelle des dispersions de montmorillonite Na C.R. Rech, 92 N 800094, PIRSEM et ARTEP.

Pusch, R. (1980). The Permeability of Highly Compacted Bentonite. *Swedish Nuclear Fuel and Waste Management Company.* Technical Report 80–16.

Pusch, R., & Güven, N. (1990). Electron microscopic examination of hydrothermally treated bentonite clay Engineering Geology, 28 (3), pp. 303-314.

Pusch, R. (2001). The Buffer and Backfill Handbook, Part2: Materials and Techniques. Technical Report TR-02-12, Swedish Nuclear Fuel and Waste Management Co, ISSN 1404-0344, Stockholm.

Raiko, H. (2012). Canister Design 2012. Eurajoki, Finland: Posiva Oy. Report POSIVA 2012-13.

Rashid, H.M.A.; Wanigarathna, J.A.D.K.; Kurukulasuriya, L.C.; Priyankara, N.H.; Alagiyawanna, A.M.N.; Saito, T., & Kawamoto, K. (2017). Characterization of locally available soil as a liner material for solid waste landfills in Sri Lanka. Environmental Earth Sciences, 76(11), 396.

Rivas, P., Villar, M.V., Campos, R., Pelayo, M., Martı´n, P.L.,Go´mez, P., Turrero, M.J., Herna´ndez, A.I., Co´zar, J.S., & Min-garro, E. (1991). Caracterizacio´n de materiales de relleno y sel-lado para almacenamiento de residuos radiactivos: bentonitasespan˜olas. CIEMAT, Madrid. 196 pp., Unpublished report (inSpanish).

Robinet, J. C., Rahbaoui, A., Plas, F., & Lebon, P. (1996). A constitutive thermomechanical model for saturated clays. *Eng Geol*. https://doi.org/10.1016/0013-7952(95)00049-6.

Romero, E., Gens, A., & Lloret, A. (2001). Temperature effects on the hydraulic behaviour of an unsaturated clay. Geotechnical and Geological Engineering, 19, 311–332.

Rowe, R. K, Quigley, R. M, Brachman, R.W. I, & Broker, J.R. (2004). Barrier systems for waste disposal facilities. Taylor & Francis Books Ltd., London.

Rowe, R. K. (2005). Long-term performance of contaminant barrier system. Géotechnique 55(9):631–678.

Saix, C., Devillers, P., & Youssoufi, M.S. (2000). Element de couplage thermomecanique dans la consolidation de sols non satures. *Can. Geotech*. J. 37, 308–317.

Schmertmann, J. H. (2012). New Concepts for the Mobilization of the Components of Shear Resistance in Clay. Publication 208, Norwegian Geotechnical Institute, Oslo.

Sellin, P., & Leupin, O. X. (2013). The use of clay as an engineered barrier in radioactive-waste management - A review. *Clays and Clay Minerals*, *61*(6), 477–498.

Sezgin, M., Davraz, M., & Gündüz, L. (2005). Pomza Endüstrisine Sektörel Bakış. edited by L. Gündüz 453 and V. Deniz.

Shariatmadari, N., & Saeidijam, S. (2011). The Effect of Elevated Temperature on Compressibility and Swelling of Bentonite-Sand Mixtures. Electronic Journal of Geotechnical Engineering. 16.

SKBF, KBS. (1983). Final Storage of Spent Nuclear Fuel—KBS-3. Swedish Nuclear Fuel Supply Company, Stockholm.

Simmons, G. R., & Baumgartner, P. (1994). The disposal of Canada's nuclear fuel waste: engineering for a disposal facility. Atomic Energy of Canada Limited Report AECL-10715, COG-93-05.

Sinha, A. N., & Kusakabe, O. (2008). Temperature Effects On Volume Change Of Bentonite-Sand Liner.

Smith, M. J. et al. (1980). Engineered barrier development for a nuclear waste repository in basalt: an integration of current knowledge. In: RHO-BWI-ST-7, Rockwell Hanford Operations, WA.

Stewart, S. (2002). Exploring the continental shelf for low geological risk nuclear waste repository site using petroleum industry databases: A UK case study. Engineering Geology. 67. 139-168. 10.1016/S0013-7952(02)00150-3.

Sultan, N. (1997). Etude du comportement thermo-mécanique de l'argile de Boom: expériences et modélisation (PhD thesis) Ecole Nationale des Ponts et Chaussées, p. 217.

Sultan, N., Delage, P., & Cui, Y. J. (2002). Temperature effects on the volume change behavior of Boom clay. Engineering Geology, 64: 135–145.

Tchobanoglous, G., Theisen, H., & Vigil, S. A. (1993). Integrated solid waste management: Engineering principles and management issues, McGraw-Hill, New York.

Thomas, F., Jin, H.M., & Cases, J. M .(1994). Définition du comportement des argiles au cours des forages C.R. Rech, 92 N 80003, PIRSEM et ARTEP.

Towhata, I., Kuntiwattanaku, P., Seko, I., & Ohishi, K. (1993). Volume change of clays induced by heating as observed in consolidation tests. *Soils Found*. https://doi.org/10.3208/sandf1972.33.4_170.

Tupsakhare, S., Moutushi, T., Castaldi, M. J., Barlaz, M. A., Luettich, S., & Benson, C. H.(2020). The impact of pressure, moisture and temperature on pyrolysis of municipal solid waste under simulated landfill conditions and relevance to the field data from elevated temperature landfill.Science of The Total Environment, Volume 723,138031,https://doi.org/10.1016/j.scitotenv.2020.138031.

Van, Impe, W. F. (1998). Environmental geotechnics. ITC 5 activities. State of the art. In: Sêcoe P (ed) Environmental geotechnics. A. A. Balkema, Rotterdam, pp 121–126.

Veliscek Carolan, J. (2016). Separation of Actinides from Spent Nuclear Fuel: A Review. Journal of Hazardous Materials. 318. 266. 10.1016/j.jhazmat.2016.07.027.

Verschaffel-Drefke, C., Schedel, M., Balzer, C., Hinrichsen, V., & Sass, I. (2021). Heat Dissipation in Variable Underground Power Cable Beddings: Experiences from a Real Scale Field Experiment. Energies, 14, 7189. https://doi.org/10.3390/en14217189

Villar, M. V., & Gomez-Espina, R. (2009). Report on Thermo-Hydro-Mechanical Laboratory Tests Performed by CIEMAT on Febex Bentonite 2004-2008.

Villar, M. V., & Lloret, A. (2004). Temperature Influence on the Mechanical Behaviour of a Compacted Bentonite. Elsevier Geo-Engineering Book Series, 2(C), 305–310.

Villar, M. V., Gómez-Espina, R., & Lloret, A. (2010). Experimental investigation into temperature effect on hydro-mechanical behaviours of bentonite. *Journal of Rock Mechanics and Geotechnical Engineering*. 2010, 2 (1): 71–78.simmons

Wanger, R., & Clauser, C. (2005). Evaluating thermal response tests using parameter estimation for thermal conductivity and thermal capacity. J. Geophys. Eng., 2, 349–356. doi:10.1088/1742-2132/2/4/S08.

Westsik J.H, Jr., Bray, L.A, Hodges, F.N., & Wheelwright, E.J. (1982). Permeability, swelling, and radionuclide retardation properties of candidate backfill materials, scientific basis for nuclear waste management. In: Topp SV (ed) Proceedings of the Materials Research Society Annual Meeting, Boston, vol 6, 1981. New York, pp 329–336.

Xiang, G., Lv, L., & Ge, L. (2020). Simple method for evaluating swelling of GMZ01 Na-bentonite affected by temperature at osmotic swelling. *Soils and Foundations.* Volume 60, Issue 5, Pages 1312-1321,ISSN 0038-0806, https://doi.org/10.1016/j.sandf.2020.09.003.

Xie, J., & Qin, Y. (2021). Heat Transfer and Bearing Characteristics of Energy Piles: Review. *Energies 2021,* 14, 6483. https://doi.org/10.3390/en14206483.

Xu, X., Zhang, W., Fan, C., & Li, G. (2020). Effects of temperature, dry density and water content on the thermal conductivity of Genhe silty clay, Results in Physics, Volume 16, 102830, ISSN 2211-3797, https://doi.org/10.1016/j.rinp.2019.102830.

Xu, Y., & Jiang, Linhua & LIU, Jiaping & Zhang, Yan & Xu, Jinxia & He, G.. (2016). Experimental study and modeling on effective thermal conductivity of EPS lightweight concrete. Journal of Thermal Science and Technology. 11. 10.1299/jtst.2016jtst0023.

Yavari, N., Tang, A.M., Pereira, J.-M., & Hassen, G. (2016). Effect of temperature on the shear strength of soils and the soil–structure interface. Can. Geotech. J. 53 (7), 1186–1194.

Ye, W. M., Wan, M., Chen, B., et al. (2013). Temperature effects on the swelling pressure and saturated hydraulic conductivity of the compacted GMZ01 bentonite. Environ Earth Sci. https://doi.org/10.1007/s12665-012- 1738-4

Yeşiller, N., Hanson, J.L., & Liu, W.L., (2005). Heat generation in municipal solid waste landfills. *Journal of Geotechnical and Geoenvironmental Engineering*. 131(11), pp.1330-1344.

Yong, R.N., Boonsinsuk, P., & Wong, G. (1986). Formulation of backfill material for a nuclear fuel waste disposal vault. Canadian Geotechnical Journal, 23(2), 216-228.

Yong, R.N., & Mohamed, A.M.O. (1992). A study of particle inter-action energies in wetting of unsaturated expansive clays. Cana-dian Geotechnical Journal, 29 : 1060–1070.

Yoo, D. Y. Kang, S.T., & Yoon, Y. S. (2014). Effect of fiber length and placement method on flexural behavior, tension-softening curve, and fiber distribution characteristics of UHPFRC, Construction and Building Materials,Volume 64, Pages 67-81, https://doi.org/10.1016/j.conbuildmat.2014.04.007

Youssef, M.S., Sabry, A., & El Ramli A.H. (1961). Temperature changes and their effects on some physical properties of soils. Proceedings of the Fifth International Conference on Soil Mechanics and Foundation Engineering 2 : 419-421, Paris.

Yun, T.S., Santamarina, J.C. (2008). Fundamental study of thermal conduction in dry soils. Granular Matter 10, 197. https://doi.org/10.1007/s10035-007-0051-5.

Zang, A. (1993a). Finite element study on the closure of thermal microcracks in feldspar/quartz-rocks-I. Grain-boundary cracks. Geophysical Journal International. 113:17-31. https://doi.org/10.1111/j.1365-246X.1993.tb02526.x

Zhang, J., & Zhan, M. (2004). Visual experiments for water absorbing process of fibre reinforced composites. Journal of Composite Materials, 38(9), 779-790.

Zheng, L., Rutqvist, J., Birkholzer, J.T., & Liu, H.H. (2015). On the impact of temperatures up to 200 °C in clay repositories with bentonite engineer barrier systems: a study with coupled thermal, hydrological, chemical, and mechanical modeling Eng. Geol., 197, pp. 278-295.